Fabrication of functional basal ganglia circuitry *in vitro*: from nano- and micro-scale topographies to microfluidic devices.

Munyaradzi Kamudzandu

PhD

December 2015

Keele University

SUBMISSION OF THESIS FOR A RESEARCH DEGREE

DECLARATION by the candidate for a research degree

Degree for which thesis being submitted PhD

Title of thesis Fabrication of functional basal ganglia circuitry *in vitro*: from nano- and micro-scale topographies to microfluidic devices.

Date of submission 30/03/2015 Original registration date 03/10/2011
(Date of submission must comply with Regulation 2D)

Name of candidate Munyaradzi Kamudzandu

Research Institute Institute for Science and Technology in Medicine

Name of Lead Supervisor Rosemary A. Fricker

I certify that:

(a) The thesis being submitted for examination is my own account of my own research
(b) My research has been conducted ethically. Where relevant a letter from the approving body confirming that ethical approval has been given has been bound in the thesis as an Annex
(c) The data and results presented are the genuine data and results actually obtained by me during the conduct of the research
(d) Where I have drawn on the work, ideas and results of others this has been appropriately acknowledged in the thesis
(e) Where any collaboration has taken place with one or more other researchers, I have included within an 'Acknowledgments' section in the thesis a clear statement of their contributions, in line with the relevant statement in the Code of Practice (see Note overleaf).
(f) The greater portion of the work described in the thesis has been undertaken subsequent to my registration for the higher degree for which I am submitting for examination
(g) Where part of the work described in the thesis has previously been incorporated in another thesis submitted by me for a higher degree (if any), this has been identified and acknowledged in the thesis
(h) The thesis submitted is within the required word limit as specified in the Regulations

Total words in submitted thesis (including text and footnotes, but excluding references and appendices) …42,532……

Signature of candidate …… Date …….

Note
Extract from Code of Practice: If the research degree is set within a broader programme of work involving a group of investigators – particularly if this programme of work predates the candidate's registration – the candidate should provide an explicit statement (in an 'Acknowledgments' section) of the respective roles of the candidate and these other individuals in relevant aspects of the work reported in the thesis. For example, it should make clear, where relevant, the candidate's role in designing the study, developing data collection instruments, collecting primary data, analysing such data, and formulating conclusions from the analysis. Others involved in these aspects of the research should be named, and their contributions relative to that of the candidate should be specified (*this does not apply to the ordinary supervision, only if the supervisor or supervisory team has had greater than usual involvement*).

Abstract

According to the European Brain Council, the annual total cost of brain disorders such as Huntington's disease (HD) and Parkinson's disease (PD) in Europe is approximately €386 billion. In order to develop therapies for neurodegenerative diseases, model systems that accurately reproduce the complex circuitry of the adult brain are needed. Neuron circuits developed *in vitro* could be used for studying pathogenesis of disorders and for high-throughput screening of potential therapies. *In vitro* models may offer the potential for highly reproducible and controllable cell circuitry, mimicking to some extent the complex neural connectivity required for function. Nano- and micro-scale substrates could be fabricated using techniques such as electrospinning, lithography and microfluidics to direct neurite orientation in order to build *in vitro* models that mimic *in vivo* circuitry. Poly-lactic acid (PLA) nano-fibres and polydimethylsiloxane (PDMS) micro-groove constructs were either pre-coated with poly-D-lysine (PDL) and laminin (LN) or pre-aligned astrocytes to study attachment and orientation of striatal neurites. Neurites were more responsive to substrates made up of combined topography and chemical cues; PDL and LN coated PDMS micro-grooves yielded the best neurite alignment. Excitability of striatal and cortical neurons was verified via an electrophysiology technique of patch clamp. PDMS microfluidic devices fabricated via lithographic techniques, were developed for co-culturing basal ganglia (BG) cells to model BG *in vivo* circuitry. Cell populations in the microfluidic device displayed electrical activity monitored using a calcium imaging technique. Connectivity was determined by eliminating activity of one cell population using tetrodotoxin (TTX) and studying response of remaining cell populations. Micro-contact printing was further explored as a technique for patterning BG cell circuitry instead of microfluidic devices. The microfluidic-based functional and complex model developed herein provides platform technology that can be useful for pharmaceutical and regenerative therapy and evaluation, therefore massively reducing costs currently associated with neurodegenerative diseases.

Contents

Declaration ..... **i**

Abstract ..... **ii**

Contents ..... **iii**

List of tables and figures ..... **vii**

Acknowledgments ..... **x**

Chapter 1. Introduction **1**

1.1 Anatomy of the Basal ganglia (BG) 2

1.1.1 Components of the BG 2

1.1.2 The BG pathways and neurotransmitters 4

1.1.3 Existing HD models: *in vivo* models 10

1.1.4 Neuronal circuitry formation: *in vitro* models 14

Electrophysiology: patch clamp 15

Multi-electrode arrays (MEAs) 18

Calcium imaging 18

1.2. Cellular responses to patterned substrates 23

1.2.1 Natural patterning 23

1.2.2 Biomaterial patterning 24

1.2.3 Electrospinning 25

1.2.4 Lithographic techniques 29

1.2.5 Micro-contact printing and surface chemistry 34

1.2.6 Cell compartmentalisation via microfluidic devices 35

1.3. Thesis aims and objectives 37

Chapter 2. Materials and methods **39**

2.1 Fabrication of nano-fibre substrates 40

2.2 Fabrication of PDMS micro-groove substrates 41

2.3 Fabrication of two and five-port microfluidic devices 42

2.3.1 Fabrication of masters 42

2.3.2 Fabrication of PDMS devices 44

2.3.3 Preparing devices for cell culture 45

2.4 Fabrication of micro-contact printing substrates 45

2.5 Brain tissue dissection 46

2.5.1 Preparation for dissection 46

2.5.2 Dissection 47

2.5.3 Cell suspension preparation 48
2.6 Purifying astrocytes and co-culture with neurons....49
2.7 Microfluidic device cell loading....49
2.8 Micro-contact printing cell culture and immunocytochemistry....50
2.9 Microfluidics, nano- and micro-scale substrates immunocytochemistry 51
2.10 Digital imaging and quantification of nano-fibre and micro-groove substrates....52
2.11 Statistical analysis for neurite alignment (nano- and micro-scale substrates) 52
2.12 Whole-cell recording 53
2.12.1 Intracellular and extracellular (bath) solutions 53
2.12.2 Whole cell voltage clamping 53
2.13 Calcium imaging....55
2.13.1 Microfluidic inter-port leakage test: fluorescence intensity measurements....56
Chapter 3: Alignment of striatal neurites on nano- and micro-scale substrates....58
3.1 Introduction 59
3.2 Experimental methods 60
3.3 Results and discussion 60
3.3.1. Neurites' response to PLL and LN-coated substrates 60
3.3.2 Neurite behaviour on PLL and LN pre-coated micro-grooves 66
3.4 Conclusions....69
Chapter 4: Design and fabrication of a microfluidic neuronal device 71
4.1 Introduction 72
4.2 Experimental procedures 75
4.2.1 Design considerations 75
4.3 Results and discussion 77
4.3.1 Design of microfluidic devices 77
4.3.2 Microfluidic device fabrication 79
4.3.2.1 Photolithography....79
4.3.2.2 Soft lithography and device fabrication....84
4.3.2.3 Cell culture in microfluidic devices....86
Chapter 5: Fabrication of a complex, functional basal ganglia circuit – an *in vitro* model built using microfluidics 98
5.1 Introduction 99
5.2 Experimental procedures 100

5.2.1 Whole cell voltage clamp 101
5.2.2 Calcium imaging 101

5.3 Results and discussion 101
5.3.1 Electrophysiology of cortical and striatal neurons 101
5.3.2. Ca^{2+} imaging analysis 104
5.3.3 Upstream and downstream cells' response to TTX in the cortex port 105
a. Activity of cortical cells on coverslips 105
b. Activity of cortical cells before and after treatment with TTX 106
c. Activity of striatal cells before and after the treatment of cortical cells with TTX 107
d. Activity of SN cells before and after the treatment of cortical cells with TTX 109
e. Activity of GP cells before and after treatment of cortical cells with TTX 111
5.3.4 Upstream and downstream cells' response to TTX loaded into the striatum port. 112
a. Activity of striatal cells on coverslips, and device before and after treatment with TTX 113
b. Activity of cortical cells before and after the treatment of striatal cells with TTX 114
c. Activity of SN cells before and after the treatment of striatal cells with TTX 116
d. Activity of GP cells before and after the treatment of striatal cells with TTX 117
5.3.5 Upstream and downstream cells' response to TTX loaded into the GP port. 118
a. Activity of GP cells before and after treatment with TTX 118
b. Activity of striatal cells before and after the treatment of GP cells with TTX 119
c. Activity of cortical cells before and after the treatment of GP cells with TTX 120
d. Activity of SN cells before and after the treatment of GP cells with TTX 121

5.4 Electrophysiology techniques 122

5.5 Conclusion 124

Chapter 6. Patterning basal ganglia neurons - towards fabricating an *in vitro* complex micro-contact printed circuit 126

6.1 Introduction 127

6.2 Experimental procedures 128

6.3 Results and discussion 129
6.3.1 Micro-contact printing and substrate characterization 129
6.3.2 Cell culture on micro-contact printed substrates 133
3T3 cell culture 134
SH-SY5Y cell culture 136
Primary neuronal cultures 138
Micro-patterning issues with neuronal cultures 140

6.4 Conclusion 141

Chapter 7: General discussion 142

7.1 Fabrication of functional BG circuitry *in vitro*: from nano- and micro-scale topographies to microfluidic devices 143

7.2 Directed neurite orientation: first stage of BG circuitry fabrication 143

7.3 Design of the microfluidic device for BG circuitry fabrication 146

7.4 Electrophysiological recording of BG single cells 148

7.5 BG circuitry fabrication and Ca^{2+} imaging 149

7.5 Multi-electrode arrays (MEAs) 151

7.6 Microfluidic vs. micro-contact printed circuitry 152

7.7 Conclusions 153

Reference list 154

Appendix 180

1. Abbreviations 181

2. Manuscripts published, submitted or in preparation 185

List of tables and figures

Table 2.1 Summary of parameters used for photolithography 43

Table 4.1 Summary of benefits of using microfluidic devices versus conventional vessels for cell culture 72
Table 4.2 Optimisation of the soft baking process for both SU-8 10 and SU-8 50 photoresists 80
Table 4.3 Optimisation of the PEB process for both SU-8 10 and SU-8 50 photoresists 83
Table 4.4 Optimal baking and exposure parameters used for photolithography of master.....84

Table 5.1 Examples of neuron studies where sodium currents were eliminated by TTX.....104

Figure 1.1 Cross-section of brain showing the basal ganglia and related structures.....4
Figure 1.2 Photomontage of a medium spiny neuron 5
Figure 1.3 Topography of synaptic input onto a medium spiny neuron 6
Figure 1.4 Schematic of the basal ganglia circuit.....7
Figure 1.5 Early stages of HD and the basal ganglia indirect pathway.....9
Figure 1.6 Late stages of HD and the basal ganglia direct pathway.....9
Figure 1.7 Generation of an excitatory postsynaptic potential 12
Figure 1.8 Corpus callosum stimulating intensity and EPSP amplitude for pre- and post-symptomatic transgenic mice.....13
Figure 1. 9 Corpus callosum intensity and EPSP amplitude for WT control and transgenic mice ...14
Figure 1. 10 Schematic showing the patch clamp technique 16
Figure 1. 11 Schematic showing variations of the patch clamp technique.....17
Figure 1. 12 Multi or microelectrode arrays.....18
Figure 1. 13 Calcium homeostasis.....20
Figure 1. 14 Fura-2 dye binding to a free calcium ion.....22
Figure 1. 15 Chemical structures of Fluo-3 and Fluo-4 calcium indicators 22
Figure 1. 16 Photomicrograph of a growth cone at the tip of a ganglion cell axon 24
Figure 1. 17 Electrospinning set-up. 26
Figure 1. 18 Fabrication of the hydrogel-nano-fibre 3D scaffold 28
Figure 1. 19 Photolithography process 30
Figure 1. 20 Soft lithography process 31
Figure 1. 21 Glass coverslip patterned via photolithography 32
Figure 1. 22 Schematic showing process of microfluidic device fabrication 37

Figure 2.1 PLA electrospinning process 40
Figure 2.2 Fabrication of PDMS micro-groove constructs via soft lithography 41
Figure 2.3 Schematic of a two-port fabrication process.....42
Figure 2.4 Schematic of soft lithography following master fabrication 44
Figure 2.5 Dissection of E15/16 cortex, LGE and MGE tissue 47

Figure 2.6 Dissection of E12/13 VM tissue 48
Figure 2.7 Five-port microfluidic device cell loading 50
Figure 2.8 Schematic showing measurement of neurite angles against aligned topography 52
Figure 2.9 Micropipettes used for whole cell recordings 54
Figure 2.10 Analysis of calcium fluorescence intensities using ImageJ....56
Figure 2.11 Fluorescence intensity measurements for testing inter-port diffusion within devices ...56

Figure 3.1 Topographic cues presented to cells 61
Figure 3.2 Neuron response to non-coated nano-fibre substrates....61
Figure 3.3 Fluorescence images of response of neurons to PLL and LN coated grooves 62
Figure 3.4 Micrographs of neurite alignment on nano-fibres pre-coated with PLL and LN 62
Figure 3.5 Fluorescence micrograph indicating the response of neurons to different substrates....64
Figure 3.6 Astrocytes aligned on non-coated nano-fibres....65
Figure 3.7 Neuronal culture on PLL and LN-coated micro-grooves....68
Figure 3.8 Neurite alignment on grooves pre-coated with PLL and LN versus groove width 69

Figure 4.1 Microfluidic device and the basal ganglia circuit 75
Figure 4.2 Schematic showing fabrication of the five-port microfluidic device 76
Figure 4.3 AutoCAD designs for a two-port microfluidic device 77
Figure 4.4 AutoCAD designs for a five-port microfluidic device 78
Figure 4.5 Assessment of SU-8 10 features after the photolithography process....81
Figure 4.6 Assessment of SU-8 50 photolithography features....82
Figure 4.7 SEM photographs of SU-8 10 and SU-8 50 structures built on silicon surfaces....83
Figure 4.8 PDMS microfluidic device 85
Figure 4.9 FITC and TRITC intensity profiles for inter-port diffusion test in a microfluidic device....86
Figure 4.10 Immunocytochemistry of cortical and SN neurons....87
Figure 4.11 Immunocytochemistry of striatal and GP neurons 88
Figure 4.12 Photographs captured inside the cortical cell port of a microfluidic device 90
Figure 4.13 Cortical axons guidance through micro-grooves in a microfluidic device 91
Figure 4.14 Photographs of developing striatal cells in a microfluidic device 93
Figure 4.15 Striatal axons guidance through micro-grooves in a microfluidic device 93
Figure 4.16 Photographs of developing GP cells in a microfluidic device....94
Figure 4.17 Photographs of developing SN cells in a microfluidic device 95
Figure 4.18 Photographs of axonal extension and guidance through tapered micro-groooves....96

Figure 5.1 Schematic of basal ganglia circuitry developed in vitro 100
Figure 5.2 Depolarisation of a cortical neuron 103
Figure 5.3 Depolarisation of a striatal neuron 104
Figure 5.4 Schematics of calcium imaging set-up in microfluidic devices....105
Figure 5.5 Calcium oscillations of cortical cells....106
Figure 5.6 Calcium oscillations of cortical cells before and after TTX treatment 107

Figure 5.7 Calcium oscillations of striatal cells before and after TTX treatment of cortical cells....108
Figure 5.8 Calcium oscillations of upstream SN cells before and after TTX in cortical cells.....110
Figure 5.9 Calcium oscillations of GP cells before and after TTX treatment of cortical cells.....112
Figure 5.10 Calcium oscillations of striatal cells on coverslips.....113
Figure 5.11 Calcium oscillations of striatal cells before and after TTX treatment 114
Figure 5.12 Calcium oscillations of cortical cells before and after TTX treatment of striatal cells..115
Figure 5.13 Calcium oscillations of downstream SN cells before and after TTX in cortical cells ...116
Figure 5.14 Calcium oscillations of GP cells before and after TTX treatment of striatal cells.....117
Figure 5.15 Calcium oscillations of GP cells before and after TTX treatment.....119
Figure 5.16 Calcium oscillations of striatal cells before and after TTX treatment of GP cells.....120
Figure 5.17 Calcium oscillations of cortical cells before and after TTX treatment of GP cells 121
Figure 5.18 Calcium oscillations of upstream SN cells before and after TTX in GP cells.....122

Figure 6.1 Micro-contact printing PDMS stamp fabrication.....128
Figure 6.2 Photograph of a PDMS elastomeric stamp in a petri dish 129
Figure 6.3 SEM micrographs of the micro-groove pattern on a PDMS stamp 130
Figure 6.4 TRITC and FITC labelling of SAM patterns generated via micro-contact printing 131
Figure 6.5 Wettability test of micro-contact printed substrates 132
Figure 6.6 PDMS stamp feature aspect ratio 133
Figure 6.7 Schematic of cell plating on micro-contact printed substrata.....134
Figure 6.8 Brightfield photographs of 3T3 cells at 2 h after plating.....135
Figure 6.9 Brightfield photographs of 3T3 cells in culture 136
Figure 6.10 Photographs of SH-SY5Y cells 138
Figure 6.11 Primary cells' response to micro-contact printed substrata 140

Figure 7.1 Schematics of BG in vivo and in vitro circuitry 145
Figure 7.2 Basal ganglia cells in the microfluidic device and fabricated model 149
Figure 7.3 Experiment set-up for studying response of cells in devices after TTX treatment.....151

Acknowledgments

I thank Jehovah God for his love and leading me to Keele and allowing me to get to this stage of my life. I found my project challenging and exciting and this has been truly an amazing experience. I owe my deepest gratitude to my supervisors Dr. Rosemary Fricker and Dr. Paul Roach for the patience, knowledge, enthusiasm and support they showed towards the project. They believed in me from the start and I will always be grateful for that. I also thank my other supervisor Dr. Ying Yang for the knowledge and support she provided in all the work we did involving nano-fibres starting from my DTC mini-project. I would like to thank Dr. Michael Evans for assisting with the patch clamp technique and the patience and persistence he showed during our electrophysiology experiments. I also want to thank all my CTD in Regenerative Medicine people, particularly the CTD 3 2010 clique including Tina Dale and Chris Adams based here at Keele. Thanks again to Chris and Mike, Dr. Alinda Fernandes and Diana Maradze for their useful comments in some of my thesis chapters. I would also like to thank Dr. Rowan Orme who is now based in Cardiff, Drs Folashade Kuforiji and Dr. Rupert Wright for all their assistance around the lab; the feedback and advise they offered concerning my lab work during group meetings was valuable. I want offer my gratitude to Drs Alan Weightman, Deepak Kumar, Samantha Wilson and Ian Wimpenny for discussions and advice on work concerning nano-fibres. I thank Dr. Monte Gates for his feedback from my first year viva, Dr. Divya Chari for her feedback on my postgraduate symposium and Lisa Cartilage for sorting out my credits/modules, learning and personal plans among other things. I also thank Dr. Stuart Jenkins and Jacqueline Tickle (the occasional cup of coffee offered was much appreciated) for their assistance and advice concerning lab matters. I want express my sincere gratitude to Síle Griffin for her suggestions and feedback during our Huxley group meetings, for sorting out the lab including ordering lab materials as well as for the occasional chat about work and other stuff. I wish her the best in her PhD. Last but not least, I would like to thank my family and friends including those from JesusJam and Christian union at Keele, for their prayer and support. I am eternally grateful to my mum, Alice who raised us on her own; I hope to make her proud – *Makaita basa mhai*. I thank my little sister Vimbai and my brother Mutsa for their constant love and support in my work and life. God bless them.

Chapter 1. Introduction

Chapter 1. Introduction

Huntington's disease (HD) is an incurable disease characterized by impaired movement, dementia and ultimately death (Purdon *et al*. 1994; Cheng *et al.* 2011; Quarrell *et al*. 2013). It disrupts the synaptically connected basal ganglia (BG) circuitry, located at the base of the brain, mainly responsible for regulating movement (Bolam *et al*., 2000). This thesis covers fabrication of an *in vitro* model, which is made up of dissociated cultured neuronal circuitry; to facilitate discovery of the most effective therapy for HD. BG neural circuitry affected by HD is detailed within this chapter, giving an indication of the complexity involved and required cross communication or connectivity between multiple cell types. Engineered topographic structures enable control of axon orientation, a phenomenon called 'contact guidance' (Weiss 1945; Weiss 1947). Contact guidance of axons is a valuable tool for building *in vitro* neuronal circuitries since connectivity between various neuronal populations is established via axons. Techniques used to engineer topographic structures include: photolithography, soft lithography and electrospinning. In addition to anatomy of the BG, studies of how these techniques were used to fabricate topographic patterns as well as compartmentalised, microfluidic devices were carried out. A compartmentalised device provides an ideal platform for fabricating neuronal circuitry *in vitro* since different neuronal cell types can be cultured separately, i.e. in different compartments, whilst establishing connectivity via micro-channels between the compartments. Techniques used to study excitability of neurons as well as connectivity between different neuronal populations in culture include electrophysiology and calcium (Ca^{2+}) imaging. These techniques will also be discussed in this chapter.

1.1 Anatomy of the Basal ganglia (BG)

1.1.1 Components of the BG

The BG are a group of brain nuclei interconnected by synapses and located beneath the cerebral cortex in the forebrain. These nuclei have no direct communication with the spinal cord; an aspect dissimilar to other motor components of the brain. They transmit projections to the spinal cord via the thalamus and the cerebral cortex (Tarsy et al., 2003; Kandel *et al.*, 1991; Shepherd, 1998).

The term ganglia in this instance should not be confused with the *ganglia* referring to peripheral nervous system cell bodies. Nerve cell bodies located outside the central nervous system are within *ganglia*, whereas those located inside are within *nuclei*. The BG regulates movement and the degeneration of this part of the brain has been implicated in psychomotor diseases such as Huntington's and Parkinson's disease (HD and PD) (Celular 2000). Psychomotor diseases relate to motor function impairment associated with cognitive disorders. A substantial reduction in the volume of BG nuclei has been shown for HD patients in comparison to control groups of the same ages (de la Monte *et al.* 1988). The BG consist of five nuclei: caudate nucleus, putamen, internal and external globus pallidus (GPi and GPe), subthalamic nucleus (STN) and substantia nigra. Input to the BG is mainly projected into the largest nuclei composed of the caudate nucleus and putamen, collectively named the striatum or neostriatum. The GPi and the substantia nigra *pars reticulata* (SNr) possess similar cellular organization and form the main output nuclei of the BG. The other part of the substantia nigra, the *pars compacta* (SNc), provides dopamine (a neurotransmitter that is lost in patients with PD) to the basal ganglia. Dopamine provides either excitatory input i.e. to promote depolarization, or inhibitory input to cause hyperpolarization of target cells (Herrero *et al.*, 2002; Kandel *et al*., 1991; Shepherd, 1998).

The cerebral cortex transmits the main input to the BG. The neostriatum is the main recipient of the axonal cortical projections and these are regulated by a neurotransmitter with an excitatory effect on the striatal neurons, glutamate. Corticostriatal outputs are conveyed to the GP and SNr in a topographical manner such that they project from defined areas of the cerebral cortex to defined areas of the striatum and from here (striatum) to defined areas of the GP and SNr. The GPi and SNr nuclei convey output axonal projections from the BG to the thalamus. The thalamic projections from the BG influence the corticospinal and corticobulbar (connection between cerebral cortex and the medulla oblongata/brain stem) projections through excitation of the cerebral cortex (Kandel *et al*., 1991).

In humans the volume of the striatum is 12 times larger than that of the GPe, 20 times larger than that of the GPi and SNr, and 60 times larger than that of the STN, which suggests a convergence of tissue size from the striatum to the STN (Figure 1.1) (Yelnik, 2002). Approximately 50% of the

111 million neurons in the human striatum send projects directly to the GPe which comprises of around 540,000 neurons. This also suggests a significant tissue convergence of ratio, 200:1 neurons, from the striatum to the GPe; this is even more for the GPi and SNr nuclei that contain fewer neurons. (Shepherd, 1998).

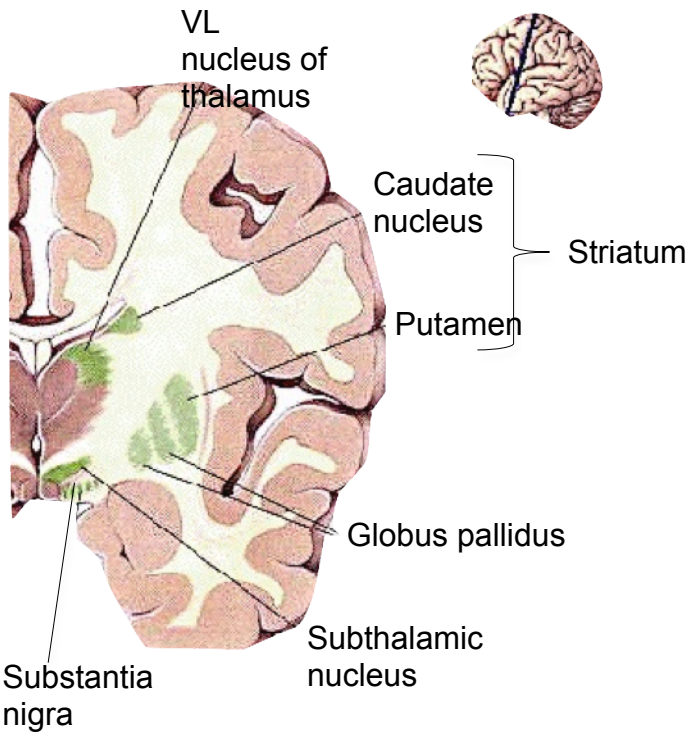

Figure 1.1: Cross-section through one hemisphere of the adult human brain showing the basal ganglia and related structures. VL nucleus = ventral lateral nucleus (Bear *et al.*, 2007).

1.1.2 The BG pathways and neurotransmitters

The medium spiny neurons (MSNs) constitute the majority of neurons in the striatum, ranging from approximately 77% in primates to 95% in cats and rodents (Shepherd, 1998). The diameters of MSNs' cell bodies range from 12-20 μm, with dendritic trunks ranging from 2-3 μm (Figure 1.2). Typically, dendritic trunks below the 10-30 μm radius of the MSN soma have no spines; the spines rapidly increase afterwards in the dendritic region up to approximately 80 μm from the soma. The dendritic branches (25-30 μm) spherically extend to a diameter ranging from 300-500 μm. The average number of spines per dendritic branch is 4-6 per μm, which makes the MSN one of the most spine-laden neurons in the brain. The main axon of the MSN branches within tens of μm from the soma to form a dense and homogeneous local collateral arborization. MSNs were recognized

as projection neurons in the 1970s, after intracellular horseradish peroxide (HRP) staining *in vivo* revealed that the axon branches were more defined that originally thought (from Golgi studies i.e. concerning silver staining of nervous tissue). Since then, further studies have shown that MSNs' arborizations in the striatum extend both externally (to other BG nuclei) and internally (to interneurons and other MSNs) (Tepper *et al.*, 2005; Shepherd, 1998; Yelnik, 2002).

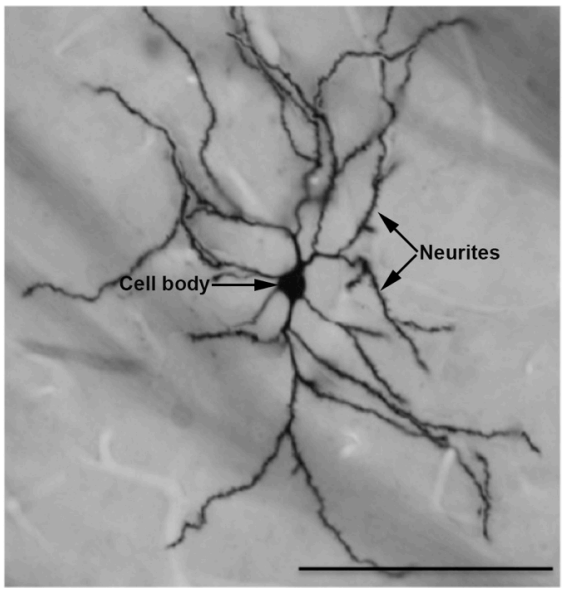

Figure 1.2: Juxtacellulary stained photomontage of a medium spiny neuron (MSN) with neurites protruding from cell body. Scale bar = 100 μm (Kita & Kita 2011).

The striatum consists of other cell types in addition to MSNs: cholinergic interneurons, gamma-aminobutyric acid (GABA)/Parvalbumin-containing interneurons and somatostatin/nitric-oxide-synthase (SOM/NOS)-containing interneurons. Cholinergic interneurons are the largest interneurons in the striatum, and make up less than 2% of the total cell population. They are usually identified by elongated soma of length 50-60 μm and diameter of 15-25 μm. Connection of cholinergic interneurons to the MSN is usually established via the dendritic shaft (Figure 1.3). The interneurons' dendrites develop from the soma, forming radial-like branching at 500-750 μm from the cell body. The interneuron's axons are initially myelinated, but their diameter decreases during the branch bifurcation process that consequently results in their non-myelination. The branch bifurcation process typically produces daughter branches of similar sizes and at 120° angle with each other covering a radius of approximately 1 mm from the soma (Shepherd, 1998; Tepper *et al*., 2010).

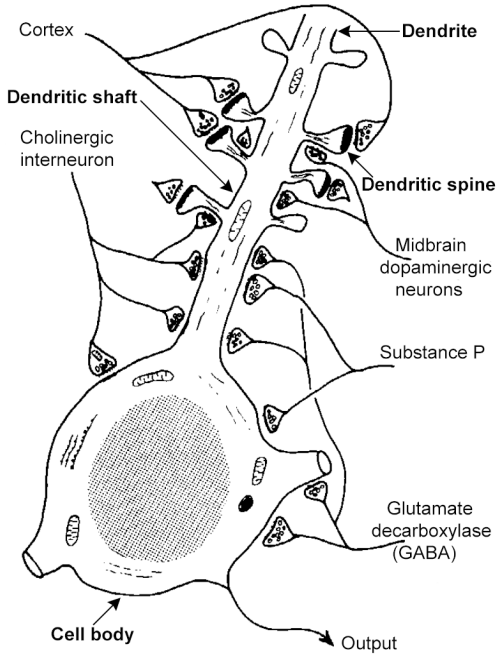

Figure 1.3: Topography of synaptic input onto a medium spiny neuron (MSN). Synaptic input from external sources such as the cortex terminate on dendritic spines. Input from local neurons (including other MSNs) containing GABA, dopamine and substance P terminate on the cell body and dendritic shaft. Input from the cholinergic interneuron terminate on dendritic spines and shaft as well as on the cell body (Smith and Bolam, 1990).

The parvalbumin-containing (PV) interneurons were first described in the 80s and 90s as striatal interneurons possessing powerful GABA intake and also immunoreactive to GAD (GABA amino-decarboxylase, a GABA synthesizing protein) (Kawaguchi, 1993). They comprise 3-5% of the total neurons in the striatum. PV interneurons are mostly medium sized and possess a mixture of smooth and varicose (swollen or enlarged) dendrites radiating from within tens of microns of the soma. They form basket-like fields extending 200-300 μm in diameter around the soma. The nature of their dendritic branching and firing pattern is somewhat similar to GABA/PV-containing interneurons found in the cortex and hippocampus. Axons extending from interneurons form highly dense arborizations, also spherical in nature; the PV interneuron possesses one of the densest axonal arborizations in the striatum. Input from the cortex to the PV interneuron form multiple synaptic contacts, which explains why it is more responsive than MSNs to cortical inputs. Somatostatin/Nitric-oxide-synthase (SOM/NOS)-containing interneurons form 1-2% of the total striatal cells. These interneurons are the second largest group of interneurons, after the cholinergic interneurons. The diameter of their soma ranges from 9-25 μm. SOM/NOS

interneurons possess the least dense arborizations in the striatum (Chang and Kita, 1992; Kawaguchi, 1993; Shepherd, 1998).

MSNs send synaptic projections into either the *direct* and *indirect* pathway. These pathways are mainly regulated by GABA, which has an inhibitory effect on target neurons. The *direct* pathway is also mediated by the neuropeptides dynorphin (DYN) and substance P (SP) released from MSNs, as well as dopamine input from the SNc, controlled via type-1 dopamine (D1) receptors expressed on their dendritic spines. MSNs projecting to the *indirect* pathway (Figure 1.4 A) express enkephalin (ENK) and type-2 dopamine (D2) receptors (Bolam *et al.* 2000).

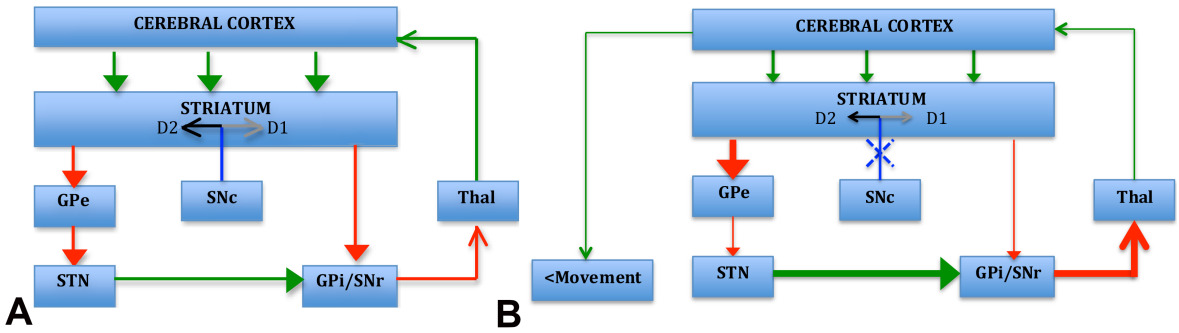

Figure 1.4: Schematic of the BG circuit. A: *Direct* and *indirect* pathways of the BG. **Green** = excitatory glutamatergic axonal projections. B: Changes to the BG pathways due to degeneration of the dopaminergic SNc neurons in PD. Loss of dopaminergic projections affects both sets of MSNs resulting in excessive inhibition of the thalamus, and consequently movement. **Red** = inhibitory GABAergic axonal projections. **Blue** = dopaminergic axonal projections to the striatum. **Black** = inhibitory dopaminergic projections to the *indirect* pathway of the basal ganglia. **Grey** = excitatory dopaminergic projections to the *direct* pathway of the basal ganglia. Line thickness indicates level of neuronal activity/firing; modified from (Albin *et al.* 1989).

MSNs in the striatum are inactive under resting conditions; they are activated when they receive projections from glutamatergic axons, mainly from the cerebral cortex. The *direct* pathway encourages movement. MSNs mediated by GABA, DYN and SP will inhibit the output neurons when they are stimulated by the projections from the cortex. This causes the GABAergic output neurons in the SNr/GPi to fire less, disinhibiting (neurons impeding the inhibitory activity of other neurons resulting in excitation) the thalamic neurons resulting in the increased activity of the motor cortical neurons receiving thalamic input. This leads to voluntary movement. When stimulated, the *indirect* pathway MSNs with their inhibitory projections will inhibit GPe neurons. This will lower the activity of the inhibitory GPe neurons, resulting in phasic disinhibition of STN neurons. STN neurons are glutamatergic, therefore disinhibition of the STN neurons allows them to fire at an

increased rate, which means they will trigger increased inhibitory output from the GABAergic neurons found in the GPi/SNr. This leads to increased inhibition of thalamic neurons, resulting in a decrease in the excitation of the motor cortical neurons, and consequently impaired movement (Kandel *et al.*, 1991; Bolam *et al*., 2000; Garcia-Munoz *et al*., 2010; Wilson, 2007).

Dopaminergic neurons transmit excitatory and inhibitory projections to the striatum via activation of D1 and D2 receptors, respectively. MSNs receiving dopaminergic afferents either project inhibitory impulses via the striatonigral and striato-GPi route (direct pathway) initiating movement or via the striato-GPe route (indirect pathway) inhibiting movement (Albin *et al.* 1989). Loss of dopaminergic neurons in the SNc nuclei (typical of PD) affects both pathways. For the *direct* pathway, dopamine released from the SNc neurons binds to D1 (type-1) receptors resulting in depolarization and subsequently enhanced activity of the MSNs. When dopaminergic neurons are lost, the *direct* pathway MSNs become less active. This means the GABAergic output neurons are less inhibitory, and this allows GPi/SNr neurons to be more active, causing excessive inhibition of the thalamus.

Dopamine binds to D2 receptors on the *indirect* pathway MSNs. This leads to hyperpolarization and reduced activity of these inhibitory MSNs. For this pathway, degeneration of the SNc nuclei results in increased activity of inhibitory MSNs, thus excessive inhibition of the GPe neurons, less inhibition of the STN neurons and excessive excitation of the output neurons, again causing excessive inhibition of the thalamus. In both instances, the excessive inhibition of the thalamus results in reduced excitation on cortical neurons and lessened movement (Figure 1.4 B) (Albin *et al*., 1989; Kandel *et al.*, 1991).

SOM/NOS/NPY and cholinergic interneurons are less affected in comparison to MSNs in the striatum. In the early stages of HD, which affects the *indirect* pathway of the BG circuit, MSNs are depleted. This means the GPe neurons are less inhibited resulting in excessive inhibition of the STN neurons. The STN neurons have a reduced excitatory effect on the output nuclei, leading to less inhibition of the thalamus nuclei and consequently excessive excitation of the cortical neurons and enhanced movement (chorea) (Reiner *et al.*, 1988) (Figure 1.5).

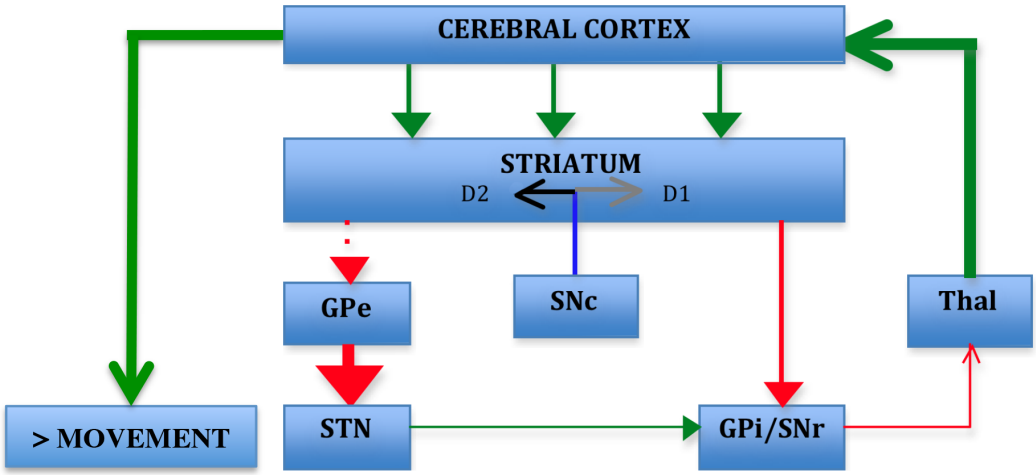

Figure 1.5: The early stages of HD affect the *indirect* pathway of the BG. **Green** = excitatory glutamatergic axonal projections. **Red** = inhibitory GABAergic axonal projections. **Blue** = Dopaminergic axonal projections to the striatum. **Black** = inhibitory dopaminergic projections to the *indirect* pathway of the basal ganglia. **Grey** = excitatory dopaminergic projections to the *direct* pathway of the basal ganglia. Line thickness indicates level of neuronal activity/firing (modified from Albin *et al*., 1989).

By late stages of HD, all MSNs are extensively lost resulting in complete inhibition of movement (akinesia) (Albin *et al*., 1992) (Figure 1.6) Loss of (*direct* pathway) MSN axonal projections to the output nuclei result in excessive inhibition of the Thal neurons. The motor cortical neurons are less excited resulting in less movement.

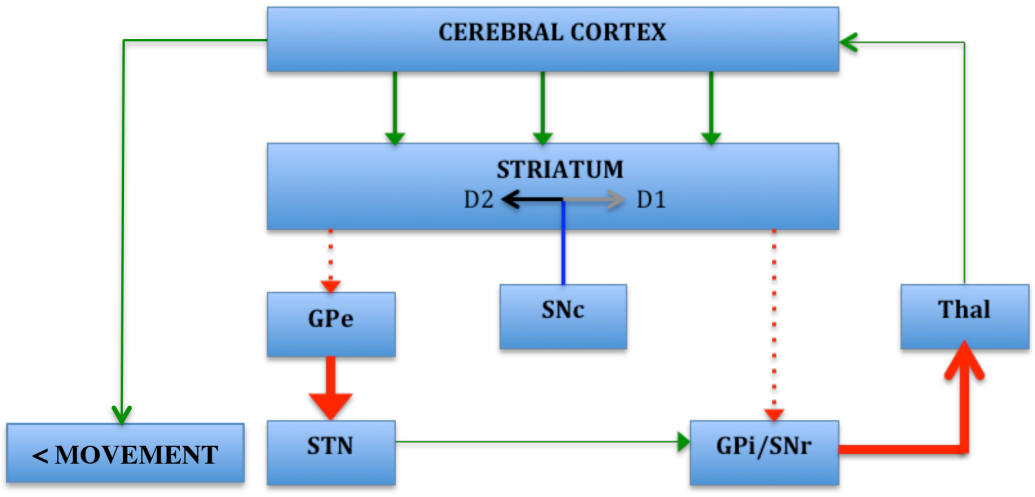

Figure 1.6: The late stages of HD affect the *direct* pathway of the BG. At later stages both populations of MSNs are depleted resulting in inhibition of movement. This effect is similar to when the SNc neurons are lost, i.e. in Parkinson's disease. **Green** = excitatory glutamatergic axonal projections. **Red** = inhibitory GABAergic axonal projections. **Blue** = dopaminergic axonal projections to the striatum. **Black** = inhibitory dopaminergic projections to the *indirect* pathway of the basal ganglia. **Grey** = excitatory dopaminergic projections to the *direct* pathway of the basal ganglia. Line thickness indicates level of neuronal activity/firing (modified from Albin *et al*., 1989).

Planert and colleagues studied the effect of dopamine applied to rat and mouse tissue slices on striatonigral and striato-GPi as well as striato-GPe MSNs (Planert *et al*. 2013). Retrograde labelling was used to distinguish direct pathway (striatonigral/striato-GPi) from indirect pathway neurons in rat slices. Transgenic mice expressing enhanced green fluorescent protein (EGFP) were used for mouse slices; EGFP is expressed by direct pathway D1 MSNs. D1 is a receptor associated with striatonigral direct pathway. Patch clamp was used for recording membrane excitability for the two MSN populations. The group found that D1 direct pathway MSNs were more excitable compared to D2 indirect pathway MSNs.

1.1.3 Existing HD models: *in vivo* models

Animal models such as rats and mice have been used to study the pathogenesis of HD in an effort to find the most effective therapies for the disease (Ramaswamy *et al.* 2007). These models can be classified into 2 categories: chemical and genetic models (Zuccato *et al.* 2010). Chemical models were the first type of HD models to be used before the mutant gene causing HD was discovered in 1993. Neurotoxins such as quinolinic acid (QA) and 3-nitro-propionic acid (3-NP) injected into the striatum are used to mimic the degeneration process of MSNs that occurs in HD. For instance, following QA injection, GABA and substance P expressing striatal neurons were selectively lost in the striatum (also in the midbrain) compared to other cell types such as somatostatin and neuropeptide Y expressing neurons (Beal *et al.* 1991).

Genetic animal models can be classified into either transgenic or knock-in models (Ramaswamy *et al.* 2007). In transgenic models, foreign DNA is introduced artificially into every cell of the host animal. The DNA is introduced at an early stage of embryonic development and modifies the function of the animal by expressing a new protein or up-regulating existing proteins (Strachan & Read 1999). Transgenic mouse models were established in 1996 and the first HD models were R6/1 and R6/2. These models express mutant exon 1 (out of the total 67 exons of the entire gene) of the *human huntingtin gene* (Li *et al.* 2005). An exon is a coding sequence found in a gene and is involved in protein synthesis. The transgene promoter is a sequence that controls the location and activation of the transgene (Strachan & Read 1999). The promoter commonly used for

R6 transgenic models is the human huntingtin (Li *et al.* 2005; Mang & Li 2005). R6/1 and R6/2 models have cytosine-adenine-guanine (CAG) length of ~ 115 and ~150 repeats and express 31% and 75% of the endogenous huntingtin protein, respectively (Mangiarini *et al*. 1996; Li *et al*. 2005). The *huntingtin gene (Htt)* consists of a sequence of the CAG trinucleotide. This CAG sequence genetically encodes for the glutamine amino acid. HD occurs when the CAG number expands and exceeds 36 repeats. This expansion results in an excessive number of glutamines in the *Htt* protein. Longer CAG extension correlates with severity and earlier onset of the disease (Bhidayasiri & Truong, 2004; Ma *et al.*, 2011; Purdon *et al.*, 1994).

Knock-in mouse models were designed to achieve better efficiency and efficacy compared to transgenic mouse models. These models allow replacement of a *normal Htt mouse gene* with single *mutant human gene* within the mouse genome. This ensures that the mouse model will only have a single mutant gene as well as a single normal gene. A knock-in mouse model also provides a more controllable transgenic setting compared to transgenic models. In transgenic models the mutant gene is randomly placed inside the mouse genome, which may disrupt functioning of other genes; however, in knock-in models the mutant gene is placed in a specific part of the genome (Menalled 2005; Ramaswamy *et al*. 2007). Examples of mouse knock-in models include CAG140 (Thomas *et al.* 2013) and CAG150 (Proenca *et al.* 2013).

Depletion of dopamine neurons affects functionality of the basal ganglia circuitry and is implicated in psychomotor impairments in PD (Samii *et al.* 2004). For instance, Kita & Kita found that loss of dopaminergic projections to indirect pathway MSNs resulted in abnormal, ‘pause and burst’ firing patterns in neurons of the succeeding BG nuclei, the GPe (Kita & Kita 2011). 6hydroxydopamine (6-OHDA) is an organic compound that was used in the study to damage dopamine neurons. Juxtacellular labelling, a labelling technique coupled with electrophysiology normally used to track single neurons *in vivo* (Pinault 2011), was used to track projections from the striatum into the GPe. This confirmed that striatum neurons established connectivity with GPe neurons. Electrical activity of 6hydroxydopamine (6-OHDA) treated and non-treated rats was recorded via microelectrodes.

The striatum receives most of its projections from the cerebral cortex (see chapter 1.1.2). Understanding how these projections are functionally integrated in the striatum and how subsequent projections are sent to the output nuclei of the BG is essential (Wilson & Groves 1981). MSNs (projection neurons forming the majority of cells in the striatum *in vivo*) switch between 2 sub-threshold membrane potential conditions, *down* and *up* states. The *down* state is a period in which the MSN is inactive. The *up* state is a more depolarized level; the MSN is active (Wilson & Kawaguchi 1996; Plenz & Kitai 1998; Plotkin *et al.* 2011; Pava *et al*. 2014). When cortical or thalamic neurons are stimulated, a signal is generated from their dendrites via axons before transmission to the target population. Generated action potentials are transmitted down the axons of the neurons to the axon boutons to establish communication with the MSNs through receptors (Wilson 2010).

MSNs are usually in a *down* state mode or inactive pending membrane depolarization from glutamatergic input (Wilson & Kawaguchi 1996; Cepeda *et al.* 2007). Stimulating cortical or thalamic tissue in intact animals releases glutamatergic neurotransmitters at the dendrites, resulting in generation of excitatory postsynaptic potentials (EPSPs) in MSNs (Shepherd, 1998). EPSPs are sub-threshold membrane potentials, short-lived and have a graded response, i.e. they need to be combined to increase the probability of a neuron to fire or generate an action potential. In general, three features measured in mV (millivolts) help define an EPSP for a neuron: reversal potential, action potential threshold and resting potential (Figure 1.7).

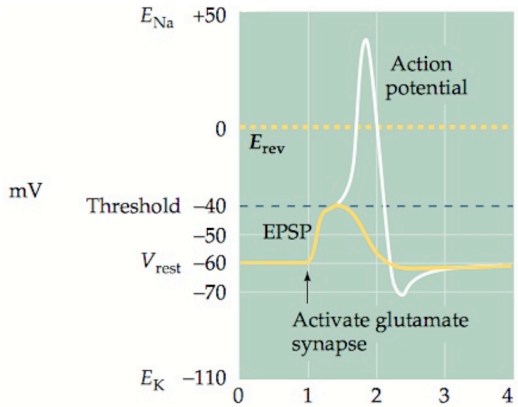

Figure 1.7: Generation of an EPSP. An EPSP is generated by activation of a glutamate synapse and consequently, glutamate receptors on the postsynaptic membrane. For a MSN, a strong enough excitation input or stimulation from the cerebral cortex or thalamus is required to generate EPSPs capable of producing an action potential (white trace). The bold yellow trace shows the EPSP from when it's activated to when it falls back to V_{rest}. V_{rest} = resting voltage, E_{Na} = sodium (Na^+)-generated potential, E_K = potassium-generated potential, E_{rev} (dotted yellow line) = reversal potential (Purves *et al.* 2004b).

Inhibitory postsynaptic potentials (IPSPs) act to reduce probability of a postsynaptic neuron firing. For instance, a neuron innervated by two EPSPs may be capable of generating an action potential but an addition of an IPSP may result in a less 'graded response' and therefore no firing (Purves *et al.* 2004b). Huntington's Disease causes electrophysiological alterations such as changes in EPSPs, which affects the way electrical signals are integrated and relayed out of the BG (Shepherd, 1998). Klapstein *et al.* studied the differences in synaptic activity of HD symptomatic and non-symptomatic mouse models (Klapstein *et al.* 2001). Synaptic responses were recorded in slice cultures of a presymptomatic and symptomatic HD mouse model expressing ~150 CAG repeats (R6/2 transgenic mouse). Wild-type (WT) mice of matching ages were used as control. MSNs were excited from *down* state by cortical afferents produced after the corpus callosum (a band of nerve fibres separating the cerebrum into two hemispheres) was stimulated. Increasing the stimulation intensity led to an increase in EPSP amplitude. Symptomatic R6/2 mice required a lot more stimulation in comparison to their WT counterparts to induce similar EPSPs (Figure 1.8).

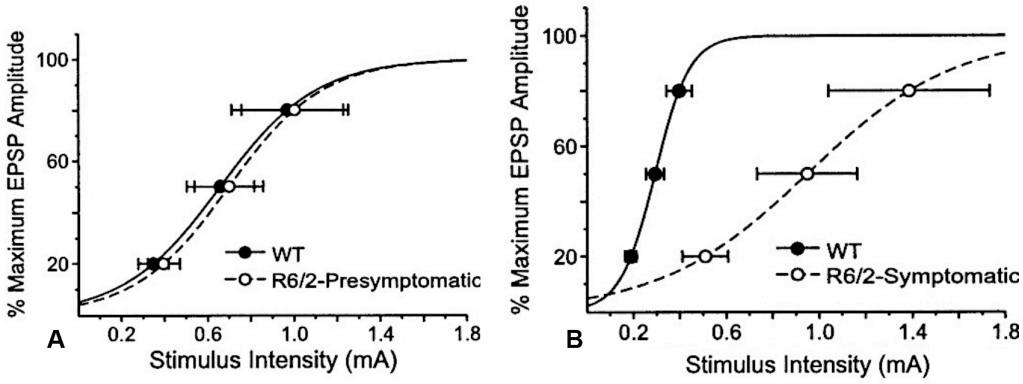

Figure 1.8: Corpus callosum stimulating intensity and EPSP amplitude for pre-symptomatic and symptomatic R6/2 transgenic mice compared with WT (wild-type) mice, control. More stimulus intensity is required for symptomatic transgenics, B in comparison to pre-symptomatic transgenics, A (Klapstein *et al.* 2001).

A number of studies have reported reduction in EPSP frequency in symptomatic HD models; for instance, a transgenic R6/2 mouse model exhibited EPSPs with significantly less frequency compared to WT controls at 11-15 weeks (André *et al.* 2006). Laforet *et al.* developed a transgenic mice model to study HD (Laforet *et al*. 2001). Slices from heterozygote transgenic mice, expressing a large N-terminal part of the human huntingtin with 100 CAG repeats, were cultured *in vitro*. The

subcortical white matter corpus callosum was stimulated to produce an EPSP response in the striatum (Figure 1.9). More intensity was required to stimulate HD transgenic MSNs compared to wild-type (WT) MSNs used as control. Even more current was required to produce a response by the MSNs, (Figure 1.9 B.).

Striatal neurite afferents and efferents *in vivo* are usually difficult to analyze on a single cell level; identifying a neuron-neuron connection can be challenging (Randall et al. 2011). *In vitro* dissociated cell culture platforms, on the other hand, enable a more detailed analysis of easily identifiable and controllable neuronal connections (Potter 2001). Randall *et al.* prepared a co-culture of dissociated cortical and striatal neurons to study synaptic connectivity between the neurons (Randall *et al.* 2011). Cortical neurons were obtained from a transgenic mouse expressing green fluorescent protein (GFP) to distinguish them from striatal neurons (non-labelled from wild-type mouse). Neurons established multiple striatocortical and corticostriatal synaptic connections recorded using a dual whole cell patch clamp technique.

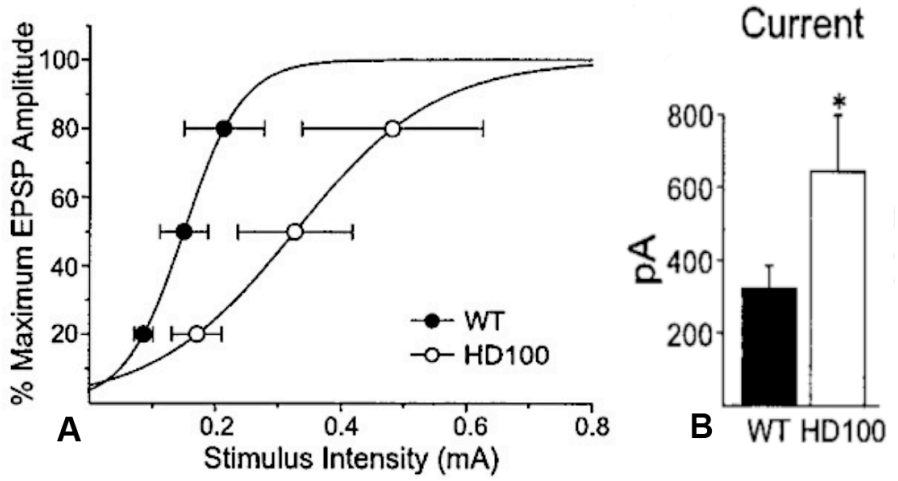

Figure 1.9: A. Corpus callosum stimulating intensity and EPSP amplitude for wild-type (WT) control and transgenic HD 100 mice. More stimulus intensity is required for symptomatic transgenics. B. Significant amounts of current input were required for HD 100 mice in comparison to WT mice. (* $p < 0.05$), pA = picoamperes (unit of electric current) (Laforet *et al.* 2001).

1.1.4 Neuronal circuitry formation: *in vitro* models

In vivo models discussed above can be limited, i.e. neurons form very complex 3D networks making it very challenging to study neuronal interaction and dynamics. Furthermore, *in vivo* circuits

involve very extensive and complex connections, which makes it challenging to manipulate and model diseases and therapies. An *in vitro* model can provide a less complex and more controllable milieu; individual neurons can be cultured in a monolayer, easily tracked, stimulated and manipulated over time with great precision. There are many fewer neurons to analyse and this makes it easy to assess the role and contribution of individual neurons within the neuronal network (Potter 2001; James *et al.* 2004). *In vitro* models, dissociated cells cultured in a dish, can be used as a tool for understanding mechanisms causing neuronal death in the striatum and for screening potential HD drugs. Various brain tissues can be dissected out and mechanically and/or enzymatically dissociated to produce primary neurons (Potter 2001). Neurons can be cultured into networks *in vitro* and subsequently used as cellular models for neurotoxicity testing or for testing potential therapies.

Analysing the electrical activity of the network is an important part of this model since it provides an insight into the function of the neural network. Neurons in networks communicate via electrical impulses or action potentials. Electrophysiology techniques that can be used to study single-cell excitability include patch clamp. The technique permit studying changes in current through plasma membrane; recordings are obtained via probing single cells, one at a time. However, simultaneously monitoring activity of large populations of cells requires other techniques such as multi-electrode arrays (MEAs) or Ca^{2+} imaging (Giugliano & Martinoia 2006; Sarkisov & Wang 2007). Both techniques are discussed after the electrophysiology: patch clamp section.

Electrophysiology: patch clamp

Changes in plasma membrane current of excitable cells, such as neurons, can be studied using an electrophysiology technique called patch clamp. The technique, developed from voltage clamp by Neher and Sakmann, allows study of electrical current across the cell membrane (Neher & Sakmann 1976). The electrical current is generated by the influx and efflux of ions through the membrane. A major development in this technique compared to previous ones was the increase in temporal resolution; it enabled the study of single cellular membrane channels (Neher & Sakmann 1976; Wood *et al.* 2004; Farre *et al.* 2008; Schramm *et al.* 2014). A glass

micropipette, with a tip of diameter from 1-2 μm, is drawn-out using an electrode puller. The end of the tip is polished using a heater filament, then waxed or coated with Sylgard to reduce, chances of recording solution leakage whilst recording occurs and noise (Levis & Rae 2002; Zhao *et al.* 2010). The micropipette is filled with an electrolyte saline (electrically conductive solution) and then placed onto a headstage, a component that holds the micropipette, with a silver/silver chloride wire designed to transport electrical signal to an amplifier (Molleman 2003). The micropipette is placed in contact with the cell membrane (Figure 1.10) and suction is applied to form a seal between the two. A high resistance seal, a 'gigaseal', ranging between 10^{9}-$10^{10}\Omega$ (Ohm, unit of electrical resistance), improves quality of recordings and minimises noise (Hamill *et al.* 1981).

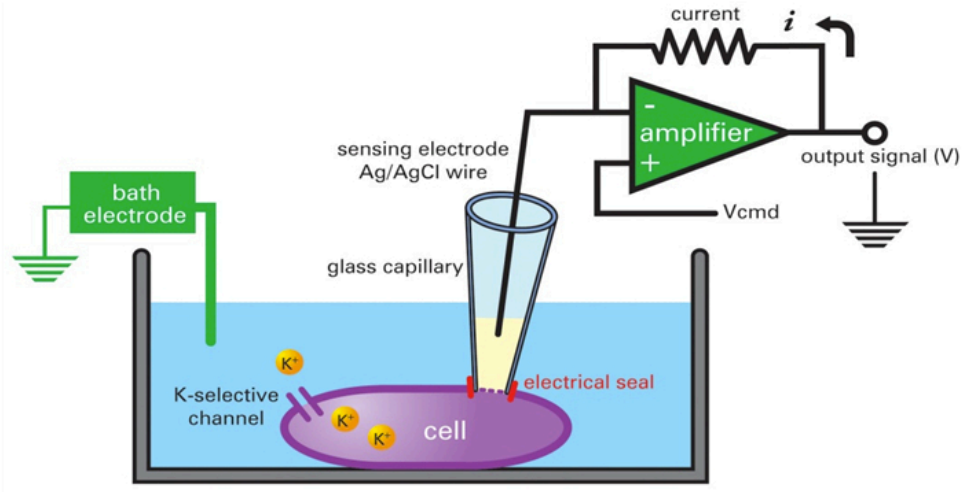

Figure 1.10: Schematic showing the patch clamp technique. Recordings are obtained from ion channels such as potassium (K-selective channels) via glass micropipettes connected to an amplifier that processes output signal. The electrical seal provides electrical continuity between inside of the cell and the micropipette. Vcmd = command voltage applied in constant steps to provoke ionic current (*i*) changes through cell membrane. Ag = silver, AgCl = silver chloride (Clare 2010).

Micropipettes are used to electrically isolate part of a cell membrane and record changes in ionic current (Neher *et al.* 1978; Ogden & Stanfield 1994). This method of recording is called cell-attached patch clamp (Figure 1.11 A). Recordings are generated from part of an intact membrane. Another method of patch clamp involves pulling part of a cell membrane using a micropipette. Inside-out patch clamp involves obtaining recordings from a completely detached cell membrane patch in which the intracellular surface is exposed to the extracellular bath solution (Figure 1.11 B). In whole-cell patch clamp, more suction is applied to the pipette attached to the

membrane until the patch breaks exposing the intracellular milieu to pipette solution (Figure 1.11 C). When this occurs, the pipette and intracellular ionic compositions become continuous, i.e. the whole intracellular microenvironment is immersed in pipette solution. In outside-out patch clamp, the intracellular surface of the patch isolated from the membrane by suction is exposed to the extracellular solution held by the pipette (Figure 1.11 D).

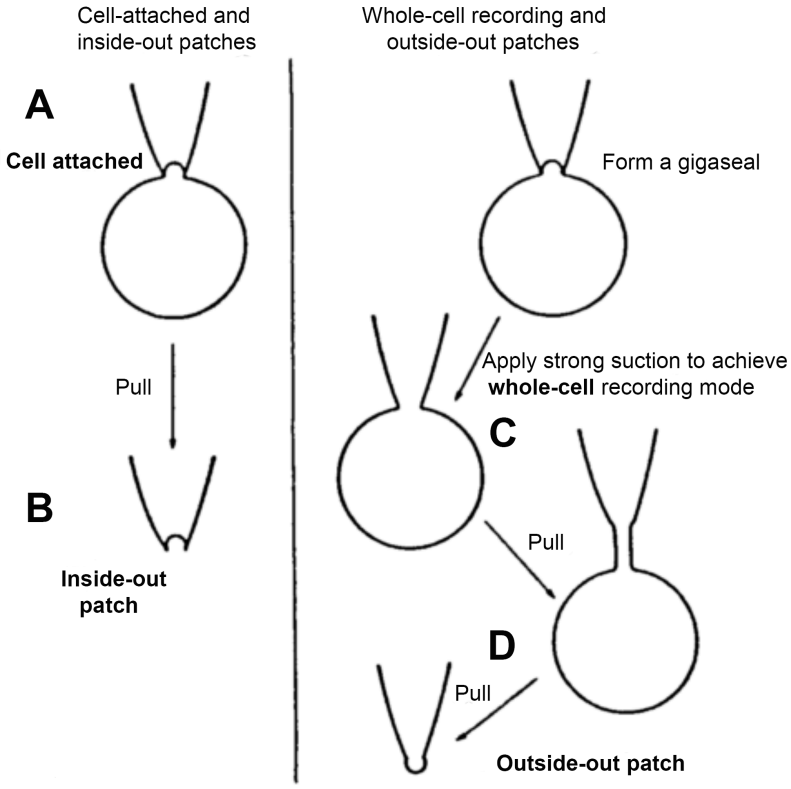

Figure 1.11: Schematic showing variations of the patch clamp technique. A: In the cell-attached method recordings are obtained without rupturing the cell membrane. B: The inside-out method involves isolating a patch of the cell membrane to expose the intracellular surface to the extracellular bath solution. C: In the whole-cell recording method, suction is applied to rupture the membrane and the intracellular environment is exposed to the solution held in the micropipette. D: The outside-out method is formed when the membrane ruptured via the whole-cell method is resealed (Ogden & Stanfield 1994).

Ionic current recordings are transferred via a conductive silver/silver chloride wire to an amplifier. Small analogue signals from the cell are amplified and transported to an analogue-to-digital (A-D) converter. Digital output is displayed on the computer. The process of signal transmission from the silver chloride wire to the output monitor applies to all forms of recording mentioned above: cell-attached, inside-out, outside-out and whole-cell patch clamp (Sontheimer & Ransom 1995; Weerakoon *et al.* 2009; Gandini *et al*. 2014).

Multi-electrode arrays (MEAs)

One of the main drawbacks associated with patch clamp is the difficulty to simultaneously monitor electrical activity of a collection of neurons (Potter, 2001). Even though it is essential to investigate electrical behaviour on an individual basis, at times there is need to monitor electrical activity at multi-cellular network level (multiple cells in multiple locations). Methods available to stimulate and measure neuron populations include multi-electrode arrays (MEAs; Figure 1.12). MEAs usually comprise 10s of electrodes of 10-30 microns in diameter. The MEA wire circuitry is normally made of gold or indium-tin oxide (ITO) and consists of electrodes usually coated with a material such as platinum black or carbon nanotubes. Electrodes are embedded within the substrates on which electrically active cells are cultured. The ionic flux across cell membranes result in spikes of extracellular change in voltage, which are detected by electrodes (Egert & Meyer 2005). This method allows for non-invasive and long-term recordings of electrical activity within a large neuronal network (Potter 2001; James *et al.* 2004). In addition to studying dissociated cells' activity, MEAs have been used to study the electrical activity within tissue slices e.g. hippocampal tissue (Novak & Wheeler 1988).

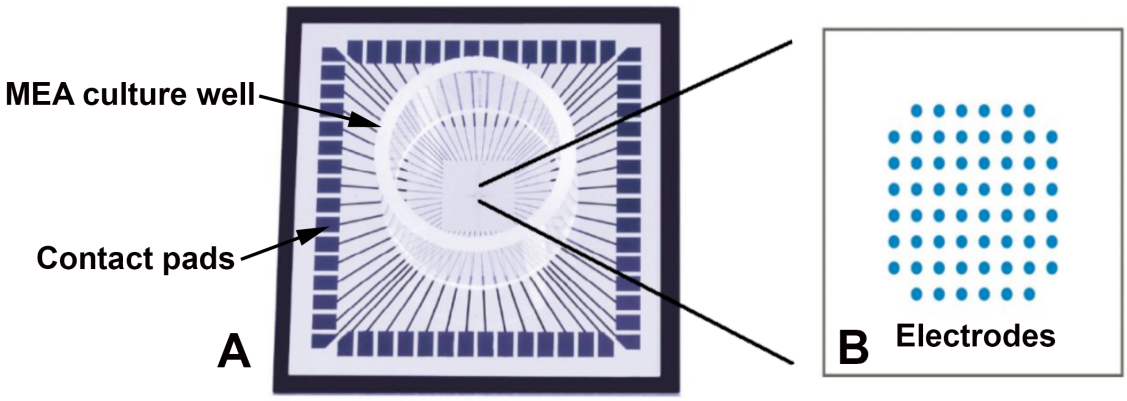

Figure 1.12: Multi or microelectrode arrays (MEAs). A: Excitable cells are cultured at the bottom of the MEA culture well; cell electrical activity is recorded and transmitted via contact pads to a computer interface. B: A close-up of electrodes located in the middle of the well (Savarraj & Chiu 2014).

Calcium imaging

Another method that can be used to simultaneously monitor electrical activity of a global neuron population is Ca^{2+} imaging. Generation of action potentials within a large population of neurons can measured indirectly by tracking the Ca^{2+} dynamics across cell membranes (Yuste *et al.* 2011). Ca^{2+}

imaging provides another means of analysing electrical activity of electrogenic cells. Ca^{2+}, a ubiquitous second messenger, plays an important role in a number of cellular signalling/physiological processes (Despa *et al.* 2014; P. Li *et al.* 2014; Ferrante *et al.* 2013; Berridge *et al*. 2000). It is involved, for instance, in the regulation of gene transcription, adenosine triphosphate (ATP) production, apoptosis and synaptic transmission (Chen *et al.* 2014; B. Li *et al*. 2014). A key point to note is that only free intracellular Ca^{2+}ions are biologically active and therefore involved in cellular signalling (Grienberger & Konnerth 2012). When inactive, most neurons contain an endogenous free Ca^{2+} concentration ranging from 100-200nM; exogenous concentration is usually around 1mM (Heizmann 1993; Rizzuto & Pozzan 2006). Ca^{2+} ion concentration rises 10 to 100 times more when neurons become active (Berridge *et al*. 2000).

The Ca^{2+} homeostasis is important in neurons since unbalanced free cytosolic Ca^{2+} ions can be toxic to cells (Clapham 2007; Stanika *et al*. 2012). Efflux of Ca^{2+} ions is achieved via 3 means: [1] Extruding excess Ca^{2+} ions from the intracellular environment; [2] Compartmentalizing Ca^{2+} ions into internal stores and [3] Chelating Ca^{2+} ions to intracellular proteins called buffers and sensors (Berridge *et al.* 2003; Clapham 2007). First, plasma membrane Ca^{2+} ATPase (PMCA) pumps are used to extrude Ca^{2+} from cytosolic to extracellular milieu. In addition to that, Na^{2+}/Ca^{2+} exchangers are used to reduce the number of free cytosolic Ca^{2+} via swapping, through the plasma membrane, 1 Ca^{2+} ion for 3 Na^{+} ions (Na^{+}- Ca^{2+} exchange or NCX) or 1 potassium (K^{+}) ion and 1 Ca^{2+} ion for 4 Na^{+} ions (Na^{+}- Ca^{2+}- K^{+} exchange or NCKX) (Berridge *et al.* 2003; Hilgemann *et al*. 2006; Noble & Herchuelz 2007; Marques-da-Silva & Gutierrez-Merino 2014). Second, sarco/endoplasmic reticulum Ca^{2+} ATPase (SERCA) as well as mitochondrial Ca^{2+} channel (MiCa), transport Ca^{2+} ions from cytosolic microenvironment to the Ca^{2+} compartments: endoplasmic reticulum (ER) and mitochondria, respectively (Clapham 2007; Chaigne-Delalande & Lenardo 2014; Wolf & Wennemuth 2014). Third, buffers such as parvalbumins (PV) and calretinin, and sensors such as calmodulin, contribute to Ca^{2+} homeostasis by binding to Ca^{2+} such that the concentration of free Ca^{2+} ions in the cytosol is reduced (Schwaller 2010).

Plasma membrane channels and internal stores determine Ca^{2+} influx (Figure 1.13). Ca^{2+} ions diffuse from either intracellular Ca^{2+} stores such as the endoplasmic reticulum (ER) or extracellular

microenvironment via voltage-operated channels (VOCs) and receptor operated channels (ROCs). Ca^{2+} ions are released from the ER storage via inositol trisphosphate (IP_3Rs); they are also released via ryanodine receptors (RyRs) (Bootman & Lipp 2001; Grienberger & Konnerth 2012).

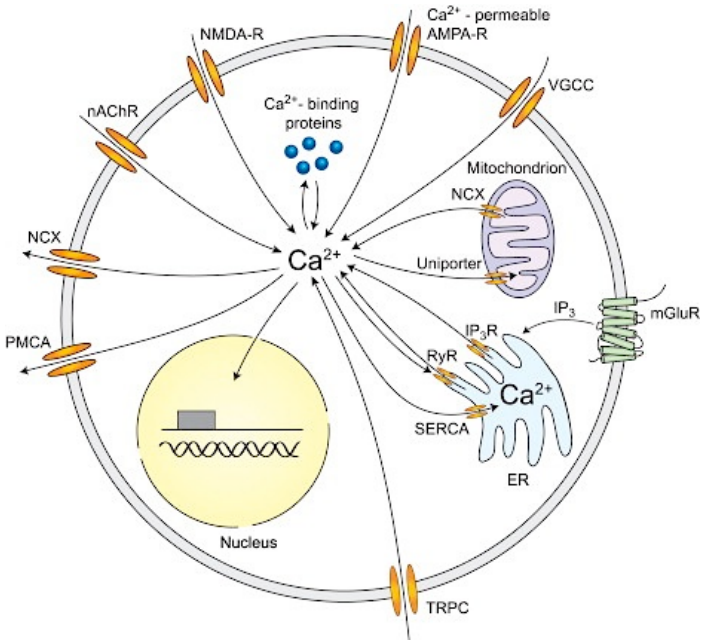

Figure 1.13: Ca^{2+} homeostasis. Ca^{2+} ions influx is sourced from internal stores (ER and the mitochondrion) and the extracellular microenvironment via voltage-operated channels (VOCs), IP_3R (inositol trisphosphate receptors), nAChR (nicotinic acetylcholine receptors), NMDA-R (N-methyl-D-aspartate receptor), AMPA-R (a-amino-3-hydroxy-5-methyl-4-isoxazolepropionic acid receptor), RyR (ryanodine receptors) and TRPC (transient receptor potential type C). Ca^{2+} efflux from the cytoplasm is mediated by NCX (Na^{+}- Ca^{2+} exchanger), PMCA (plasma membrane calcium ATPase) and SERCA (sarco-/endoplasmic reticulum Ca^{2+} ATPase) (Grienberger & Konnerth 2012).

Many excitable cells use VOCs to regulate their electrical activity; depolarization of the plasma membrane activates VOCs resulting in Ca^{2+} influx, subsequently triggering Ca^{2+}-dependent physiological process such as muscular contraction (Catterall 1991), neurotransmitter release (Dunlap *et al.* 1995; Atlas 2013; Kang *et al*. 2013) and neurite outgrowth (Sann *et al*. 2008). VOCs are classed as either high voltage activated (HVA) or low voltage activated (LVA). HVA Ca^{2+} channels (L-type), activated by large membrane depolarization of up to -30mV produce large and long lasting currents. In contrast, LVA channels (T-type) require a small membrane depolarization of around -70mV, to be activated. In addition to L-type Ca^{2+} channels, HVA also includes N-type, P/Q-type, and R-type channels mainly responsible for neurotransmission and facilitating Ca^{2+}entry into soma and dendrites in neurons (Bootman & Lipp 2001; Catterall *et al.* 2005; Welling 2009;

Catterall 2011; Simms & Zamponi 2014). Agonists such as ATP and glutamate activate ROCs when they bind to the channels; this also leads to Ca^{2+} influx into the cytosol (Bootman & Lipp 2001).

Fluorescent Ca^{2+} indicators can be used to track influx and efflux of free Ca^{2+} ions. This is made possible by fluorescent intensity produced when Ca^{2+} indicators are bound to free Ca^{2+} ions. Fluorescent intensity changes in response to changes in intracellular Ca^{2+} concentration (Takahashi *et al.* 1999; Bootman *et al*. 2013). Only free Ca^{2+} ions diffused into the cytosol (via VOCs and ROCs or internal stores such as ER) can be bound to Ca^{2+} indicators. In general, Ca^{2+} ions are not easily diffusible, for instance, only 1 of every 100 ions in the cytosol is unbound and 1 in 10, for ions in the ER (Paredes *et al.* 2008). Free Ca^{2+} ions are bound to endogenous buffers (intracellular Ca^{2+}-binding proteins) including parvalbumin and calretinin. Endogenous buffers are largely immobile and have low affinity for Ca^{2+} ions. Exogenous buffers such as Ca^{2+} indicators, on the contrary, are mobile and have high affinity for Ca^{2+} ions and hence out-compete endogenous buffers. This implies that the dynamics of Ca^{2+} ions fluxes are more influenced by exogenous buffers i.e. Ca^{2+} indicators. Therefore, the degree of Ca^{2+} flux, caused by cell depolarization, can be visualised by proportional changes in fluorescence intensity of Ca^{2+} indicators (Neher & Augustine 1992; Schwaller 2010; Grienberger & Konnerth 2012).

Bulk loading Ca^{2+} indicators on to tissue slices and dissociated neurons, for instance, provides an indirect but accurate technique for measuring generation of action potentials within a population of neurons. The output is Ca^{2+} oscillations data (demonstrated by changes in fluorescence intensity within a group of cells) with single cell resolution (Yuste *et al*. 2011). Electrical activity of a neuronal network can be monitored via Ca^{2+} imaging. For instance, spontaneous waves of impulses, moving from back to front of a cortical network in a slice, were imaged using fura-2 (chemical fluorescent Ca^{2+} indicator, Figure 1.14). Changes in field potential within the neuron network were linked to Ca^{2+} fluxes (Garaschuk *et al*. 2000). Fura-2 has been used to image fluxes of free Ca^{2+} ions within: depolarized basal forebrain cholinergic neurons (Duan *et al*. 2014), ischemic and non-ischemic hippocampal slices (ischemia was induced via slice superfusion with a solution exclusive of oxygen

and glucose) (Tanaka *et al.* 2002) and cerebellar granule neurons with and without L-glutamate stimulation (Marques-da-Silva & Gutierrez-Merino 2014).

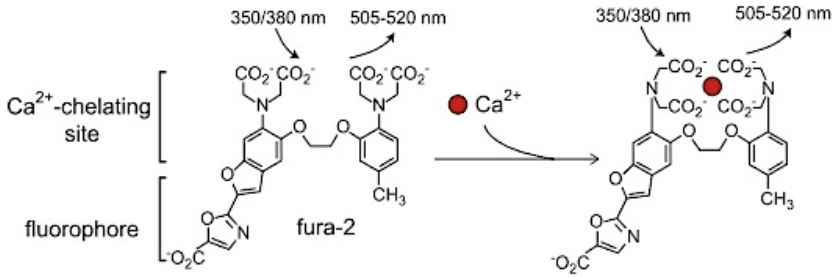

Figure 1.14: Fura-2 dye binding to a free Ca^{2+} ion (Grienberger & Konnerth 2012).

Fura-2, Quin-2 and indo-1 are some of the earlier fluorescent dyes that provided the basis for tracking intracellular Ca^{2+} changes. They permeate the cellular membrane via hydrolysis of acetoxymethyl (AM) esters and require excitation emission in the UV range; this can potentially damage cells and may lead to autofluorescence. On the other hand, fluorescent dyes like fluo-3 and fluo-4 (Figure 1.15) are excitable by visible light, therefore, avoiding drawbacks associated with UV excitation (Mintaz *et al.* 1989).

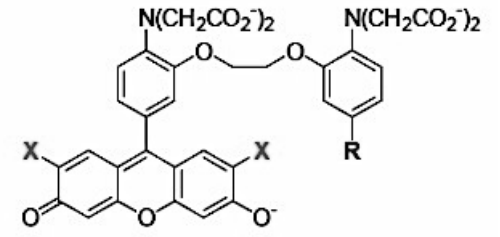

Fluo-3: X = Chlorine group & R = Methyl group
Fluo-4: X = Fluorine group & R = Methyl group

Figure 1.15: Chemical structures of Fluo-3 and Fluo-4 Ca^{2+} indicators (Mintaz *et al.* 1989; Ryan & Urayama 2012).

Fluo-4 dye has been an important tool in studying generation of action potentials via tracing Ca^{2+} fluorescent oscillations. Bipolar neurons, derived from induced pluripotent stem cells (iPSCs), for instance, were loaded with 10mM Fluo-4 Ca^{2+} fluorescent indicator to measure propagation of action potentials (Chen *et al*. 2014). Furthermore, Fluo-4 was loaded on hippocampal (B. Li *et al.* 2014; Robertson *et al*. 2014), cerebral cortical (Yuan *et al*. 2013) and striatal neurons (Peyrin *et al*. 2011), and hippocampal slices (Watters *et al*. 2014) to probe intracellular Ca^{2+} fluxes

across cellular membranes using flow cytometry, confocal and epifluorescence microscopy techniques. In a lot of Ca^{2+} imaging studies, changes in Ca^{2+} fluorescence are normally captured relative to baseline fluorescence ($\Delta F/F_0$) for each region of interest (ROI). Fluorescence ROIs correlate to Ca^{2+} oscillations profiles on different cells that are recorded within a culture (Ruffinatti *et al.* 2013).

1.2. Cellular responses to patterned substrates

1.2.1 Natural patterning

One of the major benefits of using an *in vitro* model with dissociated cells, as mentioned before, is that it provides a more controllable environment of study compared to organotypic or intact animal systems (Potter, 2001). Biomaterial surfaces can be engineered to direct the adhesion of neurons and elongation of their axons (Stevens and George, 2005; Yang, 2005). This could be developed to control the formation of neuronal circuits *in vitro*. Physical structures such as micro-channels can influence morphology of neurons and elongation of their axons from their source to their target sites; this is called contact guidance (Weiss, 1947). This phenomenon is inspired by neuronal behaviour *in vivo* during development in which axon or dendrite projections are mediated by external cues such as netrins and semaphorins (Kolodkin & Tessier-Lavigne 2011; Chak & Kolodkin 2014).

Neurons in the central nervous system (CNS) form highly complex and systematic circuitries via their axons. Any variations in the circuitry affect function, for instance, loss of neurons in the striatum alters the BG circuitry and leads to impaired movement (Figures 1.5 and 1.6). Directed axonal elongation is key in the morphogenesis process of the CNS. It is associated with the development and regeneration (after injury) of neuronal circuitries (Curinga & Smith 2008). Formation of neuronal circuits in the developing CNS is regulated by molecular guidance cues; these molecules determine the pathways to be followed by axons towards their target sites. One of the main reasons for failure of circuitry re-establishment in the adult mammalian CNS after injury is due to reactive gliosis, which involves formation of glia scars after injury; scars inhibit regeneration of axons (Silver & Miller 2004; Harel & Strittmatter 2006; Hoffman-Kim *et al.* 2010).

The growth cone at the tip of the neuronal axon senses and responds to the extracellular environmental changes imposed by guidance molecules such as netrins, slits, semaphorins, and ephrins (Kalil & Dent 2005; Kolodkin & Tessier-Lavigne 2011; Gomez & Letourneau 2014). The receptors on the surface of the growth cone are activated via interaction with guidance molecules. This leads to changes in cytoskeletal elements, particularly the actin cytoskeleton, which controls the morphology and motility of the growth cone. The flat sheet, fan-like structure at the end of an extending axon, the lamellapodia, consists of fine projections (filopodia) that sense the area around the axon (Figure 1.16).

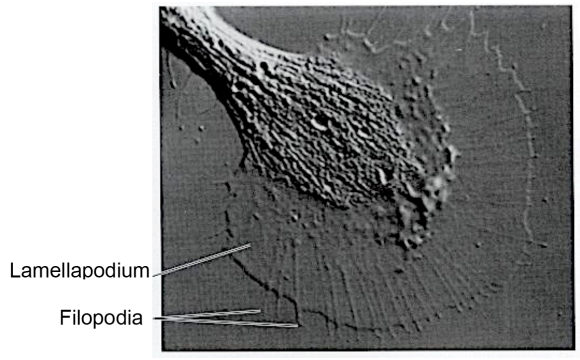

Figure 1.16: Photomicrograph of a growth cone at the tip of a ganglion cell axon. Lamellapodia and filopodia develop from the growth cone (Purves *et al*. 2001).

Filopodia normally appear when the growing axon changes direction, as noticed both *in vivo* and *in vitro*, in both the CNS and PNS (Purves *et al.* 2001; Curinga & Smith 2008; Polleux & Snider 2010). Cellular attachment and axonal elongation is clearly guided by molecular and/or topographical cues *in vivo*. This has inspired scientists to engineer microenvironments, via the use of biomaterials, with extracellular cues in order to direct or control neuronal attachment and axon elongation *in vitro*.

1.2.2 Biomaterial patterning

Fibroblasts and osteoblasts cultured *in vitro*, for instance, usually attach and align parallel to the topography present in their microenvironment. Neurons behave somewhat differently since they develop neurites from their soma. These neurites do not necessarily elongate in the same direction as their soma; alignment perpendicular to topography (perpendicular contact guidance) has been observed in some cases (Hoffman-Kim *et al.* 2010). For instance, dissociated CNS neuroblasts

cultured on lithographically-patterned substrates (130 nm deep × 1 μm wide and 320 nm × 1 μm wide) extended their processes both parallel and perpendicular to topography orientation (Nagata *et al.*, 1993; Rajnicek *et al.,* 1997). Controlling cellular behaviour on biomaterials is key since cells are guided by various environmental cues *in vivo* to follow distinct patterns during development. Surface properties of a biomaterial greatly influence the response of cells cultured on it (Murugan *et al.* 2009). A biomaterial surface can be engineered to modify its topography (structure), and its composition by either: (1) chemically manipulating molecules on a surface or (2) coating the surface with bioactive agents such as laminin (LN), in order to achieve controlled cell adhesion, growth, migration, differentiation and guidance (Stevens & George 2005; F. Yang *et al.* 2005; Roach *et al.* 2010). An ideal substrate will have the right combination of cues to provide both a neuron-friendly environment, to encourage neuron attachment and neurite development, and axonal guidance during development of a neuronal network *in vitro*. Different techniques can be utilized to design and fabricate topography for neuron culture such as: photolithography, soft lithography, microfluidics and electrospinning.

1.2.3 Electrospinning

Electrospinning has been used to fabricate topography structures that can be used to direct neuron patterning *in vitro*. The process of electrospinning uses electrostatic forces to generate polymer fibres. It evolved from electrospraying, which produces polymeric droplets as opposed to fibres. The electrospinning process has the following elements: syringe, needle, pump, voltage power source and a fibre collection device (Figure 1.17). The polymer solution is loaded into the syringe. The pump drives a volume of polymers at a set flow rate. At this time, the dominant force on the polymer is surface tension resulting in formation of droplets at the end of the needle. These droplets break and fall down due to the force of gravity. When a high voltage is applied, an electrostatic force is generated in the polymer and increases up to a point where it is greater than the surface tension. A Taylor cone is formed at the end of the needle tip leading to an elongated fluid jet. The jet is driven towards the collector due to the potential difference between the positively charged polymer at the end of the needle and the negatively charged collector. The jet undergoes bending instability due to repulsive forces formed within the polymer. This instability increases the

path length, set by distance between needle tip and collector, and time for the jet to reach the collector resulting in evaporation of solvent and consequently formation of a solid fibre. The fibres are collected on a collector, either rotating or stationary. Aligned fibres can be fabricated by using a different collection method i.e. using a rotating drum or mandrel instead of a stationary collector (Huang *et al.* 2003; Li & Xia 2004; Sill & von Recum 2008; Lee & Livingston Arinzeh 2011; Liu *et al.* 2013).

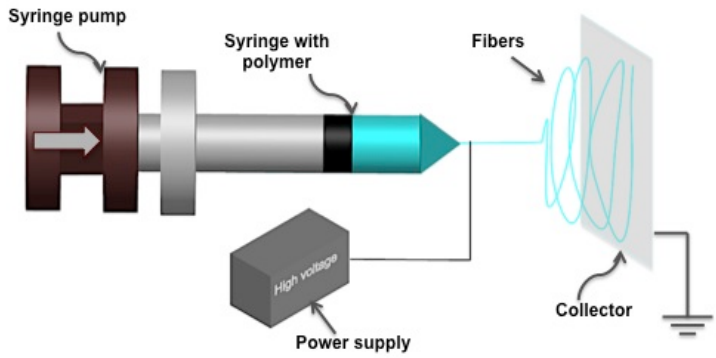

Figure 1.17: Electrospinning set-up. The polymer is driven from the end of the syringe (positively charged) to the negatively charged collector where fibre meshes are collected.

Electrospinning parameters that define the structure and formation of the fibres include: applied voltage, polymer flow rate, and needle-collector distance. For instance, increasing polymer concentration generally results in an increase in diameter of electrospun fibres (F. Yang *et al.* 2005). The effect of applied voltage on fibre diameter is somewhat controversial (Li & Wang 2013); Okutan *et al.* found that increasing voltage resulted in larger fibre diameter (Okutan *et al.* 2014). However, in some studies (Sill & von Recum 2008), fibre diameter reduced with increasing applied voltage. These relationships differ depending on polymer/solvent combination used as well as the conditions such as humidity and temperature under which the electrospinning is performed (Sill & von Recum 2008).

Electrospinning allows fabrication of aligned meshes of nano- and micro-scale diameters. It has been used to produce fibres from different polymers such as poly-lactic acid (PLA) (F. Yang *et al*. 2005; Corey *et al*. 2008; Yang *et al*. 2011) and polycaprolactone (PCL) (Schnell *et al.* 2007; Chen *et al.* 2011). These fibres resemble the natural extracellular matrix

(ECM); they are thin continuous fibres with a high surface-to-volume ratio (Schnell *et al*. 2007; Sill & von Recum 2008). Corey *et al.* fabricated PLA aligned nano-fibres using a rotating wheel collector (Corey *et al*. 2008). Primary rat spinal cord motor and sensory neurons were cultured on nano-fibre substrates for 4 days *in vitro*. Prior to cell culture, the nano-fibres were coated with polylysine and collagen I, for motor and sensory neurons, respectively. The processes for both types of neurons were elongated and aligned along the nanofibres.

Wang *et al.* cultured human embryonic stem cell (hESCs)-derived neural precursors (NPs) on tussah silk fibroin (TSF) scaffolds of both aligned and random orientation (J. Wang *et al*. 2012). On aligned TSF scaffolds, NPs differentiation and neurite outgrowth were significant in comparison to random TSF scaffolds. The study also investigated the effect of TSF diameter by comparing diameters of 400 nm to 800 nm. The smaller diameter, 400 nm scaffolds, led to better differentiation and neurite outgrowth compared to 800 nm scaffolds. A similar study by Mahairaki and colleagues used human NPs derived from ES line BGO1 to investigate directed differentiation and axonal growth (Mahairaki *et al.* 2011). The cells were cultured on micro and nano-scale PCL scaffolds pre-coated with poly-L-ornithine/LN to promote cellular attachment, viability and differentiation. Two sets of PCL scaffolds were fabricated: aligned and randomly orientated. NPs cultured on aligned nano-fibres showed higher percentage of differentiation, 86% (indicated by stain for TUJ1, a class III β-tubulin protein that identifies early stage neurons) compared to other scaffolds i.e. aligned fibres of micro-scale, 62%, random nano-fibres, 27% and random micro-fibres, 32%. Also, 40% of the NPs cultured on the tissue culture plate (no substrate) were differentiated. These studies provide essential data for finding the optimal conditions to manipulate differentiation of hESCs (human embryonic stem cells) towards neuronal regeneration.

Yang *et al.* developed 3D construct consisting of portable electrospun nano-fibres combined with hydrogel to replicates natural ECM (Yang *et al*. 2011). PLA was electrospun into aligned nano-fibres averaging 450 nm in diameter. A hydrogel base, 200 μm thick, was prepared using rat-tail collagen type 1 solution. A bottom-up approach was used for fabricating the 3D scaffold (Figure 1.18. Aa.) Multiple layers of nano-fibres were placed on top of the hydrogel base; these layers were separated by filter papers (spacers). Corneal fibroblast cells (and hydrogel) were seeded onto the

assembled nano-fibres (Figure 1.18. Ab); frames holding excessive nano-fibres were trimmed off (Figure 1.18. Ac). Cells were cultured for 48 h and orientated along nano-fibres placed at different angles relative to each other, (Figure 1.18. B-D).

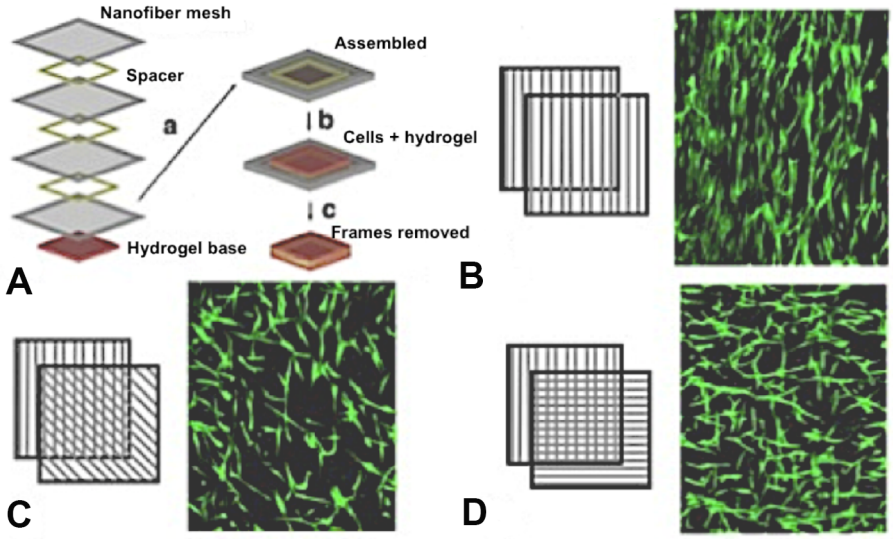

Figure 1.18. A: a-c. Fabrication of the hydrogel-nano-fibre 3D scaffold. B, Z-stacked 3D CLSM images of corneal fibroblast cells cultured on nano-fibres layered parallel to each other. C, Nano-fibres layered at 45^0 to each other. D, Fibres layered perpendicular to each other before cell culture. Cells were stained with calcein-AM (green), which stains for live cells (Yang *et al.* 2011).

In addition to contact guidance, nano-fibres have also been used to promote nerve cell morphogenesis and survival. For instance, cerebellar cortex cell types: granule and Purkinje cells, (GC) and (PC) were cultured on a hybrid scaffold consisting of collagen type 1 and peptide amphiphile (PA) nano-fibres (Sur *et al*. 2012). PAs are peptide molecules that self-assemble into nano-fibres, used for applications including supporting and signalling cells (Cui *et al*. 2010). The hybrid scaffolds fabricated had diameters ranging from 20-30 nm. The LN epitope (part of an antigen that specifically attaches to an antibody), IKVAV-hybrid scaffold was used as a platform for culturing cells. Adjusting the PA concentration and consequently the number of LN epitopes influenced the density or survival and maturation of the cells. A PA concentration range of 0.125 to 2 mg/mL was used. Both GC and PC cell density increased compared to the controls (cells cultured on collagen only). This hybrid scaffold could potentially be useful for studying cell morphogenesis and promoting cell viability (Sur *et al.* 2012). Lithographic techniques including photolithography and soft lithography have also been used to fabricate aligned topography for studies involving cell patterning.

1.2.4 Lithographic techniques

Photolithography is a microfabrication technique commonly used in electronics, for instance, for manufacture of integrated circuits (Xia & Whitesides 1998; Jones 2000). It allows formation of different geometric patterns on substrates using 3 elements: photoresist, light source and a photomask**.** Photomasks can come in many forms, either ink printed on transparency paper (for low resolution large feature size – above 50 microns) or more solid masks prepared by depositing chrome on glass (these can allow features down to 0.25 microns). Each mask presents a specific pattern, which is transferred to a photoresist-coated substrate when exposed to a light source e.g. UV-365nm (also termed the i-line). AutoCAD (computer-aided design software) can be used for designing the photomasks, allowing any type of design or pattern to be formed. The substrate to be patterned can be pre-treated to remove any surface contamination, for example, hexamethyldisilazane can be used to remove moisture and therefore, improve photoresist adhesion (Yang *et al*., 2005).

The photolithography process is as follows: [1] the substrate is spin-coated with a photoresist. A drop of the photoresist is placed onto the substrate; the photoresist is spread around, usually by spinning at ~500 rpm and finally spun at range 1,000-10,000 rpm. A thin layer of photoresist is formed on the substrate. The spin-coating process reduces the percentage of residual resist and also dries the resist through partial removal of the solvent. A process called soft baking further reduces the solvent. [2] The substrate is placed on a hot plate, or in an oven for a few seconds to minutes depending on the type of resist used and its thickness. The temperature required for soft baking depends on the glass transition temperature of the photoresist in use. [3] After soft baking the photoresist-coated substrate is exposed, via a photomask to a light source, usually using a filtered wavelength of 365 nm (Jones 2000).

A photoresist consists of: (1) a polymer, (2) a photo-active compound (PAC) which reacts to light and (3) a solvent which keeps the photoresist in liquid form prior to coating and soft baking**.** The resist can be either positive or negative indicating how it will react to UV exposure - positive photoresists, when exposed to light, are altered molecularly making them soluble in developing

solutions; negative photoresists react with light to form hardened areas which cannot be developed away**.** [4] A pattern identical to that on the photomask is imprinted on the substrate, being either an exact replica or its inverse image depending on the nature of the resist used (Figure 1.19) (Jones 2000).

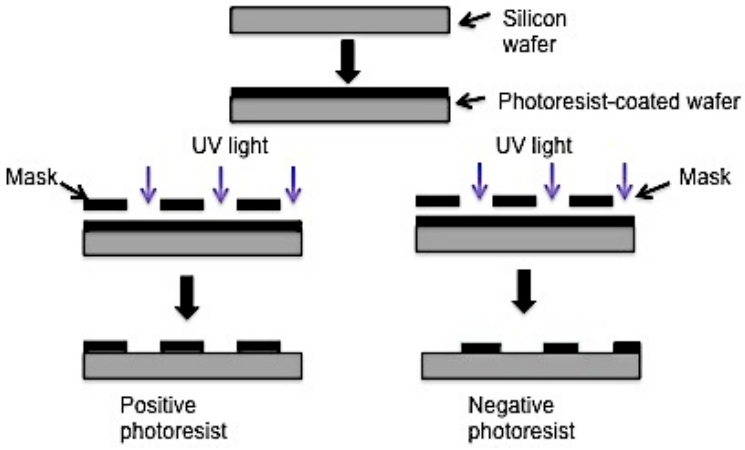

Figure 1.19: Photolithography process. A surface e.g. silicone wafer is coated with photoresist that react when exposed to light. The mask defines the pattern to be transferred onto substrate.

The main element key to the soft lithography process is an elastomeric material. Examples of elastomers used in soft lithography are: polyurethanes and polyimides and polydimethylsiloxane (PDMS) (Xia & Whitesides 1998). PDMS is commonly used due its unique properties, i.e. (1) good thermal stability, which means the polymer can be cured thermally and can withstand higher temperature within the range required for most applications (2) good optical transparency, up to ~300 nm (3) not hydroscopic, doesn't swell with humidity. The soft lithography process is as follows (Figure 1.20) an elastomer, i.e. PDMS is cast over a topographically patterned substrate, prior designed via processes such as photolithography. The topographic structure can be built on materials such as silicon. A curing agent is used to initiate cross-linking of the polymer (curing process) into a solid material. Curing can be achieved by heating the PDMS i.e. at 100 °C for ~35 min or leaving at room temperature for ~48 h. The cured PDMS elastomer block, with an inverse pattern from the master, can be easily peeled off from the master. This technique is relatively inexpensive and reproducible (you only have to design/manufacture one master which can be re-used) and can be used to construct substrates with physical structures to direct cell growth (Xia & Whitesides, 1998).

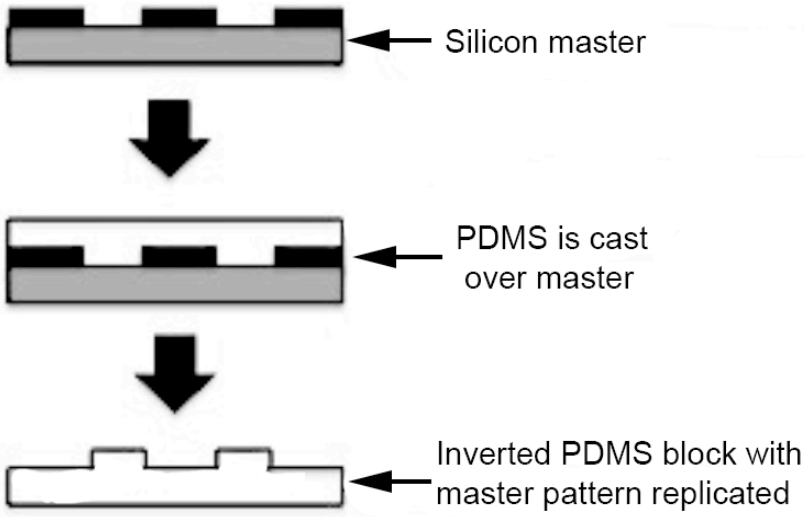

Figure 1.20: Soft lithography process. The master is fabricated via photolithography; PDMS polymer is mixed with a curing agent and cast over the master. The PDMS elastomer block with a pattern mirrored from the master is fabricated.

Photolithography can be used to form sacrificial polymer templates, which can be used for chemical patterning. These patterns have been formed from various (bio)molecules, allowing subsequent manipulation of interacting cells. For instance, a substrate can be coated with both cell inhibiting and cell promoting substances to achieve directional/morphological control (Murugan *et al.* 2009). Stenger *et al*. fabricated a chemically pattern to study response of hippocampal neurons on the substrate (Stenger *et al.* 1998). A glass coverslip was prepared with cell adhesive sites pre-coated with trimethoxysilylpropyldiethylenetriamine (DETA): somal adhesion sites of 25 µm diameter, axonal adhesion sites of length 190 µm and dendritic adhesion sites of four 5x10 µm blocks. The remainder of the coverslip was pre-coated with the non-adhesive agent, fluorinated silane (13F) (Figure 1.21). Embryonic hippocampal neurons were cultured for 3 days *in vitro* and immunostained for antibodies MAP5 and MAP2 to classify the soma, axons and dendrites. 34-48% of the cultured neurons attached on the somal site; with 65-89% of these having axons attached on the continuous adhesion site of the substrate. Processes from the soma were restricted along the continuous adhesion site (longer neurites) or broken paths at the sides of the soma (short neurites).

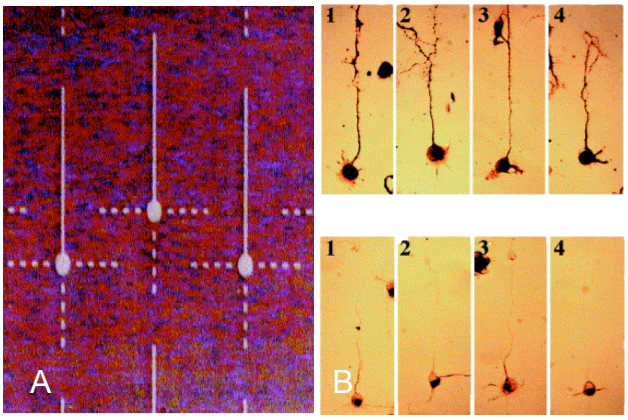

Figure 1.21: Glass coverslip patterned via photolithography. A: Blue/purple = cell inhibiting region coated with a fluorinated silane called 13F, silver pattern = cell promoting region pre-coated with DETA. B: Embryonic hippocampal neurons response to substrate patterning (Stenger *et al*. 1998).

Recknor *et al.* used the photolithography technique to fabricate substrates for astrocyte alignment *in vitro* (Recknor *et al*. 2004). Photolithography was used to design a silicon wafer (master) with a pattern for astrocyte culture. Polystyrene (PS) was then cast onto the master to inversely transfer the pattern onto the polymer (soft lithography). PS micro-grooves of 10 μm widths, 3-μm height and with separation of 20 μm were fabricated. The average thickness of the polymer (PS) substrate was ~60 μm. The PS substrate pre-coated with LN, improved adhesion and spreading of rat type-1 astrocytes resulting in over 85% astrocyte alignment. Aligned astrocytes were used as biological cues alongside topographical (PS substrate) and chemical cues (LN) to create an environment that allowed neuronal stem cell differentiation and directed axon outgrowth.

Francisco and collegues fabricated three-dimensional 'square and corridor' structures using photolithography to regulate axonal outgrowth and orientation (Francisco *et al.* 2007). The structures (chambers) had dimensions ranging from (length × width) 40×40 μm to 120×120 μm and 700 μm long corridors with widths ranging from 20 μm to 50 μm. These structures had a uniform height of 15 μm and were pre-coated with LN to promote adherence of dorsal root ganglia (DRG) neurons. Axonal outgrowth of neurons cultured within the chambers was inhibited compared to neurons cultured in corridors. The corridor structures were unconfined, i.e. they had open channels for axons to extend through. Some axons responded to the open channels and followed the structure around.

Some studies have indicated that the depth of lithography micro-grooves correlates to neurite alignment (Hirono *et al*. 1988; Clark *et al*. 1990; Miller *et al*. 2002; Tuft *et al*. 2013). Increasing the depth from 0.2 to 4 μm led to an increase in the alignment of neurites since it made it difficult for axons to cross from one groove to the next (Hoffman-Kim et al. 2010). In another case, a micro-grooved substrate with different groove depth was designed via photolithography and dry etching (Clark *et al.* 1990). Baby hamster kidney (BHK) cells were cultured on grooves and the alignment, which was defined by cells attached less than 10^0 from direction of grooves, increased relative to the depth of micro-grooves from 0.2 to 1.9 μm. In other studies, increasing the width of grooves and ridges reduced neurite alignment (Cecchini *et al.* 2008; Ferrari *et al.* 2011; Holthaus *et al.* 2012). PC12 cells cultured on a substrate with 200 nm grooves had reduced alignment from 95% to 75% when the width of the grooves and ridges was increased from 500 to 750 nm (Cecchini *et al.* 2008).

Neurons respond better to surfaces biochemically or physically modified to encourage attachment and growth, compared to unaltered surfaces (Miller *et al*. 2002; Hoffman-Kim *et al*. 2010; Roach *et al.* 2010). Gomez *et al.* studied development of primary axons on biochemical and topography patterned substrates (Gomez, Chen, *et al*. 2007). Embryonic day 18 (E18) neurons cultured on nerve growth factor/ LN (chemical) coated and PDMS patterned (topographic) substrates yielded an axonal growth of 69% and 75%, respectively, compared to unmodified surfaces. Topography was found to be an important cue for promoting the initial growth of axons (axogenesis) in culture. Biochemical cues were found to be less influential. The biochemical cues, however, encouraged more axonal growth in total compared to topographical cues. In another study by Gomez *et al.*, hippocampal neurons had a 10% increase in axonal length when cultured on a biochemically-modified surface pre-coated with immobilized nerve growth factor and LN (Gomez, Lu, *et al.* 2007). There was no increase noticed for neurons cultured on a physically modified surface (PDMS micro-grooves) only. A 25% increase in axonal growth was noticed when both cues were present on the substrate. This implies that a substrate with both biochemical and topographical cues, i.e. LN and micro-grooves encourages more enhanced neuronal response and certainly axonal growth compared to a substrate with either topographical or biochemical cues on their own (Yu & Shoichet 2005; Koh *et al*. 2008; Yao *et al.* 2009; Hoffman-Kim *et al.* 2010). DRG neurons were cultured on

polylactic acid (PLA) or poly (lactic-co-glycolic acid) (PLGA) micro-grooves pre-coated with LN (Miller *et al*. 2002). Micro-grooves provided physical guidance to the neurites, whilst LN improved the adherence and outgrowth of neurites along micro-grooves. Around 95% neurite alignment was achieved. The soft lithography technique used to build micro-grooves has also been useful in the process of fabricating micro-contact printed substrates.

1.2.5 Micro-contact printing and surface chemistry

Micro-contact printing is a chemical patterning technique that involves the use of an elastomeric stamp to print a chemical on a surface. Whitesides and colleagues developed micro-contact printing with the intention of an easy, quick and cost effective replication of patterns via a stamp build using soft lithography (Perl *et al.* 2009). A master is initially developed using photolithography; a lot of elastomeric stamps can be replicated using the master. The process used is similar to the one used for fabricating micro-grooves (Section 1.2.4). PDMS is commonly used for fabricating stamps due to its superior characteristics such as elasticity, bio-inertness and thermal stability. The polymer is chemically stable and durable, i.e. PDMS elastomeric stamps can be re-used up to 100 times (Kumar *et al*. 1994).

Patterns of cell-adhesive and non-adhesive chemistry permit cell patterning. Elastomeric stamps are inked into a chemical before they are placed into contact with a surface such as silicon dioxide, gold, silver and glass to form a pattern. The micro-contact printing technique was initially used to pattern thiol-based self-assembled monolayers (SAMs) on gold surfaces. SAMs involve assembling molecules onto a surface via adsorption. Adsorption allows binding of molecules onto a surface from a solution or gas; the process allows crystalline structures to be formed onto a surface (Perl *et al.* 2009; Kaufmann & Ravoo 2010; Alom Ruiz & Chen 2007; Larsen *et al.* 1997). Surface modification via micro-contact printing of cell-permissive and repellent molecules allows cell guidance. For instance, Jang and Nam guided outgrowth of CNS neurites using micro-contact printed ECM proteins (Jang & Nam 2012). Elastomeric stamps made of PDMS polymer were used to print LN patterns onto glass coverslips. E18 hippocampal plated on glass substrates developed neurites, which were guided by LN patterns. Neuron patterning can be used for developing artificial, *in vitro* neuron circuits for studying neurobiology including neuron-neuron synaptic

interactions. Micro-contact printing enable fabrication of neuron microcircuits that are simpler and more defined/controllable compared to complex *in vivo* micro-environments (Kwiat *et al.* 2012). Neural patterns commonly use poly-D-lysine (PDL) or LN as the cell permissive layer.

Vogt *et al.* developed an *in vitro* model for studying synaptic plasticity, which is associated with processing and storage of information in the CNS (Vogt *et al.* 2005). PDMS micro-stamps were used for contact printing cell permissive ECM-gel with PDL biomolecules on cell-repellent polystyrene petri dishes. E18 cortical neurons cultured on patterned substrates responded to cell-permissive biomolecules and established connectivity. Neurons in neighbouring locations on contact printed grids (width of 4-6 μm and node points of diameter 12-14 μm), cultured for days *in vitro* (DIV) 11-15 were patched simultaneously to demonstrate neuron-neuron synaptic connectivity. Synapses of neuron circuitry showed short-term plasticity; for instance, the second postsynaptic potentials (PSP) recorded were smaller than the first ones even though constant presynaptic action potentials were fired.

1.2.6 Cell compartmentalisation via microfluidic devices

Microfluidic devices are cell culture platforms that are also built via lithographic techniques. Instead of printing cell permissive/inhibiting patterns on surfaces, elastomeric stamps are reversibly or irreversibly (using oxygen plasma) sealed to a surface such as glass to form a microfluidic device. Devices can be used to compartmentalise dissociated cells or brain tissue. They can potentially be used to develop neuronal networks *in vitro*, designed to mimic *in vivo* circuitry. Connectivity established in the brain is in the order of microns and device has dimensions of similar scale. Dissociated cells or tissue of different types can be co-cultured in different compartments or ports of the same substrate. Microfluidic device permit different ports to be treated separately. For instance, two-port microfluidics have been used to study axonal damage and regeneration (Brunello *et al.* 2013). In the studies, cells were cultured in one port and developing axons were guided through to the next port by micro-grooves separating the ports. Axons invading the next port were studied separately without disturbing cell bodies in the other port (Li *et al.* 2012; Millet & Gillette 2012; Bhatia & Ingber 2014).

Fabrication of a typical microfluidic device uses both photolithography and soft lithography techniques. A master is manufactured using photolithography and it consists of grooves and chambers/channels (Figure 1.22 A-D). The soft lithographic technique, using PDMS used to build the final device (Figure 1.22 E-F) (Taylor *et al.* 2003; Harris *et al.* 2007). When neurons placed in device compartments mature, they develop protrusions, neurites that extend from soma in one compartment into another where synaptic connectivity is established. Elongation/protrusion of neurites is directed via contact guidance by micro-grooves situated between compartments. Different studies have shown that this device can isolate the soma from axons in addition to aligning axons (Taylor *et al*. 2003; Taylor *et al.* 2005; Park *et al.* 2012). This is enabled by micro-grooves narrow enough to allow axons to extend from one channel to another whilst physically restricting cell bodies from entering the grooved areas.

Moreover, micro-grooves can be tapered to ensure axon elongations are unidirectional (Peyrin *et al*. 2011). It follows that isolated axons can be analysed separately without interference from the soma. In a two-compartment microfluidic device, for instance, neurons can be plated in one compartment with axons extending into another such that studies like axon degeneration and regeneration (Ben-Yakar *et al*. 2009) can be carried out separately. Microfluidic devices have been used to culture CNS dissociated neurons such as cortical (Taylor *et al*. 2009; Coquinco *et al.* 2014), hippocampal (Barbati *et al*. 2013) and striatal (Peyrin *et al.* 2011) neurons. Taylor *et al.* used a two-port microfluidic device to culture E18 rat cortical neurons inside the device (Taylor *et al.* 2003). Compartments were connected with 120 micro-grooves, 10 μm wide, 3 μm high, and 150 μm in length, separated by 50 μm. At around day 3-4 *in vitro*, the axons extended from the soma to the axon compartment at an outgrowth rate of 50-100 μm per day. The device also allows neurons to be co-cultured with other cell types such as astrocytes and oligodendrocytes, but keeping the different cell types physically separated.

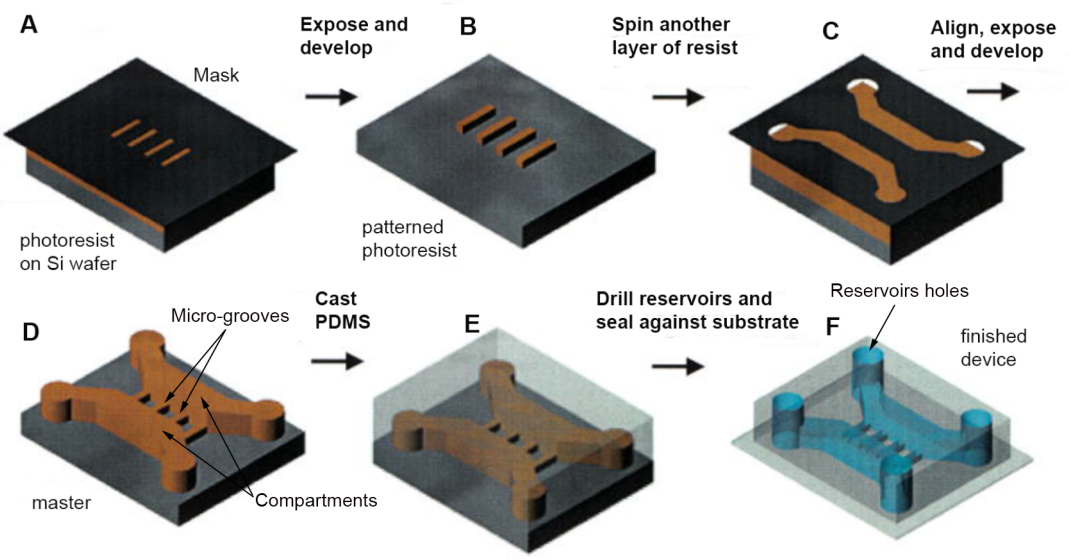

Figure 1.22: Schematic showing process of microfluidic device fabrication. A-D: Photolithography was used to fabricate the master. E-F: Soft lithography was used to complete the device. PDMS was cast onto the master and once cured, the reservoirs holes were drilled and the device was bonded to a glass coverslip using oxygen plasma (Taylor *et al.* 2003).

Majumdar *et al.* fabricated a device for co-culturing dissociated E19 hippocampal neurons with glia isolated from post-natal day 2 (P2) pup brains (Majumdar *et al*. 2011). The cells were split into two compartments; the neurons' compartment was pre-coated with LN and the glia chamber was pre-coated with type 1 collagen to encourage cell attachment and development. Neurons and glia cells were cultured in separate chambers for 2-3 days to allow the glia cells to reach confluence. After the glia cells reached confluence, the chambers were connected to allow exchange of nutrients between the cell types. Glia provided the neurons with nutrients to maintain their viability for up to 3 weeks in culture.

1.3. Thesis aims and objectives

The mammalian brain is made up of very complex circuits involving billions of neurons synaptically intercommunicating via trillions of connections. Neurobiology research is concerned with studying how these circuits develop and how neurodegenerative diseases, such as HD and PD damage function. Micro-engineering techniques such as electrospinning and lithography produce substrates that can be used for contact guidance of neurites (axons and dendrites) for fabricating oriented

neuronal networks. The current work was concerned with fabricating a complex and functional *in vitro* neuronal circuit. One of the main benefits of using an *in vitro* model compared to an *in vivo* model is that it provides a simpler neuronal network with less complex synaptic connectivity and controllable environment of study. Micro-engineering techniques were used to fabricate substrates for neurite alignment and neuronal network fabrication. The work discussed in the current thesis involves:

a. The fabrication of PLA nano-fibres and PDMS micro-groove constructs (Chapter 3). Investigation of striatal neurite alignment on PDL and LN-coated constructs and pre-aligned astrocytes was also carried out.
b. Design and fabrication of two- and five-port microfluidic devices (Chapter 4). Microfluidic devices were pre-coated with PDL and LN, similarly to constructs built in Chapter 3.
c. Cortical, striatal, GP and SN cell culture in five-port microfluidic devices (Chapter 5) built and characterised in Chapter 4.
d. Measuring excitability of cortical and striatal neurons using electrophysiology techniques as well as functional connectivity of neurons in five-port microfluidic devices using Ca^{2+} imaging (Chapter 5).
e. Fabrication of micro-contact chlorotrimethylsilane and trichlorosilane printed substrates (Chapter 6). The elastomeric stamp used to print substrates was of a five-port microfluidic device designed in Chapter 4 and used for neuron sub-type co-culture in Chapter 5. Study of 3T3, SH-SY5Y and cortical cells' response to micro-printed substrates was carried out.

Chapter 2. Materials and methods

2.1 Fabrication of nano-fibre substrates

Aligned nano-fibres used to guide neurite orientation were fabricated via electrospinning (Figure 2.1). 2% poly-L,D-lactic acid (PLA: 96% L/4% D; Purac BV, Gorinchem, Netherlands) polymer was dissolved in a mixture of dichloromethane and dimethylformamide (7:3 volume ratio, both solvents from Sigma-Aldrich, Dorset, United Kingdom) following a protocol established in the lab (Yang *et al.* 2011). The flow rate of the polymer solution out of an 18G needle ranged from 0.022-0.025 mL/min. A mobile parallel electrode collector was used to collect aligned nano-fibres charged at a range of ±5.5 kV to ±6.5 kV (Spellman HV, Pulborough, United Kingdom). Fibres from the collector were transferred to acetate frames (4.5 × 4.5 cm); an aerosol adhesive (3M CraftMount, 3M, Bracknell, UK) was used to attach fibres onto frames. Fibres were then anchored to coverslips using silicon glue (RS Components, Smithfield, Australia).

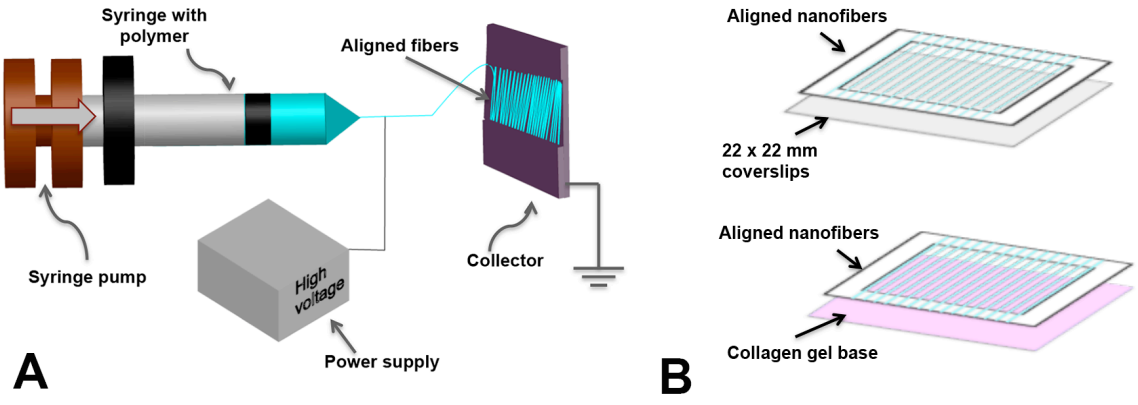

Figure 2.1: Electrospinning process. A: PLA polymer was pumped from the syringe and drawn by electrostatic forces towards the collector where aligned fibres were collected. B: Portable aligned nano-fibres were either placed on coverslips or collagen gel.

Silicon glue securing the nano-fibres was allowed to dry for 30 min before nano-fibre constructs were placed in square petri dishes and covered with foil paper with small holes punched on top. The constructs were vacuum dried for 30 min to remove any solvents before cell culture. After vacuum drying, the constructs were sterilized under ultraviolet (UV) light for 4.5 min. Nano-fibre constructs were pre-coated with 100 µg/mL poly-L-lysine (PLL, Sigma-Aldrich, Dorset, United Kingdom) overnight at room temperature; unbound PLL was removed by washing constructs three

times using sterile distilled water (dH_2O), and then 10 µg/mL LN (Sigma-Aldrich, Dorset, United Kingdom) for approximately 4 h. 13 mm circular glass coverslips (Menzel-Gläser, Braunschweig, Germany) were used as positive controls for each experiment. These were sterilized in 100% ethanol and left to dry before they were coated with PLL and LN similarly to nano-fibres. LN was carefully aspirated off constructs or coverslips just before cell seeding.

2.2 Fabrication of PDMS micro-groove substrates

PDMS micro-grooves were fabricated via soft lithography, as discussed in section 1.2.4 (Figure 2.2) (Xia & Whitesides 1998). Initially, silicon masters with dimensions: groove width ranging from 20-80 µm and depth of 2.2 µm were imprinted onto polymethylmethacrylate (PMMA) templates. A two-part kit consisting of silicone elastomer and curing agent (10:1 weight ratio) (Sylgard 184©, Dow Corning, Midland, MI) was used to prepare the PDMS solution. The solution was left at room temperature for 1 h to get rid of bubbles before casting onto PMMA templates placed in a 6 well plate (Greiner Bio-One, Stonehouse, UK). The solution was cured at 60 °C for 1 h to form PDMS micro-grooves.

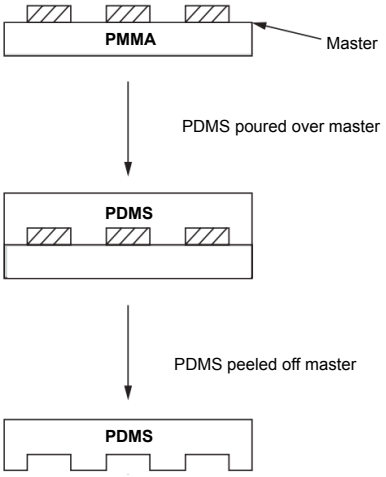

Figure 2.2: Fabrication of PDMS micro-groove constructs via soft lithography. PDMS polymer was cast over the PMMA master then peeled off, after curing, to form the PDMS micro-grooves. Adapted from (Tang & Whitesides 2009).

PDMS micro-grooves were incubated in 100% ethanol for 0.5-1 h at room temperature. The constructs were left to dry for a few minutes before they were washed with dH_2O to get rid of any remaining ethanol. Thereafter, micro-grooves were coated with 0.1 µg/mL PLL overnight at room

temperature, followed by three washes in dH_2O, and then 10 µg/mL LN for approximately 4 h. Circular glass coverslips were also used as positive controls for these experiments.

2.3 Fabrication of two and five-port microfluidic devices

2.3.1 Fabrication of masters

Microfluidic devices consisting of either 2 or 5 ports were fabricated via photolithography and soft lithography techniques. Parts of the protocol in this section were modified from (Park *et al.* 2006). First, photolithography; 2 layers of photoresist were fabricated for reservoirs and micro-grooves to produce a master template (Figure 2.3). SU-8 10 (MicroChem, Chestech Ltd, Warwickshire) photoresist was deposited onto clean silicon (Si) wafer (IDB Technologies, Wiltshire, UK) and spun (Solitec, Milpitas, CA) at 4,400 rpm for 60 s to produce a film of approximately 5 µm thickness (Brigham Young University, 2014). The wafer was pre-baked at 95 °C for 1 min to remove photoresist solvent and to promote cross-linking and hardening of film. It was then UV exposed through a super high-resolution transparency mask (128k, JD Photo-Tools, Manchester, UK) containing micro-groove patterns and alignment marks, for ~18 s, at an exposure energy of approximately 280 mJ/cm^2. Micro-grooves had widths tapered from 50, 25 and 15 to 5 µm, a length of 1,050 µm and spacing ranging 25-50 µm.

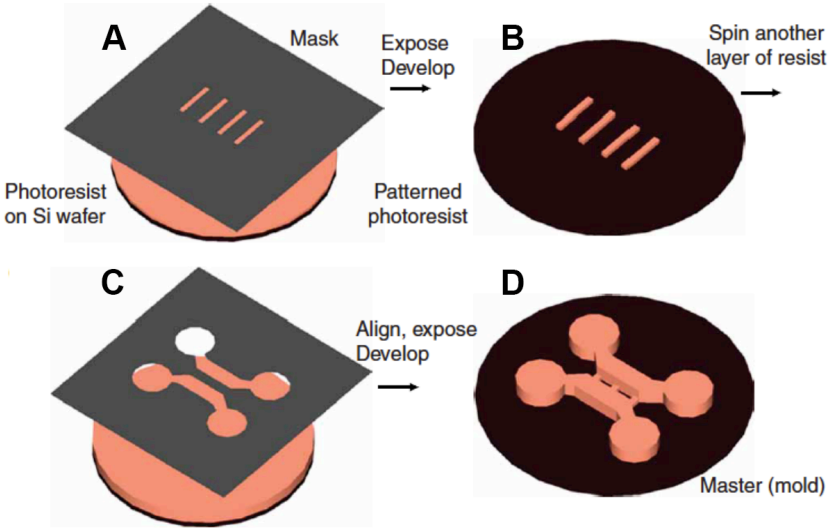

Figure 2.3: Schematic of a two-port master fabrication process. The fabrication procedure followed for a five-port master was similar to the one in this figure. A: Silicon wafer was coated with the first photoresist and exposed to UV light through micro-groove transparency mask. B: Micro-groove patterns were fabricated on silicon wafer. C: Silicon wafer was coated with second layer of photoresist for microfluidic device ports. D: Microfluidic device master was fabricated (Park *et al.* 2006).

After exposure the wafer was baked, (post-exposure baking, PEB), at 65 °C for 1 min followed by PEB at 130 °C for 2 min. The wafer was developed in ethyl lactate solvent (Microposit EC solvent, Rohm and Haas Electronic Materials, Coventry, UK) for approximately 1 min to remove unexposed parts of the film. The patterned wafer was rinsed in propan-2-ol (Fisher Scientific, Loughborough, UK), and rinsed again with developer if the sample had a cloudy film forming across it (an indication the substrate was underdeveloped). The wafer was dried using an air gun (Airmaster Tiger 8/64 air compressor, Nottingham, UK).

Another layer of photoresist, SU-8 50 (MicroChem, Chestech Ltd, Warwickshire), was spun onto the micro-groove-patterned wafer. Photoresist was spread at 300 rpm for 10 s, and then spun at 1,000 rpm for 50 s to fabricate a 100 µm thick film. Pre-bake was performed at 65 °C for 10 min and soft bake at 95 °C for 30 min. On the same plate, the temperature was ramped up, to soft bake again at 110 °C for 10 min; thereafter, the wafer was exposed through a second super high-resolution transparency mask (128k, JD Photo-Tools, Manchester, UK) with the reservoir/channel pattern and alignment marks, for ~33 s at approximately 280 mJ/cm^2. The instrument uses light integra, which relates the energy exposed to a surface to changes in exposure power, as the intensity of the UV light bulb drops. PEB was done at 65 °C for 1 min then at 95 °C for 10 min. Afterwards, the wafer was developed for approximately 10 min to ensure only the unexposed parts of the film were removed. The summation of parameters used for fabrication of two and five-port masters are displayed in Table 2.1. The wafer was rinsed again in fresh ethyl lactate developer and subsequently washed with propan-2-ol.

Table 2.1: Summary of parameters used for photolithography.

SU-8	Spin speed	Soft bake at 65 °C	Soft bake at 95 °C	Exposure Time/s (Integra)	PEB at 65 °C	PEB at 95 °C	PEB at 130 °C	Developing time
10	4,400 rpm	-	1	18.2 s (50)	1 min	-	2	1
50	1,000 rpm	10	30	33.0 s (100)	1 min	10 min	-	10

2.3.2 Fabrication of PDMS devices

Photolithographic master templates were used to fabricate complete PDMS (QSil 216 A/B, Farnell, Leeds, UK) microfluidic devices (Figure 2.4). PDMS pre-polymer was weighed out and mixed for approximately 5 min with a curing agent at a ratio of 10:1. The PDMS mixture was then poured onto a master, placed in a petri dish. A vacuum desiccator and an air gun were used to ensure bubbles from the mixture were completely removed around the patterned parts of the mould. The petri dish was placed in an oven at 60-70 °C for 50-60 min. The PDMS mixture was cured into a mould that was cut out using a plastic-handle disposable scalpel (Swann-Morton, Sheffield, UK). The PDMS mould was placed patterns up and punches were used to cut out reservoirs. Any remaining debris was removed; care was taken to ensure the side contacting the mould i.e. the side with the micro-grooves on was kept clean and dust-free.

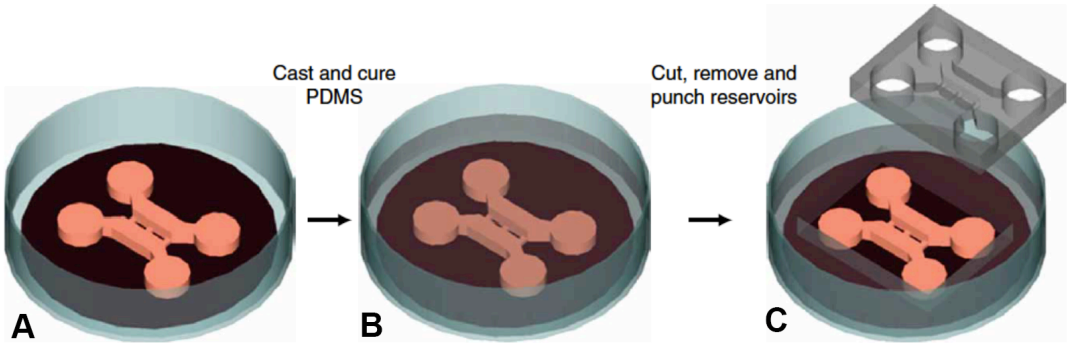

Figure 2.4: Schematic of soft lithography process following master fabrication. A: A master was placed in a vessel e.g. petri dish. B: PDMS was cast onto the master and cured in an oven. C: Once set, the PDMS mould was cut out and reservoirs (on the ports) were removed (Park *et al.* 2006).

The PDMS mould was irreversibly bonded to microscope slides (26 mm width, 76 mm length, 1-1.2 mm height from Fisher Scientific, Loughborough, UK) using oxygen plasma treatment (Diener electronic, Ebhausen, Germany). Slides were cleaned using propan-2-ol and dried using pressurized air. PDMS devices, micro-grooves up, and slides, were placed into the plasma chamber (Diener electronic, Ebhausen, Germany). This was followed by plasma treatment for 30 s at 30 W, and 0.5-mBar oxygen; the PDMS moulds were then placed upside down on glass slides to form irreversible bonded microfluidic devices.

2.3.3 Preparing devices for cell culture

Microfluidic devices were coated with PLL and LN to encourage attachment of cells. Beforehand, devices were filled with 1% Penicillin Streptomycin Fungizone (PSF, Invitrogen, Paisley, UK) in PBS (Sigma-Aldrich, Dorset, United Kingdom) and incubated at 37 °C for at least 1 h. PSF solution was then removed and devices were rinsed with PBS. Devices were fully loaded with 100 µg/mL PLL solution (around 250 µm for each port) in dH_2O overnight (or ~12 h). PLL solution was then unloaded from devices and rinsed 3 times with dH_2O; care was taken not to empty micro-grooves, as this would have resulted in bubbles. Thereafter, devices were filled with dH_2O and left for at least 20 min to ensure all unbound PLL was removed. LN solution was subsequently added for a minimum of 1 h, before it was replaced with neuronal culture medium (NCM). PLL, LN and medium incubation were all carried out at 37 °C. PDMS devices were incubated in NCM up to until cells were plated.

2.4 Fabrication of micro-contact printing substrates

The five-port microfluidic master (Section 2.3) was used to fabricate PDMS stamps via soft lithography (Xia & Whitesides 1998; Park *et al.* 2006). A master was placed into a glass petri dish and PDMS pre-polymer and curing agent solution (PDMS, QSil 216 A/B, Farnell, Leeds, UK) was cast and placed into an oven at 60-70 °C for 50-60 min to allow PDMS to cross-link. Two PDMS stamps were fabricated. Chlorotrimethylsilane and trichloro(1*H*,1*H*,2*H*,2*H*-perfluorooctyl)silane (this will be shortened to trichlorosilane in the thesis) solutions (both from Sigma-Aldrich, Dorset, United Kingdom) were prepared in toluene (Fisher Scientific, Loughborough, UK) at a concentration of 100 µL/mL. The first stamp was used for printing chlorotrimethylsilane and the second one, trichlorosilane substrates. Approximately 500 µL of each solution was placed on a cover slide (Menzel-Gläser, Braunschweig, Germany); the PDMS stamp was inked into the solution for a few seconds and dried off using nitrogen pressure (BOC, Surrey, UK). Inked stamps were placed onto coverslips and lightly pressed down using a pair of Dumont tweezers (Fine Science Tools, Cambridge, UK) to ensure all protruding surface features of the stamp were fully in contact with the coverslips. Stamps were removed from coverslips using tweezers after a few seconds of contact.

Printed coverslips (for both chlorotrimethylsilane and trichlorosilane substrates) were hovered upside down over boiling water for steam to collect. This was done to determine whether patterns were successfully printed. Steam was expected to accumulate on stamped sites where protruding features of the PDMS stamp formed contact with coverslips. These sites were expected to be more hydrophilic (hence, water attracting) parts of the substrate as opposed to non-stamped sites. Substrates for primary cells were incubated in PDL (100 µg/mL) overnight at room temperature and LN (10 µg/mL) for approximately 4 h, also at room temperature. They were rinsed with PBS buffer to remove any unbound LN. To determine whether LN was bound to cell culture surfaces fluorescent dyes were used. Fluorescein isothiocyanate (FITC) and tetramethyl rhodamine (TRITC) dyes (both from Sigma-Aldrich, Dorset, United Kingdom) were dissolved in a buffer. PDL and LN substrates were incubated in dye solutions at 37 °C for approximately 45 min, before they were rinsed 3 times with buffer. Substrates were dried at room temperature before imaging was carried out using the Nikon Eclipse 80i microscope.

2.5 Brain tissue dissection

2.5.1 Preparation for dissection

The following items were sterilized using a glass bead sterilizer (Steri 250, Simon Keller AG, Burgdorf, Switzerland) for approximately 15 s at 250 °C: large and small scissors (Fine Science Tools, Cambridge, UK), bracken forceps (Roboz Surgical Instrument Co, Kent, UK) and Dumont forceps (Fine Science Tools, Cambridge, UK). After cooling down, materials were placed in a sterile container. Trypsin and deoxyribonuclease (DNase) solutions were thawed at room temperature. Trypsin solution was made up of: 0.1% trypsin and 0.05% DNase (both from Worthington Biochemical Corp., Reading, UK) in Dulbecco's Modified Eagle's Medium/Nutrient F-12 Ham's medium (DMEM-F12, Sigma-Aldrich, Dorset, United Kingdom) and DNase solution was made up of 0.05% DNase also in DMEM-F12. Both solutions were kept in 1.5 mL Eppendorf tubes (Greiner Bio-One, UK) at -20^{0}C. 50 mL tubes (Greiner Bio-One, UK) were filled with DMEM-F12 medium and placed on ice; the number of tubes filled depended on the types of tissue to be dissected. For instance, an E13 and E15 tissue dissection would require at least 2 tubes of medium since E15 and E13 embryos will need to be separated.

2.5.2 Dissection

Pregnant Sprague-Dawley rats and their embryos, bred in-house at Keele University, were killed by approved Schedule 1 methods, following guidelines from the UK Animals, Scientific procedures Act, 1986 and authorization from Keele University's local ethics committee. The embryos were either 15-16 days old (E15-E16) or 12-13 days old (E12-E13), with E0 defined as date of observing vaginal plug. After Schedule 1, the peritoneum was opened using scissors; first horizontally through the skin then vertically to expose the uterine horns containing the rat embryos. Sterilized forceps were used to lift each uterine horn whilst a pair of small scissors was used to trim off tissue attached to the abdomen. Uterine horns were transferred into a 50 mL tube and were transported to the dissection hood. Uterine horns were then transferred into a sterile 100 mm petri dish (Greiner Bio-One, UK). Scissors and forceps were used to remove one embryo at a time and to transfer embryos into a petri dish with DMEM-F12 medium. Rat brains were then dissected out. Since they were older than E11, embryos were decapitated following the Schedule 1 procedure set out in the UK Animals, Scientific procedures Act, 1986. Scissors and forceps were re-sterilized using the bead sterilizer for 10-15 s. For cortical, medial and lateral ganglionic eminence (MGE and LGE) tissue dissection the heads were placed on their side in the petri dish, a vertical cut was made (Figure 2.5) using a pair of small scissors (Fine Science Tools, Cambridge, UK) and the brains were extracted. Brains were transferred into a petri dish containing DMEM-F12 medium (Dunnett & Björklund 2000; Dunnett *et al.* 2006).

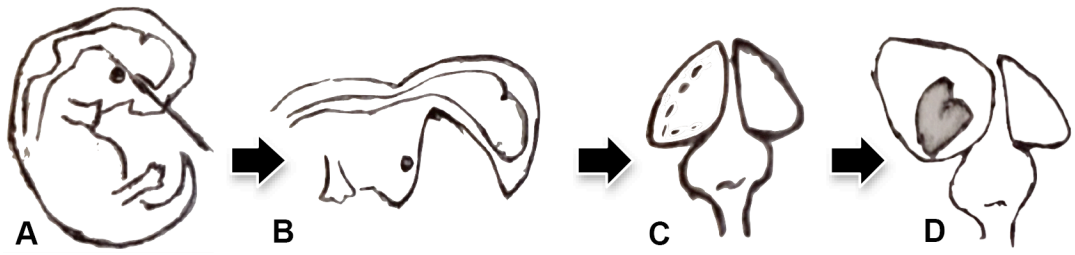

Figure 2.5: Dissection of E15/16 brain tissue. A cut is made, just above the eyes, to expose the rat brain, A and B. Another cut is made, C, to expose the ganglionic eminence. LGE and MGE are split from the ganglionic eminence; the cortex surrounds the ganglionic eminence, D (Dunnet & Björklund 1992).

A longitudinal cut was made along the medial dorsal cortex, close to the midline using fine Vannas dissection scissors (Fine Science Tools, Cambridge, UK). It was opened up to reveal the ganglionic eminence (heart-shaped structure, Figure 2.5). A vertical cut was made, to divide the LGE from MGE tissue. Afterwards, a horizontal cut was made to remove tissue. Tissue pieces were transferred into small Eppendorfs containing DMEM-F12 kept on ice. The tissue covering the ganglionic eminence forms the cortex; pieces of it were collected as well. For dissection of ventral mesencephalon (VM) tissue, 2 vertical cuts were made on the mesencephalic flexure as indicated in Figure 2.6 A. Dissection scissors were used to make 2 cuts: cut 3, horizontal line across the flexure and cut 4, to isolate VM tissue (butterfly shaped) (Figure 2.6 B).

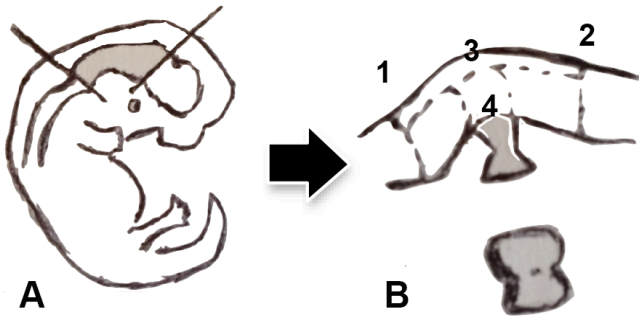

Figure 2.6: E12/13 ventral mesencephalon (VM) tissue dissection. 2 vertical cuts are made on the ventral mesencephalic flexure, A. On the separated flexure, further cuts are made to isolate VM tissue, B (Dunnet & Björklund 1992).

2.5.3 Cell suspension preparation

Tissue pieces were placed into a 1.5 mL Eppendorf containing approximately 1 mL of DMEM-F12. Tissue pieces were washed twice with DMEM-F12 and placed in 0.1% trypsin (Worthington Biochemical Corp., Reading, UK) / 0.05% DNase (Worthington Biochemical Corp., Reading, UK) in DMEM-F12 for 20 min. The pieces were then washed three times with DNase solution before they were mechanically triturated using a Gilson P200 pipette, into individual cells. The cells were centrifuged at 1,200 rpm for 3 min. The supernatant was aspirated out and cells were re-suspended in 200 µL of NCM consisting of: 95% Neurobasal, 1% fetal calf serum (FCS), 1% PSF, 1% B27 supplement (all from Invitrogen, Paisley, UK), 200 mM L-glutamine (PAA, UK), 0.45% glucose (Sigma-Aldrich, Dorset, United Kingdom) (dissolved in deionized water). Dissociated cells were counted using a hemocytometer (Fisher Scientific, Loughborough, UK) and their viability

checked using trypan blue (Sigma-Aldrich, Dorset, United Kingdom) before cell culture. Cells were plated as a drop culture. Seeding density was approximately 20,000-30,000 cells suspended in 50 µL of NCM. Constructs were then flooded with NCM: 300-400 µL for 15.6 mm diameter (24-well plate) substrates, 2-3 mL for 34.8 mm diameter (6-well plate) substrates, after cells were attached to the surfaces.

2.6 Purifying astrocytes and co-culture with neurons

Dissociated cells from LGE tissue were cultured in T-25 flasks with astrocyte culture medium made of: DMEM-F12, 10% FCS, 1% PSF, 1% B27 supplement (all Invitrogen, Paisley, UK), 10 µM L-glutamine, 0.45 % glucose and 10 ng/mL epidermal growth factor (EGF, human recombinant; R&D Systems). Cells were fed with approximately 2 mL of astrocyte medium every 2 days. When cells were approximately 80% confluent, medium was removed and cells were washed once with PBS. After washing, cells were incubated in 1 mL of 0.025% trypsin (Invitrogen, Paisley, UK) for approximately 3 min; the flask was lightly tapped at the sides to make sure the cells were detached. 4 mL of astrocyte culture medium was added to quench the trypsin and the suspension transferred to a 15 mL Falcon tube for centrifugation at 1,200 rpm for 3 min. The supernatant was removed and cells were re-suspended in 2 mL of astrocyte medium. Cells were counted and approximately 30,000 cells in 50 µl were seeded onto non-coated nano-fibres or micro-grooves for 4 h before wells were flooded with media. Pre-seeded astrocytes on scaffolds were cultured for 48 h in astrocyte medium. Thereafter, astrocyte medium was removed and E15-16 LGE neurons were seeded at a density of 30,000 cells in 50 µl of NCM and incubated for 2 h before adding sufficient culture media to submerge the constructs. LGE neurons were kept in culture for 7 days before they were fixed and stained.

2.7 Microfluidic device cell loading

After dissection, dissociated neuronal suspension, for all tissue types, was prepared at a density of 10,000 to 20,000 cells/µL in NCM. NCM was aspirated from reservoirs but not from channels (to avoid bubbles) and a volume of 10 µL cell suspension was loaded into: the cortical, SNc, SNr and GP ports for the five-port microfluidic device (Figure 2.7) and both ports for the two-port

device. A volume range of 15 -20 µL was used for the striatum port since it has a larger volume compared to other ports. For the five-port devices, cell suspension was loaded into the outer compartments first and then the middle (striatum) compartment. Cells were incubated for ~2 h at 37 °C to allow cells to attach. Thereafter, devices were filled up with 150-200 µL of NCM per port and were placed in the incubator and monitored for 12-18 days. NCM was replaced every 2-3 days.

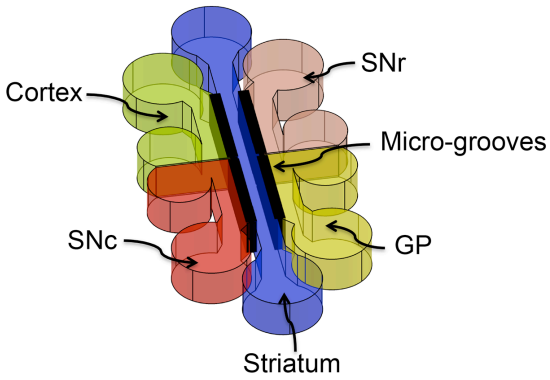

Figure 2.7: Five-port microfluidic device cell loading. Cells were loaded into five ports, one at a time. Different colours indicate ports. Black (separating ports) = tapered micro-grooves.

2.8 Micro-contact printing cell culture and immunocytochemistry

Vials of 3T3 and SH-SY5Y cell lines were removed from a liquid nitrogen freezer. Cell suspensions were thawed and immediately placed in 15 mL tubes containing 4 mL of cell culture medium. The medium consisted of DMEM supplemented with 10% FCS and 1% PSF, (all Invitrogen, Paisley, UK). Tubes were centrifuged at 1500 rpm for 5 min; the supernatant was removed from each tube and was replaced with 1 mL of fresh medium. Cells were re-suspended and placed in T-25 flasks holding 5 mL of medium. Cells were allowed to reach 70-80% confluence at 37 °C, 5% CO_2 before passages 20 and 4 were carried out for 3T3 and SH-SY5Y cells, respectively. For cell passaging, medium was removed from flasks and cells were rinsed with PBS buffer. Trypsin (1 mL) was added to flasks to detach cells. Thereafter, cells were incubated at 37 °C for around 4 min; flasks were agitated slightly to help detach cells from the bottom. Flasks were rinsed with around 4 mL of culture medium and placed (along with the cell suspension in trypsin) into 15 mL tubes. Tubes were centrifuged at 1,500 rpm for 5 min and supernatant was removed and replaced with fresh medium.

Cells were re-suspended and then plated onto printed substrates. Primary cells were obtained from the rat embryonic cortex (details in Section 2.4). 3T3 cells were seeded in suspension in a full volume of medium. SH-SY5Y and primary cells were plated as drop cultures and incubated for ~2 h before they were flooded with medium. After around 7 days in culture, some SH-SY5Y cells were fixed with 4% paraformaldehyde (PFA, Sigma-Aldrich, Dorset, United Kingdom) at 4°C for 20 min and washed with tris-buffered saline (TBS) for 3 times before staining. Cells were incubated in TRITC-conjugated phalloid (dissolved at ~2 µL/mL of distilled water) at room temperature for ~2 h to visualise the structure of the cells. Cells were washed with distilled water 3 times, then the last wash was replaced with DAPI (Vector laboratories, UK), added to cells to identify cell nuclei.

2.9 Microfluidics, nano- and micro-scale substrates immunocytochemistry

Primary cells were washed in PBS to remove cell debris and medium. They were fixed in 4% PFA for 20 min. Cells were washed three times for 5 min in TBS (12 g trizma base from MERCK, Germany, 9 g NaCl, 1 L dH_2O). Afterwards, cells were blocked at 4 °C in 5% normal goat serum (NGS) in TBS-T (200 mL TBS with 400 µL triton X-100) for 1 h. Primary antibodies: GFAP (2.4 g/L Anti-Glial Fibrillary Acidic Protein, Dako, UK) and beta-III tubulin (1 mg/mL, Covance, UK) in 1% NGS in TBS-T were added to the cultures and left overnight at 4 °C. Cells were washed in TBS three times for 5 min. Secondary antibodies (goat anti-mouse fluoprobe 547H and goat anti-rabbit fluoprobe 488 both at dilution ratio of 1:300, Interchim) in 1% NGS and TBS-T were added to the cultures that were then stored in the dark at room temperature for 2 h before washing in TBS. Vectashield hardset mounting medium with DAPI (Vector laboratories, UK) was placed on 22×22 mm coverslips (VWR International, UK) and then upside down onto each nano-fibre and micro-groove construct; for microfluidic devices small amounts (enough to cover cell bodies) of mounting medium was loaded into cell culture ports.

2.10 Digital imaging and quantification of nano-fibre and micro-groove substrates

A Nikon Eclipse 80i microscope (Nikon, Surrey, UK) was used to view constructs and ensure that topographical patterns (nano-fibres and micro-grooves) were visible. Images were captured using a Nikon DS-U2/L2 camera and the measurements for processes angles were carried out using NIS Elements (BR3.00, SP3) imaging software (Nikon, Surrey, UK). The direction of neurite elongation was measured relative to aligned nano-fibres or micro-grooves (Figure 2.8). A best line of fit of the longest part of the neurite was drawn and the angle between this line and groove orientation calculated. Angle measurements were collected and were 'binned' into ranges of: 0-10°, 11-20°, 21-30°, 31-40°, 41-50°, 51-60°, 61-70°, 71-80° and 81-90° angles.

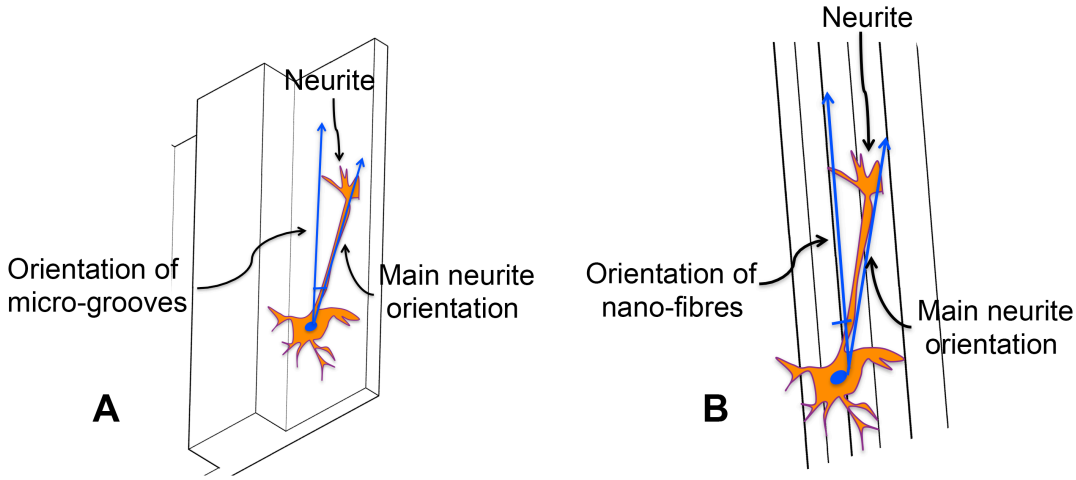

Figure 2.8: Schematic showing measurement of neurite angles against aligned topography. Best line of fit or the longest part of the neurite from cell body was considered as appropriate. A shows how neurite alignment was measured on micro-grooves; B shows measurement on nano-fibres.

2.11 Statistical analysis for neurite alignment (nano- and micro-scale substrates)

GraphPad Prism v6 software was used for statistical data analysis. Two-way analysis of variance (ANOVA) was carried out for: different surface treatments vs. % of neurites aligned and single neurites % of alignment vs. clustered neurites % of alignment. In both cases data used for analysis was obtained from three repeated independent experiments. ANOVA was followed by Bonferroni's tests for post-hoc multiple comparisons. For correlation of the angle of neurite alignment vs. groove width treatment Fisher's exact test for R^2 correlation was performed. Data used for analysis was obtained from a combination of three independent experiments. Values of $p < 0.05$ were considered significant.

2.12 Whole-cell recording

Patch-clamp techniques (Neher & Sakmann 1976) such as whole-cell recording were used to study electrophysiological activity including Na^+ current and spike generation of single cortical and striatal neurons.

2.12.1 Intracellular and extracellular (bath) solutions

Intracellular solution loaded into micropipettes for patch clamp experiments consisted of (mM): KCl 140, $MgCl_2$ 3, EGTA 1, HEPES 5, NaGTP 0.3, pH 7.3 with KOH. Bath solution (neuronal culture medium) was made up of neurobasal medium supplemented with: 1% fetal calf serum (FCS), 1% PSF, 1% B27 supplement (all from Invitrogen, Paisley, UK), 0.5% L-glutamine (PAA, UK), 0.45% glucose (Sigma-Aldrich, Dorset, United Kingdom) (dissolved in deionized water). For acute application of drugs, the puffer pipette was aimed at the cell (a few µm away). To block Na^+ channels, this pipette was filled with 5 µM tetrodotoxin (TTX, Tocris Bioscience, Bristol, UK) dissolved in PBS.

2.12.2 Whole cell voltage clamping

Glass micropipettes were pulled using a vertical electrode puller (GC120TF-10, Clark Electromedical Instruments) with a resistance of 3-4 MΩ. The shanks of the pipettes were coated with cross-country ski wax (Toko AG, Altstatten, Switzerland) to reduce capacitance transients and noise. Whole cell patch clamp recordings were obtained from E15 striatal and cortical neurons cultured for DIV 14-18 days. The microscope (Olympus BX51, UK) was mounted on an anti-vibration table in order to avoid disturbance. Cells grown on a coverslip were transferred from a 24 well plate and placed in the recording chamber (glass microscope slide) with silicon around it to hold the bath solution. The coverslip was secured by placing it on top of a small drop of Sylgard polymer. Bath solution at room temperature was added onto the coverslip. Cells were viewed under the microscope with a 40× objective lens and relayed onto a video monitor using a monochrome solid-state video camera (Cairn, Kent, UK) connected to a frame grabber (PixelSMART).

Two micropipettes were used in the experiment (Figure 2.9). The first one was filled with intracellular solution for recording both cortical and striatal Na^+ currents; the second one was filled with 5 μM TTX to block the Na^+ current generated by striatal neurons. TTX is a neurotoxin, found in some pufferfish, which blocks generation of action potentials in excitable cells by binding to voltage-gated Na^+ channels. For the first pipette, suction was applied to form a seal or 'patch' on the cell membrane via a tube connected to the micropipette holder. Increased suction was then applied to rupture the patch to achieve the 'whole-cell' state. In whole cell recording mode, capacitance transients were manually cancelled. Membrane series resistance compensation (either off or 30-50%) was applied via amplifier controls (EPC-7, List-Medical, Darmstadt, Germany).

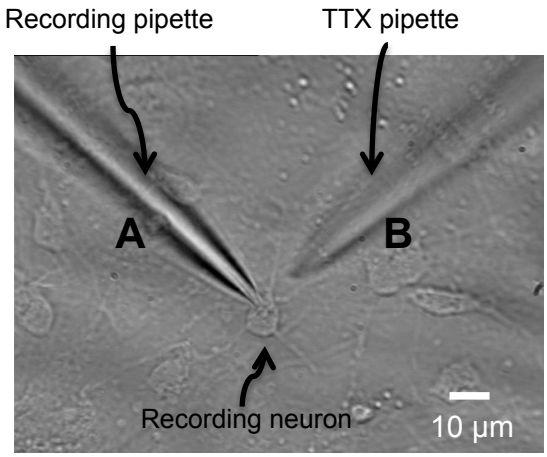

Figure 2.9: Micropipettes used for whole cell recordings. A: The first pipette was used to patch and record intracellular current through the cell. B: The second pipette was used to deliver TTX to the cell.

Resting potential for cortical and LGE cells was −24 to −54 mV; holding potential ranged from −60 to −80 mV. Whole-cell currents were digitized and stored on disk. For the second micropipette, a pneumatic picopump (PV 820, World Precision Instruments, FL, USA) was used to eject TTX onto the cell. TTX was used to confirm the presence of Na^+ current. Signal software with a 1401-*plus* interface (Cambridge Electronic Design, Cambridge, UK) was used for running these experiments.

2.13 Calcium imaging

Five-port microfluidic devices with cortical, striatal, SN and GP cells cultured for DIV 14 to 18 were rinsed with loading saline consisting of (all from Sigma-Aldrich, Dorset, UK, unless otherwise stated): 150 mM NaCl (Merck, Darmstadt, Germany), 4 mM KCl, 1 mM $MgCl_2$, 10 mM glucose, 2 mM $CaCl_2$ and 10 mM HEPES, dissolved in sterile, deionized water (dH_2O). Devices were loaded with a Ca^{2+} indicator, Fluo-4 (Peyrin *et al.* 2011) acetoxymethyl ester (AM) (Life Technologies Ltd, Paisley, UK). Fluo-4 dye was dissolved in dimethyl sulfoxide (DMSO) mixed with 20% pluronic F-127 solution (Sigma-Aldrich, Dorset, UK) and a stock of 0.5 mM was made up. Cells were exposed to 2 μM of dye in dH_2O for 30 min at room temperature. Afterwards, the dye was washed off with loading buffer and DMEM-F12 was added to cells.

Recordings of Ca^{2+} fluorescence oscillations were captured on a Nikon Eclipse 80i microscope; NIS elements software (BR3.00, SP3.) was used to record activity at 5 frames per second for 3-5 min. At certain periods after recording Ca^{2+} oscillations in the 5-port device, in one of the 5 ports, DMEM-F12 was replaced with TTX (1 μM in DMEM-F12). This was done to enable comparison between oscillations within the whole network before and after TTX was applied. Analysis of Ca^{2+} fluorescence intensities were performed using an ImageJ (National Institutes of Health, Maryland, USA) function called 'plot Z-axis profile'. The function plots the mean of the values of changes in intensity against number of slices through an image for a particular ROI (Figure 2.10). Fluorescence intensity read-outs (X and Y values, Figure 2.10B), corresponding to mean intensity and slice number (Figure 2.10A), were exported to a Microsoft Excel spreadsheet. Mean intensity or changes in fluorescence relative to background fluorescence (F/F_0) were plotted against number of slices or time (t).

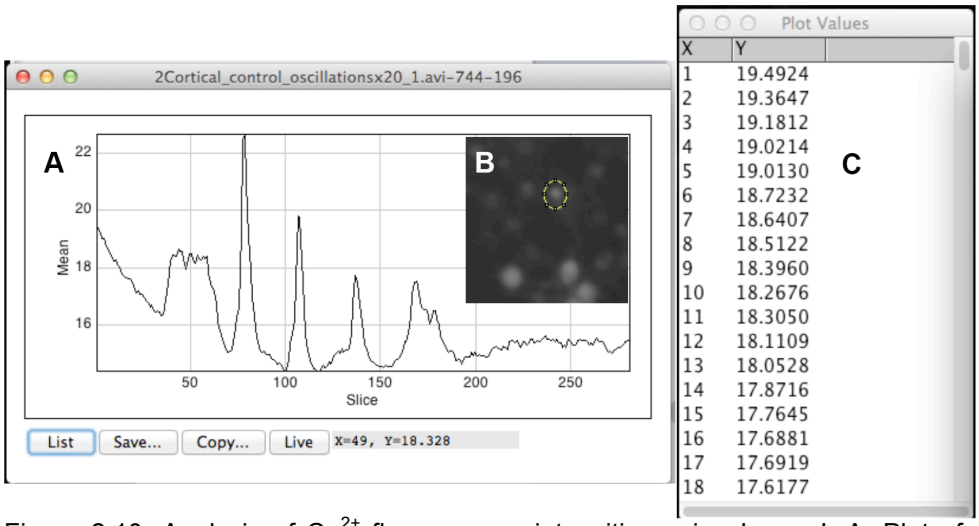

Figure 2.10: Analysis of Ca^{2+} fluorescence intensities using ImageJ. A: Plot of slice number vs. mean intensity values. B: A ROI with the plot summary displayed in part A of the figure. C: Plot values for B, corresponding to plot slice number vs. mean intensity in A.

2.13.1 Microfluidic inter-port leakage test: fluorescence intensity measurements

Rhodamine B isothiocyanate dye (Sigma-Aldrich, Dorset, United Kingdom) was used for a test to ensure TTX-medium i.e. 1 µM TTX in DMEM-F12 medium (Section 2.10) was not spilling into neighbouring ports. The dye (rhodamine) powder was dissolved in a buffer and the solution was loaded into the middle port (Figure 2.11). The rest of the ports were filled with undiluted Na^{+} carbonate buffer (0.1 M from Sigma-Aldrich, Dorset, United Kingdom, prepared in distilled water). A Nikon Eclipse 80i microscope (Nikon, Surrey, UK) was used for imaging.

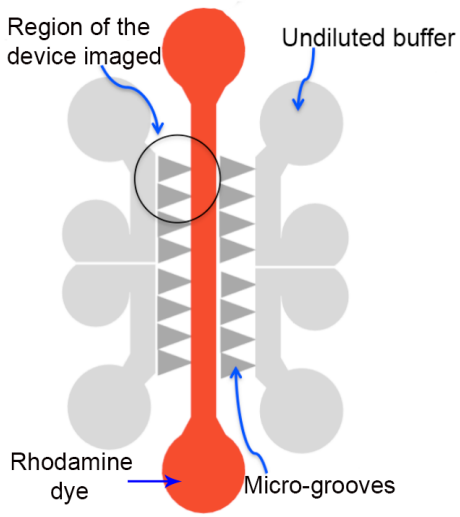

Figure 2.11: Fluorescence intensity measurements for testing inter-port diffusion within the microfluidic device. Schematic of a microfluidic device showing the middle port loaded with rhodamine dye and the rest of the ports loaded with undiluted buffer.

Images were captured at: 0, 10, 30, 60 and 120 min for the middle port as well as the upstream port; and the middle port with the downstream port were also captured at 120 min. Fluorescence intensity measurements from the middle port were compared to other ports. ImageJ (National Institutes of Health, Maryland, USA) application was used to analyse intensity. First, fluorescence (.tiff) images were opened in ImageJ. For each image, the type was changed to an 8-bit grey scale before analysis. The '*mean grey value'* option was selected under the '*analyse*' tab and the '*set measurements'* option. A line was drawn across the image as depicted in Figure 2.11. The '*plot profile*' function was used to measure intensity. If there was inter-port leakage, the fluorescence intensity across ports surrounding the middle port was expected to rise as the concentration of the dye rises in the ports. The intensity measurements were exported from ImageJ to Microsoft Excel to determine changes in intensity across the image.

Chapter 3: Alignment of striatal neurites on nano- and micro-scale substrates

3.1 Introduction

Alignment of CNS neurites on fabricated substrata was evaluated. PLA nano-fibres and PDMS micro-grooves were fabricated to provide contact guidance to developing processes for primary striatal cells. Patterned surfaces were also coupled with astrocytes to provide biological cues, to promote neuronal adhesion and guide neurite extension. Glia cells in the CNS and PNS support neurons in a number of functions. Schwann cells in the PNS and oligodendrocytes in the CNS produce myelin sheath that wraps around neurons to provide insulation and hence, speed up impulse transmission. Glial cells provide directional cues for neurons *in vivo*. During development of the cerebral cortex, progenitor cells within the ventricular zone (VZ) differentiate into radial glia cells and projection neurons. Radial glia extend their processes from the VZ to the cortical plate. The processes provide a path for projection neurons to migrate towards the cortical plate (Hatten 2002; Fricker-Gates 2006; Pinto & Götz 2007).

In vitro, macroglial cells such as astrocytes can provide topography and/or biological cues to direct axon extension (Recknor *et al.* 2004; Deumens *et al.* 2004; Schnell *et al*. 2007; East *et al*. 2010). Some studies have reported that culturing DRG neurons on pre-aligned astrocytes led to DRG axons orientating parallel to aligned astrocytes (Recknor *et al*. 2004; Alexander *et al.* 2008). In addition to directional cues, i.e. imposed by chemoattraction or chemorepulsion, and biological topography cues, other important cues are involved during development of the CNS. Adhesive cues, such as those received from LN and fibronectin in the ECM or cell adhesion molecules expressed by glial cells, generate micro-environment permissive to neuronal attachment and axon protrusion (Raper & Mason 2010).

In the current study, PLA nano-fibres were directly compared with PDMS micro-grooves to see which topography best aligned striatal neurites. Topographies were coated with either PLL-LN or astrocytes to explore how these biological/biochemical cues influenced neurite alignment. Micro-groove structures fabricated with groove width ranging from 20-80 μm enabled evaluation of whether varying groove width would affect neurite alignment. Furthermore, an evaluation was made on neurites emanating from clusters of cell bodies on micro-groove substrates and different alignment tendency compared to those extending from single cell bodies.

3.2 Experimental methods

Fabricated nano- and micro-scale substrata were either incorporated with chemical or biological cues. For chemical cues, constructs were pre-coated with 100 µg/mL PLL and 10 µg/mL LN (sections 2.1 and 2.2); for biological cues, constructs were pre-seeded with pure astrocytes (section 2.6), prior to neuron culture. Glass coverslips, pre-coated with PLL then LN, were used as positive controls for each experiment. Primary dissociated cells acquired from brain tissue, as discussed in section 2.5, were cultured on both nano- and micro-scale constructs. Striatal neurons were kept in culture for 7 days before they were fixed and stained for GFAP and beta-III tubulin. Mounting medium with DAPI was used to stain nuclei. Images were acquired via an epi-fluorescent microscope and the measurements for processes angles, as previously studied by (Mahoney *et al.* 2005; O'Dell *et al.* 2012; Riblett *et al.* 2012; Chua *et al.* 2014), were carried out using NIS Elements imaging software. Neurite orientation was measured relative to nano-fibres' or micro-grooves' main orientation axis. Angle measurements, as discussed in section 2.10, were 'binned' into: 0-10°, 11-20°, 21-30°, 31-40°, 41-50°, 51-60°, 61-70°, 71-80° and 81-90° angles.

3.3 Results and discussion

3.3.1. Neurites' response to PLL and LN-coated substrates

Aligned nano-fibres (Figure 3.1 A), attached to coverslips, had an average diameter of 500 nm (Yang *et al.* 2011). PDMS micro-grooves (Figure 3.1 B) had width ranging from 20-80 µm and depth of 2.2 µm. Dissociated cells cultured on non-coated substrates (of both nano-fibres and micro-grooves) did not readily attach and had poor viability i.e. cell bodies neither elongated nor produced neurites (Figure 3.2). Cells, particularly neurons, are required to adhere to cell culture surfaces and develop neurites in order to study response (of neurites) to topography features. Permissive reagents promote cell adherence to surfaces; this is achieved by interaction between integrins on cell surfaces with either ligands provided by ECM proteins such as LN or polyamino acids such as polylysine (Khan & Newaz 2010).

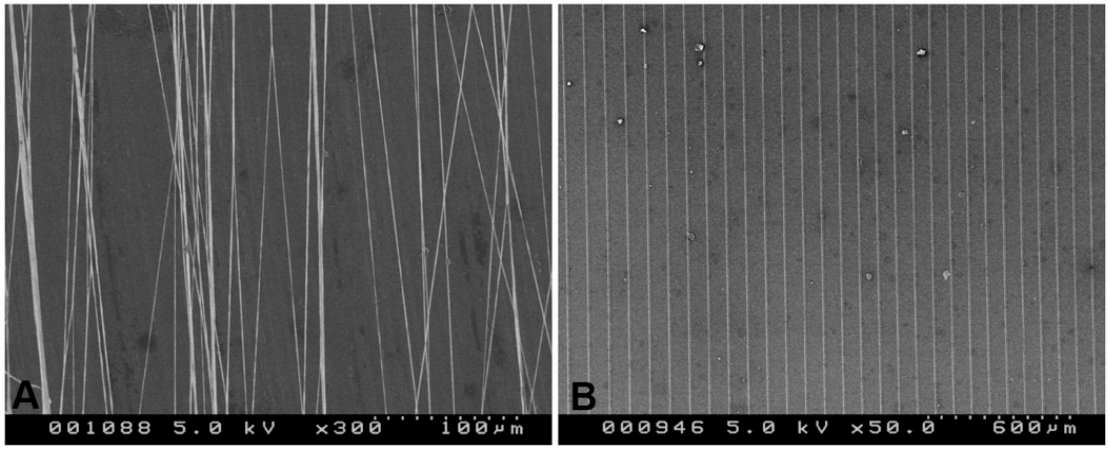

Figure 3.1: Topographic cues presented to cells. A: Aligned PLA nano-fibres B: PDMS micro-grooves.

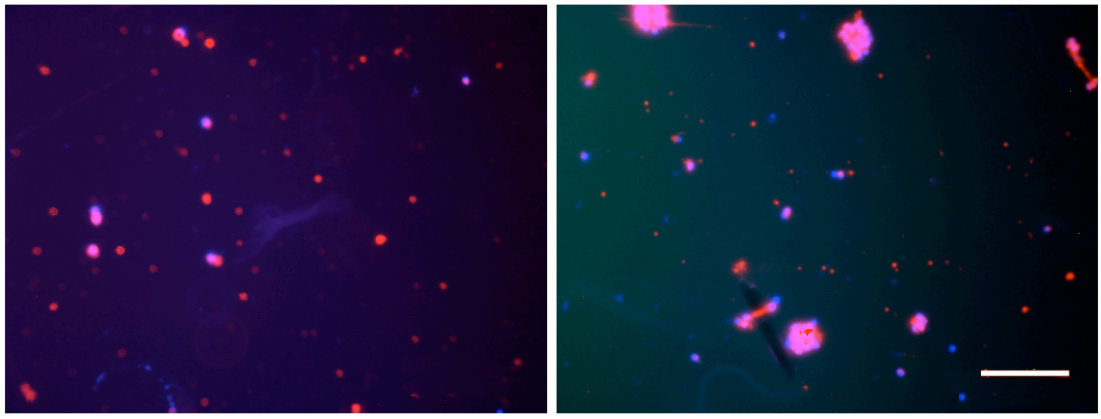

Figure 3.2: Neuron response on non-coated nano-fibre substrates. Neurons attached to the substrate, but had low viability; red dots/clusters indicate neurons that are in the process of or have undergone cell death. Red = β-III-tubulin stained neurons, blue = DAPI stain for cellular nuclei. Scale bar = 100 µm.

Viability of neurons as well as response of neurites to topography on substrates was studied. Striatal neurons on PLL and LN coated micro-grooves (MPL) had very good viability; neurites developing from soma were guided by micro-scale topography (Figure 3.3). Electrospun nano-fibres were coated with PLL and LN biochemical cues (NPL) prior to striatal cell culture. As mentioned before, chemical cues promote adherence of neurons as well as neurite protrusion (Miller *et al.* 2002; Hoffman-Kim *et al*. 2010). Cell attachment to the substrate and viability were very good. Nano-fibres provided topography cues to direct orientation of neurites developing from soma (Figure 3.4). PLL and LN cell adhesion molecules have previously been used in primary cell culture studies in the lab. For instance, Shin *et al.* studied the functional properties such as spontaneous postsynaptic and Na^+-dependent electrical activity (using patch clamp), of striatal

neurons derived from mouse embryonic stem cells (mESCs) (Shin *et al*. 2012). These properties were compared with properties of primary striatal neurons cultured on PLL and LN coated coverslips.

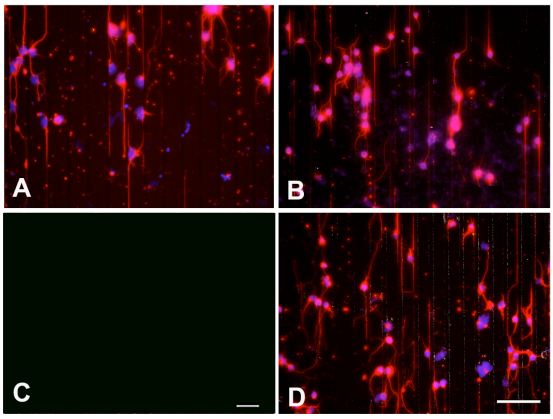

Figure 3.3: Micrographs indicating the response of neurons to PLL and LN coated micro-grooves (MPL). Red = β-III-tubulin labelled neurons, blue = DAPI stained cellular nuclei. Micrograph C indicates negative control, non-specific staining of grooves in the absence of cells, scale bar = 100 µm. Scale bar on D = 100 µm and applies to A and B micrographs as well.

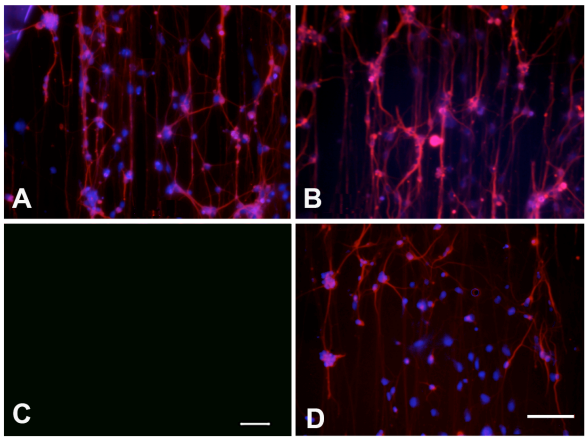

Figure 3.4: Micrographs of neurite alignment on electrospun nano-fibres pre-coated with PLL and LN (NPL). Red = β-III-tubulin labelled neurons, blue = DAPI stained cellular nuclei. Micrograph C indicates negative control, non-specific staining of nano-fibres in the absence of cells, scale bar = 100 µm. Scale bar on D = 100 µm; applies to micrographs A and B as well.

Neurons on all substrates: micro-grooves with PLL and LN (MPL, Figure 3.5 A), micro-grooves with pre-seeded astrocytes (MpA, Figure 3.5 B), nano-fibres with PLL and LN (NPL, Figure 3.5 C) and control (PLL and LN on glass coverslips with no topographic structure, Figure 3.5 D) had very good attachment and viability. This supports reports from several studies of the importance of poly(amino acids) including PLL and ECM proteins including LN, in promoting cell attachment and development of neurites (Ruardij *et al*. 2000; Khan & Newaz 2010; Roach *et al*. 2010; Gladwin *et al*. 2013).

Neurons were attached to the constructs approximately 2 h after seeding; it was possible to check morphology of the cells to distinguish neurons from astrocytes at this point. Small neurites were easily noticeable emanating from cell bodies at approximately 24 h after neurons were seeded. Some processes were not easily observable (i.e. before immunostaining) since they were very fine and for MPL, extending closely along the lower corners of the micro-grooves. Following immunohistochemistry most neuronal cell bodies were observed randomly orientated, but their processes (mainly for single neurons on MPL substrates) were orientated along the topographic structure. As discussed in section 2.10, the direction of neurite elongation was measured with respect to the topographic pattern, data being binned in terms of the degree of alignment, e.g. greater alignment was recorded as a smaller angle between the neurite and surface topography direction.

Neurites on control substrates were randomly oriented due to the absence of topography cues, and neurite angles measured on these control coverslips were evenly distributed across all bins i.e. from 0-10° through to 81-90° (Figure 3.5 D and E). Combination of both topography and chemical cues had a significant effect on neurite alignment (Figure 3.5 E; 2 Way ANOVA: $F_{(24,72)} = 13.10$, $p < 0.0001$). MPL and NPL had the most significant effect on neurite alignment compared to control (MPL vs. control: Tukey, $t = 32.70$, $p < 0.0001$ and NPL vs. control: Tukey, $t = 24.27$, $p < 0.0001$). On both micro- and nano-topographies, significantly more neurites were aligned within 0-10° of the topographical cue. Approximately 44% of neurites on MPL were angled within 0-10° of the topography and 36% for NPL (Figure 3.5 E).

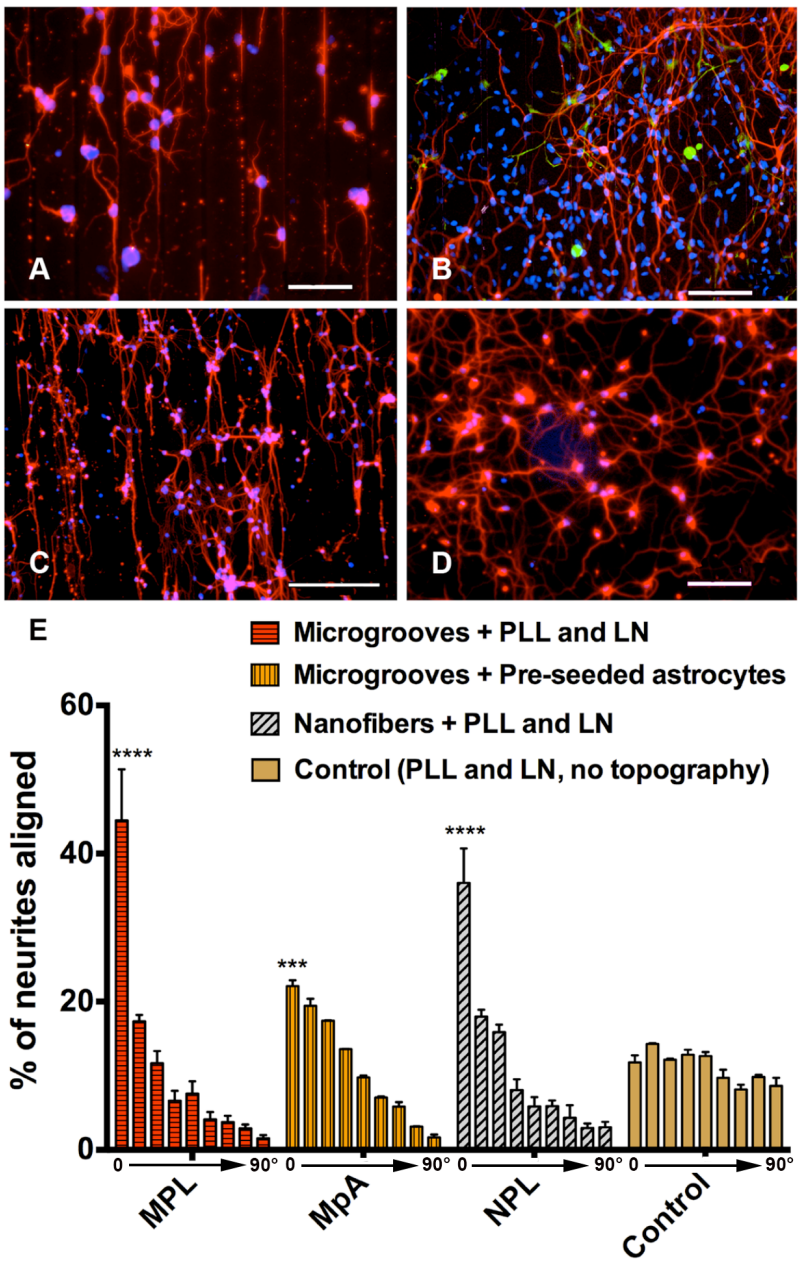

Figure 3.5: Fluorescence micrographs indicating neurite behaviour on various substrates: A = micro-grooves coated with PLL and LN, MPL; B = micro-grooves coated with astrocytes, MpA; C = nano-fibres coated with PLL and LN, NPL; & D = control coverslips coated with PLL and LN. Red = β-III-tubulin labelled neurons, green = GFAP labelled astrocytes and blue = DAPI stained cellular nuclei. Scale bars = 100 µm. Graphs (below micrographs, E) indicate the angle of neurites with respect to topographic direction, from 0-10° (first bar) to 80-90° (final bar) for each treatment. (****, $p < 0.0001$ & ***, $p < 0.001$) indicate significant alignment vs. controls. Data obtained from three independent repeated experiments.

Neurites responded less well to topography on substrates pre-seeded with astrocytes. Neurons were seeded on to astrocytes at 48 h. At this point in time, it was observed that most of the astrocytes pre-seeded on non-coated micro-groove substrates had failed to attach effectively. After 48 h in culture, any attached astrocytes were still spherical; they were mainly individual cells

evenly distributed over the substrate. However, after 7 days immunohistochemistry revealed that astrocytes were clearly present in the cultures, had attached and developed a typical morphology and had extended processes (Figure 3.5 B). Neurons responded to MpA constructs (micro-grooves with pre-seeded astrocytes) but to a lesser extent than MPL (~21% for MpA at 0-10^0 compared with ~12% for non-topography substrate, Tukey, $t = 9.20$, $p < 0.001$).

Astrocytes on non-coated micro-grooves did not show alignment of their processes with the grooves. Most neurons in these pre-seeded cultures formed colonies, often closely associated with astrocytes. Observations from the current study suggest neurites that were aligned, i.e. oriented within 0-10° of the micro-grooves, only occurred when they extended from neurons not in contact with astrocytes. However, it was found that astrocytes were highly directionally responsive to non-coated nano-fibres (Figure 3.6). At approximately 4 h after seeding, astrocyte alignment could be seen in some areas of the substrates, i.e. astrocytes initially rounded just after seeding, were starting to elongate along topography. Most astrocytes were aligned parallel to topography after 72 h in culture.

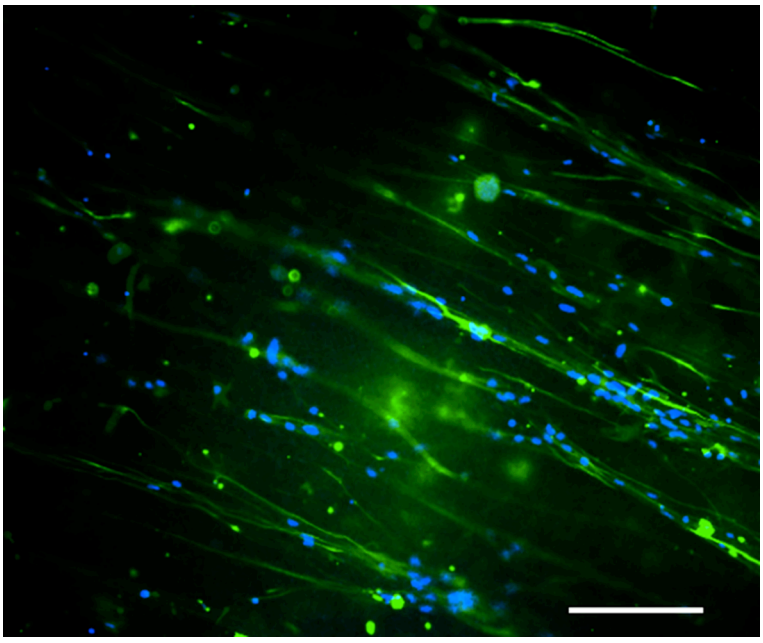

Figure 3.6: Astrocytes aligned on non-coated nano-fibres after DIV 7 in culture. Green stained GFAP astrocytes response to aligned nano-fibres (diagonally positioned). Scale bar = 50 µm. Blue indicates DAPI-labelled nuclei of all cells.

Substrates with topographic structures were compared against each other to determine whether there was any significant difference amongst them. Substrates with PLL and LN coating (MPL and NPL) showed significantly better alignment of neurites than neurites from neurons cultured on MpA substrates (MPL vs. MpA, Tukey, $t = 23.50$, $p < 0.0001$ and NPL vs. MpA, Tukey, $t = 15.06$, $p < 0.0001$). Comparing the two PLL and LN conditions, micro-grooves had more aligned neurites (within $0\text{-}10^0$ of the topographical structure) than nano-fibres (Tukey, $t = 8.43$, $p < 0.01$).

As mentioned earlier, astrocytes have been reported to provide adhesion and growth promoting cues to neurons as well as neurite outgrowth and directional guidance cues. Astrocytes promote cell proliferation (Lim & Alvarez-Buylla 1999), stem cell differentiation (Yang *et al*. 2014) and survival and extension of neurites *in vitro* (Sørensen *et al*. 2007). Findings in the current study suggest that the presence of pre-plated astrocytes on micro-groove surfaces, even though they initially did not attach well to non-coated grooves, promoted adherence and development of striatal cells. Striatal cells cultured on non-coated micro-groove substrate, i.e. in the absence of chemical (PDL and LN) or biological (astrocytes) cues were rounded, dark, shrivelled and did not develop neurites.

3.3.2 Neurite behaviour on PLL and LN pre-coated micro-grooves

It was discovered that groove height (2.2 µm) restricted, and therefore directed, the orientation of neurites on MPL substrata. Studies have reported the influence of groove depth, ranging from 0.2 µm to 15 µm (Francisco *et al*. 2007), on neurite alignment. Hoffman-Kim *et al.* established a relationship between groove depth and cell alignment or neurite outgrowth (Hoffman-Kim *et al.* 2010). Alignment and outgrowth increased with increase in depth from 0.2 µm to 4 µm; no alignment was observed below 0.2 µm; where neurites almost ignored the topography structure. Increase in groove height correlated to increase in alignment for DRG neurites since they were physically restricted to grooves on which they were located and therefore found it difficult to cross to adjacent grooves (Miller *et al*. 2002; Hoffman-Kim *et al.* 2010).

In the current study, dissociated cells were spread out such that no clumps or clusters were observed after seeding. However, it was discovered that some cells had formed clusters after

immunostaining; a cluster of cells was defined as being when two or more soma (cell bodies) were located at a distance approximately 20 μm or less than each other. Most neurites emanating from single or isolated neurons were much more influenced by topography cues compared to those from clusters of two or more neurons (Figure 3.7). Neurites from 'single' neurons were significantly better aligned to micro-grooves (Single vs. cluster: Sidak, $t = 44.95$, $p < 0.0001$) than neurites from '*clusters*' of neurons. It is likely that orientation of neurites from clusters was influenced more by cues from close by cells rather than topography cues.

Dissociated cells were cultured on micro-grooved substrates with varying groove width (20 μm to 80 μm) to determine if alignment of neurites extending from soma was affected by changes in groove width. Neurite orientation did not correlate to groove width (Figure 3.8, $R^2 = 0.0284$). It is possible this was due to most cells extending neurites that followed groove walls after contact, regardless of where the cell soma was located within the groove, their processes finding a groove edge and then extending along this. This finding is somewhat contrasting to what other studies have reported. In general, it has been shown that groove or micro-channel width influences alignment. For example, alignment of PC12 neurites reduced from 90% to 75% when the width of gratings 200 μm deep was reduced from 750 nm to 500 nm (Cecchini *et al.* 2008).

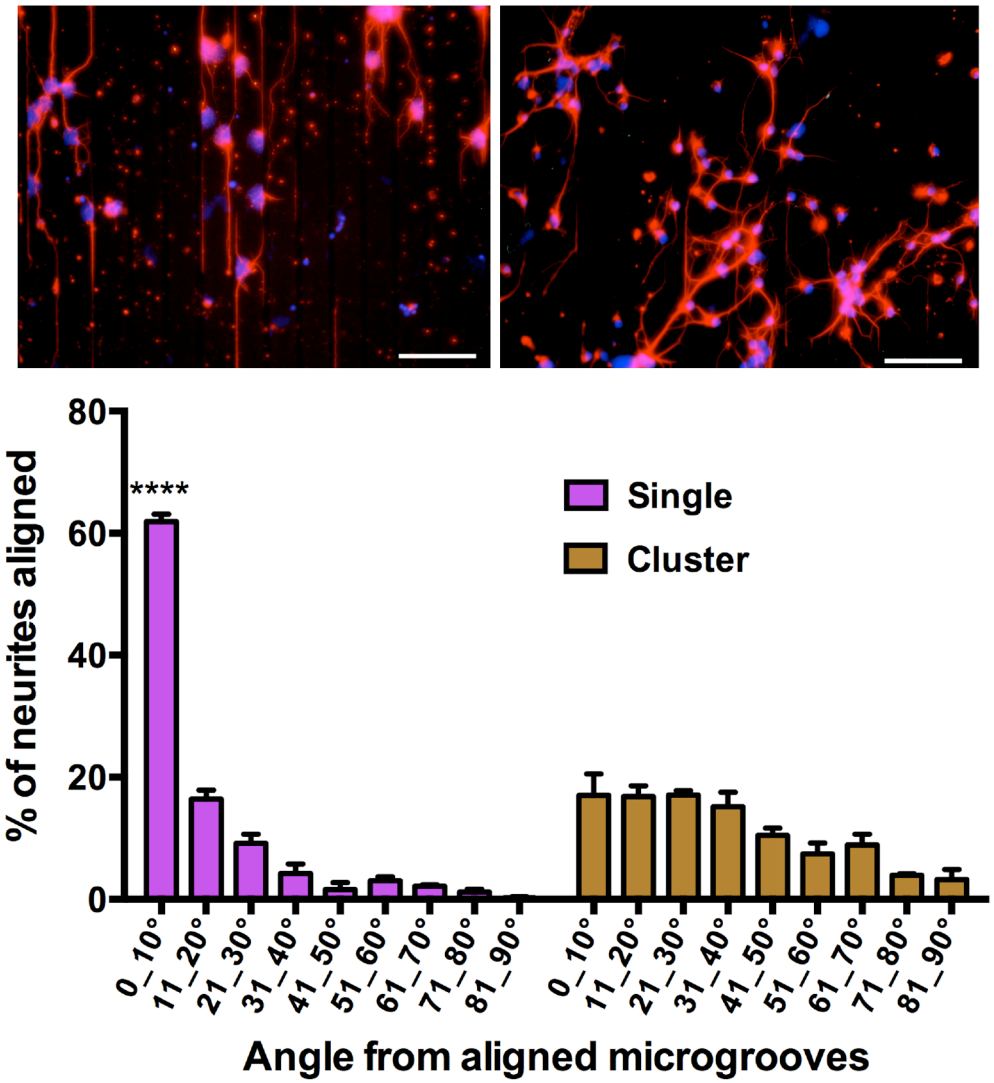

Figure 3.7: Neuronal culture on PLL and LN-coated micro-grooves. Neurites from single cells, A, are more responsive to micro-grooves than neurites from clusters, B. Red = β-III-tubulin labelled neurons and blue = DAPI stained cellular nuclei. Scale bars = 100 μm. Graphs (below micrographs) indicate quantification of angle of neurites with respect to topographic direction. (****, $p < 0.0001$) indicates significant alignment of neurites from single cells vs. clusters. Data obtained from three independent repeated experiments.

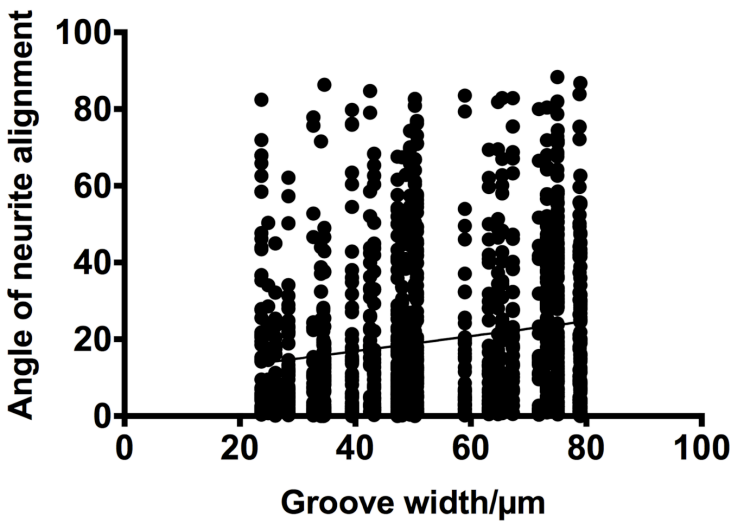

Figure 3.8: Neurite alignment on grooves pre-coated with PLL and LN (MPL) versus groove width. Black dots represent individual neurite angles measured. Line of best fit R^2 = 0.0284, indicating no correlation. Data combined from three independent experiments.

When the same cell type was cultured on 2-3 μm deep substrates with 5 μm and 10 μm widths, more alignment was observed on 5 μm wide stripes (Yao *et al.* 2009). Furthermore, polyimide patterns with height of 11 μm and width ranging from 20-60 μm showed that all widths were effective in guiding neurite orientation, however more significant alignment was observed on smaller channels of 20-30 μm width (Mahoney *et al*. 2005). Therefore, cell response to groove width may be strongly dependent on the cell type as well as the topography. Findings from the current study suggest that groove height of 2.2 μm was more influential in guiding neurite extension compared to width ranging from 20-80 μm. Future work will involve studies to determine if neurites exposed to widths below 20 μm and above 80 μm would also be influenced by height of groove walls.

3.4 Conclusions

Dissociated CNS neurons were sensitive to nano-, micro-scale topographic substrates; they provided directional guidance of neurites. The chemical cues PLL and LN, introduced to the surfaces, are essential for dissociated CNS neurons to attach and develop neurites. Pre-seeded astrocytes were used as biological cues but diverted the neurites from aligning to topographic cues to some extent. Micro-grooved substrata with chemical cues (MPL) yielded the best neurite

alignment, ~44% compared to ~36% for nano-fibres (NPL) and ~21% for micro-grooves with pre-seeded astrocytes (MpA).

On MPL substrata, it was found that to achieve even better neurite alignment cells needed to be spread out to ensure that the topography cue was dominant; otherwise neurites receive cues from other cells and disregard the topographic structure. Changes in groove width did not affect the degree of neurite alignment whereas groove height (2.2 μm) strongly influenced alignment. The results presented here imply that PDMS micro-grooves coated with PLL and LN provide a valuable technology for controlling CNS neurite orientation. These findings were used as foundation for building basal ganglia neuronal circuitry using microfluidics in Chapters 4-5.

Chapter 4: Design and fabrication of a microfluidic neuronal device

4.1 Introduction

The BG circuitry is compartmentalised, i.e. it consists of discrete nuclei such as the striatum and the GP, located in distinct regions of the deep brain and interconnected via extending axons (Bolam *et al.* 2000; Yelnik 2002). Designing compartmentalised systems that closely mimic the architecture of neuronal populations in the brain is essential. Advances in microfabrication techniques, inspired by established procedures used to manufacture integrated circuits in the semiconductor industry (Voldman *et al*. 1999), have led to fabrication of microfluidic devices for cell culture (Park & Shuler 2003). Microfluidic devices involve manipulation of small volumes of fluid ranging from μL to aL (attolitres, 10^{-18} litres) (Whitesides 2006; Halldórsson *et al.* 2014). The microfluidic, compartmentalized cell culture system addresses a number of challenges faced by conventional cell culture methods (Table 4.1). Microfluidic devices offer substrate design flexibility; architectures of cell culture vessels and channels can be designed via computer aided design software, such as AutoCAD. Therefore, surface chemical and topography microfabrication can be tailored to address specific challenges depending on a number of factors including: cell type, material biocompatibility and device application (Millet & Gillette 2012; Halldórsson *et al.* 2014).

Table 4.1: Summary of benefits of using microfluidic devices for separated cell co-culture compared to conventional or macroscopic cell culture vessels such as flasks and well plates (Millet & Gillette 2012; Halldórsson *et al.* 2014).

Microfluidic devices	**Conventional cell culture vessels**
Cell culture substrate design flexibility	Fixed substrate design
Small volumes – less reagent consumption	Larger volumes required to flood cells – more reagent consumption
Laminar, steady and controllable fluid flows	Cells exposed to turbulent forces
Portable and self-contained	Not easily portable
Perfusion is possible	Perfusion is difficult to achieve
Controlled and reproducible co-cultures	Co-cultures difficult to control and reproduce

Microfluidic devices permit co-culture of different cell types within defined compartments. For instance, Majumdar *et al* developed a two-port microfluidic device for co-culturing neurons and glia cells (Majumdar *et al.* 2011). Cells were cultured in separate ports with: length, width and height of 6,000, 800 and 100 μm, respectively. The device, fabricated using polydimethylsiloxane (PDMS) polymer via soft lithography, consisted of a valve barrier that enabled reversible isolation between the neuron and glia ports. Micro-channels connecting the two ports had: length, width and height of 10,000, 100 and 5 μm, respectively. Prior to cell culture the neuron chamber was coated with LN, whilst the glia chamber was coated with type 1 collagen. Cells were cultured separately until glial cells reached confluence. Thereafter, the valve barrier separating the glia and neuron ports was deactivated to enable connectivity between neuron and glia ports. The study found that neurons remained viable for more than 3 weeks in the presence of glia or glia-conditioned media compared to less than 1 week, in their absence.

Microfluidic devices have been used to enable co-culture of diseased and healthy cell populations for studying development of different diseases (Lippens *et al*. 2007; Kunze *et al.* 2011; J.-Z. Wang *et al.* 2013). For example, in a study by Kunze *et al.* a microfluidic-based model for an *in vitro* study of Alzheimer's disease was developed (Kunze *et al.* 2011). The Tau protein is associated with axonal transport and stabilization of the microtubule structure of neurons. The abnormal function or hyperphosphorylation of the tau protein is associated with the pathology of Alzheimer's disease. Two populations of primary cortical neurons were cultured separately in device compartments consisting of length, width and height of 3,000, 200 and 100 μm. Okadaic acid (OA) was loaded into one cortical cell population to induce neurotoxicity. OA causes hyperphosphorylation of the tau protein. In its normal state, the Tau protein consists of 2-3 moles of phosphate, whereas in the abnormal, hyperphosphorylation state the protein consists of 5-9 moles of phosphate. The study found that cells in OA-loaded port exhibited phosphorylated Tau aggregates, whereas cells in the other port (i.e. healthy cells not exposed to OA) presented evenly distributed Tau.

In addition to design flexibility, microfluidic devices also offer material versatility. Polymers are mainly used for device fabrication since they are less expensive and flexible (easily conforms to different surfaces) compared to glass and silicon (Tang & Whitesides 2009). PDMS is the most commonly used polymer due to its optical transparency and good thermal stability (Xia & Whitesides 1998; Whitesides 2006; Tang & Whitesides 2009; Mehling & Tay 2014); it is inert and can easily form irreversible sealing without the need for high temperature, pressure or voltage, compared to glass, thermoplastic and silicon devices (Tang & Whitesides 2009). PDMS is well suited for use with aqueous solvent, such as cell culture media, although has limitations for widespread usage due to swelling of the PDMS caused by ingress of some organic solvents. Tailor-made design masks fabricated from computer-aided drawings are used for building master templates via a process of photolithography. An exact replica or its inverse, of the design pattern is imprinted via light exposure onto a substrate using photoresists (light-sensitive polymers, Chapter 2, Section 3) (Jones 2000).

In the previous chapter it was found that biochemical cues were required to promote adherence of dissociated primary neurons and consequently, development and extension of neurites. Biochemical cues were supplied by polyamino acid molecules and ECM proteins provided by PDL and LN, respectively. Directional guidance of neurites extending from soma was provided by aligned micro-grooves (Chapter 3). This chapter discussed the fabrication of more complex *in vitro* neuronal circuitry to mimic *in vivo* BG circuitry. Compartmentalised devices are paramount when trying to mimic brain circuitry since multiple cell populations can be co-cultured in one device in a more controllable and reproducible manner compared to other cell culture methods. Herein, design and fabrication of a compartmentalised, five-port microfluidic device was evaluated for its ability to direct the development of neuronal circuitry in culture. SN, GP and striatal cells, developing from the VM, MGE and the LGE, respectively; and cortical cells were co-cultured in a five-port microfluidic device to fabricate BG circuitry.

4.2 Experimental procedures

4.2.1 Design considerations

AutoCAD software was used to draw templates for building microfluidic devices. Design of the five-port microfluidic device (Figure 4.1A) was influenced by the BG circuitry model depicted in Figure 4.1B. Positioning of ports in the device was designed to reflect the arrangement of *in vivo* BG circuitry. Micro-grooves separating cell culture ports were designed to provide directed guidance to orientation or outgrowth of axons, e.g. orientation of cerebral cortex axons is directed from the cortex to the striatum port. Groove openings of 15 µm were designed to limit cell bodies entering the micro-grooves. In addition to the 15 µm openings, 25 and 50 µm groove openings were used for groove opening optimisation, particularly to study and compare the number of axons entering the micro-grooves. Exit ends for all devices were 5 µm wide. Groove length of 1,050 µm was designed to selectively allow axons to extend into neighbouring ports and establish connectivity.

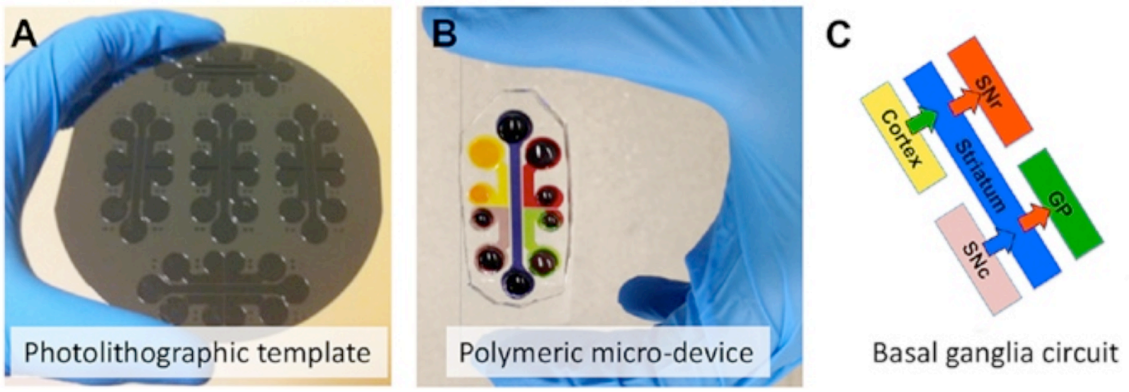

Figure 4.1: Microfluidic design and the basal ganglia circuit (A) Photolithographic master template (B) Polymeric microfluidic or micro-device. Colours displayed on photograph correspond to colours on the basal ganglia circuit (C). Arrows shown in C: green = glutamatergic excitatory axonal projections, red = GABAergic inhibitory projections and blue = dopaminergic projections.

Following AutoCAD design, two masks were printed on chrome/soda lime glass: one for micro-grooves and another for cell culture ports; this was carried out by JD PhotoTools LTD. Masks were then used to fabricate microfluidic devices following the two-stage procedure displayed in Figure 4.2. For the photolithography process, two photoresists, SU-8 50 (viscous) and SU-8 10 (less viscous) were used. The spin speed and viscosity of the photoresist determined the resulting thickness, or height of the structure built on the silicon wafer surface. The first photoresist,

SU-8 10, was used to produce micro-groove patterns (Figure 4.2 A). Cell ports or compartments (Figure 4.2 B) were then overlaid, using the second photoresist, SU-8 50, on top of micro-grooves to produce a photoresist master (Figure 4.2 C). Following the photolithography process, i.e. fabrication of master, PDMS was cast onto the master using the soft lithography technique (Figure 4.2 D) to produce an elastic mould of ports and micro-grooves. The height of micro-grooves was intended to provide physical constraint and guidance to developing axons. The mould was irreversibly bonded to a glass slide to form a complete microfluidic device (Figure 4.2 E).

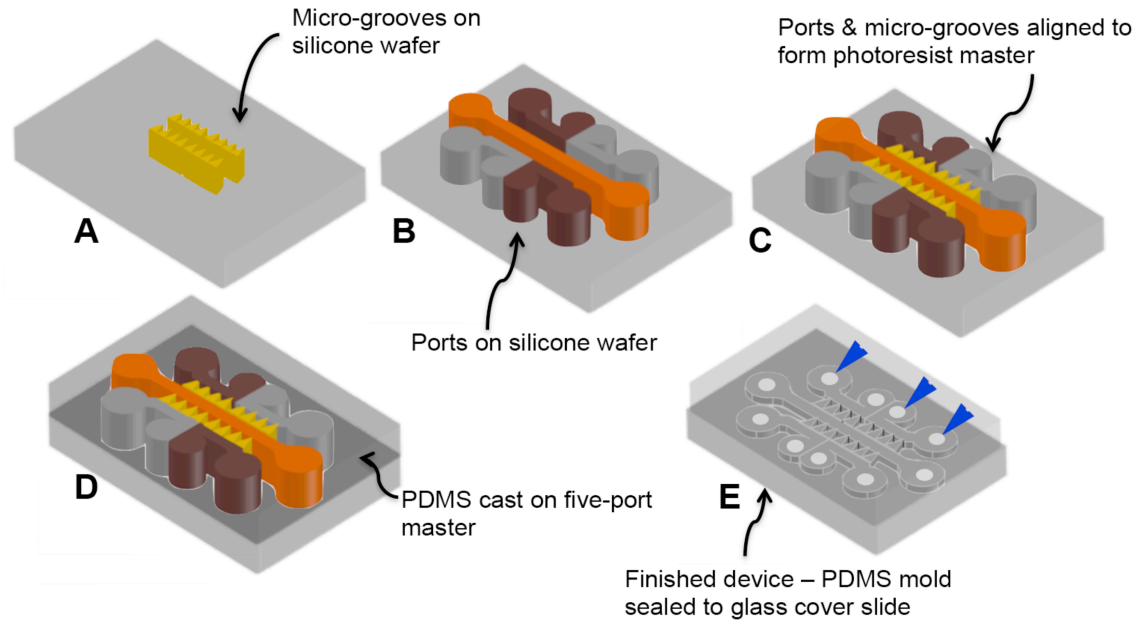

Figure 4.2: Schematic of fabrication of the microfluidic device. A-C, Photolithography was used to fabricate the master. D-E, Soft lithography was used to complete the device. Holes indicated by blue arrowheads in E, allowed access to microfluidic devices and were drilled on PDMS moulds before sealing to cover slides.

Devices were coated with PDL and LN prior to cortical, SN, GP and striatal cell culture. As discussed in section 2, cells on coverslips were cultured for DIV 12-19 before they were fixed with 4% PFA and stained as follows: cortical neurons - vesicular glutamate transporter 2 (VGlut 2), SN - tyrosine hydroxylase (TH), GP - phosphotyrosine (Py) and striatal - GABA. Cells in microfluidic devices used for studying axonal extension from one port to another were stained with β-III-tubulin for neurons and GFAP for astrocytes. Some cultures were labelled with PKH-26 and Fluo4 dyes to track the extension of axons through micro-grooves.

4.3 Results and discussion

The main processes involved in building microfluidic devices were: device design, photolithography and soft lithography.

4.3.1 Design of microfluidic devices

Computer-aided design software such as AutoCAD, is used for designing cell culture microfluidic devices (Conn *et al.* 2014; Crane *et al.* 2014; J. Lee *et al.* 2014; Shih *et al*. 2013; L. Wang *et al*. 2013) due to their precision, which is essential since devices usually consist of very small features (Ferry *et al*. 2011). AutoCAD was used in the current study to design two sets of templates. The first templates (Figure 4.3) were designed for a two-port microfluidic device, for studying connectivity between two cell populations. The term port refers to a cell culture compartment. Four sets (replicates) of micro-grooves (Figure 4.3A) of length, width and spacing of 375, 50 and 450 µm, respectively, were drawn within an area of approximately 3,800 mm^2. The area, surrounded by crosses in Figure 4.3 A and C, was designed to allow the two-port device template to comfortably fit onto a 101.60 mm (diameter) silicon wafer. Microfluidic ports covered an area of approximately 120 mm^2 each.

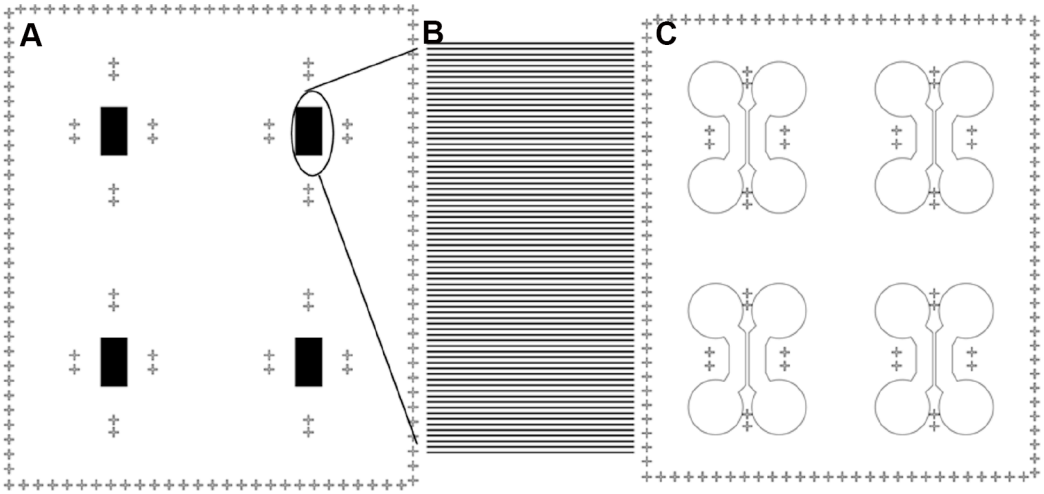

Figure 4.3: AutoCAD designs for a two-port microfluidic device. The design was made for simultaneous fabrication of 4 devices. A: 50-µm-width microgroove design separating 2 ports. B: Close-up of microgroove design. C: Ports for cell culture. Grooves (A) and ports (C) were fabricated separately and crosses (in A and C) were designed to ensure masks were aligned during the photolithography process.

Some groups have studied use of two-port microfluidic devices for cell culture, for instance, Taylor *et al.* developed a two-port microfluidic device to culture two populations of rat hippocampal neurons (Taylor *et al.* 2010). Synaptic connectivity established between the sets of neurons was assessed. Neurites (axons and dendrites) emanating from soma in both ports extended into micro-grooves separating the ports. Micro-grooves had length, width and height of: 900, 7.5 and 3 µm, respectively. After DIV 14, ~50% of micro-grooves contained dendrites of at least 100 µm of length. The average dendritic length extended to 214 µm after DIV 21. Thereafter, not much increase in dendritic length was noticed. Both cell populations were then transfected with either red fluorescent protein or GFP-Sindbis virus to visualise synaptic connectivity. Pre- and post-synaptic neurites were tracked back to their soma from either port to confirm that inter-port synaptic connectivity had occurred.

In the current study, a second set of templates was designed for a novel five-port microfluidic device. It consisted of tapered micro-grooves (Figure 4.4 A and B) and cell culture port drawings (Figure 4.4 C). Three sets of micro-grooves, with openings of 15, 25 and 50 µm, were drawn inside an area measuring approximately 10,404 mm^2 (Figure 4.4 A); cell culture ports (Figure 4.4 C) were enclosed inside the same area (identified with crosses). Micro-grooves were tapered from 50, 25 or 15 µm to 5 µm, to provide unidirectional axonal orientation (as discussed in Section 4.2.1). Design of the microfluidic device consisted of one long port in the middle with an area of approximately 180 mm^2, flanked by two ports on each side, all measuring approximately 107.5 mm^2 each.

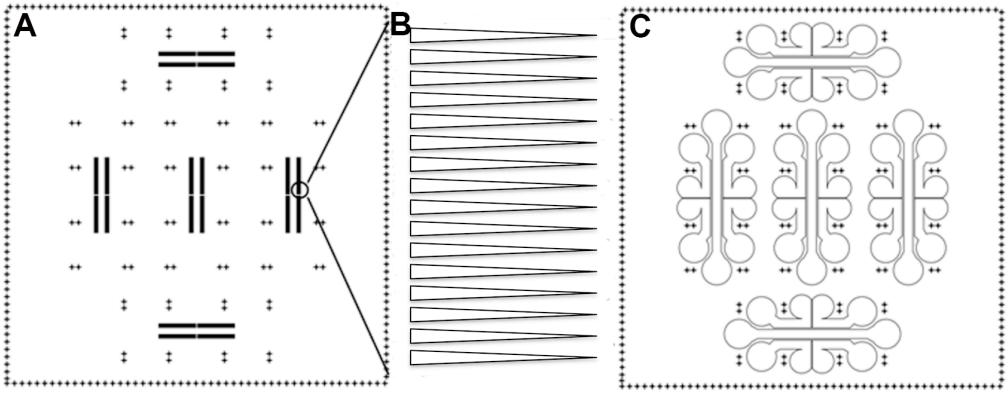

Figure 4.4: AutoCAD designs for a five-port microfluidic device. A: micro-grooves with cross patterns for alignment with ports displayed in C. Top set (A) consists of 50 to 5 µm tapered grooves; bottom set, 25 to 5 µm and middle set, 15 to 5 µm. B: close-up of 15 to 5 µm tapered micro-grooves. C: Five cell culture ports matching micro-grooves in A.

An external company manufactured photomasks using AutoCAD microfluidic designs displayed in Figures 4.3 and 4.4 (more details in Chapter 2). Lithography techniques were then used to print microfluidic device patterns at a resolution of 64,000 dots per inch (dpi). Photomasks fabricated consisted of transparent soda lime glass microfluidic patterns on opaque chrome background. The glass mask was designed to enable transfer of microfluidic designs onto a photosensitive surface via UV light exposure in a process called photolithography. Darkfield mask printing allowed a negative image of the devices to be produced such that the end product pattern would stand proud on the surface of a silicon wafer.

4.3.2 Microfluidic device fabrication

4.3.2.1 Photolithography

As discussed in section 1.2.4, the photolithography technique is used to replicate patterns on photomasks onto substrates in order to manufacture a master, usually on silicon wafers (Jones 2000). A master is a template made up of photoresists, usually on silicon wafers, that is used multiple times to fabricate device moulds e.g. PDMS device moulds (Xia & Whitesides 1998). The first photolithography step in the current study was to optimise the conditions used to fabricate photoresist (photosensitive polymer) structures on wafers. SU-8, an epoxy-based negative UV light-sensitive resist (Lorenz *et al.* 1997; Williams & Wang 2004; Ribeiro *et al.* 2005), was used in the current study; SU-8 10 and SU-8 50 photoresists were used for fabricating micro-grooves and ports, respectively. Epoxies are resins that cross-link to form solid polymeric structures. SU-8 resins are dissolved with photo-initiators in an organic solvent (gamma-butyrolacton) at different concentrations depending on application (Lorenz *et al*. 1997), e.g. SU-8 10 is less viscous than SU-8 50, which is used to fabricate thicker structures.

The SU-8 coated wafers were baked on a hot plate to ensure the removal of solvent from the photoresist (section 2.3.1). Different bake temperatures and times tested to determine the optimal soft baking parameters are summarised in Table 4.2. Optimal soft baking parameters for the SU-8 10 photoresist were found to be 95 °C for 1 min. Soft baking parameters for the SU-8 50 were optimised to 65 °C for 10 min followed by 95 °C for 30 min. Following soft baking,

photoresist-coated silicon wafers were exposed to UV light through micro-groove and cell culture port photomasks. They were rinsed in an ethyl lactate solvent to remove non-cross-linked regions of the wafers.

Table 4.2: Optimisation of the soft baking process for both SU-8 10 and SU-8 50 photoresists.

Photoresist	Soft bake temperature	Soft bake duration
SU-8 10	65 °C	10 min
	95 °C	10 min
SU-8 10	65 °C	2 min
	95 °C	5 min
SU-8 10	110 °C	1 min
SU-8 10	95 °C	1 min
SU-8 50	100 °C	30 min
SU-8 50	65 °C	10 min
	95 °C	30 min

After SU-8 structures were fabricated and cleaned, they were examined under a microscope to determine the quality of the structures, i.e. correct replication of the original AutoCAD design. Dimensions of 'alignment crosses' (for both SU-8 10 and SU-8 50), after different UV light exposure periods at an exposure energy of 280 mJ/cm^2, were analysed to determine if they conformed to specifications in AutoCAD drawings (Figures 4.5 – SU-8 10 and 4.6 – SU-8 50). Both exposures (19.8 s and 26.4 s) for the SU-8 10 resist yielded good results, i.e. dimensions were not significantly different from AutoCAD specifications. However, samples exposed for 19.8 s appeared to be sharper, with more defined structures. More experimentation centred around 19.8 s of UV light exposure followed, and it was found that optimal light exposure duration for SU-8 10 structures was 18.15 s (Figure 4.5 C).

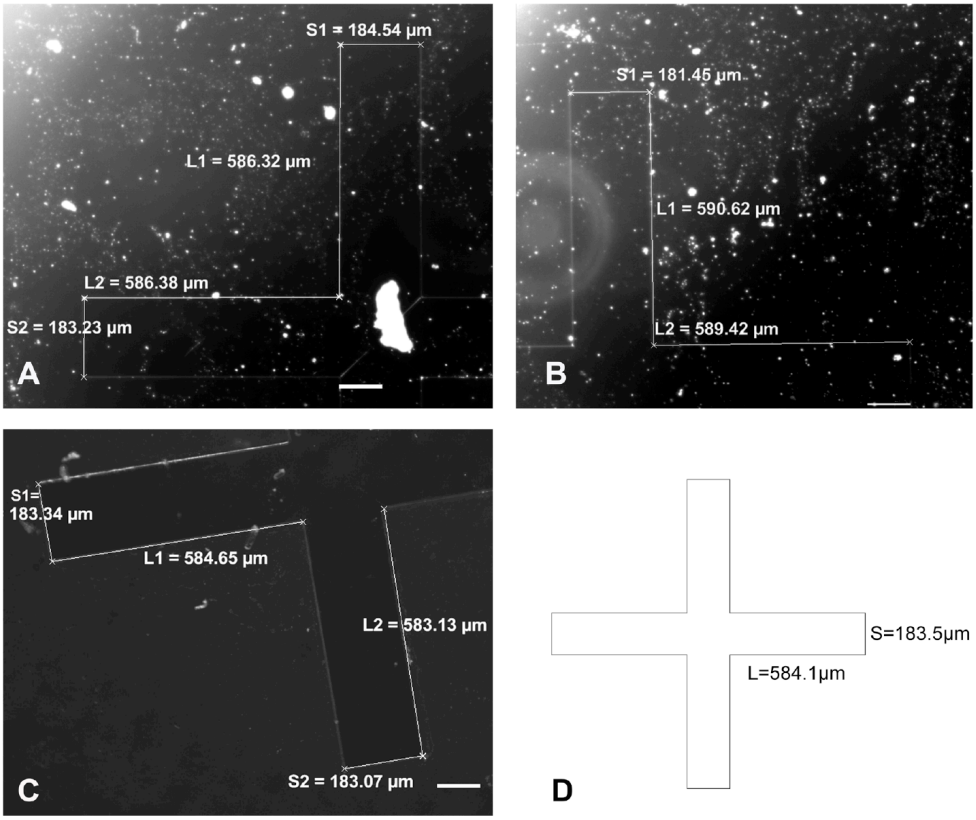

Figure 4.5: Assessment of SU-8 10 features after the photolithography process. A-C show crosses representing features built by photolithography via different exposure times – A: 19.8 s, B: 26.4 s and C: 18.15 s. Dimensions of structures were measured to determine the optimal exposure time (duration) required for building structures; measurements obtained were compared to AutoCAD specifications (D). L and S refer to long and short sides of the cross structures. Scale bars = 100 µm.

UV light exposure to SU-8 50 photoresist structures, for a duration of 49.5 s resulted in distorted features (overexposure) i.e., some features of the cell culture port structures measured less than the specification (Figure 4.6 A). Optimal UV light exposure for SU-8 50 resist was found to be 33 s (Figure 4.6 B,C).

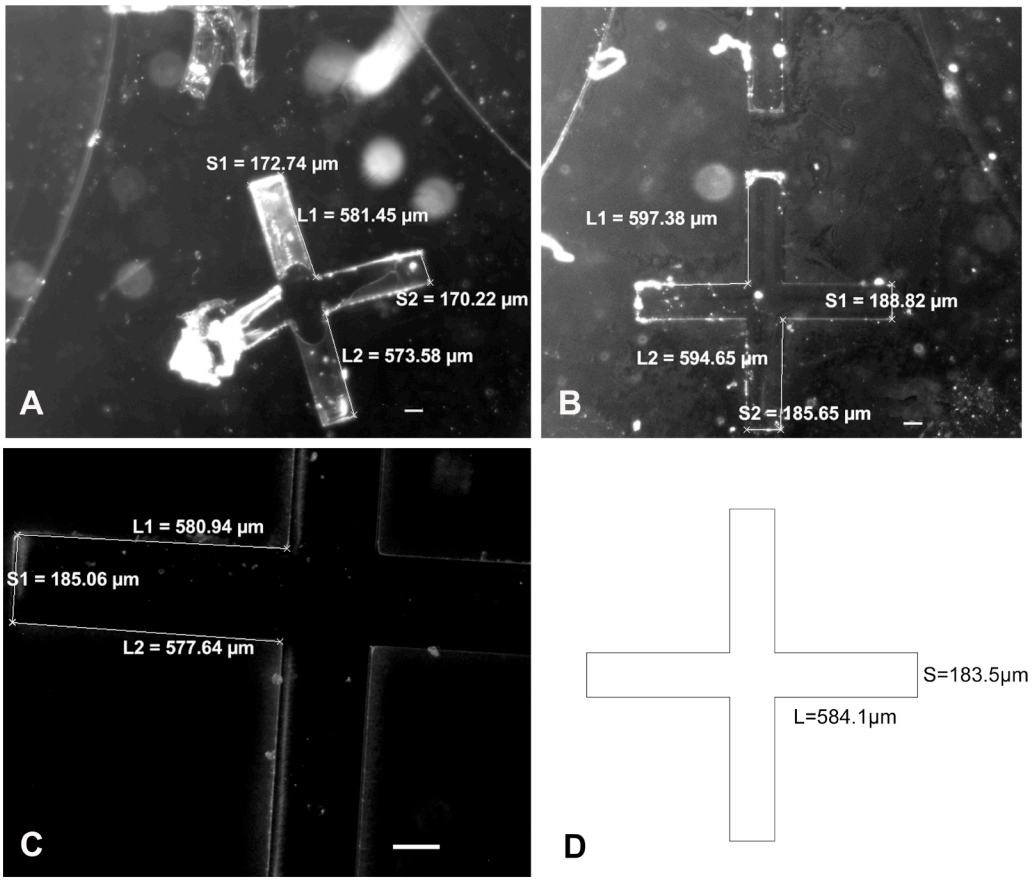

Figure 4.6: Assessment of SU-8 50 photolithography features. SU-8 50 polymeric features built from UV light exposure duration of A: 49.5 s, B and C: 33 s. D: AutoCAD structure measurement specification. Features in A are distorted and have smaller dimensions, which indicates more exposure to UV light than required (overexposure). However, features in B and C show features that are more defined and sharper and measurements are more comparable to the design specification in D. L and S refer to long and short sides, respectively, of the cross structures. Scale bars = 100 µm.

Different post-exposure baking (PEB) temperatures and times tested to determine the optimal parameters are summarised in Table 4.3. Optimal PEB parameters the SU-8 10 photoresist were found to be 65°C for 1 min followed by 130°C for 2 min. The PEB process was performed to crosslink parts of the photoresist exposed to UV light. Micro-groove structures built using the SU-8 10 photoresist yielded thickness of 5 µm (Figure 4.7 A). Optimal PEB for SU-8 10 was found to be 65°C for 1 min followed by 95 °C for 10 min. Cell ports or compartments were built using the SU-8 50 photoresist yielding thickness of 100 µm (Figure 4.7 B). A master template (Figure 4.1 A) was then fabricated by overlaying the SU-8 10 pattern with a SU-8 50 pattern. A summary of the optimal soft bake, exposure and PEB are displayed in Table 4.4.

Table 4.3: Optimisation of the PEB process for both SU-8 10 and SU-8 50 photoresists.

Photoresist	Soft bake temperature	Soft bake duration
SU-8 10	90 °C	2 min
SU-8 10	65 °C	5 min
	95 °C	5 min
SU-8 10	65 °C	1 min
	95 °C	2 min
SU-8 10	65 °C	1 min
	130 °C	2 min
SU-8 50	90 °C	5 min
SU-8 50	65 °C	1 min
	95 °C	10 min

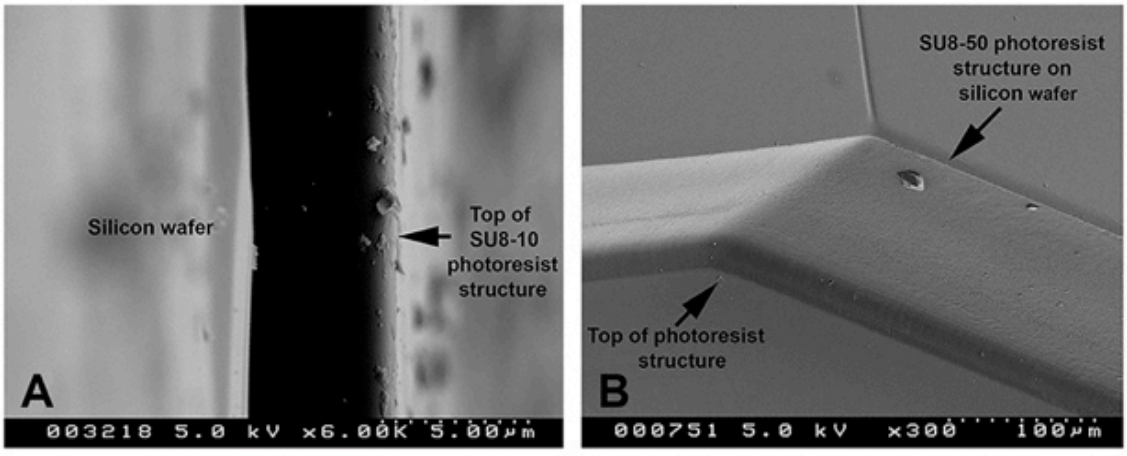

Figure 4.7: SEM photographs of SU-8 10 and SU-8 50 photoresist structures built on silicon surfaces. A: Side view of a SU-8 10 structure, 5 µm from the silicon wafer surface. B: SU-8 50 structure with height of 100 µm on silicon surface.

Table 4.4: Summary of optimal baking and exposure parameters used for photolithography of master.

SU-8	Soft-bake at 65 °C	Soft-bake at 95 °C	Exposure time/s (Integra)	PEB at 65 °C	PEB at 95 °C	PEB at 130 °C
10	-	1	18.2 s (55)	1 min	-	2
50	10	30	33.0 s (100)	1 min	10 min	-

Exposure time depends on the thickness of photoresist structures built, i.e. thicker structures require higher exposure dosage or longer exposure times. Optimal UV light exposures for SU-8 10 and SU-8 50 in the current study were ~18 s (5 µm) and ~33 s (100 µm), respectively. The instrument used for photolithography is set in light integra i.e. dosage dependant light exposure rather than controlled exposure time periods in s. The conversion to exposure time in s was based on the findings that 100 integra was approximately 33 s. Exposure times for building structures thinner than 5 µm would require less than 18.15 s and for structures more than 100 µm, exposure of more than 33 s would be required. Once masters were fabricated, microfluidic device moulds were fabricated via a technique of soft lithography.

4.3.2.2 Soft lithography and device fabrication

PDMS polymer was cast onto a five-port master fabricated via photolithography. The mould developed, a PDMS replica of the master, was then irreversibly bonded to glass cover slides to complete device fabrication (Figure 4.8). The PDMS mould can form watertight, reversible sealing with flat surfaces at room temperature. In contrast to other polymers, PDMS easily conforms to a surface when contact is established. Van der Waals (weak intermolecular attraction) forces hold the PDMS and the surface together; peeling off the mould from the surface can break the seal without damaging the mould. However, microfluidic devices fabricated via reversible sealing are prone to fluid leakage, particularly if the pressure used to introduce the fluid into the device exceeds 5 psi (Anderson *et al.* 2000; Park *et al*. 2006).

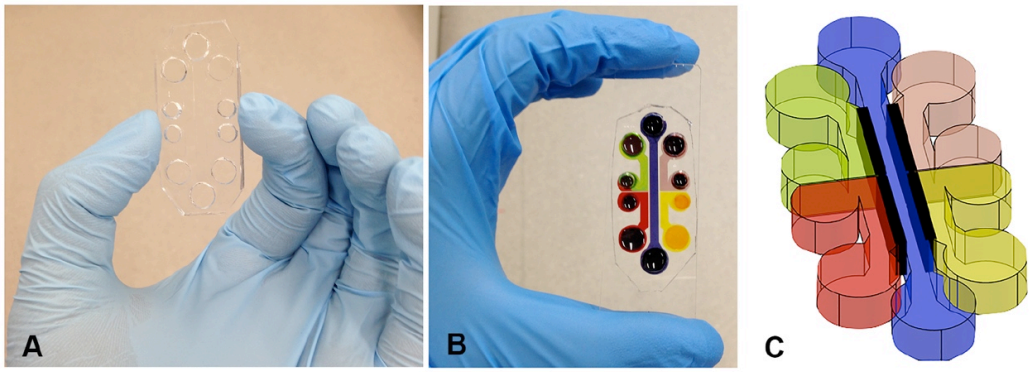

Figure 4.8: PDMS microfluidic device. A: PDMS microfluidic mold fabricated via soft lithography. B: Microfluidic mold irreversibly mounted, using oxygen plasma, onto a glass surface. The microfluidic device was loaded with food coloring to indicate five different ports. C: AutoCAD design displaying the inside of a microfluidic device.

The PDMS surface is inherently hydrophobic and contains repeating units of -O-Si$(CH_3)_2$- bonds. Oxygen plasma treatment eliminates the –(CH_3) group from the surface and introduces silanol (Si-OH) groups via oxidisation; other plasma treated materials such as silicon and glass form -OH-containing functional groups. When oxidised PDMS and plasma treated materials are brought together at room temperature, permanent covalent bonds (O-Si-O) are formed (Owen & Smith 1994; Tang & Whitesides 2009). Irreversible bonds formed are capable of withstanding pressures of 30 – 50 psi. Watertight seals are formed e.g. between plasma treated PDMS and glass, which permits reproducible fabrication of devices compared to reversible (van der Waals) bonds (Anderson *et al.* 2000; Park *et al.* 2006).

In the current study, plasma treatment was beneficial in both initiating irreversible bonding (between oxidised PDMS and glass slides) and making the glass slide and PDMS surfaces hydrophilic. The hydrophilicity can be maintained by placing plasma treated surfaces or devices in water or other polar organic solvents. This prevents resurfacing of hydrophobic groups on treated surfaces; resurfacing usually occurs within 24 h if surfaces are exposed to air (Ng *et al*. 2002). The hydrophilicity and increased wettability of microfluidic devices caused by plasma treatment in the current study, meant that virtually no applied pressure was required to introduce fluids such as PBS, PDL and LN solutions, as well as NCM into the device (Brody *et al.* 1996). It was found that fluids placed in one cell culture port were not diffusing into other ports; different food colorings placed in each port (Figure 4.8 B) did not mix.

Laminar flows govern fluid mechanics in microfluidic systems (Brody *et al*. 1996). In contrast to unpredictable and complex turbulent flows that promote fluid mixing, laminar flow is steady, controlled and permits side-by-side flow of different fluids without mixing. This is made possible by the small, micro-scale structures of microfluidic devices and makes it easier to generate reproducible experiments (Anderson *et al*. 2000; Campbell & Grzybowski 2004; Taylor & Jeon 2010; Velve-Casquillas *et al*. 2010; Ferry *et al*. 2011; Crane *et al.* 2014; Mehling & Tay 2014). To verify that fluids between microfluidic ports do not readily mix TRITC was loaded into the middle port; the rest of the ports were loaded with FITC. Intensity profiles (Figure 4.9) showed that TRITC remained contained inside the middle microfluidic port; so did FITC in a neighbouring port.

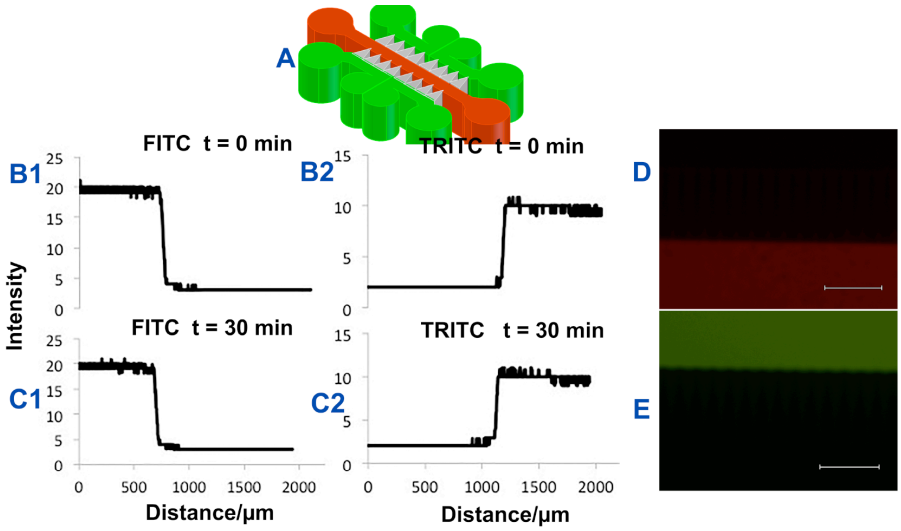

Figure 4.9: FITC and TRITC intensity profiles for inter-port fluid diffusion test in a microfluidic device. Micro-grooves had width tapering from 50 to 5 µm. (A) shows schematic of the device loaded with FITC (green) and TRITC (red) dyes. (B) Intensity profiles relating to fluidic separation between the middle port (red, TRITC positive) and the left port (FITC positive). Images captured at: (B1) FITC time (t) = 0 min and (B2) TRITC t = 0 min. (C1) FITC t = 30 min and (C2) TRITC t = 30 min. Photographs showing fluidic separation at 30 min after loading, TRITC (D) and FITC dyes (E). Scale bars = 250 µm.

4.3.2.3 Cell culture in microfluidic devices

Cell culture in microfluidic devices requires pre-coating substrates with polyamino acids e.g. PLL and polyornithine and/or ECM proteins e.g. LN and fibronectin, to promote growth and development of processes (Khan & Newaz 2010). Microfluidic devices in the current study were pre-coated with PDL and LN prior to primary cell culture. Five different cell types were successfully cultured inside devices. The middle port contained developing striatal cells from the LGE of the rat

brain. There were two input cell populations namely: cortical glutamatergic (excitatory) neurons and SNc dopamine neurons from the VM. Developing GP GABAergic (inhibitory) neurons from the MGE and SNr from the VM were the two output cell populations.

To verify the identity of different cell populations prior to microfluidic device cell culture, primary cells cultured on PDL and LN coated coverslips were fixed and stained with various antibodies. Cortical cells were positively stained for VGLUT 2 (Figure 4.10 A and B). Glutamatergic neurons express VGLUTs, proteins responsible for packing glutamate in synaptic vesicles and transporting it to the synaptic cleft to trigger postsynaptic excitatory neurotransmission (Shigeri *et al*. 2004; Wojcik *et al*. 2004; Liguz-Lecznar & Skangiel-Kramska 2007; Brumovsky *et al*. 2011). Synaptic vesicles are presynaptic organelles responsible for storage of neurotransmitters; vesicles release neurotransmitters into the synaptic cleft, a gap between presynaptic and postsynaptic neurons (Purves *et al*. 2001). Developing SN neurons from the VM positively stained for TH (Figure 4.10 C and D). TH is a catalyst involved in the hydroxylation (a process that introduces an –OH, hydroxyl group to a compound) of tyrosine into L-3, 4-dihydroxyphenylalanine (L-DOPA) which is involved in the production of the dopamine neurotransmitter. TH is expressed in dopaminergic SN neurons (Haavik & Toska 1998; Hirata 1998).

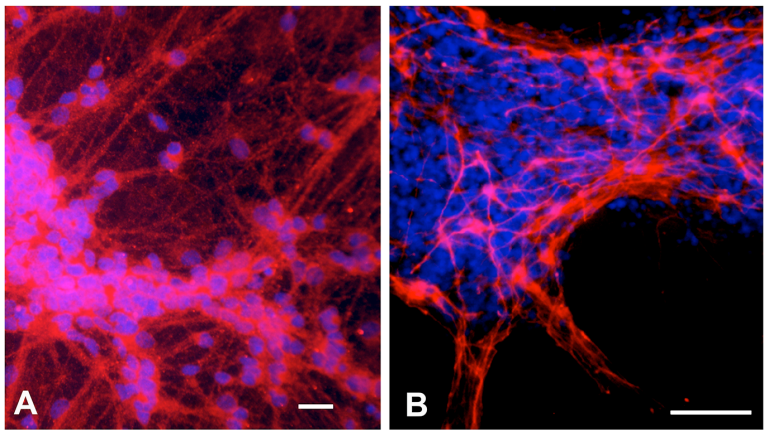

Figure 4.10: Immunocytochemistry for primary neurons. A: VGlut 2 staining for cortical neurons. B: TH staining for SN neurons developing from the VM. Red = neuron staining, blue = DAPI staining for cell nuclei. Scale bars, A = 10 µm, B = 100 µm. Some of the DAPI stained nuclei in B possibly belong to meningeal cells. Meninges are layers of tissue that protect the developing brain. At E12/13, the peak of VM neurogenesis, the meningeal tissue closely adheres to the VM tissue and often difficult to completely remove during dissection. This inevitably results in some meningeal cells present in SN cultures.

Developing GP neurons from the MGE were identified via Py immunocytochemistry. Fluorescence microscopy results (Figure 4.11A and B) suggest further experimentation is required to acquire optimal dilution to improve staining and resolution of soma and neurites. Striatal neurons developing from the LGE were visualised via GABA immunocytochemistry.

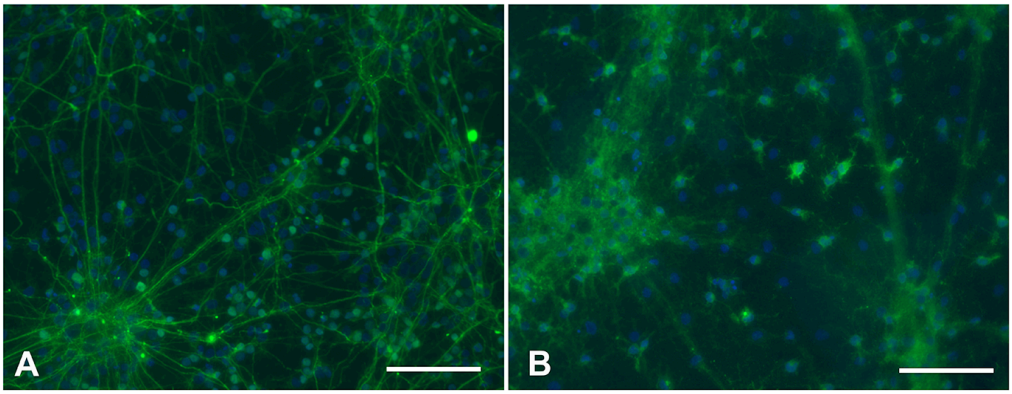

Figure 4.11: Immunocytochemistry for primary striatal and GP neurons. A: GABA staining for striatal neurons from the LGE. B: Py staining for GP neurons developing from the MGE. Green = neuron staining, blue = DAPI staining for cell nuclei. Scale bars = 100 µm.

The first set of microfluidic cell culture experiments were concerned with optimising the volume of cell suspension loaded into microfluidic device ports. Optimal volumes of cell suspension were found to be 15-20 µL for the middle port and approximately 10 µL for the rest of the ports. A concentration of 10,000 to 20,000 cells/µL was used for all ports. Smaller volumes of suspension often did not cover the whole port area and therefore required another loading, which made it difficult to reproduce cell distribution for different devices. Larger volumes (e.g. 50-100 µL) made it difficult to control flow and distribution of cells and often resulted in a lot of cells accumulating in microfluidic device reservoirs. Devices were checked under a brightfield microscope after cell suspension loading to verify even cell distribution. Following cell seeding, devices were incubated for 2 h at 37°C to allow cells to attach prior to adding NCM. After microfluidic devices were flooded with medium (at 2 h) they were placed under the microscope again to ensure none of the cells were lifting off the surfaces. It was found that almost all (cortical, striatal, GP and SN) cells remained attached to the substrata.

In the current study, one of the challenges encountered in early microfluidic cell culture experiments was medium evaporation, which resulted in poor cell viability, possibly due to hyperosmolality. Evaporation occurs faster in microfluidic devices due to high surface area to volume ratio associated with them. Hyperosmolality involves an increase in solute concentrations that can result from water evaporation, e.g. evaporation of water contents from medium. This osmolality imbalance has been found to affect long-term viability of neurons (Potter & DeMarse 2001; Blau *et al*. 2009; Halldórsson *et al.* 2014). The PDMS material used in the current study to build a microfluidic device is permeable to water vapour, in addition to oxygen (O_2) and carbon dioxide (CO_2). Even though water vapour in the cell culture incubator is low, it is not negligible. Permeability to O_2 and CO_2 allows necessary gaseous exchange between cell culture medium and the surroundings (Halldórsson *et al*. 2014). Medium evaporation was addressed by maintaining high levels of medium in microfluidic device reservoirs. In addition to changing the medium every 2-3 days, medium levels were topped up as necessary to maintain good cell viability following the protocol developed by Park and colleagues (Park *et al*. 2006).

Careful loading and unloading of fluids, e.g. PDL and LN solutions (during coating) and medium, was required to avoid formation of air bubbles inside microfluidic device ports. Complete emptying of ports, for instance during replacement of PDL with the LN coating solution, resulted in bubbles forming inside devices; a lot of pressure was required to remove bubbles. Air bubbles possess small curvatures and according to the Laplace law, which states that applied pressure is inversely proportional to curvature radii, high pressures are required to push bubbles out of microfluidic ports (Brody *et al*. 1996; Y. Wang *et al*. 2012). In addition to obstructing the view of cells inside the device, air bubbles were found to displace cells initially attached to the microfluidic substrata; in this instance, bubble formation was caused by a reduction in medium volume due to excessive evaporation.

Primary E15/16 cells loaded into the cortex port yielded good cell adherence and growth (viability) up to around DIV 19; thereafter, the cell viability was inconsistent. Good cell viability was demonstrated by pyramidal, phase-bright cell bodies with neurite outgrowth. Density and extension of neurites increased during culture from DIV 1 to 19 (Figure 4.12).

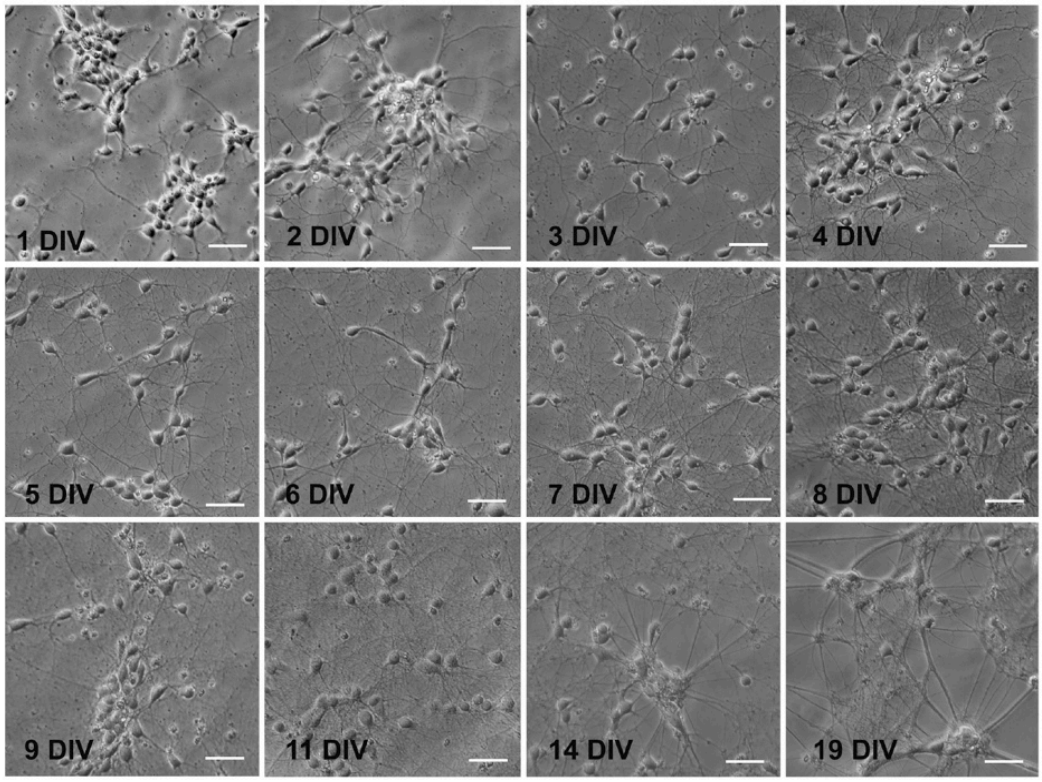

Figures 4.12: Photographs captured inside the cortical cell port of a microfluidic device. Cortical cells cultured from DIV 1 to 19. Scale bars = 20 µm.

A number of studies have demonstrated the ability of microfluidic devices to isolate soma from axons using micro-grooves (Park *et al.* 2006; Peyrin *et al*. 2011; Millet & Gillette 2012; N. Lee *et al*. 2014). As discussed in section 1.2.6, micro-grooves are usually designed to enable axon entrance whilst physically restricting cell bodies from entering the grooved areas. Isolated axons, extending from the neighbouring compartment, can be analysed separately without interference from the soma and dendrites e.g. for axonal growth, injury or degeneration studies (Taylor *et al*. 2005; Taylor *et al*. 2009; Brunello *et al.* 2013). In the current study, cortical axons extending from cell bodies were guided from the cortex port to the striatum port (Figure 4.13). This demonstrates that micro-grooves are capable of influencing orientation of cortical axons, as found in Chapter 3.

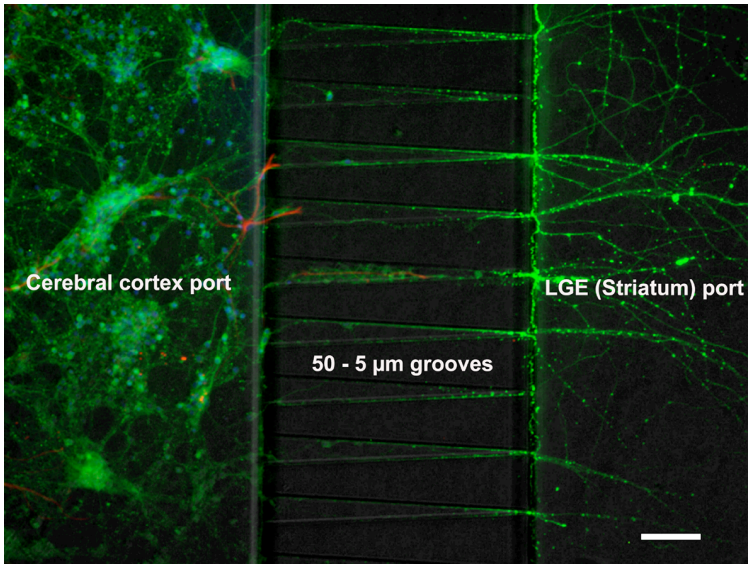

Figure 4.13: Photograph demonstrating cortical axons guidance through micro-grooves in a microfluidic device. The receiving, striatum port, did not have cells present to clearly demonstrate the axons invading the port. Micro-grooves had width tapered from 50-5 µm. Green = β-III-tubulin stained neurons, red = GFAP stained astrocytes and blue = DAPI stain for cellular nuclei. Scale bar = 100 µm.

Taylor *et al.* used a two-port microfluidic device to develop an axonal injury and regeneration model for cortical and hippocampal neurons (Taylor *et al*. 2005). Neurons cultured in one port extended neurites that were guided by micro-grooves with height and width of 3 and 10 µm, respectively. Axons, identified by Tau staining, extended through 900 µm long micro-grooves into another (axonal) port. On the other hand, microtubule-associated protein 2 (MAP2) stained dendrites did not extend past groove length of 450 µm. Isolated axons (residing in the axonal port) allowed the study of axonal protein synthesis for development of synapses; mRNA encoding for synaptophysin (Syp) was found from axon samples analysed. Syp is a protein that is majorly involved in the formation presynaptic vesicles.

Developing striatal cells, dissociated from E15/16 LGE tissue and loaded into the LGE (striatum) port (Figure 4.1 A) yielded good adherence to the microfluidic substrate (glass + PDL + LN); almost all cells remained adhered to the surface when devices were loaded with medium. Cells developed phase-bright soma as well as neurite protrusion and extension. Density and extension of striatal neurites increased during culture from DIV 1 to 19 (Figure 4.14, Figure 4.15 shows the guidance of striatal axons via micro-grooves).

In Peyrin *et al*'s the two-port microfluidic device for studying connectivity between striatal and cortical neurons, both cell populations derived from E14 mouse tissue were cultured in separate ports. Micro-grooves incorporated in devices were tapered (15-3 μm) to direct cortical axons extension into the striatal port. Cortical axons invading the striatal port induced full differentiation of striatal neurons that were previously partly differentiated pure striatal cultures before connection. Morphological assessment showed that longer dendrites and more dendritic spines were developed in connected striatal neurons compared to unconnected, pure striatal neurons; an indication that improved maturity (of striatal neurons) was encouraged by cortical connectivity. Furthermore, connected striatal neurons presented Ca^{2+} oscillations activity that was synchronous to cortical neurons' activity. Pure cortical neurons showed spontaneous Ca^{2+} oscillations, whereas pure striatal neurons displayed no oscillations. This study demonstrates that, in addition to permitting study of axon injury and regeneration, microfluidic devices provide a valuable platform for modelling neuron networks (Peyrin *et al.* 2011; Deleglise *et al.* 2013). It provided valuable data, particularly on interaction between cortical and striatal cells, towards co-culturing BG cell networks in five-port microfluidic devices.

In the current study, striatal axons outgrowth into other ports was determined by observing changes in cells' morphologies. Orientation of axons developed by cell bodies was directed by micro-grooves from the striatum port to the next (SNr) port. Axons were visualised via immunocytochemistry using a β-III-tubulin neuronal marker (Figure 4.15). Developing GP cells from the MGE and SN cells from the VM tissue yielded good viability in the microfluidic device. Cell adherence to the substrate for both populations was very good. In most cases GP cells remained more evenly distributed, with fewer clusters compared to cells in other ports.

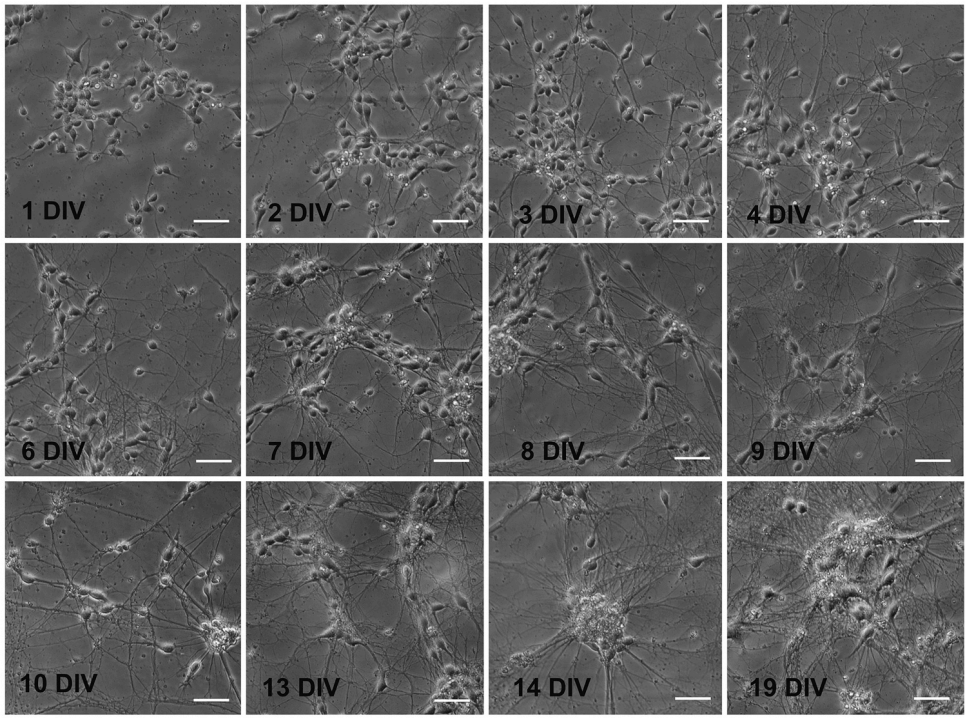

Figures 4.14: Photographs of developing striatal cells from the LGE cultured in a microfluidic device. Cells were cultured for up to DIV 19. Scale bars = 20 μm.

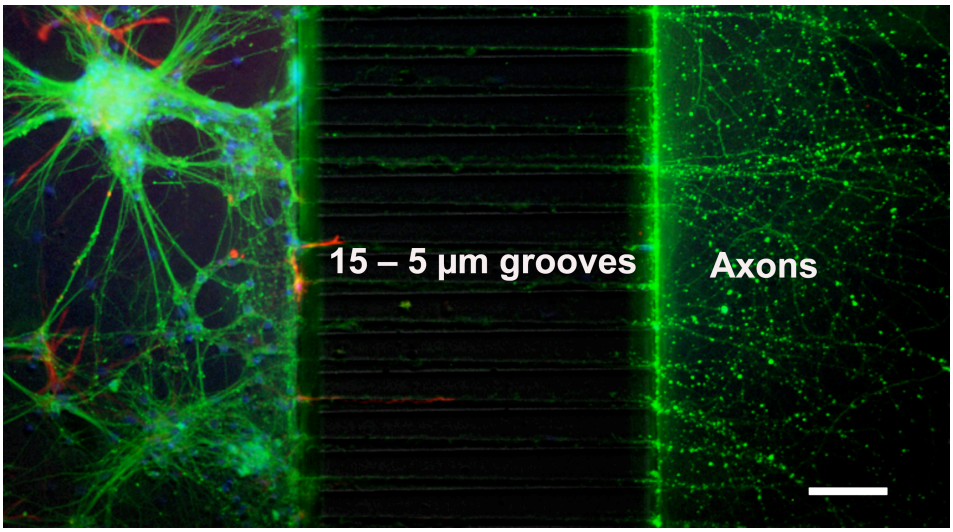

Figure 4.15: Photograph showing striatal axon guidance through micro-grooves in a microfluidic device. The neighbouring port (labelled Axons) shows striatal axonal extensions. Micro-grooves had width tapered from 15-5 μm. Green = β-III-tubulin stained neurons, red = GFAP stained astrocytes and blue = DAPI stain for cellular nuclei. Scale bar = 100 μm.

This indicates that GP cells possibly responded to the chemically modified (PDL and LN pre-coated) microenvironment more than cells in other ports. GP cells developed phase-bright soma with good neurite outgrowth. Density and extension of GP neurites increased during culture

from DIV 1 to 19 (Figure 4.16). SN cells were seeded in two ports; this was done to reflect the two types of cells (SNr and SNc) found by other studies in the BG circuitry in previous *in vivo* experiments (Bolam *et al.* 2000). SN cells cultured in the microfluidic device appeared viable; they were also phase bright and cell bodies developed neurites. SN cultures included another cell type that could have been meningeal cells. The meningeal tissue closely adheres to the VM tissue; every effort was made to remove as much of the tissue as possible during dissection however, some meningeal tissue was inevitably included in SN cultures.

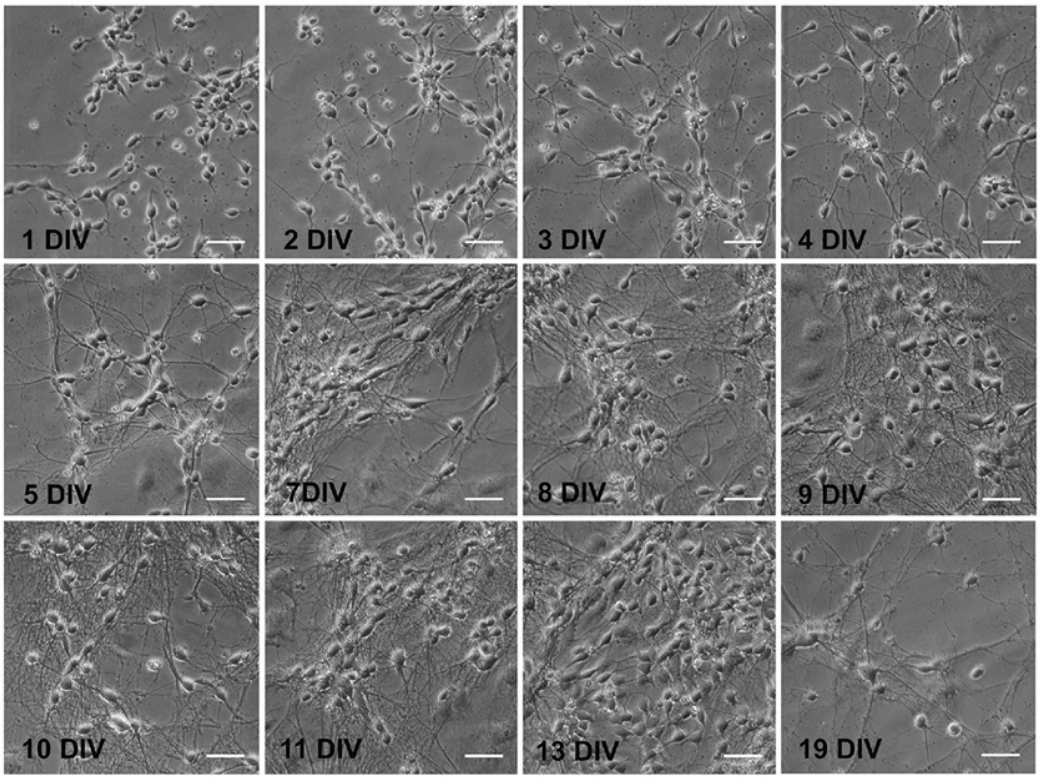

Figures 4.16: Photographs of developing GP cells from the MGE, cultured in a microfluidic device. Cells were cultured for DIV 1 to 19. Scale bars = 20 µm.

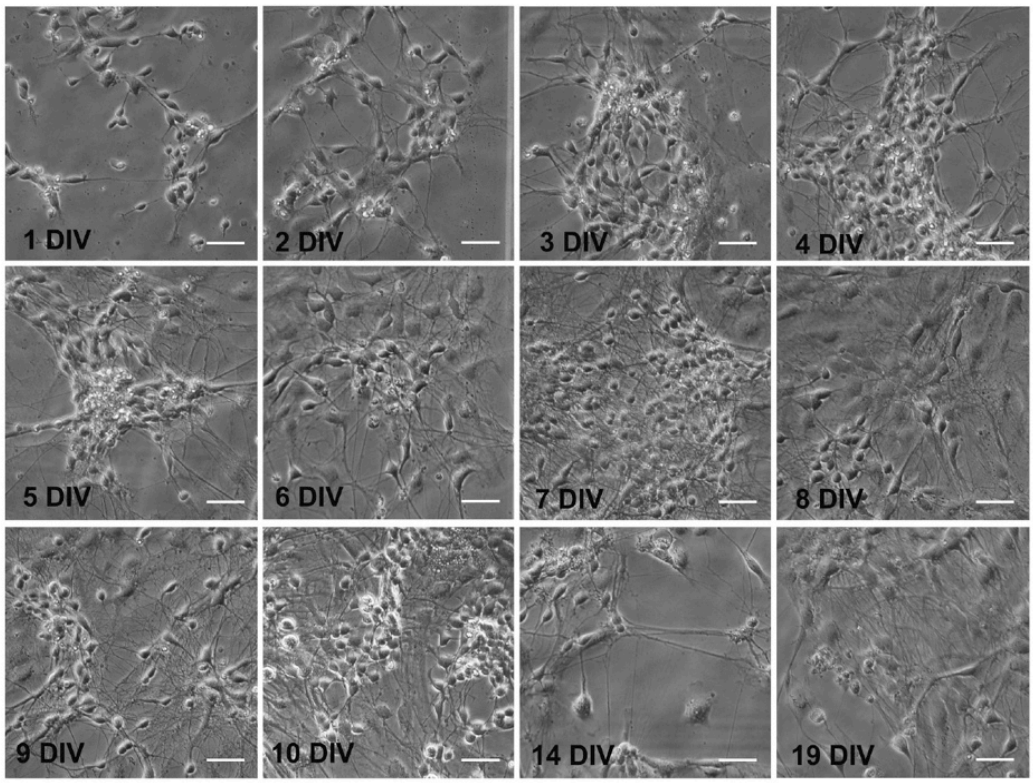

Figures 4.17: Photographs of developing SN cells from the VM cultured in a microfluidic device from DIV 1 to 19. Scale bars = 20 μm.

Three types of devices were fabricated in the current study, depending on micro-groove openings of 15, 25 and 50 μm tapering to 5 μm. All openings allowed axons to be extended from a port containing cell soma to another port, controlled by the tapering of micro-grooves. However, due to the high density of axon branches produced at the narrow ends of the micro-grooves, it was very difficult to quantify the number of axons emitted from one port to another for different openings. Due to viability differences it was challenging to determine the difference between numbers of axons emitted from 15, 25 and 50 μm openings. In some cases soma (cell bodies) were found inside micro-grooves, particularly for 50-5 μm tapered grooves (Figure 4.18). Future work will involve the use of microfluidic devices with micro-grooves of 15-5 μm tapering; 15 μm openings will reduce chances of cells migrating or seeding into micro-grooves, whilst allowing a large number of axonal extension.

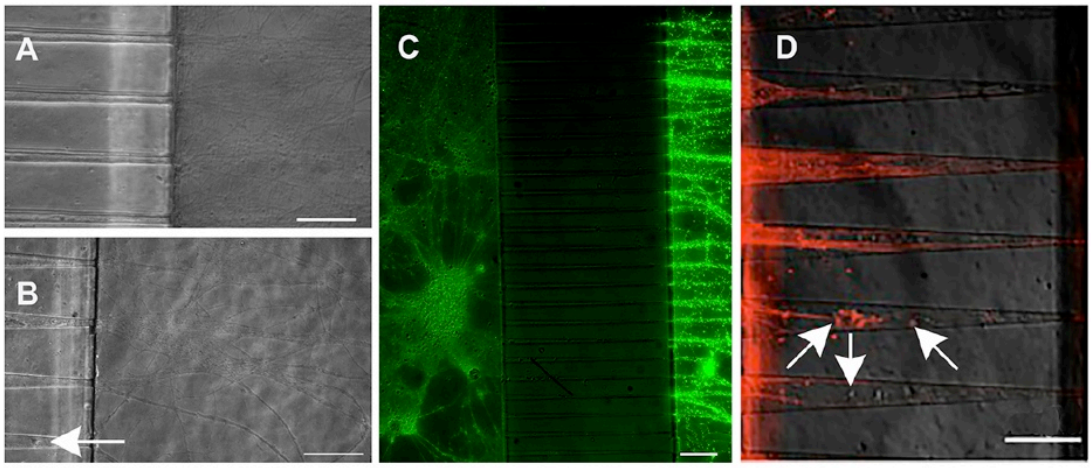

Figure 4.18: Brightfield and fluorescence photographs of axonal extension and guidance via 15 and 50 µm to 5 µm-tapered micro-grooves. Brightfield photographs of axon guidance through (A) 15-5 µm and (B) 50-5 µm micro-grooves. (C) Fluo4 dye labelling of axon guidance through 15-5 µm micro-grooves. (D) PKH-26 dye labelling of axons guided through micro-grooves tapered from 50 to 5 µm. In some cases cell bodies (white arrows) were noticed inside 50-5 µm grooves; they probably migrated through the grooves during cell loading. Scale bars for A = 50 µm and for B, C and D = 100 µm.

The design of microfluidic devices in the present study, consisting of a long port in the middle with two ports on each of its side (totalling five ports), is uniquely suited to the arrangement of BG circuitry. Cell networks generated in five-port microfluidic devices are more complex than those developed in a number of studies that often utilised fewer (two or three) cell culture ports (Park *et al.* 2012; Majumdar *et al.* 2011; Shi *et al.* 2013; Crane *et al.* 2014; J. Lee *et al.* 2014; Taylor *et al*. 2005; Park *et al*. 2006). However, the potentially complex five-port microfluidic device (and neuronal circuitry fabricated) provides the robustness required to develop a model that closely mimics BG circuitry. The design of the microfluidic device including specific arrangement of ports allows mimicry of the *in vivo* BG circuitry and provides a micro-environment that is controllable and reproducible; devices can be easily replicated since they are built using the same master template. Fluids in cell culture ports do not readily mix meaning five neuron populations can be treated separately; for instance, loading a neurotoxin in the striatum port should only directly abolish electrical activity of the 'striatal' part of the circuitry (see Chapter 5).

One of the drawbacks of using microfluidic devices is limited cell accessibility. The permanent bond between the PDMS and glass surface is designed to be strong and liquid-tight; meaning that in cases where direct cell access is required, the PDMS may have to be cleaved off from the glass,

which can potentially affect the sample. Reversible sealing (without plasma bonding) can be used, e.g. for immunocytochemistry experiments, where the PDMS top can be peeled off the glass surface prior to fixing and immunostaining experimentation. Companies such as Xona Microfluidics sell the PDMS chip or mould part of the microfluidic device only i.e. without plasma bonding to glass surfaces. However, reversibly sealed microfluidic devices are prone to problems of liquid leakage (Park *et al.* 2006). Regardless, the potential benefits of microfluidic devices particularly the high temporal and spatial resolution that enables monitoring of large neuron circuitry at single cell level, far outweighs the drawbacks. Microfluidic devices could allow the incorporation of analytical systems such as MEAs to improve efficiency of studies including disease modelling and drug screening (Berdichevsky *et al*. 2009).

4.4 Conclusion

The BG nuclei are compartmentalized, i.e. different cell populations are placed in different locations and establish communication via axonal projections. This study set out to evaluate the design and fabrication of a novel compartmentalized microfluidic device intended to serve as a platform for developing an *in vitro* BG model. Also explored in this study, was the primary neuron culture in the devices as well as controlled orientation of axons through micro-grooves. Primary cells cultured in the microfluidic device were the developing: cortical cells from the cerebral cortex, striatal cells from the LGE, GP cells from the MGE and SN from the VM brain tissue. This study demonstrated the benefits of microfluidic devices compared to other cell culture systems, e.g. conventional well plates and flasks. For instance, microfluidic devices offer design flexibility, i.e. templates can be designed, via AutoCAD, to address specific challenges. The AutoCAD drawing was specifically designed to accommodate BG circuitry. Optimal parameters and conditions were defined for lithography and cell culture, respectively. All cell populations appeared healthy and developed axons, which guided from soma in one port to specific neighbouring ports by micro-grooves. Findings from this work were used to study BG cell connectivity/communication, presented in Chapter 5.

Chapter 5: Fabrication of a complex, functional basal ganglia circuit – an *in vitro* model built using microfluidics

5.1 Introduction

Microfluidic devices can be used for developing oriented neuronal circuitry. Cells can be co-cultured in separate compartments within the device and cell-to-cell connectivity between different cell types e.g. neurons and glia cells (Hosmane *et al*. 2010) or different neuron types e.g. cortical and hippocampal neurons (Deleglise *et al.* 2014) can be studied. In the current study, the microfluidic device was used to create an *in vitro* functional model to mimic *in vivo* BG circuitry (Figure 5.1 A). As discussed in section 1.1.2, the *in vivo* circuitry involves glutamatergic input from the cerebral cortex to the striatum. GABAergic neurons from the striatum transmit inhibitory impulses to the GP and SNr. The striatum also receives dopaminergic inputs (both inhibitory and excitatory) from the SNc (Bolam *et al.* 2000).

In the present study, a model was developed using dissociated rat BG cells; the schematic of the model is displayed in Figure 5.1 B. Methods that could be used to study functional connectivity of neurons within the microfluidic device (Figure 5.1 C) include electrophysiology and Ca^{2+} imaging (section 1.1.4). Patch clamp is commonly used to study electrophysiology of excitable cells. Dynamics of ions across the plasma membrane changes a cell's electrical potential. This electrophysiology technique enables the study of changes in electrical current flowing through ion channel(s), at controlled or constant voltages (Neher & Sakmann 1976; Neher *et al.* 1978; Ogden & Stanfield 1994). Hodgkin and Huxley discovered and characterised voltage-gated Na^+ currents responsible for initiating and propagating action potentials in excitable cells. They used voltage clamp techniques to measure current through the membrane of a giant squid axon at set voltages and used their findings to create a model used to quantify generation of action potentials (A L Hodgkin & Huxley 1952; A L. Hodgkin & Huxley 1952; Catterall *et al*. 2012). The Na^+ currents can be manipulated i.e. Na^+ channels can be blocked using toxins such as TTX to avoid inward flow of ions and depolarisation of the cell membrane.

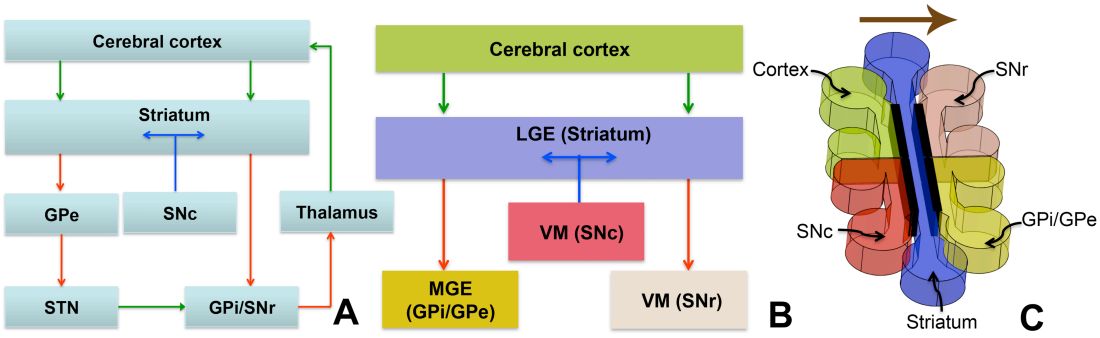

Figure 5.1: A – Schematic of basal ganglia (BG) circuitry developed *in vitro*. Blocks represent nuclei involved in forming circuitry. Connectivity is regulated by neurotransmitters and established via axons (arrows). Red arrows = inhibitory GABAergic axonal neurotransmission, green = excitatory axonal glutamatergic neurotransmission, blue = dopaminergic axonal projection to the striatum. SNr = substantia nigra pars reticulata, SNc = substantia nigra pars compacta, GPi = internal globus pallidus, GPe = external globus pallidus and STN = subthalamic nucleus. B - Schematic of the model for the current study designed to mimic BG circuitry in A, using rat dissociated brain cells. LGE = lateral ganglionic eminence, MGE = medial ganglionic eminence, VM = ventral mesencephalon. In B, the names of the developing tissue in relation to the BG circuit *in vivo* (A) are enclosed in brackets. Schematics displayed in both A and B were adapted from (Albin *et al.* 1989). C - five-port microfluidic device designed to accommodate all (five) cell types in B as well allow connectivity among them. Tapered micro-grooves were used to control direction of axon orientation; brown arrow (top of C) indicates direction of groove tapering/axon orientation. Colours in C correspond to those in B, showing how the arrangement of cells in the microfluidic device relates to model circuitry. Black parallel lines on C indicate position of the micro-grooves.

As discussed in section 1.1.4, Ca^{2+} imaging provides indirect yet accurate means of studying generation of action potentials. Unlike the patch clamp, Ca^{2+} imaging permits simultaneous recordings from large populations of neurons, at a single cell resolution. Changes in endogenous concentration of Ca^{2+} ions can be used to study generation of action potentials within a population of cells. That is, Ca^{2+} oscillations indicated by indicator dye fluorescence changes can be used to study stimulated or spontaneous firing activity (Smetters et al. 1999; Yuste et al. 2011). Ca^{2+} oscillations were studied in BG cell populations within microfluidic devices, particularly the response of specific subtypes of neurons to elimination of action potentials by TTX elsewhere within the network, to assess the functional connectivity between the ports.

5.2 Experimental procedures

Excitability of cortical and striatal neurons was studied using the whole cell voltage clamp technique (section 2.12); this technique is a form of patch clamp. Ca^{2+} imaging (section 2.13) was first carried out for cortical and striatal cells on coverslips and then, inside the microfluidic device.

5.2.1 Whole cell voltage clamp

Whole cell patch clamp recordings were obtained from striatal and cortical neurons at DIV 14-18. This work was done in collaboration with Dr Michael Evans, Keele University. Recordings were made from individual cells cultured on glass coverslip. Coverslips were used only for 2-3 h to ensure cells used for the study had optimal viability. Cells to be patched were selected based on their morphology. Two micropipettes were used in the experiment. The recording patch pipette was filled with intracellular solution (section 2.12.1). The application pipette was filled with 5μM TTX in culture medium to test TTX-sensitivity of striatal neurons. Whole-cell currents were digitized and stored on disk. For the second micropipette, a pneumatic picopump was used to eject TTX into the microenvironment of the patched cell.

5.2.2 Calcium imaging

Microfluidic devices with striatal, cortical, SN and GP cells (Figure 5.1) at DIV 14-18 were incubated in 2μM Fluo-4 for 30 min at room temperature before they were washed off with loading buffer and replaced with DMEM-F12. Ca^{2+} fluorescence oscillations were captured on an epifluorescent microscope. Recordings were obtained at 5 frames per second (fps) for 5 min for coverslips with cortical and striatal cells. 1μM of TTX in NCM was added in cortex, striatum or GP port for microfluidic devices. Pre-TTX and post-TTX recordings were simultaneously acquired 5 frames per second for 3 min for two adjacent ports, using a 4x objective lens, with ~ 2 min between each recording. Ca^{2+} fluorescence intensity recordings were obtained using the ImageJ application. Fluorescence intensity values were graphed in Microsoft Excel spreadsheets. Changes in fluorescence intensity (ΔF) were plotted against time (t).

5.3 Results and discussion

5.3.1 Electrophysiology of cortical and striatal neurons

The electrophysiology study on coverslip was carried out to verify spiking capabilities of cortical and striatal neurons before they were loaded and cultured in microfluidic devices. Voltage clamp studies were first performed for cortical neurons; studies involved recording changes of current

through a cortical neuron membrane in response to voltage-clamp steps. Neurons were identified from glial cells by morphological appearances i.e. cortical neurons had pyramidal, three-dimensional phase-bright appearance as opposed to flat, two-dimensional and non-phase-bright glia cells. Inward Na^+ currents were generated in response to voltage step inputs (Figure 5.2 A and B). Voltage-gated Na^+ current initiates generation of action potentials in excitable cells; this was first reported by Hodgkin and Huxley in a series of papers they published on the dynamics of ions flow across membrane and explanations of mechanisms involved in generation of action potentials. They used voltage clamp techniques to study current through the membrane of a squid giant axon (Catterall *et al.* 2012).

In current clamp, in the present study, it was found that E16 cortical neurons possess spontaneous and depolarisation induced spiking activity. The technique involves studying voltage changes in response to 'clamped' or constant current. Four voltage traces (indicated by blue, red, black and green colours) are shown on the voltage graph in Figure 5.2 D; they all signify voltage or neuron membrane potential in response to the current injection steps shown in corresponding colours on the bottom current (I) graph. There was a small negative holding current from around 0.5 s (Figure 5.2 D) meaning no voltage spiking was expected. However, at approximately 1 s a voltage spike (green trace, Figure 5.2 D) was generated; since this spiking occurred in the absence of depolarising current injection it represented spontaneous, cortical electrical spiking activity.

As already established, input to the BG micro-circuit *in vivo*, is mainly provided by cortical neurons (Wilson & Groves 1981; Kandel *et al.* 1991; Cepeda *et al.* 2007). The present study involved analysis of Na^+ current profiles. Hammond and colleagues cultured E18 cortical cells on MEAs pre-coated with 10% FCS medium. Cells were cultured and electrophysiological activity recorded up to DIV 61. Spontaneous firing was observed in both immature, DIV 14-25 and mature, DIV 37-61, cortical neurons. Increased impulse firing and spiking was recorded in immature neurons in comparison to mature neurons (Hammond *et al.* 2013). Wagenaar and colleagues also cultured E18 cortical cells on MEAs (Wagenaar *et al.* 2006). However, their MEAs were pre-coated with PEI and LN before cell culture. Cells had different densities, from 300-5,000 neurons/30-75 mm^2 cultured for around 5 weeks. The group found that E18 cortical neurons initiated spontaneous

activity from as early as DIV 3-4 and that the electrical activity patterns (such as shapes and sizes of burst spikes generated by cortical neurons *in vitro*, e.g. from DIV 2-32) were complex.

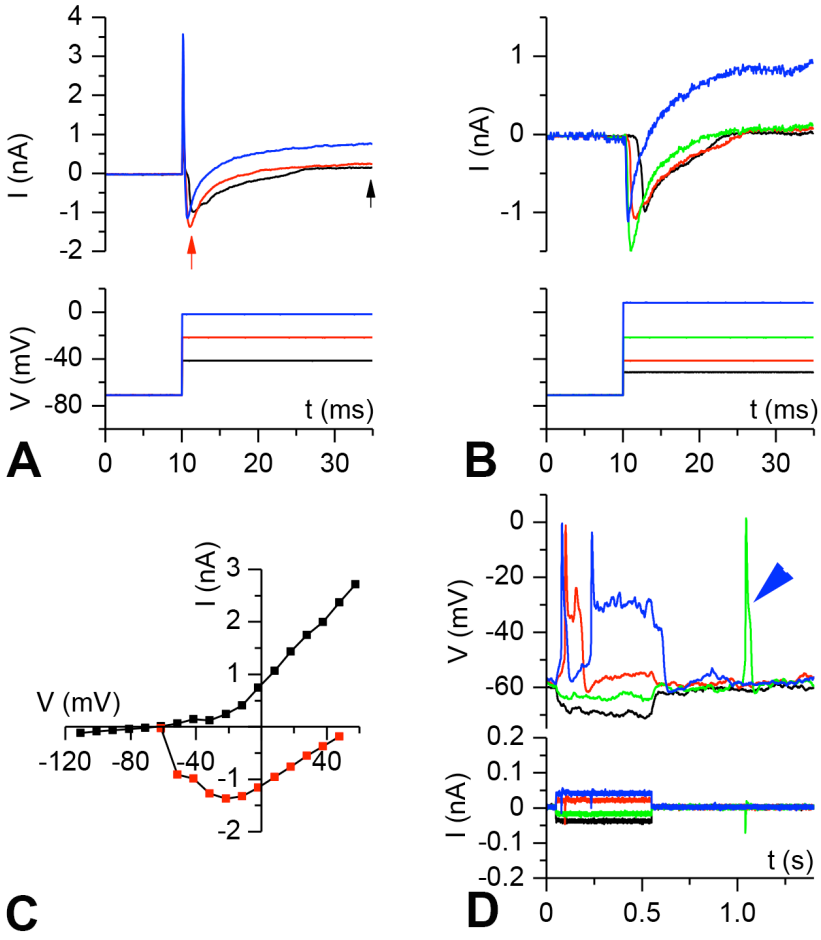

Figure 5.2: Depolarisation of a cortical neuron. (A) Voltage clamp i.e. recordings of changing current in response to constant levels of voltage injection, indicated below. The black arrow shows steady-state Na^+ current and the red arrow shows peak inward current (B) Voltage clamp data but with leak-subtracted using an equal opposite voltage step. (C) Current-voltage (I-V) graph of a cell in A showing "steady-state" current measured at ~30 ms and peak inward current. (D) Current clamp records from same cell show spontaneous spiking (blue arrowhead), at approximately 1 s.

In the current study, TTX was used to assess whether it was possible to manipulate, i.e. abolish and reinitiate, generation of action potentials in neurons. Striatal neurons with spontaneous activity were found to be sensitive to TTX (Figure 5.3). The inward Na^+ current observed before TTX, was eliminated after TTX was applied to neurons. A higher concentration of TTX (5 µM) was used compared to other studies for two reasons: to get a rapid effect of TTX and to minimise the effect of dilution of the drug in bath solution. Table 1 shows examples of studies that have used TTX to eliminate the inward Na^+ current.

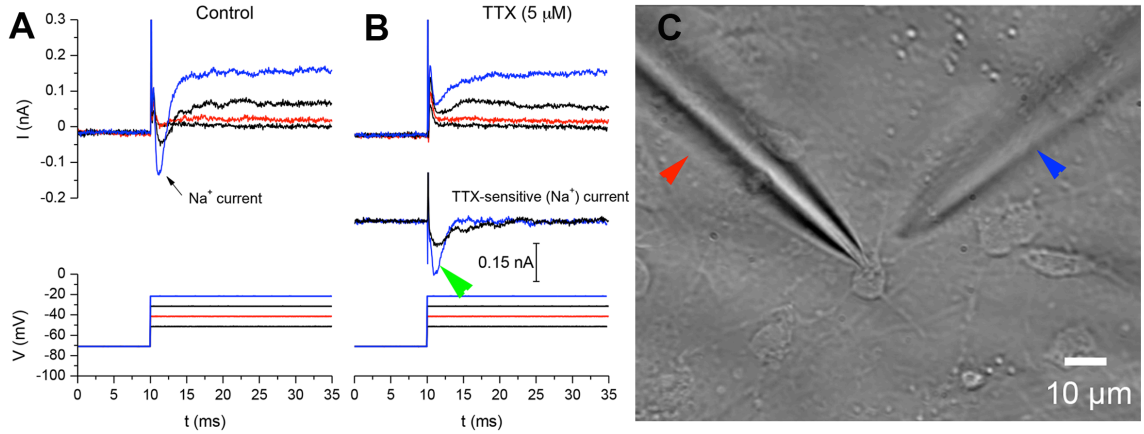

Figure 5.3: Depolarisation of a striatal neuron and its response to TTX. (A) Voltage clamp data before TTX was applied to cell (control), voltages are shown below. (B) Voltage clamp data after a puff application of 5μM TTX, from the pipette indicated by a blue arrowhead in C. TTX-sensitive currents (green arrowhead) were obtained from subtraction of TTX records from control records. (C) Recording and TTX pipettes, indicated by red and blue arrowheads, respectively.

Table 5.1: Examples of neuron studies where Na^+ currents were eliminated by TTX.

Cell type	TTX concentration	Reference
Basal forebrain cholinergic	2 μM	(Duan *et al.* 2014)
Cortical	1 μM	(Gorelova & Yang 2000)
Striatal	0.5 -1 μM	(Nisenbaum & Wilson 1995; D'Ascenzo *et al.* 2009)
Midbrain dopamine	1 μM	(Puopolo *et al.* 2007)

5.3.2. Ca^{2+} imaging analysis

Ca^{2+} oscillations were studied in BG cell populations on unconnected cells (cultured as individual populations on pre-coated coverslips) for cortical and striatal cells, and connected cells (cultured in five-port microfluidic devices). TTX was applied to various microfluidic ports to determine the functionality and connectivity of BG cells, i.e. to eliminate activity of one cell population and study subsequent responses from upstream and downstream ports (or cell populations) within the microfluidic device (Figure 5.4). The terms upstream and downstream ports refer to ports preceding and succeeding the port in question, respectively; for instance in Figure 5.4A, blue arrowheads indicate upstream and black arrowheads, downstream ports with respect to the central, striatum port.

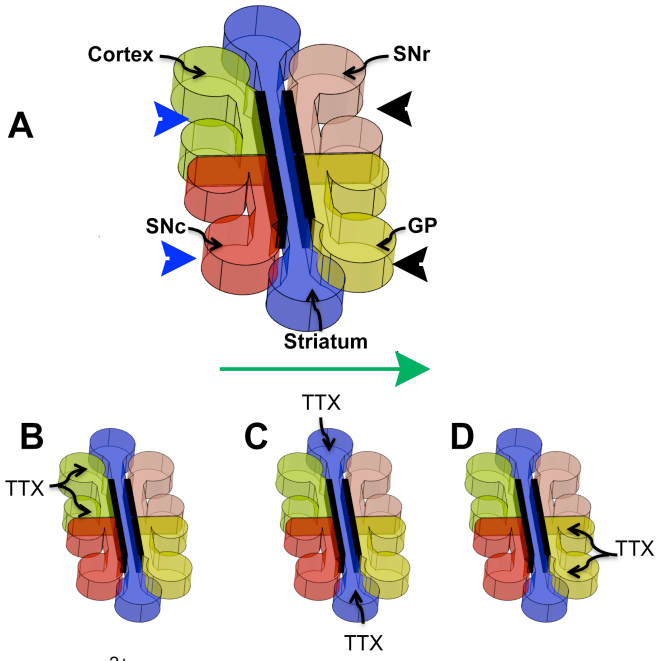

Figure 5.4: Schematics of Ca^{2+} imaging set-up in microfluidic devices. (A) Schematic showing arrangement of basal ganglia (BG) cells cultured in microfluidic devices. Green arrow indicates the direction of tapered micro-grooves i.e. from wide openings of 15, 25 or 50 µm to a narrow end of 5 µm. Blue arrowheads = upstream ports and black arrowheads = downstream ports. Studies of BG upstream and downstream cell populations' response to TTX application to the: (B) cortex, (C) striatum and (D) GP ports were performed to assess cell connectivity inside the device. Black lines on microfluidic devices indicate where micro-grooves are located.

Cells cultured on PDL and LN coated coverslips and in microfluidic devices (Chapter 4), adhered very well to the substrates and had good viability. Cells did not lift off substrates when ports or coverslips were flooded with media. Viability was determined by assessing morphological appearance of adhered cells; neuronal cell bodies appeared phase-bright, three-dimensional and developed small neurites. The following parts of this chapter cover Ca^{2+} imaging results and discussions concerning upstream and downstream cells' response to TTX applied into: 1.Cortical cells, 2.Striatal cells and 3.GP cells.

5.3.3 Upstream and downstream cells' response to TTX in the cortex port

a. Activity of cortical cells on coverslips

Increase in Fluo-4 dye fluorescence can be directly related to an increase in Ca^{2+} ion concentration (Gee *et al.* 2000; Robinson *et al.* 2004). Unconnected cortical cells displayed random spontaneous Ca^{2+} oscillations (Figure 5.5). The amplitude and time periods between oscillations in cortical cell

populations in this study varied from cell to cell. Nonetheless, changes in fluorescence (ΔF), hence Ca^{2+} oscillations, were very apparent and were likely caused by cells generating action potentials.

Other groups have reported that cortical neurons exhibit spontaneous electrical activity. Steve Potter and colleagues found that E18 cortical cells cultured *in vitro* exhibited spontaneous bursts that were variable across different cultures, e.g. different seeding density, as well as within same cultures i.e. repeats of the same cultures (Wagenaar *et al*. 2005; Wagenaar *et al.* 2006). They recorded burst patterns up to DIV 45 and discovered variations within cultures from day to day. At times, action potential bursts were delayed for several minutes, especially in early cultures (~DIV 7). Burst activity increased as cortical networks further developed in culture; most spiking activity was observed around DIV 20-25.

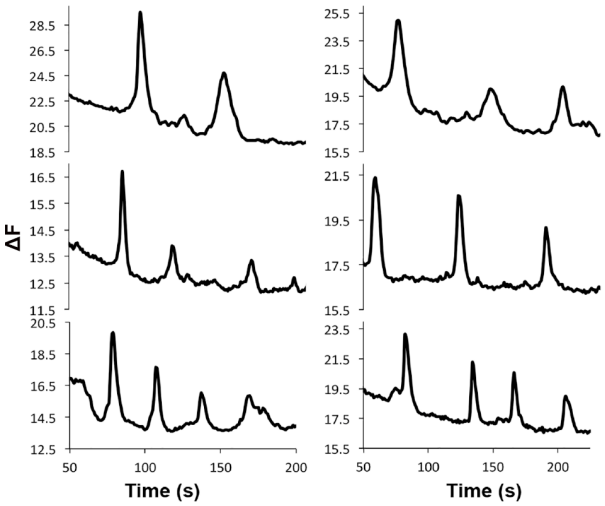

Figure 5.5: Ca^{2+} oscillations of cortical cells cultured on coverslip substrates. ΔF is the change in Fluo-4 (Ca^{2+} indicator) fluorescence.

b. Activity of cortical cells before and after treatment with TTX

The response of cortical cells located in the cortex port, to TTX, was then studied. Ca^{2+} dynamics in cortical cells were imaged before TTX was loaded into the cortex port. Ca^{2+} oscillations were observed. Cortical cells' spontaneous activity (indicated by Ca^{2+} oscillations) was abolished by application of TTX, resulting in a significant reduction in oscillations (Figure 5.6). The patterns of oscillations before TTX was applied were different for the 6 cells recorded.

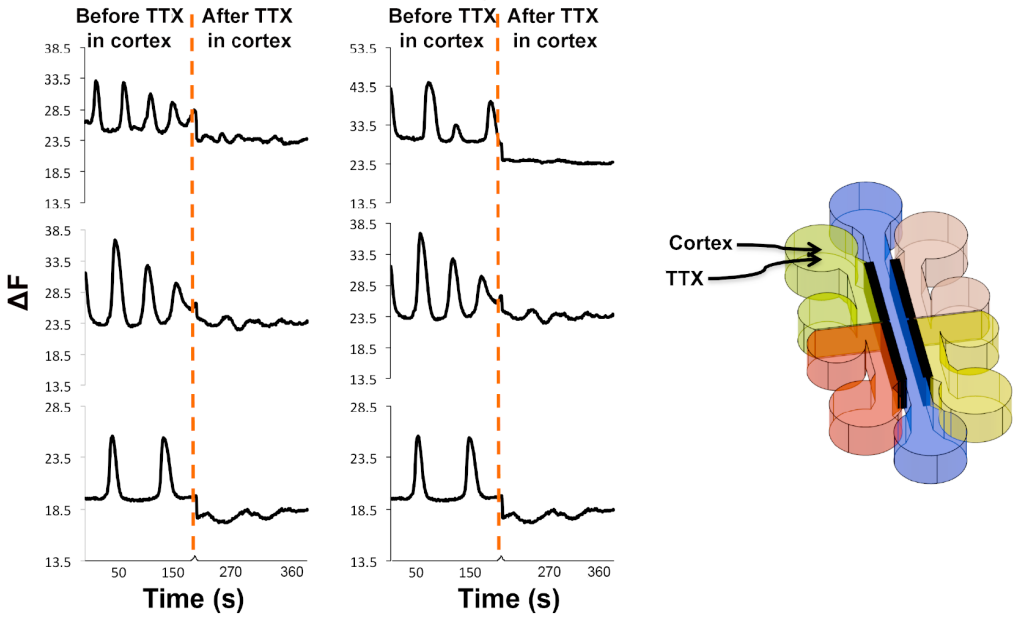

Figure 5.6: Ca^{2+} oscillations traces of cortical cells before and after TTX in the cortex port.

c. Activity of striatal cells before and after the treatment of cortical cells with TTX

Ca^{2+} dynamics of striatal cells were studied before and after TTX was applied to the cortex port. Evidence from brightfield and fluorescence photographs (Chapter 4) suggests that cortical axons had extended into the striatum port by DIV 12-13. Striatal cells yielded Ca^{2+} oscillations before TTX was applied to cortical cells. It was found that after TTX was loaded into the cortex port, the downstream striatal cells responded by abolishing their Ca^{2+} oscillations (Figure 5.7). Findings from inter-port fluid diffusion studies (section 4.3.2.2) were carried out using FITC and TRITC dye solutions suggested that TTX did not diffuse between upstream to downstream ports. Indeed, from intensity measurements it appears that any diffusion that may have occurred was most likely contained within the micro-groove area due to fluidic pressure from neighbouring ports. Analysis carried out for inter-port diffusion tests were done on fluorescence photographs captured at 30 min. The total time required to record Ca^{2+} oscillations for all BG cells in the microfluidic device, including changing port locations, was found to be approximately 18 min, which is well within the diffusion test time (30 min). This means, for at least 30 min, TTX most likely could not have diffused into the striatum port to cause reduction of Ca^{2+} oscillations. Nevertheless, there is a slight possibility that some of the TTX placed in the cortical port may have leaked into the striatum port to cause the effect.

Osanai *et al*. found that striatal cells (from a corticostriatal acute slice) exhibited spontaneous Ca^{2+} oscillations (Osanai *et al*. 2006). However, the oscillations were not triggered by excitatory input from the cortex. Membrane excitation by cortical input would have opened up VOCs. This would have led to a rise in concentration of intracellular Ca^{2+}, $[Ca^{2+}]_i$, depolarization and Ca^{2+} oscillations. Nevertheless, this was not the case in their study since TTX was not effective in eliminating Ca^{2+} oscillations. Instead, they discovered that the rise in $[Ca^{2+}]_i$ and consequently induction of Ca^{2+} oscillations, was attributed to the release of Ca^{2+} from the endoplasmic reticulum (ER) since the Ca^{2+} oscillations were significantly reduced by thapsigargin, an inhibitor that depletes the Ca^{2+} store, shown by blocking Ca^{2+}-pumps (Osanai *et al.* 2006; Tamura *et al*. 2014). The ER is a structure within a neuron that stores Ca^{2+} (Berridge 1998).

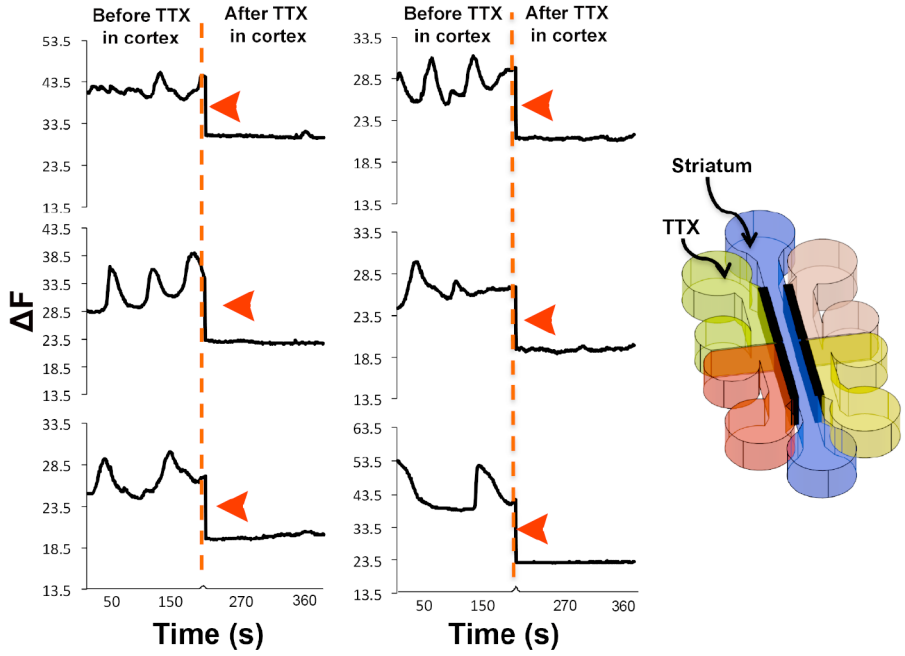

Figure 5.7: Ca^{2+} oscillations of striatal cells before and after TTX application in cortical cells (n=6). Red arrowheads indicate an immediate decrease in Ca^{2+} activity following TTX application to the cortical port. The lower baseline following TTX treatment may indicate a photobleaching effect, as there was a time-lag of ~20 min between pre-TTX and post-TTX measures.

In the current study, the response of Ca^{2+} oscillations in cortical cells to TTX confirms that the oscillations are directly related to generation of action potentials. Therefore the response of striatal cells to elimination of electrical activity in cortical cells means that the two cell populations are likely to have established functional connectivity.

d. Activity of SN cells before and after the treatment of cortical cells with TTX

The SNc and SNr ports both contain the same (SN) type of cell since the tissue is closely apposed and therefore unable to be sub-dissected from the embryonic rat brain. Based on the design of the five-port microfluidic device (inspired by the *in vivo* BG circuit, Figure 5.1), cortical cells do not form a direct connection to SN cells. Therefore, connection of cortical cells to the SNc port (upstream SN cells) is established indirectly via the striatum port. Variable Ca^{2+} oscillations were observed in SN cells' recordings before TTX was applied to cortical cells (Figure 5.8). It was found that applying TTX into the cortex port led to a reduction of Ca^{2+} oscillations in upstream SN cells. However, residual Ca^{2+} oscillations indicated by blue arrowheads in Figure 5.8 were observed in some (3/6) upstream SN cells after TTX was applied. SN cells consist of dopaminergic and GABAergic neuronal subtypes. Residual oscillations could be due to tonically active oscillations of dopamine neurons not sensitive to TTX (Yung *et al.* 1991; Nedergaard *et al*. 1993; Wilson *et al.* 2000). This may also be due the fact that there is limited direct connectivity between cortical and SN cells, and some of the SN cells are firing action potentials independently of any input from other ports. Nevertheless, the data suggest that there may be some degree of connectivity between ports since 50% of SN cells responded to TTX loading to cortical cells. TTX application in upstream cortical cells eliminated Ca^{2+} oscillations in downstream striatal cells (Figure 5.7). As mentioned earlier (Figures 5.1 and 5.4), design of microfluidic devices included tapered micro-grooves to provide directed SNc axonal extensions to striatal cells. In the current part of the study, it may be possible that upstream SNc cells responded to elimination of oscillations of their target cell group, downstream striatal cells.

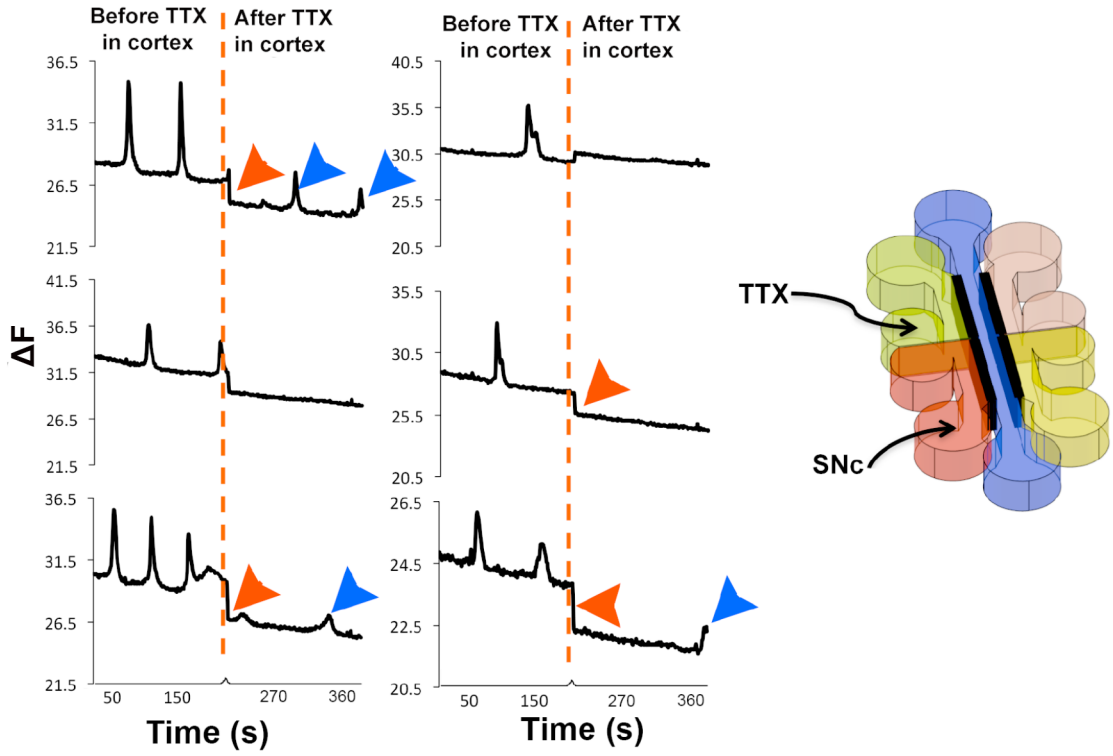

Figure 5.8: Ca^{2+} oscillations of upstream SNc cells before and after TTX loading in cortical cells. The general downward trend of the traces is possibly due to the photobleaching effect. Blue arrowheads indicate some residual electrical activity occurring in SN cells, located in the SNc port, after TTX was applied to the cortex port.

The classic BG circuitry shows that the SN does not have direct communication with the cortex (Kandel *et al.* 1991). However, an *in vivo* study by Tseng *et al.* found that slow cortical rhythmic impulses were transmitted to the SNr and GPi nuclei (output nuclei), after the SN→striatum pathway was damaged (nigrostriatal lesions) (Tseng *et al*. 2001). Membrane potentials of striatal neurons transmitting impulses to the output nuclei switch between 'up'- depolarised and 'down' – hyperpolarised state (Plenz & Kitai 1998; Wilson 2010). The 'up' state is initiated by thalamic or cortical excitatory inputs (Plenz & Aertsen 1996). Tseng *et al*. found that there was a connection between change in striatal membrane potential and the cortical firing input. So, when the nigrostriatal circuit was lesioned using 6-OHDA, the excitability of the striatum was increased and that enabled transmission of impulses from cortex to the output nuclei (GPi and SNr). Work by Tseng *et al* implies that cortical neurons are capable of evoking a response from SN neurons, which is comparable to findings of the present study. Therefore, the response of 3/6 cells no longer firing could mean that the cells belong to the SNr GABAergic cell population.

e. Activity of GP cells before and after treatment of cortical cells with TTX

The GP cells' response to TTX in the cortex port was studied. Cortical cells should not be directly connected to GP cells; it was assumed that connection is established via striatal cells located in the central, striatum port. Prior to TTX loading, GP cells showed Ca^{2+} oscillations (Figure 5.9). Cells then displayed significant reduction in Ca^{2+} oscillations after the cortical cells' activity was abolished by TTX (Figure 5.9). The response of GP cells to silencing cortical cells, suggests there is communication between the cell populations. If TTX had switched off firing in the striatal population, in a mature *in vivo* system, then the result would have been disinhibition i.e. increased firing in the GP port. One explanation for this is that it is possible striatal cells were excitatory in the current model and therefore, elimination of activity in cortical cells led to reduction in striatal oscillations and subsequently GP cells. The GABA neurotransmitter can be excitatory during early development. DRG cells and immature CNS neurons express the Na^+-K^+-$2Cl^-$ (NKCC1) cotransporter more than the K^+-Cl^- (KCC2) cotransporter. A cotransporter is a protein responsible for simultaneously transporting substances, e.g. ions, across cell membrane. More expression of NKCC1 in immature neurons raises the intracellular concentration of chloride $[Cl^-]_i$. An increase in $[Cl^-]_i$ results in Cl^- efflux and consequently, membrane depolarization and generation of action potentials. Mature neurons express more KCC2 than NKCC1. This reduces $[Cl^-]_i$ leading to Cl^- influx and hyperpolarization (Stein & Nicoll 2003; Batista-Brito & Fishell 2009).

GP cells do not receive direct afferents from the cortex *in vivo* (Bolam *et al.* 2000). However, according to Sano *et al*. GP nuclei *in vivo* respond to cortical stimulation (Sano *et al.* 2013). 37% and 33% of GP neurons for a D2 mutant and wild type mice, respectively, responded to stimulation of the cortex. The response was in 3 phases: an EPSP, followed by IPSP and then an EPSP again. The cortical→STN→GP *in vivo* pathway mediates the first (excitatory) phase. The cortical→striatal→GP pathway mediates the second (inhibitory) phase and the cortical→striatal→GP→STN→GP pathway mediated the third (excitatory) phase. When D2R-expressing striatal neurons were damaged, the response of GP neurons to cortical stimulation rose to 52% and 43% for D2R mutant and wild-type mice, respectively. Therefore, it is possible that GP cells can respond to elimination of electrical activity in cortical cells, as was found in the current study.

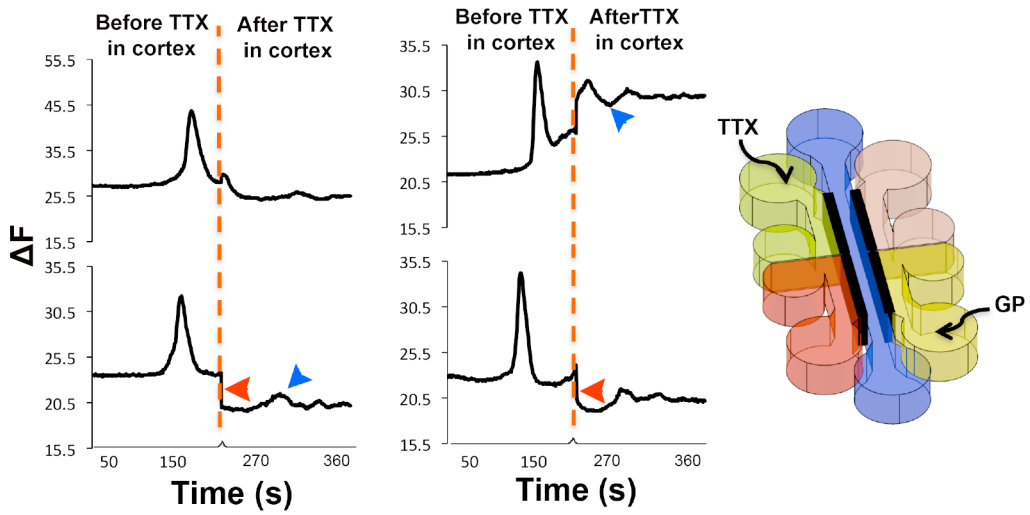

Figure 5.9: Ca^{2+} oscillations of GP cells before and after TTX in cortical cells. The drop in intensity after the break (red dotted line) indicated by red arrowheads may be due to photobleaching effect. Blue arrowheads indicate very small amplitude residual Ca^{2+} oscillations occurring in GP cells after TTX was applied to cortical cells.

Findings in this section (TTX in the cortex port), suggest that the cortical cell population is: directly connected to the downstream striatal cell population and indirectly (most probably via the striatal cell population) connected to the GP and SN cell populations. All cell populations in the microfluidic device responded to TTX loading in the cortex port. As discussed earlier, studies were performed to ensure TTX did not diffuse into neighbouring ports, particularly, into the striatum port. Furthermore, the minute dimensions of the structures involved in the microfluidic device and the length of the micro-grooves makes the fluid flow inside the device controllable i.e. in a laminar, steady state flow range and reduces chances of fluids flowing into neighbouring ports (Halldórsson *et al.* 2014; Lee *et al.* 2011).

5.3.4 Upstream and downstream cells' response to TTX loaded into the striatum port.

Studies were also carried out to measure Ca^{2+} oscillations of striatal cells cultured on pre-coated substrates and how BG cells in other ports responded to TTX in the striatum port.

a. Activity of striatal cells on coverslips, and device before and after treatment with TTX

Dissociated striatal cells were cultured on coverslip substrates for DIV 14-18. It was found that striatal cells yielded spontaneous Ca^{2+} oscillations. Ca^{2+} oscillation traces appeared to be random and variable from cell to cell (Figure 5.10). In contrast to the current study's findings, *in vivo* studies have reported that striatal neurons are inhibitory and do not exhibit spontaneous electrical activity. For animals with thalamic or cortical lesions, it was found that the striatum displayed '*hyperpolarized periods*,' i.e. periods where cell membranes were not depolarized and so did not generate action potentials. The thalamus and cortex mainly provide input to the striatum. Striatum slices cultured on their own *in vitro* also lacked spontaneous activity. This was mainly due to lack of sufficient excitatory input from the cortex and thalamus (Wilson & Groves 1981; Wilson & Kawaguchi 1996).

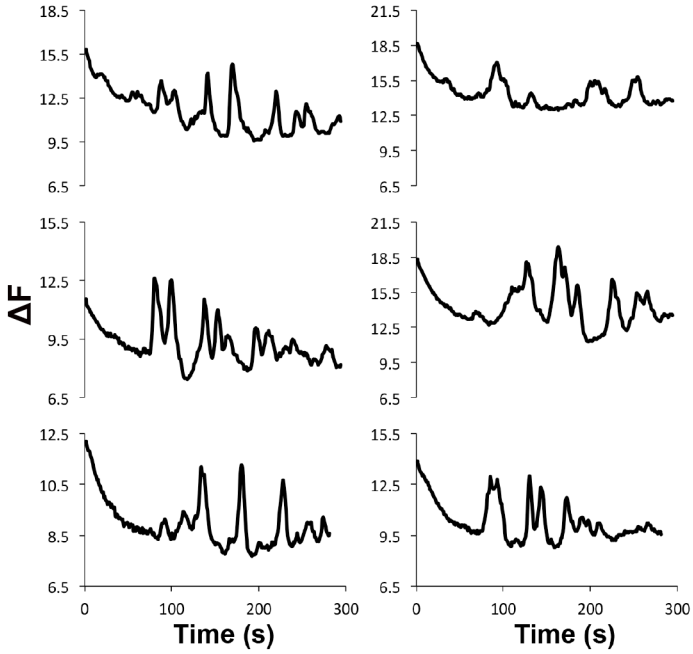

Figure 5.10: Ca^{2+} oscillations of striatal cells cultured on coverslip substrates.

Peyrin *et al*. found that pure E14 striatal neurons from a mouse cultured for DIV 12-16 did not present spontaneous activity since they did not show Ca^{2+} oscillations (Peyrin *et al.* 2011). However, in the current study Ca^{2+} oscillations were observed for striatal cells dissociated from E15/16 rat tissue. Mueller *et al*. found that the less developed GABA inhibitory system of immature rabbit hippocampus, i.e. 6-10 days after birth had a depolarizing effect. However, in mature CA1

pyramidal neurons, i.e. from rabbits 1 month after birth the EPSPs were switched to IPSPs resulting in membrane hyperpolarization (Mueller *et al*. 1984).

In the current study (Figure 5.10), it was found that striatal cells cultured in a microfluidic device also yielded Ca^{2+} oscillations. This could be due to cortical inputs making functional synapses on striatal neurons as shown by others such as Peyrin *et al*. When TTX was loaded into the striatum port, Ca^{2+} oscillations were greatly reduced (Figure 5.11.) implying oscillations were triggered by action potentials. Ca^{2+} influx through VOCs changes the cell membrane potential leading to depolarisation and generation of action potentials (Catterall 2011).

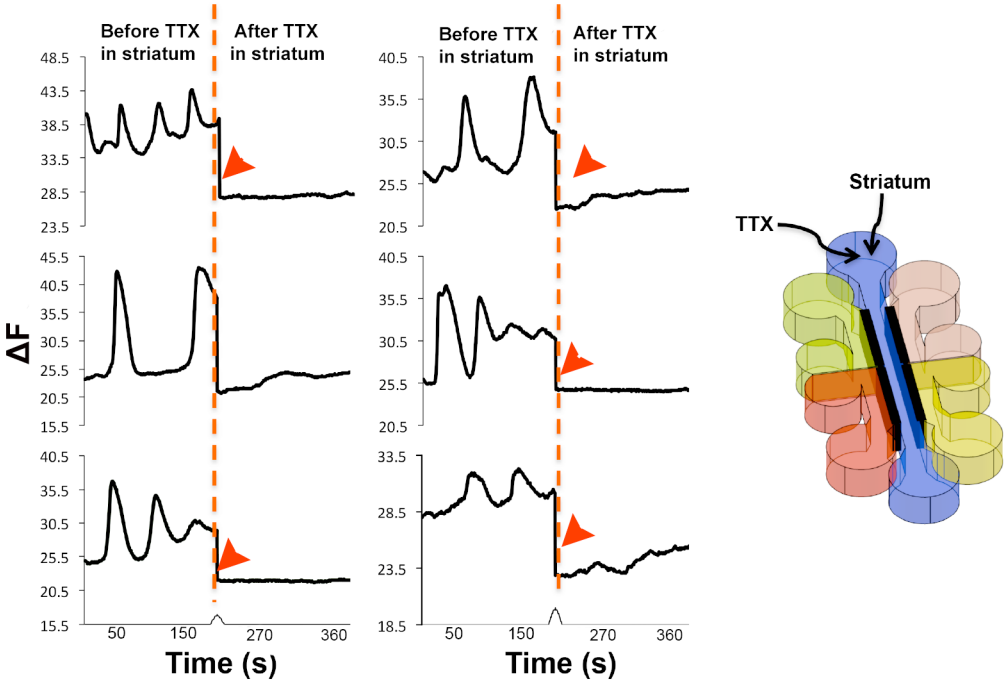

Figure 5.11: Traces of Ca^{2+} oscillations of striatal cells before and after TTX was applied in the striatum port. The drop in overall intensity indicated by red arrowheads may be due to photobleaching effect.

b. Activity of cortical cells before and after the treatment of striatal cells with TTX

Ca^{2+} oscillations of the cortical cell population were monitored using Ca^{2+} imaging. The response of cortical cells in the microfluidic device, when TTX was loaded into striatal cells was studied. It was found that Ca^{2+} oscillations of cortical cells were significantly reduced in response to TTX in the

striatum port (Figure 5.12.). This provided further evidence that connectivity was established between cortical and striatal cells in the device, since cortical cells responded to elimination of striatal Ca^{2+} oscillations. This suggests that cortical and striatal neurons in the current model established electrical connectivity.

Cepeda *et al*. developed a mouse HD model (R6/2) to study how the corticostriatal circuitry was affected by the disorder (Cepeda & Hurst 2003). In particular, how cortical input was affected by damage in the striatum. Frequency of spontaneous EPSCs generated from the cortex and transmitted into the striatum was similar in 3-4 week old transgenics and non-symptomatic controls.

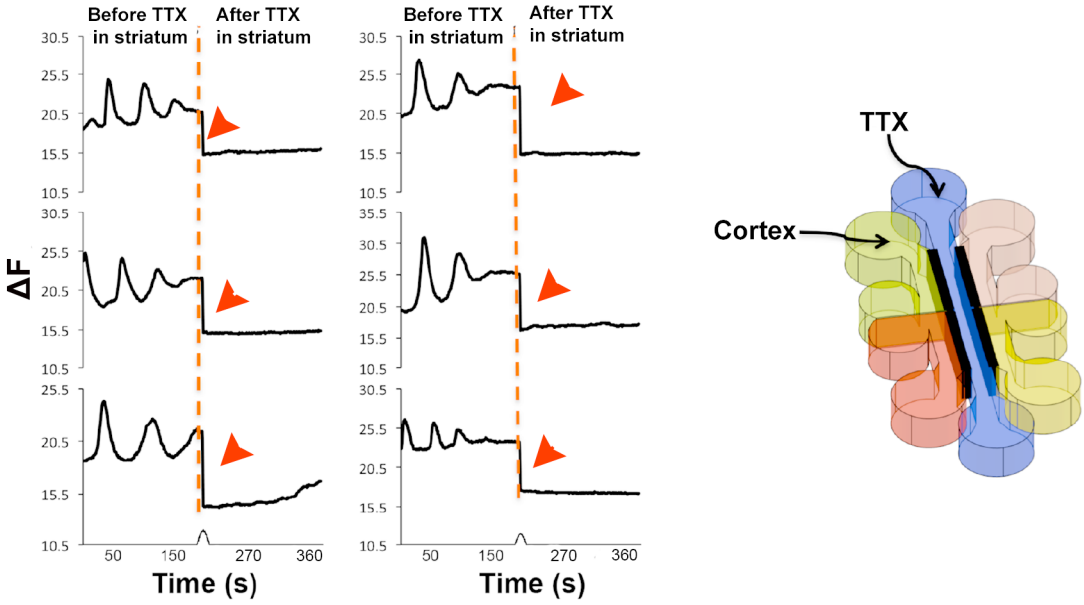

Figure 5.12: Traces of Ca^{2+} oscillation of individual cortical cells before and after TTX was applied to striatal cells in the microfluidic device. The drop in baseline indicated by red arrowheads may be due to photobleaching effect.

At older ages (11-15 week), as the HD symptoms manifested, the frequency of EPSCs from the cortex was significantly reduced in the striatum of transgenics compared to controls. This suggested that damage to the striatum (as HD symptoms progressed) resulted in changes to spontaneous electrical input from the cortex (Cepeda & Hurst 2003). Klapstein and colleagues found that R6/2 HD models required more intense stimuli to generate EPSPs in the striatum compared to their wild-type, non-symptomatic counterparts; also indicating the connectivity between the cortex and the striatum and it's alteration in the diseased state (Klapstein *et al.* 2001).

c. Activity of SN cells before and after the treatment of striatal cells with TTX

SN cells cultured in microfluidic devices demonstrated spontaneous Ca^{2+} oscillations before TTX was applied to striatal cells. Downstream SN cells responded to TTX in the striatum port by significantly reducing Ca^{2+} oscillations (Figure 5.13). This finding suggests that connectivity is established between striatal and SN cells in the microfluidic device, especially since it was found that striatal axons were capable of extending to neighbouring ports (Chapter 4).

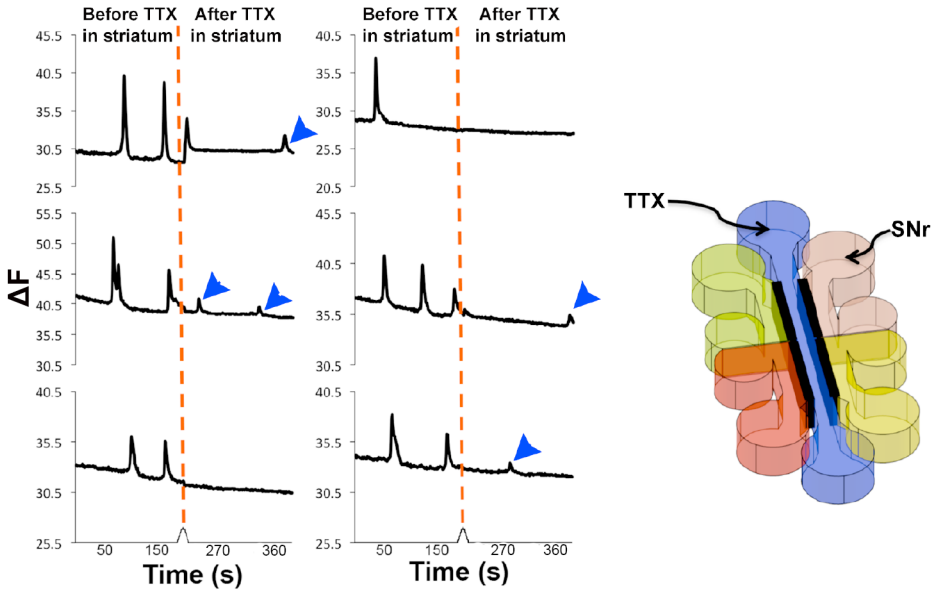

Figure 5.13: Ca^{2+} oscillations of SN cells before and after TTX in striatal cells. Blue arrowheads indicate residual electrical activity occurring in downstream SN cells located in the SNr port after TTX was applied to striatal cells.

However, small oscillation traces were observed (4/6 cells recorded) after TTX was applied. A number of studies have reported the pacemaker-like, spontaneous firing nature of SN neurons (Grace 1991; Liss *et al.* 2001; Atherton & Bevan 2005). SNc neurons transmit dopaminergic impulses into the striatum, whereas, SNr neurons receive GABAergic impulses from the striatum and transmit inhibitory impulses to the thalamus (Kandel *et al.* 1991; Bolam *et al.* 2000). Yung, *et al.* studied the electrophysiology behaviour of SNc neurons in guinea-pig midbrain slices. The group electrophysiologically distinguished the cells into 'bursting' and 'non-bursting' populations. 85% of bursting cells were discovered to be dopamine neurons; they were driven by pacemaker depolarization and demonstrated spontaneous activity with slow action potential

generation. The rest of the cells, thought to be GABAergic, were stimulated via current injection and presented rapid action potentials (Yung *et al.* 1991). SNr neurons e.g. in rat brain slices, also exhibit spontaneous activity (Atherton & Bevan 2005). Therefore, the residual spiking activity seen in the SN port following TTX application to striatal neurons, in the current study, may reflect the presence of dopamine neurons in the downstream, SNr port.

d. Activity of GP cells before and after the treatment of striatal cells with TTX

The response of downstream, GP cells to TTX loading into the striatum port was studied. GP cells in the microfluidic device showed Ca^{2+} oscillations, which indicated presence of electrical activity. The Ca^{2+} oscillations were greatly reduced after TTX was loaded into the striatum port (Figure 5.14). This suggests downstream GP cells responded to changes in the upstream striatum port; therefore, suggesting that striatal and GP cells established connectivity.

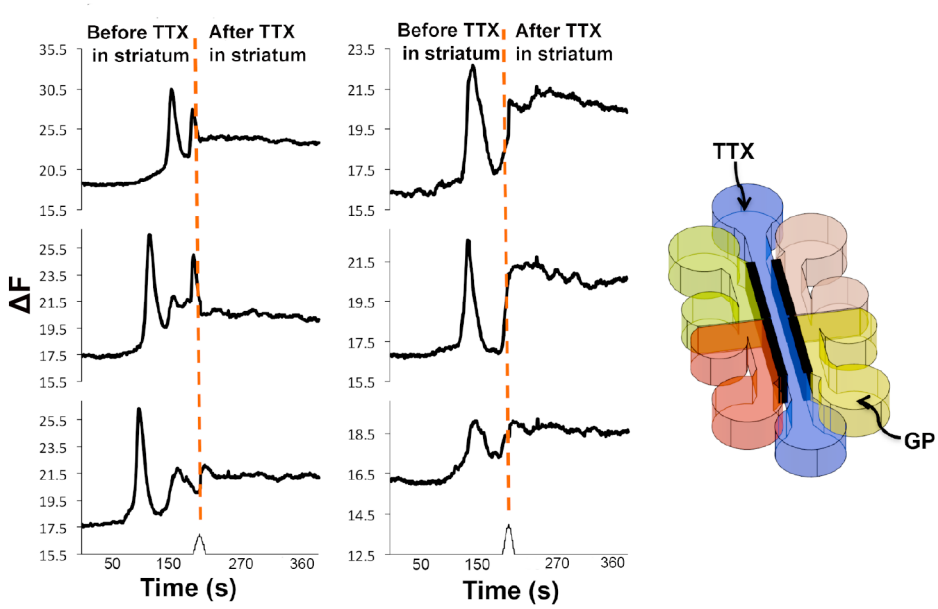

Figure 5.14: Traces of Ca^{2+} oscillations of GP cells before and after TTX was applied in striatal cells.

The striatum forms direct synaptic connection with the GP (both the internal and external parts) *in vivo*. The striatum sends GABAergic inhibitory impulses to the GP (Kandel *et al.* 1991). Since the striatum is GABAergic and therefore inhibitory, the output by GP neurons in response to TTX application in the striatal port, should be increased firing. TTX inhibits inhibitory striatal neurons

leading to disinhibition of downstream neurons. This should cause a rise in GP activity, leading to a rise in spike frequency and Ca^{2+} oscillations. However, in the current study it may be that striatal neurons are excitatory; so their inhibition would be expected to result in a drop in activity in downstream neurons (Bolam *et al.* 2000). This implies that, if the striatal and GP neurons had formed functional connections then generation of action potential (electrical activity and hence, Ca^{2+} oscillations) would have been expected in GP cells, in the absence of TTX, therefore Ca^{2+} oscillations would have been obtained (as shown in Figure 5.15).

However, eliminating activity in the striatum port using TTX would have left the GABAergic GP neurons un-inhibited and no disinhibition would have occurred; leading to increased firing in GP cells. This means more membrane depolarisation and Ca^{2+} oscillations would have been observed. Nevertheless, since GABA might have an excitatory role in the still immature cells used in the current study, it is possible that the reduction of Ca^{2+} oscillations in (excitatory) GP cells (Figure 5.14) was simply a direct response to elimination of excitatory activity in the striatal cells (also excitatory), and no disinhibition was involved.

5.3.5 Upstream and downstream cells' response to TTX loaded into the GP port.

a. Activity of GP cells before and after treatment with TTX

Ca^{2+} oscillations were recorded in GP cells inside the microfluidic device. Cells were found to be TTX-sensitive; Ca^{2+} oscillations were eliminated by the neurotoxin (TTX) (Figure 5.15.). Kita and Hashimoto investigated the firing pattern of the GPe in brain slices of juvenile rats. The whole cell patch clamp technique was used to record firing activity of GPe neurons. The neurons exhibited spontaneous firing. Phases of long depolarization and hyperpolarization, called '*slow oscillations',* noticed in GPe neurons *in vivo* were reconstructed via depolarisation and hyperpolarising of dendrites and somata, respectively. Na^{+} currents were majorly involved in generation of *slow oscillations* in GPe neurons; neurons were sensitive to TTX as a consequence (Purves *et al.* 2004a; Hashimoto & Kita 2006).

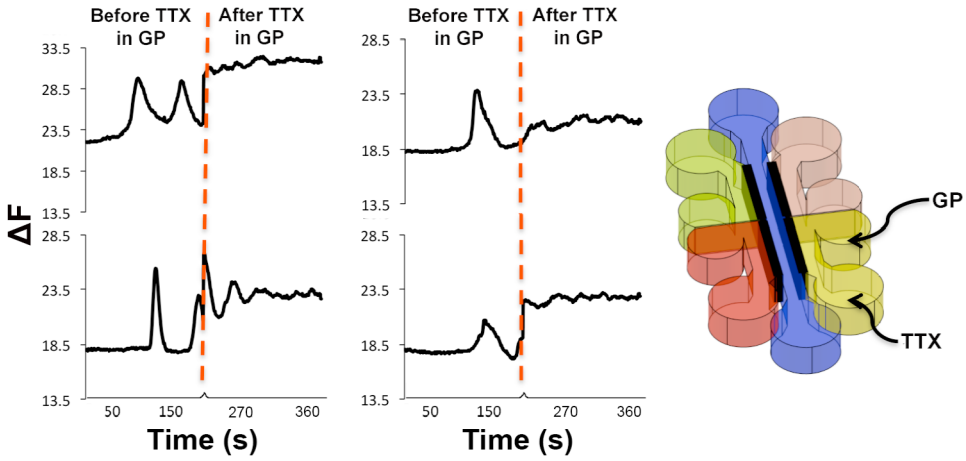

Figure 5.15: Ca^{2+} oscillations of GP cells before and after TTX in GP port.

b. Activity of striatal cells before and after the treatment of GP cells with TTX

Abolishing action potential activity in GP cells resulted in significant reduction of Ca^{2+} oscillations in striatal cells (Figure 5.16). This suggests that striatal and GP cells had formed connectivity via micro-grooves. The hypothesis was that adding TTX to the GP port should not affect the activity of the upstream striatal neurons. So the finding that the "switching off" downstream GP neurons caused a reduction in activity of their upstream striatal neurons is challenging to explain. One explanation is that because their downstream target neurons are silent, the striatal neurons have no stimulus to fire action potentials and therefore switch off their electrical activity. Alternatively, there is evidence of a sub-population of GABAergic GP neurons that project their axons back to the striatum (Spooren *et al.* 1996; Bevan *et al*. 1998). Even though the percentage of these feedback GP neurons is small, they also innervate a lot of GABA interneurons in the striatum and therefore have significant control over the activity of striatal neurons (Bolam *et al*. 2000). Due to the tapered design of the micro-grooves, the assumption is that the striatum and GP ports are connected in one direction only – i.e. axons from striatal neurons innervate the GP port, but axons from GP neurons do not innervate the striatum port. However, if there were connections in the reverse directions from the GP neurons to the striatum port, then the GP neurons could influence spiking activity. Equally, synaptic connectivity of GP and striatal cells in the current *in vitro* study could differ from connectivity established *in vivo;* since *in vivo* GABAergic cells are mature and inhibitory, whereas developing, immature cells may have exhibited excitatory behaviour (Stein & Nicoll 2003).

So, findings of the current study suggest that, if there was input from the GP neurons to the striatal neurons, then any excitatory immature striatal cells could have responded to elimination of the GP cells' excitatory input by TTX, by being switched off, causing a loss of activity in the striatum port.

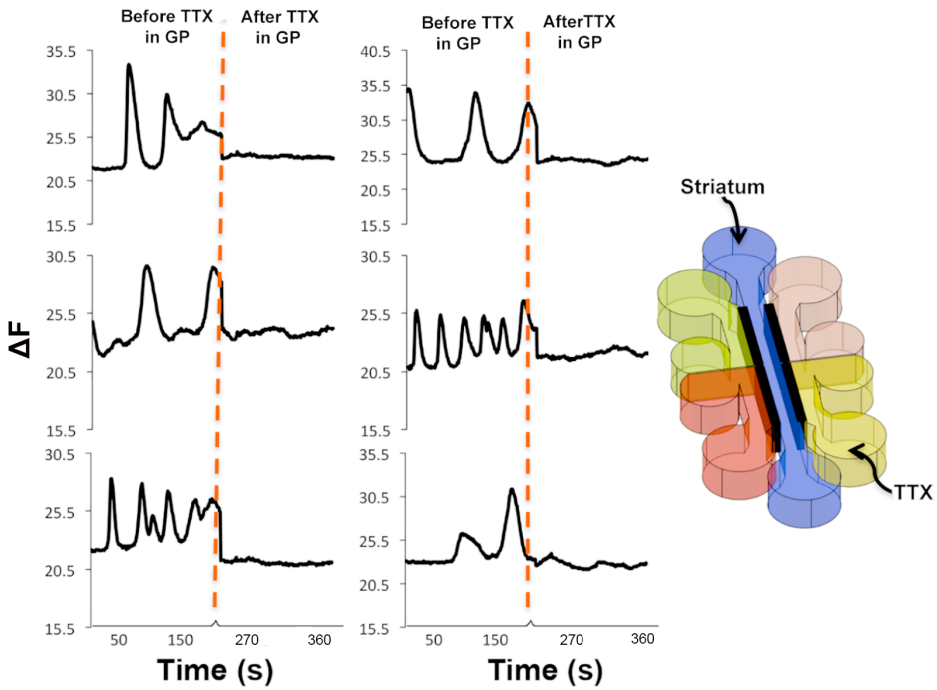

Figure 5.16: Traces of striatal cells' Ca^{2+} oscillations before and after TTX was applied to GP cells.

c. Activity of cortical cells before and after the treatment of GP cells with TTX

Ca^{2+} oscillations of cortical cells were studied after TTX was applied to the GP cell population the microfluidic device (Figure 5.17). The cortex is not directly connected to the GP in BG circuitry (Bolam *et al*. 2000), rather, it establishes communication via the striatum. In the current study, cortical cells acquired significant Ca^{2+} oscillations before TTX was applied into the GP port compared to after it was applied (Figure 5.17). The response of cortical cells, though located upstream, to TTX loading in the GP port suggests there is communication between cortical and GP cells via striatal cells. Some minor oscillations were observed in 2/6 cells recorded (blue arrowheads, Figure 5.17). Oscillations (blue arrowheads) appear much smaller than those recorded before TTX was applied. The presence of post-TTX oscillations suggests that maybe not all of the cortical cells measured were connected efficiently to other parts of the circuit, so they were less influenced by TTX application.

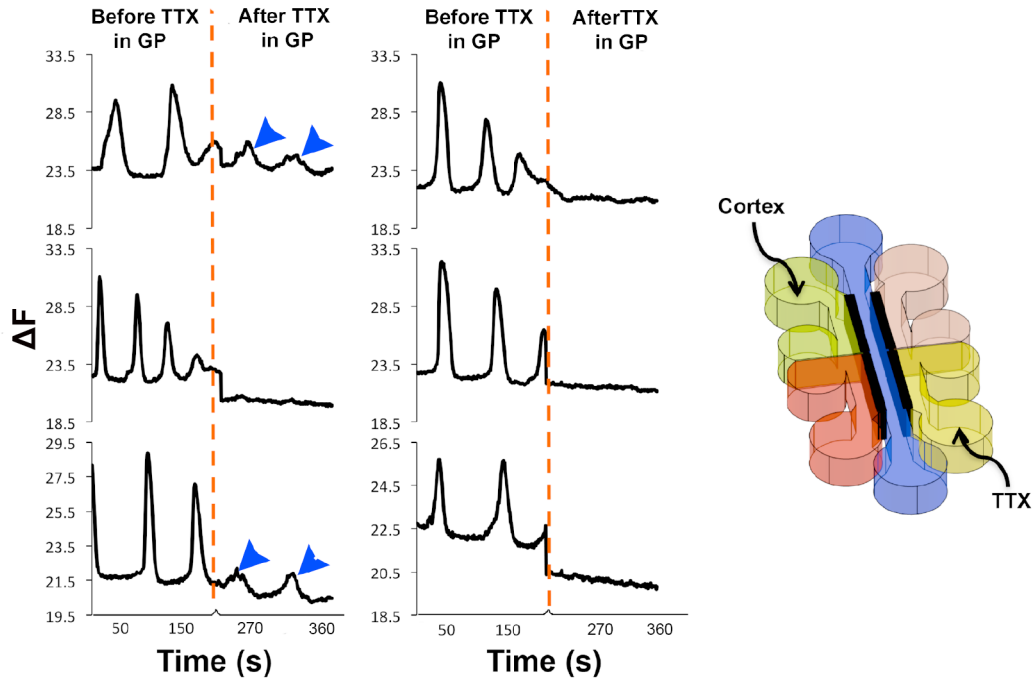

Figure 5.17: Traces of Ca^{2+} oscillations of cortical cells before and after TTX was loaded into GP cells. Blue arrowheads indicate residual electrical activity occurring in cortical cells after TTX was applied to GP cells.

d. Activity of SN cells before and after the treatment of GP cells with TTX

The response of SN cells to TTX loading in GP cells was studied. The study was carried out to determine how cells cultured in the SNc port would respond to elimination of electrical activity in GP cells. Prior to GP TTX loading, Ca^{2+} oscillations in SN cells were observed (Figure 5.18). After TTX was applied to GP cells, upstream SN cells (located in the SNc port) showed significantly reduced Ca^{2+} oscillations. There is no direct connection between SN and GP ports, so the SN cells' response to TTX in the GP port must have depended on links with the middle port, and potentially the striatal neurons residing there. The striatal neurons had to respond first (by reducing Ca^{2+} oscillations) to abolish electrical activity in SN cells. If that is the case then a SNc-striatum-GP circuit has been developed in this device. Kita and Kita established that the burst activity of GPe cells (in slice cultures) was impaired as a consequence of dopamine depletion caused by 6-OHDA (neurotoxin).

Abnormal 'pauses and bursts' generated in the GPe were reversed when a dopamine precursor, methyl-L-DOPA, was injected into the striatum (to reduce spontaneous firing). This confirmed that

alteration in the function of dopamine (SNc) neurons had led to impaired GPe firing; so, there was an electrophysiological connection between the SNc and GPe (Kita & Kita 2011). Again, both the striatal population and SN population should be upstream from the GP port, if there is unidirectional connection of axons through the tapered micro-grooves. Therefore the relationship between the three neuronal populations needs to be studied in more detail to further characterise connectivity between the three cell groups to explain the results obtained. Spiking retained (blue arrowheads, Figure 5.18) after application of TTX were likely due to presence of dopamine neurons in the upstream SNc port.

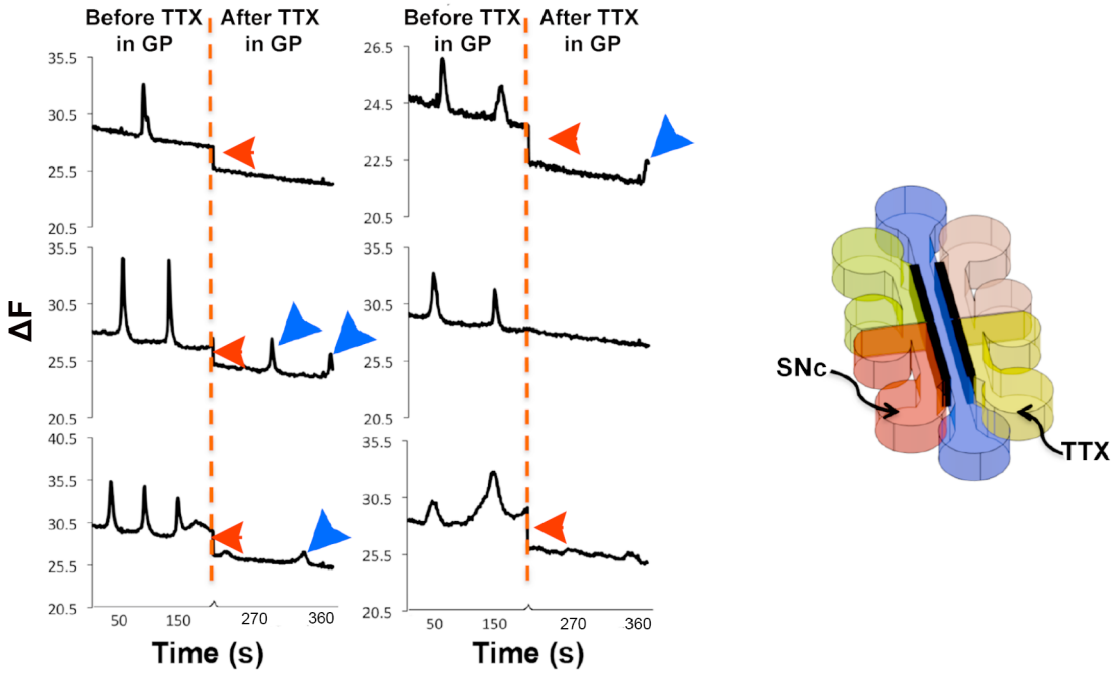

Figure 5.18: Traces of Ca^{2+} oscillation of SN cells (upstream) before and after TTX in GP cells. The general downward tendency (indicated by red arrowheads) may be due to photobleaching effect. Blue arrowheads indicate small Ca^{2+} oscillations occurring in SN cells (located in the SNc port) after TTX was applied to GP cells. SN cells still responded to TTX applied to GP cells since the amplitudes of oscillations after TTX were smaller than before TTX.

5.4 Electrophysiology techniques

Ca^{2+} imaging provides a way of monitoring the electrophysiological behaviour of populations of cells via studying Ca^{2+} dynamics across the cell membrane. As mentioned earlier, this technique provides an accurate but indirect means of studying generation of action potentials since depolarisation triggers Ca^{2+} oscillations across the membrane (Berridge 1998; Smetters *et al.*

1999; Berridge *et al.* 2000; Catterall 2011; Yuste *et al*. 2011; Grienberger & Konnerth 2012). However, the patch clamp technique provides a more direct method of measuring or studying generation of action potentials at high temporal resolution. A neuron can be 'patched' and important electrophysiology information e.g. generation and elimination of Na^+ currents, can be obtained (Sarkisov & Wang 2007; Catterall *et al*. 2012). In the current study, using the patch clamp technique to study cell connectivity within the microfluidic device presented a few challenges. First, cortical and striatal neurons cultured on pre-coated coverslips were 'patched' and recorded e.g. voltage clamp recordings were performed to study current flowing through neuron membrane and generation of action potentials. The process was very time-consuming since individual neurons had to be recorded one at a time.

Secondly, studying connectivity of neurons inside the microfluidic device was challenging, especially gaining access to cells, since the device was enclosed. An obvious option was to remove the PDMS mould off the glass surface to expose cells and simplify the 'patching' process. The PDMS device was sealed via oxygen plasma treatment (section 4.3.2.2) to form a permanent seal designed to disallow fluid leakage. An attempt was made to cut the PDMS top off from the device, however, that resulted in damage of axons that were extended between ports. Even if access had been gained inside the microfluidic device somehow without damaging the BG cell network, studying connectivity i.e. probing individual neurons in different ports would have been very time-consuming and challenging (e.g. manoeuvring the micromanipulator around the microfluidic device culture). Furthermore, sampling a large cell population would have taken longer and risked losing cell viability and affecting the quality of recordings (Giugliano & Martinoia 2006).

MEAs permit continuous, real-time and simultaneous recording of cell electrical activity; allowing multiple recordings of the same neuron over a long period of time, something virtually impossible in patch clamp and Ca^{2+} imaging (Giugliano & Martinoia 2006). Potter *et al.* reported that a dissociated cortical culture remained electrophysically active for more than 12 months (some spontaneous activity was recorded in culture after 15 months *in vitro*) (Potter & DeMarse 2001). Moreover, cultures do not have to be moved (e.g. from the incubator) for recordings to take place,

depending on the MEA system available. MEAs can be incorporated to microfluidic devices so that electrophysiological behaviour of the network developing inside the device can be monitored (Berdichevsky *et al.* 2009; Scott *et al*. 2013). Future work will involve use of MEA technology to improve connectivity and functionality studies of the BG circuit model.

5.5 Conclusion

The study intended to build an *in vitro* functional and complex model to mimic BG circuitry impaired by Huntington's disease (HD) *in vivo*. The patch clamp technique was used to examine the excitability of cortical and striatal neurons. Both neuron types generated inward Na^+ currents, spontaneous firing that were found to be sensitive to TTX. This finding meant that upstream/input cells and their target neurons in the five-port circuit model developed in the current study were excitable, as expected. The functionality and connectivity of BG cells cultured in five-port microfluidic devices was studied. The design of the microfluidic device was inspired by *in vivo* BG circuitry. Axon outgrowth was directed from one port to another via tapered micro-grooves. Ca^{2+} imaging was used to study the global generation of action potentials and connectivity between different cells in the device. Eliminating action potentials in one cell population and determining the response of other populations provided an insight into the connectivity established within the fabricated network.

All cell populations in the microfluidic device: cortical, striatal, GP and SN, displayed electrical activity. This was confirmed by Ca^{2+} oscillations, which were TTX-sensitive. When TTX was applied to cortical, striatal or GP cells to eliminate electrical activity, all remaining groups of cells in the device responded by significant reduction in Ca^{2+} oscillations. This included cells in ports that were not close to each other, or not normally connected *in vivo*. Fluid diffusion studies were carried out to ensure TTX was not diffusing into neighbouring ports. Dynamics of the impulse transmission found in the current study were not entirely compatible to the findings in literature. One of the main explanations could be the immaturity of the network established. Most immature GABAergic neurons in developing CNS exhibit excitatory instead of inhibitory behaviour (Stein & Nicoll 2003; Spitzer 2010; Ben-Ari *et al*. 2012).

Further work will be required to determine the nature of the response of neurons in the circuit, to assess whether this is due to:

1) Technical reasons e.g. leakage of TTX between ports – Liquid chromatography and mass spectrometry-based methods can be used in the future to determine the amount of TTX that could be diffusing between ports

2) Bidirectional connectivity between ports – viral transfection can be used to track synaptic connectivity between cell populations within the microfluidic device.

3) The excitatory or inhibitory nature of the immature neurons in the ports and whether this changes with time in culture – mature cell types can also be used in future models to ensure cell behaviour e.g. synaptic connectivity is comparable to *in vivo* systems.

Comparison of the model developed therein to *in vivo*, mature BG circuitry is challenging due to difference in how synaptic communication between neurons is mediated. Nevertheless, the model developed here provides a foundation, and first steps towards developing complex circuitry that can potentially be used to model neurodegenerative diseases such as Huntington and Parkinson's diseases.

Chapter 6. Patterning basal ganglia neurons - towards fabricating an *in vitro* complex micro-contact printed circuit

6.1 Introduction

The use of pre-patterned substrates for guiding orientation of neurites *in vitro* is a useful tool in developing neuronal network models for neurobiology studies. Neuronal networks developed *in vitro* provide a less complex and more defined and controllable environment compared to the *in vivo* microenvironment. For instance, microfluidic devices (Chapters 4 and 5) offer design flexibility such that cell culture vessels can be fabricated to suit specific scientific applications (Millet & Gillette 2012). However, a microfluidic device is enclosed e.g. a PDMS polymer mould is permanently sealed to a glass surface (Park *et al*. 2006), which makes it difficult to access the inside of the device. Micro-contact printed substrates, on the other hand, are usually not enclosed, which makes them easily accessible especially useful in cases where direct manipulation or measurement of cells is required.

Edwards *et al.* used deep UV photolithography to generate cell permissive and inhibitory patterns for developing a small hippocampal circuit (Edwards *et al.* 2013). N-1[3-(trimethoxysilyl)propyl] diethylenetriamine (DETA) provided the cell adhesive SAM whilst, poly(ethylene glycol) (PEG) provided non-cell adhesive SAM. The DETA SAM consisted of two 25-μm cell adhesive or permissive sites for cell body adhesion, which were connected via 5 μm lines, providing axonal guidance cues. The connectivity of the hippocampal neurons was demonstrated via dual patch clamp techniques.

As discussed in section 1.2.5, micro-contact printing involves use of a polymeric stamp, e.g. made of PDMS polymer to print material such as proteins (Bernard *et al.* 1998) and cell adhesive peptides (Hong *et al.* 2014) onto a substrate (Perl *et al*. 2009; Roa*ch et al.* 2010). Lithography techniques (section 4) are used to generate micro-contact printing stamps; photolithography enables fabrication of a master template, which is then used to develop a stamp via soft lithography (Xia & Whitesides 1998). In the current study, the five-port microfluidic device master was used to build a PDMS stamp. The goal of the study was to build a network of cells akin to that built using microfluidic devices (Chapter 5). Chemical patterning was used to fabricate cell culture devices instead of microfluidics. Chlorotrimethylsilane and trichlorosilane solutions were used for micro-contact printing. Micro-contact printed surfaces for primary cell culture were backfilled with

PDL and LN to encourage attachment of cells and development of neurites. Data presented here serve to provide an insight into general fabrication of patterned substrates using micro-contact printing and response of 3T3 mouse fibroblasts, SH-SY5Y neuroblastoma and primary cortical, GP, SN and striatal neurons to patterning.

6.2 Experimental procedures

Figure 6.1 depicts the process followed for the fabrication of PDMS stamps and patterning of cell repulsive compounds, chlorotrimethylsilane and trichlorosilane, as well as backfilling with PDL and LN. As discussed in section 2.4, two stamps were used, one for chlorotrimethylsilane and the other for trichlorosilane substrates. Chlorotrimethylsilane and trichlorosilane solutions were prepared in toluene; the PDMS stamp was inked into the solution and printed onto coverslips.

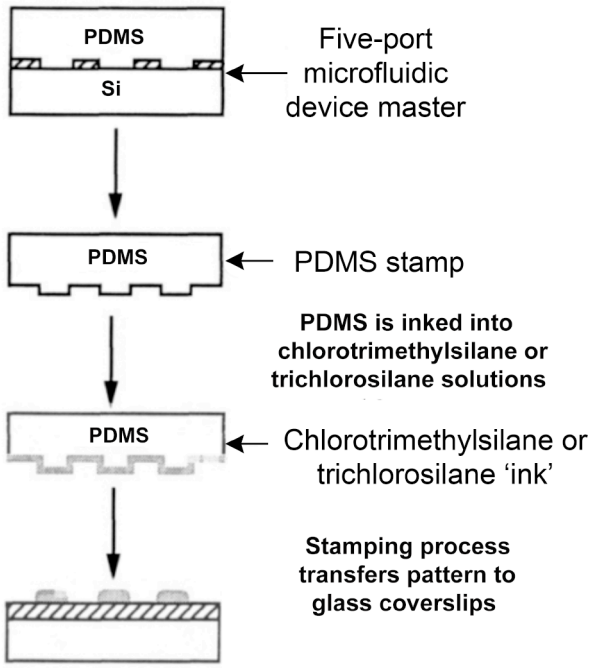

Figure 6.1: Polydimethylsiloxane (PDMS) stamp fabrication and chemical patterning. Adapted from (Kumar *et al*. 1994). Si = silicon master.

3T3 and SH-SY5Y cells were cultured onto micro-contact printed coverslips. Primary cells were obtained from rat E15 tissue. Substrates for primary cells were pre-coated with PDL and LN. 3T3 cells were seeded in medium. SH-SY5Y and primary cells were plated as a drop culture and

incubated for ~2 h before they were flooded with medium. Some SH-SY5Y cells were fixed with 4% PFA and then stained with TRITC-conjugated phalloid to visualise their actin cytoskeletons and assess their response to micro-contact printed patterns.

6.3 Results and discussion

6.3.1 Micro-contact printing and substrate characterization

As stated earlier, the five-port microfluidic master fabricated via photolithography (Jones 2000) was used for fabrication of elastomeric stamps. Stamps were peeled off and examined using bright-field microscopy to confirm pattern replication from the master template before commencing micro-contact printing.

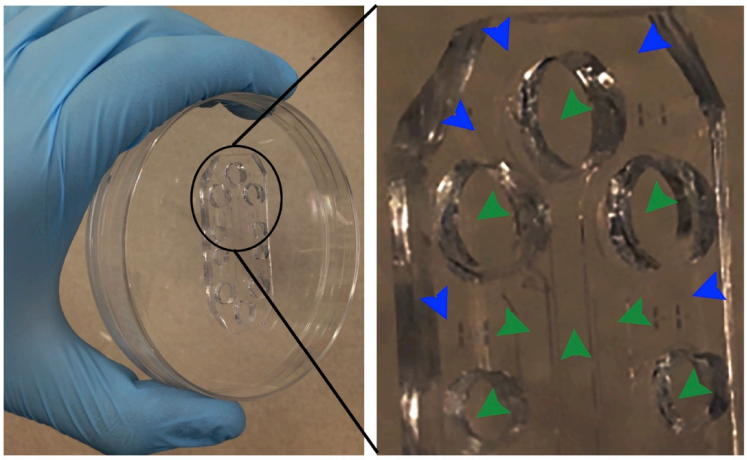

Figure 6.2: A: Photograph of a PDMS elastomeric stamp in a petri dish. B: Close-up of the elastomeric stamp in A. Punched holes and ports (green arrowheads) are regions not printed onto coverslips. Protruded (blue arrowheads) regions are printed onto coverslips.

Figure 6.3 displays SEM micrographs for the structure of the stamp used for micro-contact printing experiments. Microfluidic device features ranging from 3-100 µm (from master) were transferred onto PDMS stamps (Qin *et al.* 2010). Stamps were inked into either chlorotrimethylsilane or trichlorosilane solutions and brought into contact with coverslips to form SAM patterns. The salines were prepared in toluene to make them easily transferable to glass coverslips. Chlorotrimethylsilane or trichlorosilane were both miscible in toluene. However, the solvent caused the PDMS stamp to swell slightly; this has been reported in other studies, for instance, by Honda and colleagues (Honda *et al.* 2005). In the current study, PDMS mould swelling disappeared as the solvent evaporated.

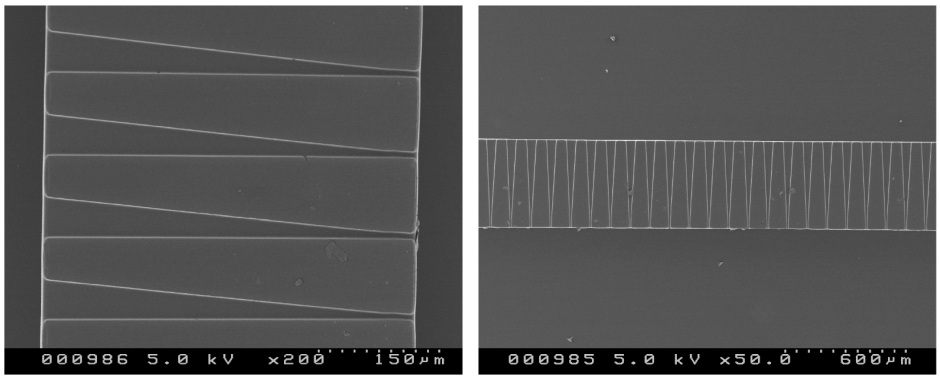

Figure 6.3 SEM micrographs of the micro-groove pattern on a PDMS stamp. Micro-grooves of width tapered from 50-5 µm are shown.

Air-drying using nitrogen gas pressure accelerated the evaporation process and it took just a few seconds for the PDMS stamp to return to its original shape from swelling. The structure of the microfluidic stamp appeared to be unaltered by swelling as indicated by printed patterns stained by TRITC and FITC dyes. SAM patterns were defined by exclusion of TRITC (red) and FITC (green). Backfilling of PDL and LN were defined by TRITC/FITC dye staining; either dye molecules tagged amine groups in the PDL/LN coating (Figure 6.4). A wettability test was performed to confirm if printing had occurred. Steam was applied to micro-contact printed substrates and accumulated on hydrophobic (stamped), as opposed to non-coated regions of the substrate (Figure 6.5).

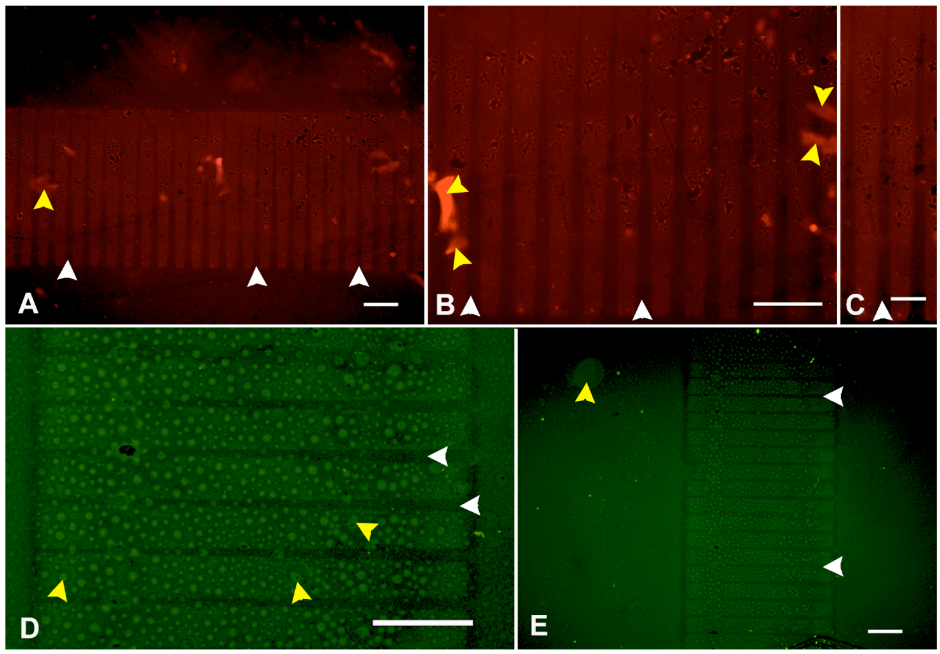

Figure 6.4: TRITC and FITC labelling of SAM patterns generated via micro-contact printing. Dark lines indicate SAM patterns (white arrowheads), backfilling of PDL and LN were defined by exclusion of TRITC (red) and FITC (green) A-C: TRITC labelling of trichlorosilane SAM patterns. D-E: FITC labelling of chlorotrimethylsilane SAM patterns. Yellow arrowheads indicate some debris from micro-contact printed samples. Scale bars: A-B, D-E = 100 µm and C = 50 µm.

PDMS is the most commonly used elastomer for soft lithography and micro-contact printing studies due to vast amount of benefits associated with it (Larsen *et al.* 1997; Xia & Whitesides 1998). As discussed earlier, the melting point and glass transition temperatures for PDMS polymer are around −50 °C and −120 °C, respectively. The polymer remains a fluid or pre-polymer at room temperature. PDMS has very good thermal stability, so elevated temperatures do not alter its structure. Furthermore, PDMS is biocompatible and chemically stable, implying it does not react or form irreversible adherence with molecules or polymers during micro-contact printing (Xia & Whitesides 1998).

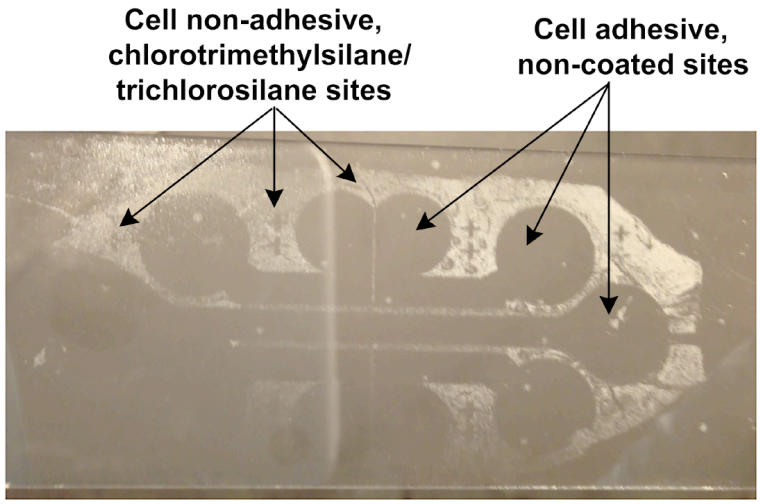

Figure 6.5: Wettability test of micro-contact printed substrates. Photograph showing steam accumulated on stamped, less hydrophilic sites of the substrate as opposed to non-coated patterns. Bottom left of the photograph is not clear due to steam evaporating on that side of the pattern.

Most studies employing micro-contact printing fabricate and utilize stamps with feature sizes greater than 0.5 μm (Xia *et al.* 1996; Qin *et al.* 2010). However, Li *et al.* found that fabrication of features with dimensions less than 0.1 μm could be facilitated by modifying PDMS stiffness. Stiffer PDMS i.e. with low elasticity and Young's modulus, or 'hard-PDMS' stamps possess increased strength and stability during micro-contact printing. Young's modulus of a material is a measure of stiffness defined as the ratio of stress, which is force per unit area, to strain, which is deformation resulting from stress (Li *et al.* 2003). Whitesides's lab found that a PDMS stamp could be re-used up to around 100 times over several months before degradation in micro-contact printing quality is noticed (Kane *et al*. 1999).

The stiffness of PDMS moulds determines the aspect ratio of structures used for micro-contact printing and the reproducibility of SAM patterns printed on substrates (Perl *et al*. 2009). Aspect ratio is the height of the stamp features divided by its lateral features' dimensions (Figure 6.6). When the ratio is too high the height is a lot greater than widths (*H>>D or H>>*L). This creates a risk of buckling or 'lateral collapse' i.e. parts of the structure touching, a phenomenon called 'pairing'. When the aspect ratio is too low the height is a lot smaller than widths (*H<<D or H<<*L). This increases the likelihood of 'sagging' where the un-protruded parts of the stamp (structures not designed to be printed onto substrates), are brought into contact with the substrate (Figure 6.6).

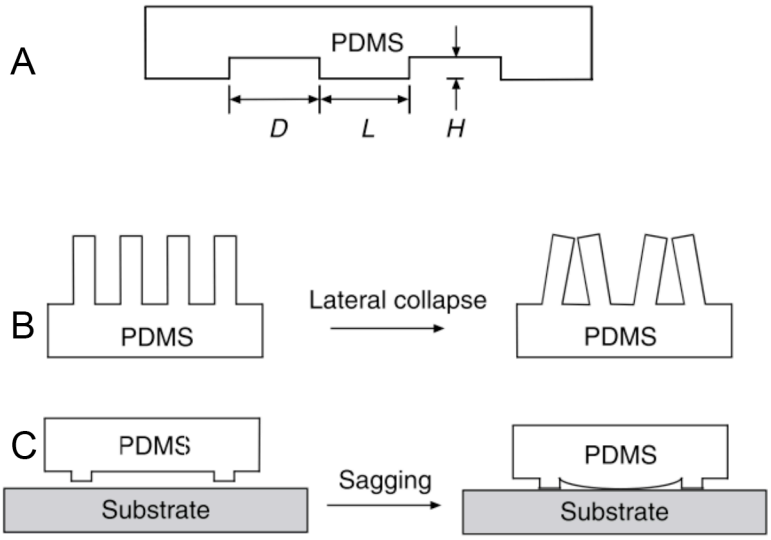

Figure 6.6: A: PDMS stamp aspect ratio, H = height, D and L = lateral dimensions. B: Stamps consisting of features with too high aspect ratio i.e. heights much greater than lateral dimensions are prone to lateral collapse. C: Stamps with too low aspect ratio i.e. small heights, are more likely to experience 'sagging' (Qin *et al*. 2010).

Compressive forces applied to stamps to achieve contact with substrates can cause sagging. Supporting material such as glass has been used in certain studies to support PDMS stamps. These materials provide rigidity to microstructures during micro-contact printing. Any form of PDMS stamp deformation affects resolution of SAM patterns (Xia & Whitesides 1998; Perl *et al*. 2009; Kaufmann & Ravoo 2010; Qin *et al.* 2010). In the current study, after the stamp was placed onto glass slides, a very minimal amount of force was applied to ensure the contact required was established with substrates. Results from pattern staining of devices (Figures 6.4) suggest that neither 'lateral collapse' nor 'sagging' occurred.

6.3.2 Cell culture on micro-contact printed substrates

Three types of cells were cultured on micro-contact printed substrata. Initial cell culture experiments involved seeding 3T3 cells across the whole substrate, consisting of regions with and without micro-groove patterns (small black dots, Figure 6.7 A). This was done to determine the response of cells to different regions of the substrate. However, primary and SH-SY5Y cells were plated as drop cultures on port-reservoir regions of the substrata (large black dots, Figure 6.7 B). The intention of the experiments was to determine whether SH-SY5Y proliferating cells and axons outgrowing from non-patterned regions were guided by patterned micro-grooves.

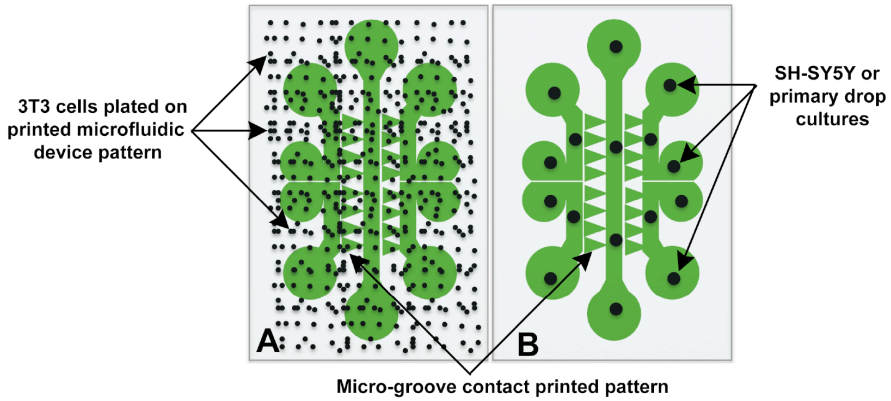

Figure 6.7: Schematic of cell plating on micro-contact printed substrata. A: 3T3 cells represented by small black dots were plated across the whole substrate. B: SH-SY5Y and cortical cells were plated on locations depicted by large black-dots so that developing axons or proliferating SH-SY5Y cells would be guided by the micro-groove pattern.

Initial experiments (Figure 6.7 A) involved contact printing of chlorotrimethylsilane SAMs on glass cover slides. Chlorotrimethylsilane is an organic compound that has been used for hydrophobic modification of surfaces. Silicon-methyl ($Si\text{-}CH_3$) groups within the compound cause hydrophilicity and therefore, less wettability; cells are repulsed by chemically modified chlorotrimethylsilane SAMs (Sah *et al.* 2004; Zhou *et al.* 2009; Ayala *et al.* 2011). Later experiments involved use of another organic compound, trichlorosilane, to provide another type of hydrophobic SAMs. Trichlorosilane is one of the commonly used polytetrafluoroethylene organosilanes that contains fluoride groups capable of modifying a surface to become hydrophobic and therefore cell repellent (Bennès *et al.* 2008; Glass *et al.* 2011). An organosilane is a compound that contains a carbon-silicon (C-Si) group (Thames & Panjnani 1996). The organosilane was used for printing SAM substrata for SH-SY5Y and primary cells.

3T3 cell culture

3T3 cells were cultured on chlorotrimethylsilane SAM patterns. This part of the study involved micro-contact printing of non-adhesive SAMs on glass substrata where the rest of the substrata remained non-coated. The 'non-coated' patterning provided adherence sites for cells. Plating of 3T3 cells across the whole substrate was done to provide a quick assessment of cell response to SAM patterning compared to non-patterned regions. The alternative was to seed cells in regions between micro-groove patterns (Figure 6.7 B) followed by analysis of their response to patterning as they proliferated and covered the cultures. It was found that in most samples cells were not evenly spread i.e. more cells were observed adjacent to micro-groove SAM patterns compared to other regions of the substrate. It is possible that the high density of cell suspension used in the study resulted in cells moving towards the centre of the substrate where micro-groove patterns are located (Figure 6.8 A). 3T3 cells had good viability on chlorotrimethylsilane-printed SAM substrata. Morphology of cells changed from being spherical to becoming flattened when checked around 2 h after plating (Figure 6.8 B).

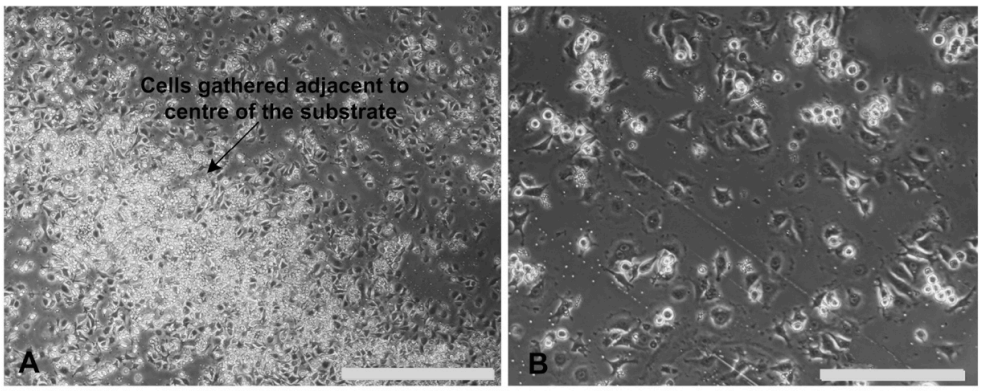

Figure 6.8: Brightfield photographs of 3T3 cells at 2 h after plating. A: Cells accumulated around centre of the substrate, where micro-groove patterns are located, after plating. B: Appearance of cells at 2 h after plating. Cells spread out and begin to develop protrusions.

Cells responded to SAM patterns; the majority of cells cultured on micro-contact printed substrata appeared to be directed by micro-groove patterns. However, cells cultured in other regions on the substrate exhibited random orientation; there was a clear distinction between cells with random processes and cells with processes forming alignment, likely due to printed patterns of aligned micro-grooves (Figure 6.9).

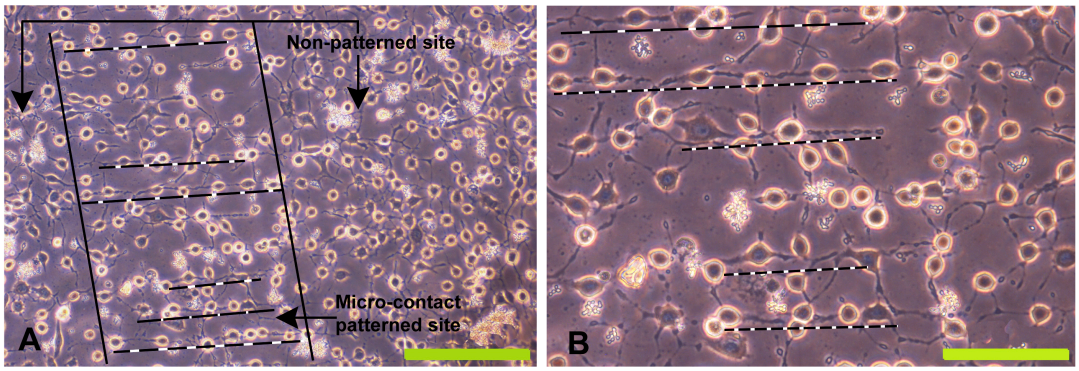

Figure 6.9: Brightfield photographs of 3T3 cells DIV 6 in culture. A: Alignment (black/white lines) was observed in micro-contact patterned compared to non-patterned sites. B: Close-up of aligned cells cultured on patterns. Scale bars: A = 200 µm and B = 100 µm. Dashed lines indicate the orientation of the microgroove pattern.

The micro-contact printing technique has been used in a number of studies for patterning 3T3 cells. Lin *et al.* developed a PDMS stamp using a photosensitive polyimide master template (Lin *et al.* 2004). PDL SAMs were printed onto glass substrates to create cell adhesion sites and backfilled with BSA to fabricate non-adhesion sites. Cells were seeded on substrata and incubated at 37°C for 5-10 min; PBS was used to wash off cells not attached to the surface. Cells preferred PDL-coated sites to BSA sites. Moreover, they found that increasing PDL concentration e.g. from 5, 10 and 50 µg/mL resulted in a lower number of cells attached to PDL-coated sites. In another study, Zhang and colleagues fabricated a RADSC-14 and EG_6SH patterned gold substrate for directing 3T3 cell orientation (Zhang *et al.* 1999). A PDMS stamp was used to print non-adhesive cell molecules (EG_6SH) onto gold surfaces. The substrate was then backfilled with RADSC-14, a peptide that promotes cell adhesion. The peptide used consisted of an amino acid sequence RADSRADSAAAAAC, where the $(RADS)_2$ repeat is a ligand that initiates cell attachment, the A's signify the alanine segment of the sequence which provides a link to the anchor, C. The anchor forms covalent bonding with the gold surface. 3T3 cells adhered and aligned to RADSC-14 patterning on the gold surface, ignoring the EG_6SH sites (Pale-Grosdemange *et al*. 1991; Prieto *et al.* 1993; Zhang *et al.* 1999).

In the current study, SAM substrata consisting of non-adhesive chlorotrimethylsilane cues printed in non-coated surfaces, required fewer steps to fabricate and were possibly less expensive (compared to the studies mentioned above) since they do not involve fabrication of adhesive cues.

Non-treated sites of the substrata provided adhesive cues. However, adhesive cues used in the studies above i.e. PDL and RADSC-14 can enhance the responsiveness of cells (compared to non-coated cues) to fabricated patterns. Future work will involve use of adhesive cues such as PDL, collagen, or PDL and LN, along with non-adhesive chlorotrimethylsilane cues to determine if that enhances the response and hence, improve alignment of cells to micro-contact printed patterns. According to Lin *et al*. increasing PDL concentration from 5 to 50 µg/mL results in a lower number of cells adhering to the substrate (Lin *et al.* 2004). Future work will involve biochemical pre-coating experimentation with different concentrations of both PDL and LN as well as comparison with non-coated substrata. The starting concentration for PDL would be 5 µg/mL and for LN would be 10 µg/mL as these are currently used for primary neurons. .

SH-SY5Y cell culture

In SH-SY5Y cell culture experiments the study focused on assessing whether cells would be guided (repelled) by SAM patterns during proliferation. Cells had good viability as indicated by good adherence and subsequent elongation on substrates. Proliferation followed, which enabled cells to cover both the trichlorosilane patterned and non-coated (adhesive) regions of the substrate. Cell alignment relative to micro-groove patterns was observed in some areas (Figure 6.10 A and B) even though it was not as apparent as in the case of 3T3 cells (Figure 6.9).

Yang *et al.* studied response of human neuroblastoma SH-SY5Y cells to micro-contact patterns generated on tissue culture dishes (I. H. Yang *et al.* 2005). A PDMS stamp was used to print a poly(PEGMA-*co*-MA) pattern designed to discourage cell adhesion. Poly(PEGMA-*co*-MA) is a random copolymer of oligo(ethylene glycol) methacrylate (PEGMA) and methacrylic acid (MA) that inhibits protein absorption and cell adherence (Kumar *et al.* 2003). Cells avoided the Poly(PEGMA-*co*-MA) and adhered to the un-coated sites of the substrate. Retinoic acid enhanced neurite extension (Dmetrichuk *et al.* 2006) and the direction of orientation of neurites was controlled by substrate patterns (I. H. Yang *et al.* 2005).

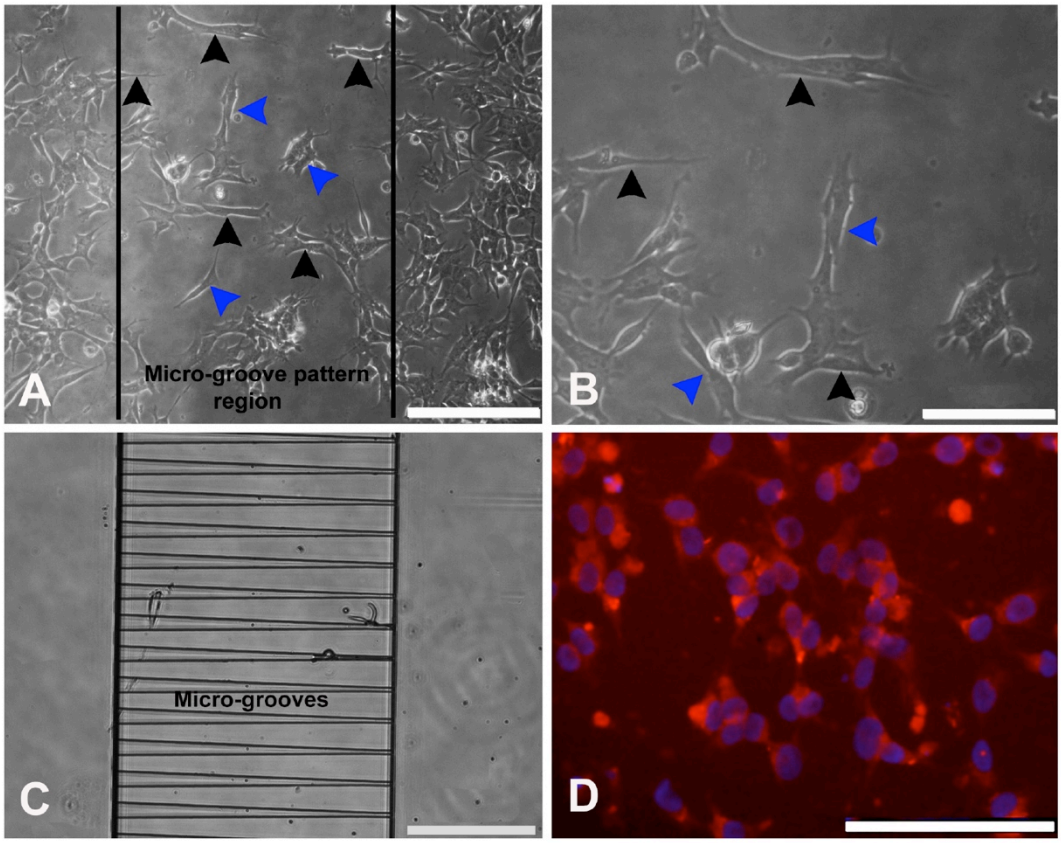

Figure 6.10: Photographs of SH-SY5Y cells. A: Bright-field photograph of cells in culture at DIV 3. B: Photograph of a close-up of part of A. Black arrowheads in A and B indicate some cells possibly responding to a printed micro-groove pattern. However, some cells completely ignored the pattern (blue arrowheads) C: Photograph of micro-grooves within an elastomeric stamp. Micro-groove width is tapered from 25 to 5 µm. D: TRITC-conjugated phalloid stained photograph of SH-SY5Y cells. Red = TRITC stain for all cells and blue = DAPI stain for cell nuclei. Scale bars: A and C = 200 µm, B and D =100 µm.

Poudel *et al.* also studied the behaviour of human neuroblastoma SH-SY5Y cells on patterned substrates (Poudel *et al.* 2013). Micro-contact printing was used to print collagen-1 (cell adhesive) patterns onto tissue culture polystyrene (TCPS) substrates. This was followed by backfilling with poly-l-lysine-g-polyethylene glycol (PLL-g-PEG) to provide cell repulsive sites. Cells were plated and incubated for 90 min to permit initial cell adherence to substrates. The group found that cells preferred collagen-1 to PLL-g-PEG regions of the substrates. Non-adhesive PLL-g-PEG backfilling repelled the cells, therefore cells were confined to aligned collagen-1 adherent sites only. Future work concerned with the current study will investigate different combinations of cell adhesive/repellent molecules that can be used to improve response of cells to printed patterns.

Primary neuronal cultures

SAM patterns were designed to provide non-adhesive cues to cells, to separate one groove from another. In the microfluidic device (Chapter 4), this separation was provided by topography i.e. a wall between grooves, rather than chemical cues. SH-SY5Y and 3T3 cells did not require adhesive cues to adhere to micro-contact printed substrata. However, dissociated E15 cortical, striatal and GP cells required backfilling of regions between the cell repellent trichlorosilane SAM printed surfaces with PDL and LN, to provide chemical cues to facilitate adherence and subsequent development of neurites. The aim was to use the micro-groove-patterned area to provide chemical cues for neurite guidance. Adherence of all cells to substrata was good in early days of culture, for instance at DIV 2 (Figure 6.11). Cells appeared viable, from observations of changes in morphology; neurons presented three-dimensional, phase-bright cell bodies with a lot of developing neurites. However, at later time points, (DIV 6; Figure 6.11), cells started to lose viability, particularly the neurons; this was determined by the morphology of cells appearing small, dark and shrunken. In some cases cells were dislodging from the substrata and forming clusters. Unfortunately, cells did not remain viable enough to produce axons to reach the micro-groove patterning.

Offenhäusser *et al.* fabricated a grid SAM via micro-contact printing for developing an *in vitro* primary neuron network (Offenhusser *et al.* 2007). An elastomeric stamp made of PDMS was inked into a cell permissive mixture of ECM-gel and polylysine and printed onto cell repellent, hydrophobic polystyrene surfaces. Grid patterns consisting of 2 μm lines and 10 μm nodes were fabricated. Dissociated E18 rat cortical neurons were cultured on contact printed patterns, in serum-free medium, to ensure that no proteins were deposited on the hydrophobic regions of the substrata. It was found that neurons adhered to printed nodes had neurites extending via the 2 μm lines. Cells were cultured for approximately 4 weeks; thereafter viability started decreasing. The patch clamp technique was used to study electrophysiology of the networks developed. Neurons cultured on grids established synaptic connectivity.

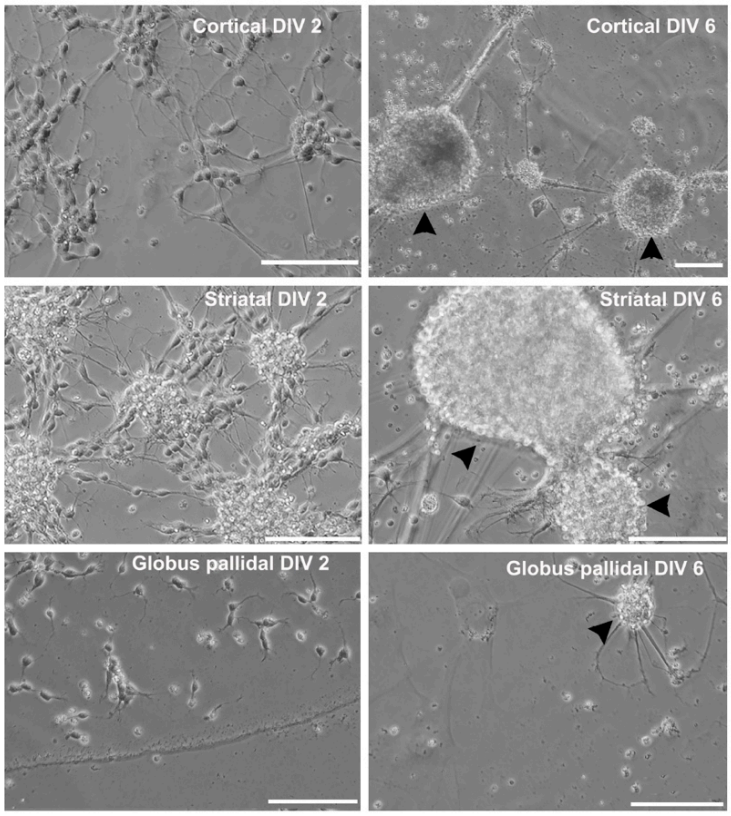

Figure 6.11: Primary cells' response to micro-contact printed substrata. The cell viability was good in the early days, for instance at DIV 2 for all primary cells involved (top row). However, viability dropped in later stages of culture starting at around DIV 6. Black arrowheads indicate clusters of unhealthy cells possibly dislodging from surfaces.

In another study, Specht *et al.* used PDMS stamps to print cell adhesive LN and collagen patterns onto a cell repellent diamond surface (Specht *et al*. 2004). Patterns were also printed on glass surfaces to use as controls for studying cortical cells' response to micro-contact printed patterns on diamond surfaces. The (single crystal) diamond material used in the study was selected due to its attractive features including optical transparency, inertness and biocompatibility. Cortical cells dissociated from an E16 mouse tissue were cultured on contact printed surfaces. It was found that LN and collagen patterns successfully directed cell adhesion and neurite outgrowth on both glass and diamond substrata.

Studies discussed above involved contact printing of cell permissive biomolecules such as PDL and ECM proteins on cell repellent surfaces such as single crystal diamond and polystyrene (Specht *et al.* 2004; Offenhusser *et al.* 2007). In the present study, cell repellent trichlorosilane molecules were printed first, followed by backfilling with adhesive PDL and LN. It is possible that

poor viability seen in later stages of culture (Figure 6.11 B) was due to repellent molecules somehow dislodging from the surface. Future work will involve contact printing of cell permissive biomolecules on non-treated and non-adherent surfaces such as polystyrene to avoid the possibility of molecules dislodging from the surface. Different methods of preparing surfaces for contact printing including piranha etching (using a mixture of hydrogen peroxide and sulfuric acid), plasma treatment and UV irradiation (Glass *et al*. 2011) will also be investigated.

Micro-patterning issues with neuronal cultures

Micro-contact printing of cell adhesive cues such as collagen, PDL, fibronectin and LN provide a means of developing neuron circuitry *in vitro*. Printing modifies the surface on which an elastomeric stamp, inked with adhesive molecules, comes into contact with. Elastomeric stamps permit design of specific architecture depending on application. The micro-contact printing technique is versatile; it allows fabrication of a variety of biomolecule patterns on different materials including gold, copper, silicon and glass. Furthermore, micro-contact printing permits direct access to cells cultured on substrata, for instance, Offenhäusser *et al.* performed triple patch clamp experimentation on a cortical cell network to determine synaptic connectivity. The experiment involved probing neurons to acquire recordings; the same patch clamp technique would have been difficult to perform in commonly 'enclosed' microfluidic devices, especially the manoeuvring of recording pipettes (Giugliano & Martinoia 2006; Offenhusser *et al.* 2007; Perl *et al.* 2009). The elastomeric stamp can be re-used, which means a lot of substrates can be rapidly fabricated (Xia & Whitesides 1998). However, the reproducibility of the contact printed geometries is limited by potential deformation that can occur on the stamp. Deformation can affect the resolution of patterns produced. Furthermore, most organic solvents required for wet inking or for transfer of organosilanes to surfaces include toluene, hexane and acetone. These solvents cause PDMS to swell, therefore distorting the structure of the elastomeric structure and dimensions of the pattern printing on a substrate (Perl *et al.* 2009).

6.4 Conclusion

This study involved micro-contact printing to develop means of culturing a network of neurons, directed by chemical patterning rather than topography (e.g. using microfluidic devices; Chapter 5). A network built on chemical patterning would provide another way of studying neuron connectivity and provide another means of modelling neural circuitry *in vitro*. It was found that the micro-contact printing technique could be used to print cell inhibiting chlorotrimethylsilane and trichlorosilane SAMs on a substrate, which does not require backfilling with cell permissive SAMs for 3T3 mouse fibroblast and SH-SY5Y neuroblastoma cells to attach. Both cell types had good cell viability during their culture period, but 3T3 cells had a better response, i.e. were more aligned to printed patterns compared to SH-SY5Y cells. Substrates used for primary cell cultures were backfilled after the micro-printing step with PDL and LN to enhance cell adhesion and neurite development. Cell viability in the early days of culture, e.g. DIV 2 was good; however, viability dropped from around DIV 6. Future work will examine potential causes of low viability for primary cells. For instance, work will involve determining if decreased viability is due to cytotoxicity potentially from chlorotrimethylsilane and trichlorosilane molecules dislodging from the substrates. Furthermore, micro-contact printing of adhesive biomolecules on non-treated surfaces may provide a better option for patterning than using repellent molecules in areas where cells should not adhere, as this could enhance cell patterning without the risk of cytotoxicity from the use of organic compounds such as chlorotrimethylsilane and trichlorosilane. This chapter provides evidence for proof-of-principle that neurons could align to micropatterned substrates, to form the complex circuitry of the basal ganglia, already modelled in microfluidic devices (Chapters 4 and 5). Future work will identify whether micropatterning is a truly viable and useful option for the study of functional basal ganglia circuitry *in vitro.*

Chapter 7: General discussion

7.1 Fabrication of functional BG circuitry *in vitro*: from nano- and micro-scale topographies to microfluidic devices

CNS circuits built *in vitro* provide means of studying progression of neurodegenerative diseases and enable screening of potential therapies. This occurs in a less complex, more controlled and reproducible microenvironment compared to *in vivo* models. Micro-engineering techniques such as lithography and microfluidics facilitate fabrication of substrates where cell patterning can be manipulated; for instance, to develop *in vitro* models mimicking *in vivo* circuitry. In the present study, PLA nano-fibres and PDMS micro-groove constructs were either pre-coated with PDL and LN or pre-aligned astrocytes (Chapter 3). The response of striatal neurites on substrates was studied. Five-port microfluidic devices were designed and fabricated via lithography techniques (Chapter 4). Cortical, striatal, GP and SN cells were cultured in devices pre-coated with PDL and LN (Chapter 4) to develop an *in vitro* BG network (Chapter 5). Excitability of cortical and striatal neurons were measured using electrophysiology techniques; functional connectivity of neurons in five-port microfluidic devices was studied using Ca^{2+} imaging (Chapter 5). Micro-contact printing was used to develop chemically patterned BG circuitry via fabrication of micro-contact chlorotrimethylsilane and trichlorosilane printed substrates and the response of 3T3, SH-SY5Y and cortical cells to micro-printed substrates was studied (Chapter 6).

7.2 Directed neurite orientation: first stage of BG circuitry fabrication

This work sets out to develop an *in vitro* model of the BG, a CNS circuit located in the deep brain. The schematic of the BG is shown in Figure 7.1A; Figure 7.1B shows a schematic based on the rat brain dissociated cell model used for the current study. An important step in the process of building an *in vitro* neuron circuit is the ability to control orientation of neurites (Chapter 3), particularly axons (Honegger *et al.* 2013). Nano- and micro-scale topographies (nano-fibres and micro-grooves) were used in this study to provide directional *contact guidance* for striatal neurites. Topographies were designed to mimic cellular and molecular structures found in the CNS that are in microns and nano-meter scales, respectively (Silva 2006a; Silva 2006b).

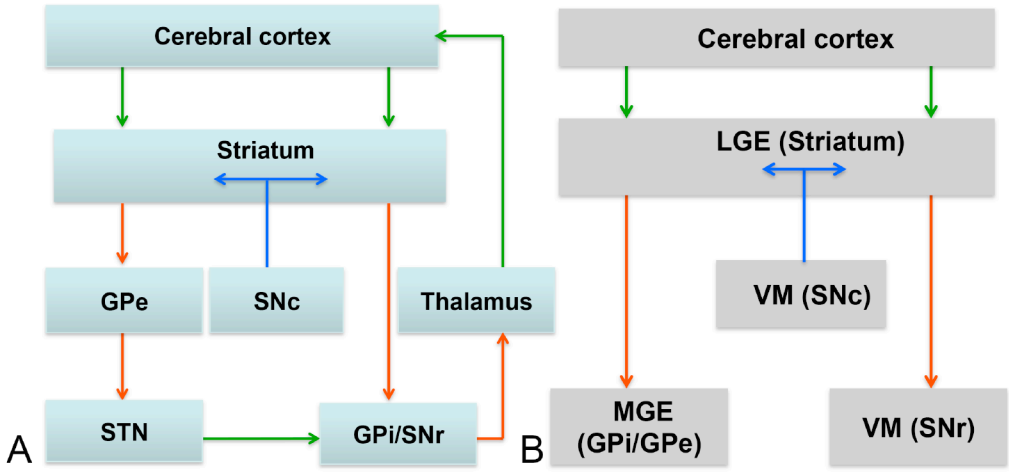

Figure 7.1: A – Schematic of BG *in vivo* and *in vitro* circuitry. Green blocks represent nuclei involved in forming circuitry. Connectivity is regulated by neurotransmitters and established via axons (arrows). Red arrows = inhibitory GABAergic axonal neurotransmission, green = excitatory axonal glutamatergic neurotransmission, blue = dopaminergic axonal projection to the striatum. SNr = substantia nigra pars reticulata, SNc = substantia nigra pars compacta, GPi = internal globus pallidus, GPe = external globus pallidus. B – Schematic of the model for the current study designed to mimic the BG in A using rat dissociated brain cells. In the developing brain LGE, MGE and VM cells displayed in B develop into corresponding blocks of cells in A, e.g. LGE develops into the striatum. VM in the rat consists of cells that develops into both SNc and SNr. Schematics displayed in both A and B were adapted from (Albin *et al.* 1989).

Striatal cells cultured on non-coated nano-fibres either failed to attach to substrates or were unhealthy, i.e. they appeared dark and shrivelled. Cell bodies remained rounded and did not develop any neurites. PDL and LN provide gold standard chemical cues for supporting neural cell cultures and were previously used to promote adherence of primary striatal and mESCs to glass substrates (Shin *et al.* 2012). These molecules were used in the present study to pre-coat nano-fibres. Nano-fibres pre-coated with PDL and LN allowed for better cell adherence and viability e.g. the neurons' soma (cell bodies) developed neurites. Consequently, micro-groove substrates were pre-coated with PDL and LN prior to striatal cell culture, resulting in neurite alignment of approximately 44%. Nano-fibre substrates yielded neurite alignment of 36%. Pre-plated astrocytes were used as biological cues for striatal neurites. Random orientation of astrocytes on micro-grooves diverted the neurites from aligning to topographic cues to some extent; approximately 21% of neurites were aligned for micro-grooves with pre-seeded astrocytes.

Use of nano-fibres for neurite contact guidance is well established in literature. For instance, Corey *et al*. fabricated poly(L-lactic acid) (PLLA) nano-fibres via the electrospinning technique (Corey *et al*. 2008). Aligned fibres were used to promote alignment of primary motor and sensory neurons from a rat spinal cord. Prior to cell culture, nano-fibres were coated with PLL and collagen I, for motor and sensory neurons, respectively to promote neuron adherence and neurite development. Neurites for both types of neurons were responsive to aligned nano-fibres (Corey *et al.* 2008). Electrospun polymers, other than PLA or PLLA, used for directing cell or neurite orientation include: PCL (Thomas *et al.* 2006; Xie *et al.* 2014), collagen (Zhong *et al.* 2006; McMurtrey 2014) and PLGA (Binder *et al*. 2013; Shin *et al*. 2014). One of the main benefits of using PLA polymer in the present study was that the polymer had been previously used in the lab. Parameters such as % of polymer, voltage applied, distance from end of needle tip to collector and polymer flow rate were already optimised and well established. Since the lab is capable of producing portable nano-fibres, for instance in a study by Yang and colleagues (Yang et al. 2011), future work may involve fabrication of three-dimensional models consisting of different sub-types of neurons cultured in layers of nano-fibre meshes.

On PDMS micro-grooves coated with PDL and LN substrata, neurites were found to achieve even better alignment when cells were spread out compared to when they were in clusters. It was discovered that cells needed to be spread out to ensure that neurites were responsive to topography cues provided by micro-grooves. Neurites emanating from cell bodies in clusters were deemed to be receiving cues from other cells in favour of topographic structures. Further work may involve studying mechanisms involved in neurite alignment for both sparse and clustered cells. Changes in groove width did not affect the degree of neurite alignment whereas the height of the topographical features (micro-scale) strongly influenced alignment. Several studies have examined the influence of changes in groove width and height on cell or neurite alignment (Hoffman-Kim *et al*. 2010; Nikkhah *et al.* 2012). Walboomers *et al.* fabricated polystyrene substrates via soft lithography to provide aligned topography cues to rat dermal fibroblast cells (Walboomers *et al.* 1999). Alignment of cells increased as micro-groove (width 1-20 μm) depth increased from 0.5-5.4 μm. The same cell type cultured on PDMS micro-groove substrates with depth of 0.5 μm yielded increased alignment on grooves with 2 μm compared to 5 and 10 μm

widths (den Braber *et al.* 1998). Uttayarat *et al*. studied influence of fibronectin coated PDMS, 0.2-5 µm width micro-grooves on bovine aortic endothelial cells orientation (Uttayarat *et al.* 2005). Changes in groove depth from 0.2-1 µm yielded increased cell alignment; however, a decrease in alignment was noticed at 5-µm groove depth. This was attributed to the changes in groove width from ~3.5 µm to ~2.6 µm for substrates with depth of 0.2-1 µm. Findings also suggest that groove width can influence cell alignment.

In the present study, the optimal substrate for promoting adherence of primary neurons as well as encouraging development and guidance of neurites was found to be PDMS micro-grooves pre-coated with PDL and LN (Chapter 3). One of the main benefits of using PDMS micro-grooves for neurite alignment (especially, compared to nano-fibres) is the reproducibility of constructs, which is enabled by use of a master template. Future studies may include studying neurite alignment on PDMS micro-groove constructs with varying heights. Drawbacks associated with cell culture on micro-grooves included lack of compartmentalisation; five-port microfluidic devices were fabricated to address this issue.

7.3 Design of the microfluidic device for BG circuitry fabrication

As established earlier in section 4.1, the nuclei involved in the *in vivo* BG circuitry are compartmentalized i.e. different cell populations are anatomically segregated and connectivity is established via axonal projections (Bolam *et al.* 2000; Turner 2009). In the present study, it was assumed that neurites from other cells forming the BG circuitry, i.e. GP, SN and cortex (Figure 7.1B) would have a response to micro-groove topography akin to striatal neurites; they would adhere to the substrate and develop neurites that aligned to topography. The findings were used as foundation for fabricating BG neuronal circuitry via microfluidic techniques. One of the main benefits of a microfluidic device is that it provides a micro-culture environment in which analysis of brain cells interaction such as synaptic connectivity between cortical and striatal neurons (Randall *et al*. 2011), is simplified in comparison to *in vivo* systems (W. Li *et al*. 2014).

Microfluidic devices permit design flexibility compared to other cell culture systems such as conventional well plates and flasks. A lot of studies involving microfluidic devices developed master templates using drawings from AutoCAD software (Xiao *et al.* 2014; Xu *et al.* 2014; Zhang *et al*. 2014). In the present study, AutoCAD software was used to design a five-port microfluidic device specific for culturing BG cells into a network (Figure 7.1B). Furthermore, microfluidic devices typically involve use of small volumes, which leads to less reagent consumption. Devices also promote laminar, steady and controllable fluids flows. They are portable and self-contained, which makes them easier to handle. Drawbacks associated with use of microfluidic devices include template design complexity. Even though devices allow design flexibility, at times fabricated devices yield complex operational systems, which makes it challenging to control cell culture. Additionally, it is often challenging to control reagent evaporation in devices consisting of small volumes compared to standard cell culture vessels such as polystyrene well plates (Halldórsson *et al*. 2014).

Other polymers used for fabricating microfluidic devices, apart from PDMS, include: silicon (Chandrasekaran *et al.* 2007), PMMA (Li *et al*. 2008) and gelatine (Paguirigan & Beebe 2006). PDMS was chosen for this study due to its attractive properties. The polymer is well established and commonly used for building devices due to its optical transparency, thermal stability, gas permeability and biocompatibility. PDMS devices were used to culture BG cells (Figure 7.2). Cells in all microfluidic device ports had good adherence and developed neurites from as early as 2 h after cells were plated. Cells remained electrophysiologically active for up to 19 days in culture. Neurite orientations were guided from one port to the other by micro-grooves separating cell culture ports.

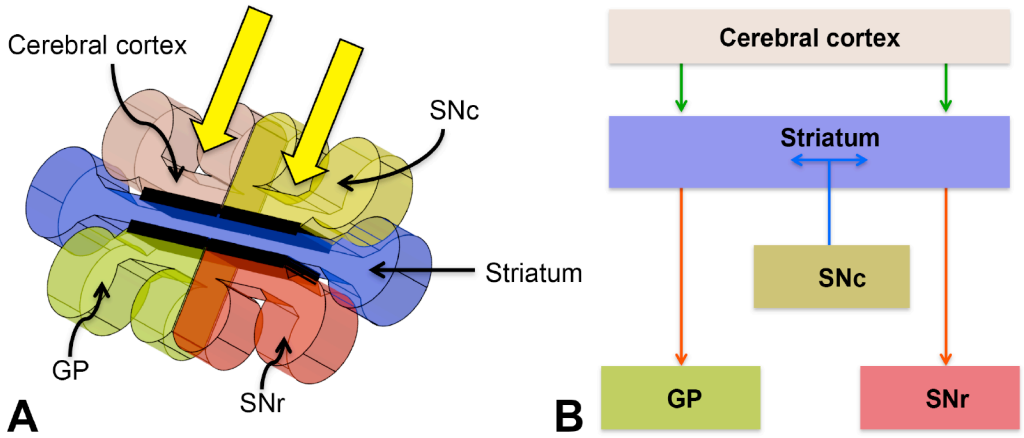

Figure 7.2: BG cells in the microfluidic device (A) and schematic of BG circuitry modelled in the current study (B). Colours of blocks in A correspond to colours of ports in B. Arrows: green = glutamatergic excitatory axonal projections, red = GABAergic inhibitory projections, blue = dopaminergic projections and yellow = shows direction of tapered micro-grooves.

7.4 Electrophysiological recording of BG single cells

Electrophysiology of cortical and striatal neurons was studied using the whole cell patch clamp technique. Voltage clamp recordings were acquired for cortical and striatal neurons (section 5.3.1). Na^+ currents, responsible for initiating action potentials (Raman & Bean 1997; Catterall *et al*. 2012), were observed for both types of neurons. Neurons were also found to be sensitive to the TTX neurotoxin. A number of studies have used whole cell recording techniques to study electrophysiology of neurons in either *in vivo* or *in vitro* preparations. For instance, *in vivo* voltage and current recordings from the cat and rat cortex were obtained using the whole cell patch clamp technique (Schramm *et al.* 2014).

The patch clamp technique used in the current study requires a glass pipette tip containing an electrolyte solution to be placed in contact with the cell membrane to record cell electrical activity (Ogden & Stanfield 1994). One of the main benefits of using this technique is its high temporal resolution (Sarkisov & Wang 2007; Brunello *et al*. 2013; Liu *et al.* 2014) from cell membrane channel recordings. This makes the patch clamp technique suited for single-cell recording (Brunello *et al.* 2013). However, the technique is highly invasive i.e. the cell membrane needs to be irreversibly damaged to gain access to the intracellular milieu and obtain current and voltage recordings. Reliable recordings can only be acquired for a very limited amount of time. Furthermore, as discussed in section 5.4, considerable expertise is required to precisely control

micromanipulation and obtain recordings from a cell (Giugliano & Martinoia 2006; Sarkisov & Wang 2007). It is very difficult to obtain simultaneous recordings using conventional patch clamp techniques from multiple sites, for instance from more than two cells, within a cell network. Recording pipettes are held by bulk micromanipulators with limited degrees of freedom, which makes them challenging to manoeuvre around samples (Potter 2001).

7.5 BG circuitry fabrication and Ca^{2+} imaging

The Ca^{2+} imaging technique provides another means of performing *in vivo* (Sullivan *et al.* 2005; Ito *et al*. 2014) or *in vitro* (Smetters *et al.* 1999; Orlandi *et al.* 2014) electrophysiology studies of cells or tissue slices. VOCs are activated when plasma membranes of excitable cells are depolarised (Bootman & Lipp 2001). Subsequently, Ca^{2+} channels are activated (Catterall 2011) and Ca^{2+} influx and efflux is tagged by fluorescent dyes sensitive to intracellular Ca^{2+} changes (Sarkisov & Wang 2007). In contrast to the single-cell recording patch clamp technique, Ca^{2+} imaging involves simultaneous monitoring and recording of large populations of cells (up to hundreds of thousands *in vitro*) at single-cell resolution, in a non-invasive manner (Stosiek *et al.* 2003; Sarkisov & Wang 2007; Grienberger & Konnerth 2012; Stetter *et al.* 2012). However, there are limitations associated with using Ca^{2+} imaging for studying electrical activity of cells. For instance, the rate of changes in voltage can be significantly faster than Ca^{2+} dynamics across cell membranes. Furthermore, sub-threshold electrical activities leading to membrane depolarisation are very difficult for Ca^{2+} indicators to detect in comparison to supra-threshold activities. This means that some Ca^{2+} dynamics data may be missed when recordings are acquired (Peterka *et al.* 2011; Gong *et al.* 2013).

Functional connectivity of BG cell networks cultured in five-port microfluidic devices (Chapter 4) was studied using Ca^{2+} imaging (Chapter 5). Figure 7.3 depicts the experimental design that was followed. As mentioned in section 5.3.2, the main port contained developing striatal neurons. There were two inputs provided by glutamatergic cortical neurons and SNc neurons; two outputs were provided by GABAergic GP and SNr neurons. Cells in all ports displayed spontaneous spiking activity. TTX was used to abolish spiking generation in one cell population at a time. Response from other cell populations in surrounding ports was then studied. When spiking activity was

eliminated from the cortical, striatum or GP ports (TTX1, 2 and 3, Figure 7.3), upstream and downstream cell populations in all conditions yielded significant reductions in spiking activity.

The micro-scale structures involved in the microfluidic device means that cells most likely experience laminar fluid flow (Velve-Casquillas *et al*. 2010); this flow is more controllable compared to the turbulent, irregular and fluctuating flow and there is less probability of inter-port fluid mixing, e.g. TTX in one port is less likely to leak into another port unless if forced into it. In the current study, a dye fluorescence test was performed to confirm that TTX placed in one port was not entering other ports. Intensity of dye placed in the middle port was measured therein and in neighbouring ports, to determine if inter-port diffusion was occurring. It was found that no diffusion occurred based on a reduction in dye intensity measured in neighbouring ports compared to the middle port. As discussed in section 5.5, future work will involve study of inter-port diffusion using other methods including liquid chromatography and mass spectrometry.

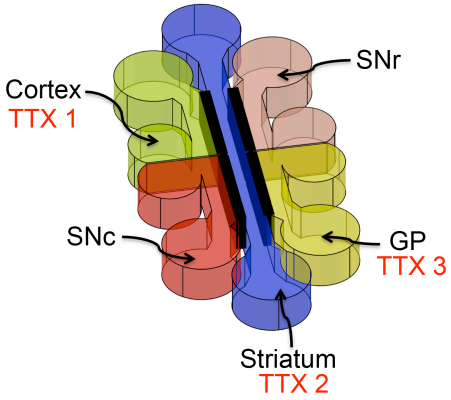

Figure 7.3: Experiment set-up for studying response of cells in microfluidic circuitry after TTX was added, on separate occasions, to: 1 – cortical, 2 – striatum and 3 – GP ports to eliminate spiking activity. Colours represent different ports within the device.

All BG cell populations in the current study presented excitatory behaviour. On the contrary, cell populations, e.g. SNr and striatal neurons within a mature *in vivo* circuitry are inhibitory, meaning they suppress spiking activity or generation of action potentials directed towards their target populations (Bolam *et al*. 2000). In the present study, it is possible that GABAergic BG cells were excitatory rather than inhibitory due to their immaturity. A number of studies have found that GABAergic CNS neurons and interneurons in early stages of development exhibit excitatory behaviour that becomes inhibitory in later stages (Ben-Ari *et al*. 1989; Stein & Nicoll 2003; Spitzer 2010). This is due to efflux of Cl^- ions from the cell caused by the $GABA_A$ receptor activation

leading to membrane depolarization (Stein & Nicoll 2003). A rise in intracellular Cl^- triggers activation of the $GABA_A$ receptor, whence GABA becomes excitatory. This mechanism causing excitatory GABAergic behaviour is implicated in pathological conditions such as spinal cord lesions, brain trauma and seizures (Ben-Ari *et al.* 2012).

Further work (on current study) would employ more mature BG cells to ensure behaviour such as inhibitory or excitatory spiking activity closely mimics the mature *in vivo* circuitry. The ages of embryos (dissected to obtain dissociated cells) used for the current study were determined by peak neurogenesis, which differs for *in vivo* BG circuitry components. For instance, the peaks of neurogenesis for SN and striatal neurons are E12-E14 and E14-E16, respectively. These are the stages of CNS early development where neurons are still small and rounded but are differentiated and just beginning neurite growth. This is an important stage for development of primary neurons since dissection before the peak would yield progenitor cells and risk limiting the possibilities of differentiating into the preferred cell type. On the other hand, dissection of tissue beyond the peak neuronal development, i.e. when axons are already developed, would risk trauma or cell death due to axotomy (cutting of axons) (Dunnett & Björklund 2000; Dunnett *et al*. 2006). Therefore, further studies are required to explore other options such as using tissue slices besides, dissecting from more mature rat BG tissue.

7.5 Multi-electrode arrays (MEAs)

In MEAs, electrodes are incorporated to the bottom of a biocompatible substrate that is usually glass, quartz or silicon. MEAs consist of electrical contacts made of materials such as ITO or gold, connecting electrodes to external components; the connection allows electrophysiological activity of cells to be continuously recorded and when necessary, stimuli can be applied to cells. Dissociated cells or tissue slices are cultured on MEA-embedded substrates. In contrast to the patch clamp technique where single cells are invasively 'patched' to acquire recordings, MEAs involve non-invasive extracellular, simultaneous recording of electrophysiological activity of large populations of cells. Transparency of array substrates enable continuous monitoring, e.g. using phase-contrast or confocal microscopy with high spatial and temporal resolution, over long periods of time (Regehr *et al*. 1989; Potter 2001; Giugliano & Martinoia 2006).

Potter *et al*. developed MEA substrata where cell culture chambers were enclosed in a permeable fluorinated ethylene-propylene membrane (Potter & DeMarse 2001). The membrane was permeable to oxygen but not to water (to avoid medium drying out and microbes entering the chamber). Rat dissociated cortical cells cultured in MEA chambers remained viable, i.e. generation of action potential were recorded, for more than 12 months after cells were plated. Chambers were pre-coated with PEI and LN to encourage adherence of cells (Potter & DeMarse 2001). Other biochemical reagents that have been used for coating MEA substrata include PDL (Rubinsky *et al*. 2007), cellulose nitrate (Chen *et al*. 2005), and fibronectin (Egashira *et al*. 2012). In contrast to Ca^{2+} imaging, MEAs provide a more direct means of recording electrical spiking. Furthermore, the recordings are acquired continuously, over a long period of time without the need to disrupt cells in culture. Future work will involve use of MEAs as a more direct technique for measuring electrical connectivity between BG cell populations.

7.6 Microfluidic vs. micro-contact printed circuitry

Microcontact printing was used in the current study to fabricate substrata for directing neuron adherence and axon growth. The objective was to build a neuron network directed by bio-chemical patterning to provide another means, besides microfluidics, of studying neuron connectivity and BG circuitry *in vitro*. Cell inhibiting (chlorotrimethylsilane and trichlorosilane) SAMs were printed on a substrate using a PDMS mould or stamp. Backfilling with PDL and LN was required for BG cells, to enhance cell adhesion and neurite development; but not for 3T3 mouse fibroblast and SH-SY5Y neuroblastoma cells. 3T3 cells had better response to bio-chemical cues compared to SH-SY5Y cells; they both appeared viable during their culture period based on their morphological appearances. BG cells appeared viable in the early days of culture. Initial adherence of cells to micro-printed surfaces was good since they started developing processes and remained attached after substrata were flooded with medium. However, viability dropped at later stages of culture, possibly due to the printed SAMs dislodging from surfaces. Further studies are required to examine causes of low viability in BG cells.

Nevertheless, cells cultured on micro-printed substrata would be easily accessible. For instance, micromanipulator positioning and 'patching' neurons for electrophysiological studies on these

substrata would be much simpler compared to microfluidic devices. The self-enclosed nature of microfluidic devices provides physical accessibility challenges for techniques such as patch clamp (Pavlovic *et al.* 2008). Micro-printed substrata have successfully been used for culturing cell networks including: cortical (Vogt et al. 2005; Santoro et al. 2014), dorsal root ganglia (Hardelauf *et al.* 2014), and hippocampal (Boehler *et al.* 2012) networks. Regardless, there are still some aspects of micro-contact printing that make it inferior to microfluidics for culturing cell networks. Localized application of treatments, e.g. TTX to abolish cell spiking, to specific cell populations on micro-printed substrata is practically impossible since all cells would be exposed to a similar solution. Furthermore, micro-printed substrata would consume more reagents compared to microfluidic devices; also, laminar flow perfusion readily provided by microfluidics would be very difficult to achieve on printed substrata (Halldórsson *et al.* 2014).

7.7 Conclusions

Findings from the current study contribute to the body of work concerned with high throughput screening of potential therapies for neurodegenerative diseases such as Huntington's (HD) and Parkinson' diseases (PD), through the use of *in vitro* circuitry. Initial stages of building *in vitro* circuitry involved directional guidance of neurites via nano- and micro-scale topography, coupled with either PDL and LN chemical cues or pre-seeded astrocyte biological cues. PDL and LN pre-coated micro-scale substrata yielded the optimal neurite guidance. BG cells were cultured in compartments or ports of microfluidic devices, separated by micro-scale tapered grooves to induce unidirectional orientation of axons. Functional connectivity of BG cell circuitry fabricated as a consequence, was studied using Ca^{2+} imaging. The dynamics of the circuitry were different from the *in vivo* circuitry the study intended to mimic. This was attributed to the excitatory nature of immature GABAergic neurons (they exhibit inhibitory behaviour *in vivo*) used in the current study. Further studies are required: to find means of improving BG cell viability on micro-printed substrata and to fabricate a more mature BG cell circuitry. It appears that the optimal substrate for performing future *in vitro* BG circuitry studies will involve microfluidic devices incorporated with MEAs. Nevertheless, the findings presented herein provide first steps towards developing complex circuitry to model neurodegenerative disorders.

Reference list

Albin, R.L. et al., 1992. Preferential Loss of Striato-External Palhdal Projection Neurons in Presymptomatic Huntington ' s Disease. *Annals of Neurology*.

Albin, R.L. et al., 1989. The functional anatomy of basal ganglia disorders. *Trends in neurosciences.*, 12(10), pp.366–375.

Alexander, J.K., Fuss, B. & Colello, R.J., 2008. Electric field-induced astrocyte alignment directs neurite outgrowth. *Neuron Glia Biology*, 2(2), pp.93–103.

Alom Ruiz, S. & Chen, C.S., 2007. Microcontact printing: A tool to pattern. *Soft Matter*, 3(2), pp.168–177. Available at: http://xlink.rsc.org/?DOI=b613349e [Accessed July 9, 2014].

Anderson, J. et al., 2000. Fabrication of microfluidic systems in poly(dimethylsiloxane). *Electrophoresis.*, 21(1), pp.27–40. Available at: http://gmwgroup.unix.fas.harvard.edu/pubs/pdf/691.pdf [Accessed January 28, 2015].

André, V.M. et al., 2006. Altered cortical glutamate receptor function in the R6/2 model of Huntington's disease. *Journal of neurophysiology*, 95(4), pp.2108–19. Available at: http://www.ncbi.nlm.nih.gov/pubmed/16381805 [Accessed September 12, 2014].

Atherton, J.F. & Bevan, M.D., 2005. Ionic mechanisms underlying autonomous action potential generation in the somata and dendrites of GABAergic substantia nigra pars reticulata neurons in vitro. *The Journal of neuroscience : the official journal of the Society for Neuroscience*, 25(36), pp.8272–81. Available at: http://www.ncbi.nlm.nih.gov/pubmed/16148235 [Accessed November 17, 2014].

Atlas, D., 2013. The voltage-gated calcium channel functions as the molecular switch of synaptic transmission. *Annual review of biochemistry*, 82, pp.607–35. Available at: http://www.ncbi.nlm.nih.gov/pubmed/23331239 [Accessed August 25, 2014].

Ayala, R. et al., 2011. Engineering the cell-material interface for controlling stem cell adhesion, migration, and differentiation. *Biomaterials*, 32(15), pp.3700–3711. Available at: http://dx.doi.org/10.1016/j.biomaterials.2011.02.004.

Barbati, A. et al., 2013. Culture of Primary Rat Hippocampal Neurons: Design, Analysis, and Optimization of a Microfluidic Device for Cell Seeding, Coherent Growth, and Solute Delivery. *Biomedical microdevices*, 15(1), pp.97–108. Available at: http://link.springer.com/article/10.1007/s10544-012-9691-2 [Accessed September 13, 2014].

Batista-Brito, R. & Fishell, G., 2009. The developmental integration of cortical interneurons into a functional network. *Current topics in developmental biology*, 87(09), pp.81–118. Available at: http://www.ncbi.nlm.nih.gov/pubmed/19427517 [Accessed October 20, 2014].

Beal, F.. et al., 1991. Chronic Quinolinic Acid Lesions in Rats Closely Resemble Huntington's Disease. *Journal of Neuroscience*, 11(6), pp.1649–1659.

Bear, M.F., Connors, B.W. & Paradiso, M.A., 2007. Brain Control of Movement. In *Neuroscience: Exploring the brain*. Baltimore: Lippincott Williams & Wilkins, p. 465.

Ben-Ari, Y. et al., 1989. Giant synaptic potentials in immature rat CA3 hippocampal neurones. *The Journal of physiology*, 416, pp.303–325. Available at: http://jp.physoc.org/content/416/1/303.short [Accessed December 30, 2014].

Ben-Ari, Y. et al., 2012. The GABA excitatory/inhibitory shift in brain maturation and neurological disorders. *The Neuroscientist : a review journal bringing neurobiology, neurology and psychiatry.*, 18(5), pp.467–86. Available at: http://www.ncbi.nlm.nih.gov/pubmed/22547529 [Accessed December 17, 2014].

Ben-Yakar, A., Chronis, N. & Lu, H., 2009. Microfluidics for the analysis of behavior, nerve regeneration, and neural cell biology in C. elegans. *Current opinion in neurobiology*, 19(5), pp.561–7. Available at: http://www.pubmedcentral.nih.gov/articlerender.fcgi?artid=3107678&tool=pmcentrez&rendertype=abstract [Accessed September 1, 2014].

Bennès, J., Ballandras, S. & Chérioux, F., 2008. Easy and versatile functionalization of lithium niobate wafers by hydrophobic trichlorosilanes. *Applied Surface Science*, 255(5), pp.1796–1800.

Berdichevsky, Y. et al., 2009. Microfluidics and multielectrode array-compatible organotypic slice culture method. *Journal of Neuroscience Methods*, 178(1), pp.59–64.

Bernard, A. et al., 1998. Printing Patterns of Proteins. *Langmuir*, 14(9), pp.2225–2229. Available at: http://pubs.acs.org/doi/abs/10.1021/la980037l [Accessed December 9, 2014].

Berridge, M., 1998. Neuronal Calcium Signaling. *Neuron*, 21(1), pp.13–26. Available at: http://yadda.icm.edu.pl/yadda/element/bwmeta1.element.elsevier-ae823ffe-597c-3e83-9526-299c92f99918/c/00805103.pdf [Accessed August 19, 2014].

Berridge, M., Bootman, M. & Roderick, H., 2003. Calcium signalling: dynamics, homeostasis and remodelling. *Nature reviews. Molecular cell biology*, 4(7), pp.517–29.

Berridge, M., Lipp, P. & Bootman, M., 2000. The versatility and universality of calcium signalling. *Nature reviews. Molecular cell biology*, 1(1), pp.11 – 21.

Bevan, M. et al., 1998. Selective Innervation of Neostriatal Interneurons by a Subclass of Neuron in the Globus Pallidus of the Rat. *The Journal of neuroscience*, 18(22), pp.9438–9452. Available at: http://www.jneurosci.org/content/18/22/9438.short [Accessed November 16, 2014].

Bhatia, S.N. & Ingber, D.E., 2014. Microfluidic organs-on-chips. *Nature biotechnology.*, 32(8), pp.760–772. Available at: http://www.ncbi.nlm.nih.gov/pubmed/25093883 [Accessed August 7, 2014].

Bhidayasiri, R. & Truong, D., 2004. Chorea and related disorders. *Postgrad Med J. 2004 Sep;80(947):527-34.*, 80(247), pp.527 – 534.

Binder, C. et al., 2013. Influence of micro and submicro poly(lactic-glycolic acid) fibers on sensory neural cell locomotion and neurite growth. *Journal of biomedical materials research. Part B, Applied biomaterials*, 101b(7), pp.1200–8. Available at: http://www.ncbi.nlm.nih.gov/pubmed/23650277 [Accessed December 19, 2014].

Blau, A. et al., 2009. Replica-moulded polydimethylsiloxane culture vessel lids attenuate osmotic drift in long-term cell cultures. *Journal of Biosciences*, 34(1), pp.59–69.

Boehler, M. et al., 2012. Hippocampal networks on reliable patterned substrates. *Journal of neuroscience methods*, 203(2), pp.344–353. Available at: http://www.sciencedirect.com/science/article/pii/S0165027011005681 [Accessed December 18, 2014].

Bolam, J.P. et al., 2000. Synaptic organisation of the basal ganglia. *Journal of anatomy*, 196 (Pt 4), pp.527–42. Available at:

http://www.pubmedcentral.nih.gov/articlerender.fcgi?artid=1468095&tool=pmcentrez&rendertype=abstract.

Bootman, M. & Lipp, P., 2001. Calcium Signalling and Regulation of Cell Function. In *eLS*. John Wiley & Sons, Ltd, pp. 1–7. Available at: http://onlinelibrary.wiley.com/doi/10.1002/9780470015902.a0001265.pub3/full [Accessed August 20, 2014].

Bootman, M.D. et al., 2013. Ca2+-sensitive fluorescent dyes and intracellular Ca2+ imaging. *Cold Spring Harbor protocols*, 2013(2), pp.83–99. Available at: http://www.ncbi.nlm.nih.gov/pubmed/23378644 [Accessed August 8, 2014].

Den Braber, E. et al., 1998. Orientation of ECM protein deposition, fibroblast cytoskeleton, and attachment complex components on silicone microgrooved surfaces. *Journal of Biomedical Materials Research.*, 40(2), pp.291 – 300. Available at: http://onlinelibrary.wiley.com/doi/10.1002/(SICI)1097-4636(199805)40:2%3C291::AID-JBM14%3E3.0.CO;2-P/abstract [Accessed December 20, 2014].

Brody, J. et al., 1996. Biotechnology at low Reynolds Numbers. *Biophysical journal*, 71(6), pp.3430–3441. Available at: http://www.sciencedirect.com/science/article/pii/S0006349596795383 [Accessed January 28, 2015].

Brumovsky, P. et al., 2011. Expression of Vesicular Glutamate Transporters Type 1 and 2 in Sensory and Autonomic Neurons Innervating the Mouse Colorectum. *J Comp Neurol.*, 159(16), pp.3346–3366.

Brunello, C. a et al., 2013. Microtechnologies to fuel neurobiological research with nanometer precision. *Journal of nanobiotechnology*, 11, p.11. Available at: http://www.pubmedcentral.nih.gov/articlerender.fcgi?artid=3636074&tool=pmcentrez&rendertype=abstract.

Campbell, C.J. & Grzybowski, B. a, 2004. Microfluidic mixers: from microfabricated to self-assembling devices. *Philosophical transactions. Series A, Mathematical, physical, and engineering sciences.*, 362(1818), pp.1069–86. Available at: http://www.ncbi.nlm.nih.gov/pubmed/15306485.

Catterall, W. a, 1991. Excitation-contraction coupling in vertebrate skeletal muscle: a tale of two calcium channels. *Cell*, 64(5), pp.871–4. Available at: http://www.ncbi.nlm.nih.gov/pubmed/1848157.

Catterall, W. a et al., 2012. The Hodgkin-Huxley heritage: from channels to circuits. *The Journal of neuroscience : the official journal of the Society for Neuroscience*, 32(41), pp.14064–73. Available at: http://www.pubmedcentral.nih.gov/articlerender.fcgi?artid=3500626&tool=pmcentrez&rendertype=abstract.

Catterall, W. a, 2011. Voltage-gated calcium channels. *Cold Spring Harbor perspectives in biology*, 3(8), p.a003947. Available at: http://www.pubmedcentral.nih.gov/articlerender.fcgi?artid=3140680&tool=pmcentrez&rendertype=abstract [Accessed July 10, 2014].

Catterall, W.A. et al., 2005. International Union of Pharmacology . XLVIII . Nomenclature and Structure-Function Relationships of Voltage-Gated Calcium Channels. *Pharmacological Reviews*, 57(4), pp.411–425.

Cecchini, M., Ferrari, a & Beltram, F., 2008. PC12 polarity on biopolymer nanogratings. *Journal of Physics: Conference Series*, 100(1), p.012003. Available at: http://stacks.iop.org/1742-

6596/100/i=1/a=012003?key=crossref.f6c1a8754ffe672e28995140e443c117 [Accessed April 15, 2012].

Celular, B., 2000. Evolution of the basal ganglia : new perspectives through a. *Review Literature And Arts Of The Americas*, pp.501–517.

Cepeda, C. et al., 2007. The Corticostriatal Pathway in Huntington's Disease. *Mental Retardation*, 81(310), pp.253–271.

Cepeda, C. & Hurst, R., 2003. Transient and Progressive Electrophysiological Alterations in the Corticostriatal Pathway in a Mouse Model of Huntington ' s Disease. *The Journal of Neuroscience.*, 23(3), pp.961–969. Available at: http://www.jneurosci.org/content/23/3/961.short [Accessed September 12, 2014].

Chaigne-Delalande, B. & Lenardo, M.J., 2014. Divalent cation signaling in immune cells. *Trends in immunology*, 35(7), pp.332–344. Available at: http://www.ncbi.nlm.nih.gov/pubmed/24932518 [Accessed August 14, 2014].

Chak, K. & Kolodkin, A.L., 2014. Function of the Drosophila receptor guanylyl cyclase Gyc76C in PlexA-mediated motor axon guidance. *Development (Cambridge, England)*, 141(1), pp.136–47. Available at: http://www.pubmedcentral.nih.gov/articlerender.fcgi?artid=3865755&tool=pmcentrez&rendertype=abstract [Accessed August 28, 2014].

Chandrasekaran, A. et al., 2007. Hybrid Integrated Silicon Microfluidic Platform for Fluorescence Based Biodetection. *Sensors*, 7(9), pp.1901–1915. Available at: http://www.mdpi.com/1424-8220/7/9/1901/.

Chang, H. & Kita, H., 1992. Interneurons in the rat striatum: relationships between parvalbumin neurons and cholinergic neurons. *Brain Res*, 574(1-2), pp.307 –311.

Chen, A.-H. et al., 2005. Luminance adaptation increased the contrast sensitivity of retinal ganglion cells. *NeuroReport*, 16(4), pp.371–375. Available at: http://content.wkhealth.com/linkback/openurl?sid=WKPTLP:landingpage&an=00001756-200503150-00013.

Chen, H. et al., 2011. Electrospun chitosan-graft-poly (ε-caprolactone)/poly (ε-caprolactone) nanofibrous scaffolds for retinal tissue engineering. *International journal of nanomedicine.*, 6, pp.453–61. Available at: http://www.pubmedcentral.nih.gov/articlerender.fcgi?artid=3075910&tool=pmcentrez&rendertype=abstract [Accessed September 14, 2014].

Chen, H.M. et al., 2014. Transcripts involved in calcium signaling and telencephalic neuronal fate are altered in induced pluripotent stem cells from bipolar disorder patients. *Translational Psychiatry*, 4(3), p.e375. Available at: http://www.nature.com/doifinder/10.1038/tp.2014.12 [Accessed July 20, 2014].

Cheng, Y. et al., 2011. Structural MRI detects progressive regional brain atrophy and neuroprotective effects in N171-82Q Huntington's disease mouse model. *NeuroImage*, 56(3), pp.1027–34. Available at: http://www.pubmedcentral.nih.gov/articlerender.fcgi?artid=3372851&tool=pmcentrez&rendertype=abstract [Accessed April 15, 2014].

Chua, J.S. et al., 2014. Extending neurites sense the depth of the underlying topography during neuronal differentiation and contact guidance. *Biomaterials*, 35(27), pp.7750–61. Available at: http://www.ncbi.nlm.nih.gov/pubmed/24954734 [Accessed September 2, 2014].

Clapham, D.E., 2007. Calcium signaling. *Cell*, 131(6), pp.1047–58. Available at: http://www.ncbi.nlm.nih.gov/pubmed/18083096 [Accessed July 11, 2014].

Clark, P. et al., 1990. Topographical control of cell behaviour: II. Multiple grooved substrata. *Development (Cambridge, England)*, 108(4), pp.635–44. Available at: http://www.ncbi.nlm.nih.gov/pubmed/7640662.

Conn, C. a et al., 2014. Visualizing oil displacement with foam in a microfluidic device with permeability contrast. *Lab on a chip*, 14, pp.3968–3977. Available at: http://www.ncbi.nlm.nih.gov/pubmed/25112724 [Accessed August 29, 2014].

Coquinco, A. et al., 2014. A microfluidic based in vitro model of synaptic competition. *Molecular and cellular neurosciences.*, 60, pp.43–52. Available at: http://www.ncbi.nlm.nih.gov/pubmed/24662423 [Accessed September 13, 2014].

Corey, J.M. et al., 2008. The design of electrospun PLLA nanofiber scaffolds compatible with serum-free growth of primary motor and sensory neurons. *Acta Biomater.*, 4(4), pp.863–875.

Crane, M.M. et al., 2014. A microfluidic system for studying ageing and dynamic single-cell responses in budding yeast. *PloS one*, 9(6), p.e100042. Available at: http://www.pubmedcentral.nih.gov/articlerender.fcgi?artid=4065030&tool=pmcentrez&rendertype=abstract [Accessed November 3, 2014].

Cui, H., Webber, M. & Stupp, S., 2010. Self-assembly of peptide amphiphiles: from molecules to nanostructures to biomaterials. *Biopolymers.*, 94(1), pp.1–18.

Curinga, G. & Smith, G.M., 2008. Molecular/genetic manipulation of extrinsic axon guidance factors for CNS repair and regeneration. *Experimental neurology*, 209(2), pp.333–342.

D'Ascenzo, M. et al., 2009. Activation of mGluR5 induces spike afterdepolarization and enhanced excitability in medium spiny neurons of the nucleus accumbens by modulating persistent Na+ currents. *The Journal of physiology*, 587(Pt 13), pp.3233–50. Available at: http://www.pubmedcentral.nih.gov/articlerender.fcgi?artid=2727034&tool=pmcentrez&rendertype=abstract [Accessed October 29, 2014].

Deleglise, B. et al., 2013. Synapto-Protective Drugs Evaluation in Reconstructed Neuronal Network. *PLoS ONE*, 8(8), pp.1–9.

Deleglise, B. et al., 2014. B-Amyloid Induces a Dying-Back Process and Remote Trans-Synaptic Alterations in a Microfluidic-Based Reconstructed Neuronal Network. *Acta Neuropathologica Communications*, 2, p.145. Available at: http://www.actaneurocomms.org/content/2/1/145.

Despa, S. et al., 2014. Junctional cleft [Ca2+]I measurements using novel cleft-targeted Ca2+ sensors. *Circulation Research*, 115(3), pp.339–47.

Deumens, R. et al., 2004. Alignment of glial cells stimulates directional neurite growth of CNS neurons in vitro. *Neuroscience*, 125(3), pp.591–604. Available at: http://www.ncbi.nlm.nih.gov/pubmed/15099673 [Accessed June 4, 2013].

Dmetrichuk, J.M., Carlone, R.L. & Spencer, G.E., 2006. Retinoic acid induces neurite outgrowth and growth cone turning in invertebrate neurons. *Developmental biology*, 294(1), pp.39–49. Available at: http://www.ncbi.nlm.nih.gov/pubmed/16626686 [Accessed November 30, 2014].

Duan, L. et al., 2014. Stem cell derived basal forebrain cholinergic neurons from Alzheimer ' s disease patients are more susceptible to cell death. *Molecular Neurodegeneration*, 9(3), pp.1–14.

Dunlap, K., Luebke, J.I. & Turner, T.J., 1995. Exocytotic Ca2'channels in mammalian central neurons. *Trends in neurosciences*, 18(2), pp.89–98.

Dunnet, S. & Björklund, A., 1992. Staging and dissection of rat embryos. In S. Dunnet & A. Björklund, eds. *Neural Transplantantion: A Practical Approach*. London: Oxford University Press.

Dunnett, S. & Björklund, A., 2000. Dissecting Embryonic Neural Tissues for Transplantation. In S. Dunnett, A. Boulton, & G. Baker, eds. *Neural Transplantation Methods.* Totowa, New Jersey: Humana Press Inc., pp. 3–24.

Dunnett, S.B. et al., 2006. Neural transplantation. In T. Tatlisumak & M. Fisher, eds. *Handbook of Experimental Neurology: Methods and Techniques in Animal Research.* Cambridge, UK: Cambridge University Press, pp. 269–308.

East, E. et al., 2010. Alignment of astrocytes increases neuronal growth in three-dimensional collagen gels and is maintained following plastic compression to form a spinal cord repair conduit. *Tissue engineering. Part A*, 16(10), pp.3173–84. Available at: http://www.pubmedcentral.nih.gov/articlerender.fcgi?artid=2958448&tool=pmcentrez&rendertype=abstract [Accessed July 3, 2011].

Edwards, D. et al., 2013. Two Cell Circuits of Oriented Adult Hippocampal Neurons on Self-Assembled Monolayers for Use in the Study of Neuronal Communication in a Defined System. *ACS chemical Neuroscience*, 4(8), pp.1174 – 1182. Available at: http://pubs.acs.org/doi/abs/10.1021/cn300206k [Accessed December 3, 2014].

Egashira, T. et al., 2012. Disease characterization using LQTS-specific induced pluripotent stem cells. *Cardiovascular Research*, 95(4), pp.419–29. Available at: http://www.ncbi.nlm.nih.gov/pubmed/22739119 [Accessed January 3, 2015].

Egert, U. & Meyer, T., 2005. Heart on a chip - Extracellular multielectrode recordings from cardiac myocytes in vitro. In S. Dhein, F. W. Mohr, & M. Delmar, eds. *Practical Methods in Cardiovascular Research*. Berlin, Heidelberg: Springer Berlin Heidelberg New York, pp. 432–453.

Farre, C. et al., 2008. Ion channel screening - automated patch clamp on the rise. *Drug discovery today: Technologies*, 5(1), pp.e23 – e28. Available at: http://www.ncbi.nlm.nih.gov/pubmed/24125503 [Accessed August 14, 2014].

Ferrante, C. et al., 2013. Analysis of osmotic stress-induced Ca2+ spark termination in mammalian skeletal muscle. *Indian journal of biochemistry & biophysics*, 50(5), pp.411–418. Available at: http://scholar.google.com/scholar?hl=en&btnG=Search&q=intitle:Analysis+of+osmotic+stress-induced+Ca2++spark+termination+in+mammalian+skeletal+muscle.#0 [Accessed August 19, 2014].

Ferrari, A. et al., 2011. Nanotopographic control of neuronal polarity. *Nano letters*, 11(2), pp.505–11. Available at: http://www.ncbi.nlm.nih.gov/pubmed/21241061.

Ferry, M.S., Razinkov, I.A. & Hasty, J., 2011. *Microfluidics for synthetic biology: from design to execution.* 1st ed., Elsevier Inc. Available at: http://www.ncbi.nlm.nih.gov/pubmed/21601093 [Accessed September 3, 2014].

Francisco, H. et al., 2007. Regulation of Axon Guidance and Extension by 3-Dimensional Constraints. *Biomaterials.*, 28(23), pp.3398–3407.

Fricker-Gates, R. a, 2006. Radial glia: a changing role in the central nervous system. *Neuroreport*, 17(11), pp.1081–4. Available at: http://www.ncbi.nlm.nih.gov/pubmed/16837831.

Gandini, M. a, Sandoval, A. & Felix, R., 2014. Patch-clamp recording of voltage-sensitive Ca2+ channels. *Cold Spring Harbor protocols*, 2014(4), pp.329–5. Available at: http://www.ncbi.nlm.nih.gov/pubmed/24692484 [Accessed August 23, 2014].

Garaschuk, O. et al., 2000. Large-scale oscillatory calcium waves in the immature cortex. *Nature neuroscience*, 3(5), pp.452–9.

Garcia-Munoz, M., Carrillo-Reid, L. & Arbuthnott, G.W., 2010. Functional anatomy: dynamic States in Basal Ganglia circuits. *Frontiers in neuroanatomy*, 4, p.144. Available at: http://www.pubmedcentral.nih.gov/articlerender.fcgi?artid=2996244&tool=pmcentrez&rendertype=abstract [Accessed August 26, 2011].

Gee, K.R. et al., 2000. Chemical and physiological characterization of fluo-4 Ca(2+)-indicator dyes. *Cell calcium*, 27(2), pp.97–106. Available at: http://www.ncbi.nlm.nih.gov/pubmed/10756976 [Accessed July 30, 2014].

Giugliano, M. & Martinoia, S., 2006. Substrate Arrays of Microelectrodes for in vitro Electrophysiology. In *Wiley Encyclopedia of Biomedical Engineering.* John Wiley & Sons, Inc, pp. 1–8.

Gladwin, K.M. et al., 2013. In vitro biocompatibility of multiwalled carbon nanotubes with sensory neurons. *Advanced healthcare materials*, 2(5), pp.728–35. Available at: http://www.ncbi.nlm.nih.gov/pubmed/23184463 [Accessed June 4, 2013].

Glass, N.R. et al., 2011. Organosilane deposition for microfluidic applications. *Biomicrofluidics*, 5(3), pp.1–7.

Gomez, Lu, Y., et al., 2007. Immobilized nerve growth factor and microtopography have distinct effects on polarization versus axon elongation in hippocampal cells in culture. *Biomaterials.*, 28(2), pp.271–284.

Gomez, Chen, S. & Schmidt, C., 2007. Polarization of hippocampal neurons with competitive surface stimuli: contact guidance cues are preferred over chemical ligands. *Journal of the Royal Society Interface*, 4(13), pp.223–33. Available at: http://www.pubmedcentral.nih.gov/articlerender.fcgi?artid=2359858&tool=pmcentrez&rendertype=abstract [Accessed March 29, 2012].

Gomez, T.M. & Letourneau, P.C., 2014. Actin dynamics in growth cone motility and navigation. *Journal of neurochemistry*, 129(2), pp.221–34. Available at: http://www.ncbi.nlm.nih.gov/pubmed/24164353.

Gong, Y., Li, J.Z. & Schnitzer, M.J., 2013. Enhanced Archaerhodopsin Fluorescent Protein Voltage Indicators. *PloS one*, 8(6), p.e66959. Available at: http://www.pubmedcentral.nih.gov/articlerender.fcgi?artid=3686764&tool=pmcentrez&rendertype=abstract [Accessed November 14, 2014].

Gooding, J.J. et al., 2003. Self-Assembled Monolayers into the 21st Century: Recent Advances and Applications. *Electroanalysis*, 15(2), pp.81–96. Available at: http://dx.doi.org/10.1002/elan.200390017.

Gorelova, N. & Yang, C., 2000. Dopamine D1/D5 Receptor Activation Modulates a Persistent Sodium Current in Rat Prefrontal Cortical Neurons In Vitro. *Journal of Neurophysiology*, 84(1), pp.75–87. Available at: http://jn.physiology.org/content/84/1/75.short [Accessed November 13, 2014].

Grace, A., 1991. Regulation of spontaneous activity and oscillatory spike firing in rat midbrain dopamine neurons recorded in vitro. *Synapse.*, 7(3), pp.221–34.

Grienberger, C. & Konnerth, A., 2012. Imaging calcium in neurons. *Neuron*, 73(5), pp.862–85. Available at: http://www.ncbi.nlm.nih.gov/pubmed/22405199 [Accessed July 10, 2014].

Haavik, J. & Toska, K., 1998. Tyrosine hydroxylase and Parkinson's disease. *Molecular Neurobiology*, 16(3), pp.285–309.

Halldórsson, S. et al., 2014. Advantages and challenges of microfluidic cell culture in polydimethylsiloxane devices. *Biosensors and Bioelectronics*, 63, pp.218–231. Available at: http://linkinghub.elsevier.com/retrieve/pii/S0956566314005302 [Accessed July 28, 2014].

Hamill, O.P. et al., 1981. Improved Patch-Clamp Techniques for High-Resolution Current Recording from Cells and Cell-Free Membrane Patches. *Pflügers Archiv: European Journal of Physiology*, 391(2), pp.85–100.

Hammond, M.W. et al., 2013. Endogenous cholinergic tone modulates spontaneous network level neuronal activity in primary cortical cultures grown on multi-electrode arrays. *BMC neuroscience*, 14, p.38. Available at: http://www.pubmedcentral.nih.gov/articlerender.fcgi?artid=3644495&tool=pmcentrez&rendertype=abstract.

Hardelauf, H. et al., 2014. Micropatterning neuronal networks. *The Analyst*, 139(13), pp.3256–64. Available at: http://www.ncbi.nlm.nih.gov/pubmed/24855658 [Accessed December 18, 2014].

Harel, N.Y. & Strittmatter, S.M., 2006. Can regenerating axons recapitulate developmental guidance during recovery from spinal cord injury? *Nature reviews. Neuroscience*, 7(8), pp.603–16. Available at: http://www.pubmedcentral.nih.gov/articlerender.fcgi?artid=2288666&tool=pmcentrez&rendertype=abstract [Accessed August 6, 2014].

Harris, J. et al., 2007. Fabrication of a microfluidic device for the compartmentalization of neuron soma and axons. *Journal of visualized experiments : JoVE*, (7), p.261. Available at: http://www.pubmedcentral.nih.gov/articlerender.fcgi?artid=2565860&tool=pmcentrez&rendertype=abstract [Accessed March 21, 2012].

Hashimoto, K. & Kita, H., 2006. Slow oscillatory activity of rat globus pallidus neurons in vitro. *The European journal of neuroscience.*, 23(2), pp.443–53. Available at: http://www.ncbi.nlm.nih.gov/pubmed/16420451 [Accessed November 16, 2014].

Hatten, M., 2002. New directions in neuronal migration. *Science (New York, N.Y.)*, 297(5587), pp.1660–1663.

Heizmann, C.W., 1993. Calcium signaling in the brain. *Acta neurobiologiae experimentalis*, 53(1), pp.15–23. Available at: http://www.ncbi.nlm.nih.gov/pubmed/8317243.

Herrero, M.-T., Barcia, C. & Navarro, J., 2002. Functional anatomy of thalamus and basal ganglia. *Child's Nervous System*, 18(8), pp.386–404.

Hilgemann, D.W. et al., 2006. Molecular control of cardiac sodium homeostasis in health and disease. *Journal of cardiovascular electrophysiology*, 17(Suppl 1), pp.S47–S56. Available at: http://www.ncbi.nlm.nih.gov/pubmed/16686682 [Accessed August 19, 2014].

Hirata, Y., 1998. Tyrosine Hydroxylase: Biochemical Properties and Short-term Regulation in vitro and in vivo. In A. Moser, ed. *Pharmacology of Endogenous Neurotoxins: A Handbook*. Cambridge, MA: Birkhauser Boston, pp. 209–220.

Hirono, T. et al., 1988. Recognition of artificial microstructures by sensory nerve fibers in culture. *Brain Research*, 446(1), pp.189–9.

Hodgkin, A.L. & Huxley, A.F., 1952. A quantitative description of membrane current and its application to conduction and excitation in nerve. *Journal of physiology*, 117(4), pp.500–544.

Hodgkin, A.L. & Huxley, A.F., 1952. Currents carried by sodium and potassium ions through the membrane of the giant axon of Loligo. *The Journal of physiology*, 116, pp.449–472.

Hoffman-Kim, D., Mitchel, J.A. & Bellamkonda, R. V, 2010. Topography, Cell Response, and Nerve Regeneration. *Annual Review of Biomedical Engineering*, 12, pp.203–231.

Holthaus, M.G. et al., 2012. Orientation of human osteoblasts on hydroxyapatite-based microchannels. *Acta biomaterialia*, 8(1), pp.394–403. Available at: http://www.ncbi.nlm.nih.gov/pubmed/21855660 [Accessed September 13, 2014].

Honda, T. et al., 2005. Controllable polymerization of N-carboxy anhydrides in a microreaction system. *Lab on a chip*, 5(8), pp.812–8. Available at: http://www.ncbi.nlm.nih.gov/pubmed/16027931 [Accessed December 6, 2014].

Honegger, T. et al., 2013. Electrokinetic confinement of axonal growth for dynamically configurable neural networks. *Lab on a Chip*, 13(4), pp.589–598. Available at: http://pubs.rsc.org/en/content/articlehtml/2013/lc/c2lc41000a [Accessed December 18, 2014].

Hong, D. et al., 2014. Generation of Cellular Micropatterns on a Single-Layered Graphene Film. *Macromolecular …*, 14(3), pp.314–9. Available at: http://www.ncbi.nlm.nih.gov/pubmed/24821665 [Accessed December 9, 2014].

Hosmane, S. et al., 2010. Circular compartmentalized microfluidic platform: Study of axon-glia interactions. *Lab on a chip*, 10(6), pp.741–747.

Huang, Z.-M. et al., 2003. A review on polymer nanofibers by electrospinning and their applications in nanocomposites. *Composites Science and Technology*, 63(15), pp.2223–2253. Available at: http://linkinghub.elsevier.com/retrieve/pii/S0266353803001787 [Accessed July 11, 2014].

Ito, T. et al., 2014. Determining auditory-evoked activities from multiple cells in layer 1 of the dorsal cortex of the inferior colliculus of mice by in vivo calcium imaging. *Brain research*, 1590, pp.45–55. Available at: http://www.ncbi.nlm.nih.gov/pubmed/25278189 [Accessed December 29, 2014].

James, C.D. et al., 2004. Extracellular recordings from patterned neuronal networks using planar microelectrode arrays. *IEEE transactions on bio-medical engineering*, 51(9), pp.1640–8. Available at: http://www.ncbi.nlm.nih.gov/pubmed/15376512.

Jang, M.J. & Nam, Y., 2012. Aqueous micro-contact printing of cell-adhesive biomolecules for patterning neuronal cell cultures. *Biochip Journal*, 6(2), pp.107–113.

Jones, S.W., 2000. Photolithography. In *Silicon Integrated Circuit Process Technology.* pp. 1–5.

Kalil, K. & Dent, E.W., 2005. Touch and go: guidance cues signal to the growth cone cytoskeleton. *Current opinion in neurobiology*, 15(5), pp.521 – 526. Available at: http://www.ncbi.nlm.nih.gov/pubmed/16143510 [Accessed March 2, 2012].

Kandel, E.R., Schwartz, J.H. & Jessell, T.M., 1991. The Basal Ganglia. In *Principles of Neural Science*. Basal Ganglia Components: Prentice-Hall International Inc., pp. 647 – 658.

Kane, R., Takayama, S. & Ostuni, E., 1999. Patterning proteins and cells using soft lithography. *Biomateria*, 20(23 24), pp.2363–2376. Available at: http://www.sciencedirect.com/science/article/pii/S0142961299001659 [Accessed December 5, 2014].

Kang, S.J. et al., 2013. N-type voltage gated calcium channels mediate excitatory synaptic transmission in the anterior cingulate cortex of adult mice. *Molecular pain*, 9, p.58. Available at: http://www.pubmedcentral.nih.gov/articlerender.fcgi?artid=3842823&tool=pmcentrez&rendertype=abstract.

Kaufmann, T. & Ravoo, B.J., 2010. Stamps, inks and substrates: polymers in microcontact printing. *Polymer Chemistry*, 1(4), pp.371–387. Available at: http://xlink.rsc.org/?DOI=b9py00281b [Accessed October 6, 2014].

Kawaguchi, Y., 1993. Physiological, morphological, and histochemical characterization of three classes of interneurons in rat neostriatum. *The Journal of neuroscience : the official journal of the Society for Neuroscience*, 13(11), pp.4908–23. Available at: http://www.ncbi.nlm.nih.gov/pubmed/7693897.

Khan, S. & Newaz, G., 2010. A comprehensive review of surface modification for neural cell adhesion and patterning. *Journal of biomedical materials research. Part A*, 93(3), pp.1209–24. Available at: http://www.ncbi.nlm.nih.gov/pubmed/20229523 [Accessed April 29, 2014].

Kita, H. & Kita, T., 2011. Role of Striatum in the Pause and Burst Generation in the Globus Pallidus of 6-OHDA-Treated Rats. *Frontiers in systems neuroscience*, 5(June), p.42. Available at: http://www.pubmedcentral.nih.gov/articlerender.fcgi?artid=3113166&tool=pmcentrez&rendertype=abstract [Accessed July 18, 2014].

Klapstein, G.J. et al., 2001. Electrophysiological and Morphological Changes in Striatal Spiny Neurons in R6 / 2 Huntington ' s Disease Transgenic Mice. *Journal of Neurophysiology*, 86(6), pp.2667–2677.

Koh, H.S. et al., 2008. Enhancement of neurite outgrowth using nano-structured scaffolds coupled with laminin. *Biomaterials.*, 29(26), pp.3574–82. Available at: http://www.ncbi.nlm.nih.gov/pubmed/18533251 [Accessed September 9, 2014].

Kolodkin, A.L. & Tessier-Lavigne, M., 2011. Mechanisms and molecules of neuronal wiring: a primer. *Cold Spring Harbor perspectives in biology*, 3(6). Available at: http://www.ncbi.nlm.nih.gov/pubmed/21123392 [Accessed May 22, 2013].

Kumar, A., Biebuyck, H. & Whitesides, G., 1994. Patterning Self-Assembled Monolayers: Applications in Materials Science. *Langmuir*, 10(5), pp.1498–1511. Available at: http://pubs.acs.org/doi/abs/10.1021/la00017a030 [Accessed December 7, 2014].

Kumar, A. & Whitesides, G., 1993. Features of gold having micrometer to centimeter dimensions can be formed through a combination of stamping with an elastomeric stamp and an alkanethiol "ink" followed by chemical etching. *Applied Physics Letters*, 63(14), pp.2002–2004. Available at: http://scitation.aip.org/content/aip/journal/apl/63/14/10.1063/1.110628 [Accessed December 9, 2014].

Kumar, G. et al., 2003. Spatially Controlled Cell Engineering on Biomaterials Using Polyelectrolytes. *Langmuir*, 19(25), pp.10550–10556. Available at: http://pubs.acs.org/doi/abs/10.1021/la035309l [Accessed December 9, 2014].

Kunze, A. et al., 2011. Co-pathological connected primary neurons in a microfluidic device for Alzheimer studies. *Biotechnology and bioengineering*, 108(9), pp.2241–5. Available at: http://www.ncbi.nlm.nih.gov/pubmed/21391208 [Accessed December 21, 2014].

Kwiat, M. et al., 2012. Highly ordered large-scale neuronal networks of individual cells - toward single cell to 3D nanowire intracellular interfaces. *ACS applied materials & interfaces*, 4(7), pp.3542–9. Available at: http://www.ncbi.nlm.nih.gov/pubmed/22724437.

De la Monte, S., Vonsattel, J. & Richardson, E.J., 1988. Morphometric demonstration of atrophic changes in the cerebral cortex, white matter, and neostriatum in Huntington's disease. *J Neuropathol Exp Neurol.*, 47(5), pp.516 – 525.

Laforet, G.A. et al., 2001. Changes in Cortical and Striatal Neurons Predict Behavioral and Electrophysiological Abnormalities in a Transgenic Murine Model of Huntington ' s Disease. *Journal of Neuroscience*, 21(23), pp.9112–9123.

Larsen, N. et al., 1997. Order in Microcontact Printed Self-Assembled Monolayers. *Journal of the American Chemical Society*, 119(13), pp.3017–3026. Available at: http://pubs.acs.org/doi/abs/10.1021/ja964090c [Accessed December 5, 2014].

Lee, C.-Y. et al., 2011. Microfluidic mixing: a review. *International journal of molecular sciences*, 12(5), pp.3263–87. Available at: http://www.pubmedcentral.nih.gov/articlerender.fcgi?artid=3116190&tool=pmcentrez&rendertype=abstract [Accessed October 12, 2014].

Lee, J. et al., 2014. A microfluidic device for evaluating the dynamics of the metabolism-dependent antioxidant activity of nutrients. *Lab on a chip*, 14(16), pp.2948–57. Available at: http://www.ncbi.nlm.nih.gov/pubmed/24920301 [Accessed November 18, 2014].

Lee, N. et al., 2014. Monitoring the differentiation and migration patterns of neural cells derived from human embryonic stem cells using a microfluidic culture system. *Molecules and cells*, 37(6), pp.497–502. Available at: http://www.pubmedcentral.nih.gov/articlerender.fcgi?artid=4086344&tool=pmcentrez&rendertype=abstract.

Lee, Y.-S. & Livingston Arinzeh, T., 2011. Electrospun Nanofibrous Materials for Neural Tissue Engineering. *Polymers*, 3(1), pp.413–426. Available at: http://www.mdpi.com/2073-4360/3/1/413/ [Accessed March 6, 2012].

Levis, R.A. & Rae, J.L., 2002. Technology of Patch-Clamp Electrodes. In W. Walz, A. A. Boulton, & G. B. Baker, eds. *Patch-Clamp Analysis: Advanced Techniques*. Totowa, New Jersey: Humana Press Inc, pp. 10 – 33.

Li, B. et al., 2014. Nuclear BK channels regulate gene expression via the control of nuclear calcium signaling. *Nature neuroscience*, 17(8), pp.1055–1063. Available at: http://www.ncbi.nlm.nih.gov/pubmed/24952642 [Accessed July 16, 2014].

Li, D. & Xia, Y., 2004. Electrospinning of Nanofibers: Reinventing the Wheel? *Advanced Materials*, 16(14), pp.1151–1170. Available at: http://doi.wiley.com/10.1002/adma.200400719 [Accessed July 9, 2014].

Li, H. et al., 2003. Nanocontact Printing : A Route to Sub-50-nm-Scale Chemical and Biological Patterning. *Langmuir*, 19(6), pp.1963–1965. Available at: http://pubs.acs.org/doi/abs/10.1021/la0269098 [Accessed December 6, 2014].

Li, J.M. et al., 2008. PMMA microfluidic devices with three-dimensional features for blood cell filtration. *Journal of Micromechanics and Microengineering*, 18(9), p.095021. Available at: http://stacks.iop.org/0960-1317/18/i=9/a=095021?key=crossref.99a9a6b9f616c35b5cbe311750398c0e [Accessed December 22, 2014].

Li, J.Y., Popovic, N. & Brundin, P., 2005. The Use of the R6 Transgenic Mouse Models of Huntington ' s Disease in Attempts to Develop Novel Therapeutic Strategies. *NeuroRx*, 2(3), pp.447–464.

Li, P. et al., 2014. Cyclic ADP-Ribose and NAADP in Vascular Regulation and Diseases. *Messenger (Los Angeles, Calif. : Print)*, 2(2), pp.63–85.

Li, W. et al., 2014. NeuroArray: a universal interface for patterning and interrogating neural circuitry with single cell resolution. *Scientific reports*, 4, p.4784. Available at: http://www.pubmedcentral.nih.gov/articlerender.fcgi?artid=3998032&tool=pmcentrez&rendertype=abstract [Accessed December 1, 2014].

Li, X. et al., 2012. Microfluidic 3D cell culture: potential application for tissue- based bioassays. *Bioanalysis.*, 4(12), pp.1509–1525. Available at: http://www.future-science.com/doi/abs/10.4155/bio.12.133 [Accessed September 13, 2014].

Li, Z. & Wang, C., 2013. Effects of Working Parameters on Electrospinning. In *One-Dimensional nanostructures: Electrospinning Technique and Unique Nanofibers*. SpringerBriefs in Materials. Berlin, Heidelberg: Springer Berlin Heidelberg, pp. 15–29. Available at: http://link.springer.com/10.1007/978-3-642-36427-3 [Accessed July 23, 2014].

Liguz-Lecznar, M. & Skangiel-Kramska, J., 2007. Vesicular glutamate transporters (VGLUTs): The three musketeers of glutamatergic system. *Acta Neurobiologiae Experimentalis*, 67(3), pp.207–218.

Lim, D. & Alvarez-Buylla, A., 1999. Interaction between astrocytes and adult subventricular zone precursors stimulates neurogenesis. *Proceedings of the National Academy of Sciences of the United States of America*, 96(13), pp.7526–7531. Available at: http://www.pnas.org/content/96/13/7526.short [Accessed January 13, 2015].

Lin, S. et al., 2004. Design of Microscopy-based Microcontact Printing Stamp and Alignment Device for Patterned Neuronal Growth. *Journal of Medical and Biomedical Engineering*, 24(1), pp.45–49. Available at: http://jmbe.bme.ncku.edu.tw/index.php/bme/article/viewArticle/113 [Accessed December 7, 2014].

Lippens, G. et al., 2007. Tau Aggregation in Alzheimer's Disease What Role for Phosphorylation? *Prion*, 1(1), pp.21–25.

Liss, B. et al., 2001. Tuning pacemaker frequency of individual dopaminergic neurons by Kv4. 3L and KChip3. 1 transcription. *The EMBO Journal*, 20(20), pp.5715–5724. Available at: http://onlinelibrary.wiley.com/doi/10.1093/emboj/20.20.5715/full [Accessed November 17, 2014].

Liu, H. et al., 2013. Electrospinning of Nanofibers for Tissue Engineering Applications. *Journal of Nanomaterials.*, 2013, pp.1–11.

Liu, T. et al., 2014. Detection of insulin granule exocytosis by an electrophysiology method with high temporal resolution reveals enlarged insulin granule pool in BIG3-knockout mice. *American Journal of Physiology - Endocrinology and Metabolism*, 307(7), pp.E611–E618.

Lorenz, H. et al., 1997. SU-8: a low-cost negative resist for MEMS. *Journal of Micromechanics and Microengineering*, 7(3), pp.121–124. Available at: http://iopscience.iop.org/0960-1317/7/3/010 [Accessed November 21, 2014].

Love, J.C. et al., 2005. Self-assembled monolayers of thiolates on metals as a form of nanotechnology. *Chemical reviews*, 105(4), pp.1103–69. Available at: http://www.ncbi.nlm.nih.gov/pubmed/15826011.

Ma, B. et al., 2011. Huntingtin mediates dendritic transport of β-actin mRNA in rat neurons. *Scientific reports*, 1, p.140. Available at:

http://www.pubmedcentral.nih.gov/articlerender.fcgi?artid=3216621&tool=pmcentrez&rendertype=abstract [Accessed March 6, 2012].

Mahairaki, V. et al., 2011. Nanofiber Matrices Promote the Neuronal Differentiation of Human Embryonic Stem Cell-Derived Neural Precursors In Vitro. *Tissue engineering. Part A*, 17(5 - 6), pp.855–863.

Mahoney, M.J. et al., 2005. The influence of microchannels on neurite growth and architecture. *Biomaterials*, 26(7), pp.771–8. Available at: http://www.ncbi.nlm.nih.gov/pubmed/15350782 [Accessed May 23, 2013].

Majumdar, D. et al., 2011. Co-Culture of Neurons and Glia in a Novel Microfluidic Platform. *Journal of neuroscience methods*, 196(1), pp.38–44.

Mang, D. & Li, Y., 2005. Generation of Transgenic and Gene-Targeted Mouse Models of Movement Disorders. In M. LeDoux, ed. *Movement Disorders: Genetics and Models*. London: Elsevier Academic Press, pp. 33–44.

Mangiarini, L. et al., 1996. Exon 1 of the HD gene with an expanded CAG repeat is sufficient to cause a progressive neurological phenotype in transgenic mice. *Cell*, 87(3), pp.493–506. Available at: http://www.ncbi.nlm.nih.gov/pubmed/8898202.

Marques-da-Silva, D. & Gutierrez-Merino, C., 2014. Caveolin-rich lipid rafts of the plasma membrane of mature cerebellar granule neurons are microcompartments for calcium/reactive oxygen and nitrogen species cross-talk signaling. *Cell calcium*, 56(2), pp.108–23. Available at: http://www.ncbi.nlm.nih.gov/pubmed/24996880 [Accessed August 20, 2014].

McMurtrey, R.J., 2014. Patterned and functionalized nanofiber scaffolds in three-dimensional hydrogel constructs enhance neurite outgrowth and directional control. *Journal of neural engineering*, 11(6), p.066009. Available at: http://www.ncbi.nlm.nih.gov/pubmed/25358624 [Accessed December 19, 2014].

Mehling, M. & Tay, S., 2014. Microfluidic cell culture. *Current opinion in biotechnology*, 25, pp.95–102. Available at: http://www.sciencedirect.com/science/article/pii/S0958166913006794 [Accessed November 18, 2014].

Menalled, L.B., 2005. Knock-In Mouse Models of Huntington's Disease. *NeuroRx*, 2(3), pp.465–470.

Miller, C., Jeftinija, S. & Mallapragada, S., 2002. Synergistic effects of physical and chemical guidance cues on neurite alignment and outgrowth on biodegradable polymer substrates. *Tissue Eng.*, 8(3), pp.367–378.

Millet, L.J. & Gillette, M.U., 2012. New perspectives on neuronal development via microfluidic environments. *Trends in neurosciences*, 35(12), pp.752–61. Available at: http://www.pubmedcentral.nih.gov/articlerender.fcgi?artid=3508261&tool=pmcentrez&rendertype=abstract [Accessed August 14, 2014].

Mintaz, A., Kao, J.P.Y. & Tsieng, R.Y., 1989. Fluorescent Indicators for Cytosolic Calcium Based on Rhodamine and Fluorescein Chromophores*. *The Journal of biological chemistry*, 264(14), pp.8171–8178.

Molleman, A., 2003. Requirements. In *Patch Clamping: An Introductory Guide To Patch Clamp Electrophysiology*. Chichester, England: John Wiley & Sons, Ltd, pp. 43 – 93.

Mueller, A., Taube, J. & Schwartzkroin, P., 1984. Development of hyperpolarizing inhibitory postsynaptic potentials and hyperpolarizing response to gamma-aminobutyric acid in rabbit

hippocampus studied in vitro. *The Journal of neuroscience*, 4(3), pp.860–867. Available at: http://www.jneurosci.org/content/4/3/860.short [Accessed November 16, 2014].

Murugan, R. et al., 2009. Biomaterial Surface patterning of self assembled monolayers for controlling neuronal cell behavior. *Journal of Biomedical Engineering*, 2(2), pp.104–134.

Nagata, I., Kawana, A. & Nakatsuji, N., 1993. Perpendicular contact guidance of CNS neuroblasts on artificial microstructures. *Development (Cambridge, England)*, 117(1), pp.401–8. Available at: http://www.ncbi.nlm.nih.gov/pubmed/8223260.

Narahashi, T., Moore, J. & Scott, W., 1964. Tetrodotoxin Blockage of Sodium Conductance Increase in Lobster Giant Axons. *The Journal of General Physiology*, 47, pp.965–974. Available at: http://jgp.rupress.org/content/47/5/965.abstract [Accessed November 13, 2014].

Nedergaard, S., Flatman, J. a & Engberg, I., 1993. Nifedipine- and omega-conotoxin-sensitive Ca2+ conductances in guinea-pig substantia nigra pars compacta neurones. *The Journal of physiology*, 466, pp.727–747.

Neher, E. & Augustine, G.J., 1992. Calcium gradients and buffers in bovine chromaffin cells. *The Journal of physiology*, 450, pp.273–301. Available at: http://www.pubmedcentral.nih.gov/articlerender.fcgi?artid=1176122&tool=pmcentrez&rendertype=abstract.

Neher, E. & Sakmann, B., 1976. Single-channel currents recorded from membrane of denervated frog muscle fibres. *Nature*, 260(5554), pp.799–802. Available at: http://books.google.com/books?hl=en&lr=&id=p_P1Wm5MnVAC&oi=fnd&pg=PA224&dq=Single-channel+currents+recorded+from+membrane+of+denervated+frog+muscle+fibres&ots=XmCVCAdwdC&sig=YSnL-qOf8x4GXdmTVMDX3kX77JI [Accessed August 14, 2014].

Neher, E., Sakmann, B. & Steinbach, J., 1978. The extracellular patch clamp: a method for resolving currents through individual open channels in biological membranes. *Pflügers Archiv: European Journal of Physiology*, 375(2), pp.219–228. Available at: http://link.springer.com/article/10.1007/BF00584247 [Accessed August 14, 2014].

Ng, J.M.K. et al., 2002. Components for integrated poly(dimethylsiloxane) microfluidic systems. *Electrophoresis*, 23(20), pp.3461–3473.

Nikkhah, M. et al., 2012. Engineering microscale topographies to control the cell-substrate interface. *Biomaterials*, 33(21), pp.5230–46. Available at: http://www.pubmedcentral.nih.gov/articlerender.fcgi?artid=3619386&tool=pmcentrez&rendertype=abstract [Accessed November 25, 2014].

Nisenbaum, E. & Wilson, C., 1995. Potassium currents responsible for inward and outward rectification in rat neostriatal spiny projection neurons. *The Journal of neuroscience*, 15(6), pp.4449–4463. Available at: http://www.jneurosci.org/content/15/6/4449.short [Accessed November 13, 2014].

Noble, D. & Herchuelz, A., 2007. Role of Na/Ca exchange and the plasma membrane Ca2+-ATPase in cell function. Conference on Na/Ca exchange. *EMBO reports*, 8(3), pp.228–32. Available at: http://www.pubmedcentral.nih.gov/articlerender.fcgi?artid=1808037&tool=pmcentrez&rendertype=abstract [Accessed August 20, 2014].

Novak, J. & Wheeler, B., 1988. Multisite hippocampal slice recording and stimulation using a 32 element microelectrode array. *J Neurosci Methods*, 23(2), pp.149–159.

O'Dell, R.S. et al., 2012. Layer 6 cortical neurons require Reelin-Dab1 signaling for cellular orientation, Golgi deployment, and directed neurite growth into the marginal zone. *Neural development*, 7(1), p.25. Available at: http://www.pubmedcentral.nih.gov/articlerender.fcgi?artid=3466444&tool=pmcentrez&rendertype=abstract [Accessed October 14, 2014].

Offenhusser, A. et al., 2007. Microcontact printing of proteins for neuronal cell guidance. *Soft Matter*, 3, pp.290–298.

Ogden, D. & Stanfield, P., 1994. Patch clamp techniques for single channel and whole-cell recording. In D. Ogden, ed. *Microelectrode Techniques: The Plymouth Workshop Handbook*. Company of Biologists, pp. 53–78. Available at: http://bbs.bioguider.com/images/upfile/2005-10/2005102725113.pdf [Accessed August 20, 2014].

Okutan, N., Terzi, P. & Altay, F., 2014. Affecting parameters on electrospinning process and characterization of electrospun gelatin nanofibers. *Food Hydrocolloids.*, 39, pp.19–26. Available at: http://linkinghub.elsevier.com/retrieve/pii/S0268005X13004062 [Accessed August 22, 2014].

Orlandi, J.G. et al., 2014. Transfer entropy reconstruction and labeling of neuronal connections from simulated calcium imaging. *PloS one*, 9(6), p.e98842. Available at: http://www.pubmedcentral.nih.gov/articlerender.fcgi?artid=4048312&tool=pmcentrez&rendertype=abstract [Accessed August 4, 2014].

Osanai, M., Yamada, N. & Yagi, T., 2006. Long-lasting spontaneous calcium transients in the striatal cells. *Neuroscience letters*, 402(1-2), pp.81–5. Available at: http://www.ncbi.nlm.nih.gov/pubmed/16714081 [Accessed November 15, 2014].

Owen, M.J. & Smith, P.J., 1994. Plasma treatment of polydimethylsiloxane. *Journal of Adhesion Science and Technology*, 8(10), pp.1063–1075. Available at: http://www.tandfonline.com/doi/abs/10.1163/156856194X00942 [Accessed November 21, 2014].

Paguirigan, A. & Beebe, D.J., 2006. Gelatin based microfluidic devices for cell culture. *Lab on a chip*, 6(3), pp.407–13. Available at: http://www.ncbi.nlm.nih.gov/pubmed/16511624 [Accessed November 20, 2014].

Pale-Grosdemange, C. et al., 1991. Formation of self-assembled monolayers by chemisorption of derivatives of oligo(ethylene glycol) of structure HS(CH2)11(OCH2CH2)mOH on gold. *Journal of the American Chemical Society*, 113(1), pp.12–20. Available at: http://pubs.acs.org/doi/abs/10.1021/ja00001a002 [Accessed December 9, 2014].

Paredes, R. et al., 2008. Chemical Calcium Indicators. *Methods*, 46(3), pp.143–151. Available at: http://www.sciencedirect.com/science/article/pii/S104620230800159X [Accessed August 14, 2014].

Park, J. et al., 2012. Multi-compartment neuron-glia co-culture platform for localized CNS axon-glia interaction study. *Lab on a chip*, 12(18), pp.3296–304. Available at: http://www.pubmedcentral.nih.gov/articlerender.fcgi?artid=3426455&tool=pmcentrez&rendertype=abstract [Accessed May 14, 2014].

Park, J.W. et al., 2006. Microfluidic culture platform for neuroscience research. *Nature protocols.*, 1(4), pp.2128–36. Available at: http://www.ncbi.nlm.nih.gov/pubmed/17487204 [Accessed August 5, 2014].

Park, T. & Shuler, M., 2003. Integration of Cell Culture and Microfabrication Technology. *Biotechnology progress*, 19(2), pp.243–253. Available at: http://onlinelibrary.wiley.com/doi/10.1021/bp020143k/full [Accessed November 19, 2014].

Pava, M.J. et al., 2014. Endocannabinoid modulation of cortical up-states and NREM sleep. *PloS one*, 9(2), p.e88672. Available at: http://www.pubmedcentral.nih.gov/articlerender.fcgi?artid=3919802&tool=pmcentrez&rendertype=abstract [Accessed September 9, 2014].

Pavlovic, E. et al., 2008. Microfluidic Device Architecture for Electrochemical Patterning and Detection of Multiple DNA Sequences. *Langmuir*, 24(3), pp.1102–1107. Available at: http://pubs.acs.org/doi/abs/10.1021/la702681c [Accessed January 2, 2015].

Perl, A., Reinhoudt, D.N. & Huskens, J., 2009. Microcontact Printing: Limitations and Achievements. *Advanced Materials*, 21(22), pp.2257–2268. Available at: http://doi.wiley.com/10.1002/adma.200801864 [Accessed September 26, 2014].

Peterka, D.S., Takahashi, H. & Yuste, R., 2011. Imaging voltage in neurons. *Neuron*, 69(1), pp.9–21. Available at: http://www.pubmedcentral.nih.gov/articlerender.fcgi?artid=3387979&tool=pmcentrez&rendertype=abstract [Accessed December 9, 2014].

Peyrin, J.-M. et al., 2011. Axon diodes for the reconstruction of oriented neuronal networks in microfluidic chambers. *Lab on a chip*, 11(21), pp.3663–73. Available at: http://www.ncbi.nlm.nih.gov/pubmed/21922081 [Accessed July 14, 2014].

Pinault, D., 2011. The Juxtacellular Recording-Labeling Technique. In R. P. Vertes & R. W. Stackman, eds. *Electrophysiological Recording Techniques.* Neuromethods. Totowa, NJ: Humana Press, pp. 41–75. Available at: http://link.springer.com/10.1007/978-1-60327-202-5 [Accessed July 21, 2014].

Pinto, L. & Götz, M., 2007. Radial glial cell heterogeneity--the source of diverse progeny in the CNS. *Progress in neurobiology*, 83(1), pp.2–23. Available at: http://www.ncbi.nlm.nih.gov/pubmed/17580100 [Accessed May 24, 2013].

Planert, H., Berger, T.K. & Silberberg, G., 2013. Membrane properties of striatal direct and indirect pathway neurons in mouse and rat slices and their modulation by dopamine. *PloS one*, 8(3), p.e57054. Available at: http://www.pubmedcentral.nih.gov/articlerender.fcgi?artid=3585935&tool=pmcentrez&rendertype=abstract [Accessed July 28, 2014].

Plenz, D. & Aertsen, A., 1996. Neural dynamics in cortex-striatum co-cultures--I. anatomy and electrophysiology of neuronal cell types. *Neuroscience*, 70(4), pp.861–891. Available at: http://www.sciencedirect.com/science/article/pii/0306452295004068 [Accessed November 17, 2014].

Plenz, D. & Kitai, S.T., 1998. Up and down states in striatal medium spiny neurons simultaneously recorded with spontaneous activity in fast-spiking interneurons studied in cortex-striatum-substantia nigra organotypic cultures. *The Journal of neuroscience : the official journal of the Society for Neuroscience*, 18(1), pp.266–83. Available at: http://www.ncbi.nlm.nih.gov/pubmed/9412506.

Plotkin, J.L., Day, M. & Surmeier, D.J., 2011. Synaptically driven state transitions in distal dendrites of striatal spiny neurons. *Nature neuroscience*, 14(7), pp.881–8. Available at: http://www.pubmedcentral.nih.gov/articlerender.fcgi?artid=3235762&tool=pmcentrez&rendertype=abstract [Accessed July 14, 2014].

Polleux, F. & Snider, W., 2010. Initiating and growing an axon. *Cold Spring Harbor perspectives in biology.*, 2(4), p.a001925. Available at: http://www.pubmedcentral.nih.gov/articlerender.fcgi?artid=2845204&tool=pmcentrez&rendertype=abstract [Accessed August 18, 2014].

Potter, S.M., 2001. Distributed processing in cultured neuronal networks. In M. A. L. Nicolelis, ed. *Advances in Neural Population Coding*. Amsterdam, The Netherlands: Elsevier, pp. 49–62. Available at: http://www.ncbi.nlm.nih.gov/pubmed/11480288.

Potter, S.M. & DeMarse, T.B., 2001. A new approach to neural cell culture for long-term studies. *Journal of neuroscience methods*, 110(1-2), pp.17–24. Available at: http://www.ncbi.nlm.nih.gov/pubmed/11564520.

Poudel, I. et al., 2013. Micropatterning-retinoic acid co-control of neuronal cell morphology and neurite outgrowth. *Acta biomaterialia*, 9(1), pp.4592–8. Available at: http://www.ncbi.nlm.nih.gov/pubmed/22939924 [Accessed December 9, 2014].

Prieto, A., Edelman, G. & Crossin, K., 1993. Multiple integrins mediate cell attachment to cytotactin / tenascin. *Proceedings of the National Academy of Sciences of the United States of America*, 90(21), pp.10154–10158. Available at: http://www.pnas.org/content/90/21/10154.short [Accessed December 9, 2014].

Proenca, C.C. et al., 2013. Atg4b-dependent autophagic flux alleviates Huntington's disease progression. *PloS one*, 8(7), p.e68357. Available at: http://www.pubmedcentral.nih.gov/articlerender.fcgi?artid=3704647&tool=pmcentrez&rendertype=abstract [Accessed September 9, 2014].

Puopolo, M., Raviola, E. & Bean, B.P., 2007. Roles of subthreshold calcium current and sodium current in spontaneous firing of mouse midbrain dopamine neurons. *The Journal of neuroscience*, 27(3), pp.645–56. Available at: http://www.ncbi.nlm.nih.gov/pubmed/17234596 [Accessed November 13, 2014].

Purdon, S.E. et al., 1994. Huntington ' s Disease : Pathogenesis , Diagnosis and Treatment. *Psychiatry (Abingdon)*, 19(5), pp.359–367.

Purves, D. et al., 2004a. *Neuroscience* 3rd ed., Sunderland, MA: Sinauer Associates, Inc.

Purves, D. et al. eds., 2004b. Synaptic transmission. In *Neuroscience*. Sunderland (MA): Sinauer Associates, Inc., pp. 93–128.

Purves, D., Augustine, G. & Fitzpatrick, D., 2001. *Neuroscience.* 2nd editio., Sunderland (MA): Sinauer Associates.

Qin, D., Xia, Y. & Whitesides, G.M., 2010. Soft lithography for micro- and nanoscale patterning. *Nature protocols*, 5(3), pp.491–502. Available at: http://www.ncbi.nlm.nih.gov/pubmed/20203666 [Accessed July 9, 2014].

Quarrell, O. et al., 2013. Managing juvenile Huntington's disease. *Neurodegenerative disease management*, 3(3), pp.1–16. Available at: http://www.futuremedicine.com/doi/abs/10.2217/nmt.13.18 [Accessed April 15, 2014].

Rajnicek, A., Britland, S. & McCaig, C., 1997. Contact guidance of CNS neurites on grooved quartz: influence of groove dimensions, neuronal age and cell type. *Journal of cell science*, 110 (Pt 2, pp.2905–13. Available at: http://www.ncbi.nlm.nih.gov/pubmed/9359873.

Raman, I. & Bean, B., 1997. Resurgent Sodium Current and Action Potential Formation in Dissociated Cerebellar Purkinje Neurons. *The Journal of neuroscience*, 17(12), pp.4517–4526. Available at: http://www.jneurosci.org/content/17/12/4517.short [Accessed December 28, 2014].

Ramaswamy, S., McBride, J.L. & Kordower, J.H., 2007. Animal Models of Huntington's Disease. *ILAR Journal*, 48(4), pp.356–370.

Randall, F.E. et al., 2011. The corticostriatal system in dissociated cell culture. *Frontiers in systems neuroscience*, 5(June), p.52. Available at: http://www.pubmedcentral.nih.gov/articlerender.fcgi?artid=3127227&tool=pmcentrez&rendertype=abstract [Accessed March 3, 2012].

Raper, J. & Mason, C., 2010. Cellular strategies of axonal pathfinding. *Cold Spring Harbor perspectives in biology*, 2(9), p.a001933. Available at: http://www.pubmedcentral.nih.gov/articlerender.fcgi?artid=2926747&tool=pmcentrez&rendertype=abstract [Accessed May 28, 2013].

Recknor, J.B.J.B. et al., 2004. Oriented astroglial cell growth on micropatterned polystyrene substrates. *Biomaterials.*, 25(14), pp.2753–67. Available at: http://www.ncbi.nlm.nih.gov/pubmed/14962554 [Accessed September 7, 2011].

Regehr, W. et al., 1989. Sealing cultured invertebrate neurons to embedded dish electrodes facilitates long-term stimulation and recording. *Journal of neuroscience methods*, 30(2), pp.91–106. Available at: http://www.sciencedirect.com/science/article/pii/0165027089900551 [Accessed January 5, 2015].

Reiner, a et al., 1988. Differential loss of striatal projection neurons in Huntington disease. *Proceedings of the National Academy of Sciences of the United States of America*, 85(15), pp.5733–7. Available at: http://www.pubmedcentral.nih.gov/articlerender.fcgi?artid=281835&tool=pmcentrez&rendertype=abstract.

Ribeiro, J.C. et al., 2005. A SU-8 fluidic microsystem for biological fluids analysis. *Sensors and Actuators A: Physical*, 123-124, pp.77–81. Available at: http://linkinghub.elsevier.com/retrieve/pii/S0924424705001639 [Accessed November 21, 2014].

Riblett, B.W. et al., 2012. Ice-Templated Scaffolds with Microridged Pores Direct DRG Neurite Growth. *Advanced Functional Materials*, 22(23), pp.4920–4923. Available at: http://doi.wiley.com/10.1002/adfm.201201323 [Accessed October 14, 2014].

Rizzuto, R. & Pozzan, T., 2006. Microdomains of Intracellular Ca 2+ : Molecular Determinants and Functional Consequences. *Physiological reviews*, 86(1), pp.369–408.

Roach, P. et al., 2010. Surface strategies for control of neuronal cell adhesion: A review. *Surface Science Reports*, 65(6), pp.145–173. Available at: http://linkinghub.elsevier.com/retrieve/pii/S0167572910000397 [Accessed July 28, 2011].

Robertson, G., Bushell, T. & Zagnoni, M., 2014. Chemically induced synaptic activity between mixed primary hippocampal co-cultures in a microfluidic system. *Interactive biology: quantitative biosciences from nano to micro*, 6(6), pp.636–44.

Robinson, J. a. et al., 2004. Ratiometric and nonratiometric Ca2+ indicators for the assessment of intracellular free Ca2+ in a breast cancer cell line using a fluorescence microplate reader. *Journal of Biochemical and Biophysical Methods*, 58(3), pp.227–237.

Ruardij, T.G., Goedbloed, M.H. & Rutten, W.L., 2000. Adhesion and patterning of cortical neurons on polyethylenimine- and fluorocarbon-coated surfaces. *IEEE transactions on bio-medical engineering*, 47(12), pp.1593–9. Available at: http://www.ncbi.nlm.nih.gov/pubmed/11125594.

Rubinsky, L. et al., 2007. Study of hypothermia on cultured neuronal networks using multi-electrode arrays. *Journal of neuroscience methods*, 160(2), pp.288–93. Available at: http://www.ncbi.nlm.nih.gov/pubmed/17081617 [Accessed January 3, 2015].

Ruffinatti, F.A. et al., 2013. Spatial wavelet analysis of calcium oscillations in developing neurons. *PloS one*, 8(10), p.e75986. Available at: http://www.pubmedcentral.nih.gov/articlerender.fcgi?artid=3796547&tool=pmcentrez&rendertype=abstract [Accessed August 4, 2014].

Ryan, J. & Urayama, P., 2012. Characterizing the dual-wavelength dye indo-1 for calcium-ion sensing under pressure. *Analytical Methods*, 4(1), p.80. Available at: http://xlink.rsc.org/?DOI=c1ay05486d [Accessed September 24, 2014].

Sah, A. et al., 2004. Hydrophobic modification of γ-alumina membranes with organochlorosilanes. *Journal of Membrane Science*, 243(1-2), pp.125–132.

Samii, A., Nutt, J.G. & Ransom, B.R., 2004. Parkinson ' s disease. *Lancet*, 363(9423), pp.1783–1793.

Sann, S.B. et al., 2008. Neurite outgrowth and in vivo sensory innervation mediated by a Ca(V)2.2-laminin beta 2 stop signal. *The Journal of neuroscience : the official journal of the Society for Neuroscience*, 28(10), pp.2366–74. Available at: http://www.ncbi.nlm.nih.gov/pubmed/18322083 [Accessed August 6, 2014].

Sano, H. et al., 2013. Signals through the striatopallidal indirect pathway stop movements by phasic excitation in the substantia nigra. *The Journal of neuroscience : the official journal of the Society for Neuroscience*, 33(17), pp.7583–94. Available at: http://www.ncbi.nlm.nih.gov/pubmed/23616563 [Accessed November 13, 2014].

Santoro, F., Panaitov, G. & Offenhausser, A., 2014. Defined Patterns of Neuronal Networks on 3D Thiol-functionalized Microstructures. *Nano letters*, 14(12), pp.6906–9. Available at: http://pubs.acs.org/doi/abs/10.1021/nl502922b [Accessed January 2, 2015].

Sarkisov, D. & Wang, S., 2007. Combining Uncaging Techniques with Patch-Clamp Recording and Optical Physiology. *Patch-Clamp Analysis*, 38, pp.149–168. Available at: http://link.springer.com/protocol/10.1007/978-1-59745-492-6_5 [Accessed December 29, 2014].

Savarraj, J.P.J. & Chiu, A.W.L., 2014. Network Dynamics and Spontaneous Oscillations in a Developing Neuronal Culture. *American Journal of Biomedical Engineering*, 4(1), pp.17–24.

Schnell, E. et al., 2007. Guidance of glial cell migration and axonal growth on electrospun nanofibers of poly-epsilon-caprolactone and a collagen/poly-epsilon-caprolactone blend. *Biomaterials*, 28(19), pp.3012–25. Available at: http://www.ncbi.nlm.nih.gov/pubmed/17408736 [Accessed July 19, 2011].

Schramm, A.E. et al., 2014. The Touch and Zap method for in vivo whole-cell patch recording of intrinsic and visual responses of cortical neurons and glial cells. *PloS one*, 9(5), p.e97310. Available at: http://www.pubmedcentral.nih.gov/articlerender.fcgi?artid=4038476&tool=pmcentrez&rendertype=abstract [Accessed July 29, 2014].

Schwaller, B., 2010. Cytosolic Ca2+ buffers. *Cold Spring Harbor perspectives in biology*, 2(11), pp.1–20. Available at: http://cshperspectives.cshlp.org/content/2/11/a004051.short [Accessed August 18, 2014].

Scott, A. et al., 2013. A microfluidic microelectrode array for simultaneous electrophysiology, chemical stimulation, and imaging of brain slices. *Lab on a Chip*, 13(4), pp.527–535. Available at: http://pubs.rsc.org/EN/content/articlehtml/2013/lc/c2lc40826k [Accessed May 6, 2014].

Sherpherd, G., 1998. Basal Ganglia. In *The Synaptic Organisation of the Brain*. New York, pp. 329 – 375.

Shi, M. et al., 2013. Glia co-culture with neurons in microfluidic platforms promotes the formation and stabilization of synaptic contacts. *Lab on a chip*, 13(15), pp.3008–21. Available at: http://www.ncbi.nlm.nih.gov/pubmed/23736663 [Accessed April 29, 2014].

Shigeri, Y., Seal, R.P. & Shimamoto, K., 2004. Molecular pharmacology of glutamate transporters, EAATs and VGLUTs. *Brain Research Reviews*, 45(3), pp.250–265.

Shih, M.-C. et al., 2013. A gel-free multi-well microfluidic device utilizing surface tension for cell culturing. *Sensors and Actuators B: Chemical*, 177, pp.295–307. Available at: http://linkinghub.elsevier.com/retrieve/pii/S092540051201180X [Accessed November 18, 2014].

Shin, E. et al., 2012. GABAergic Neurons from Mouse Embryonic Stem Cells Possess Functional Properties of Striatal Neurons In Vitro, and Develop into Striatal Neurons In Vivo in a Mouse Model of Huntington's. Disease. *Stem Cell Reviews and Reports*, 8(2), pp.513 – 531.

Shin, Y. et al., 2014. PLGA nanofiber membranes loaded with epigallocatechin-3-O-gallate are beneficial to prevention of postsurgical adhesions. *International journal of nanomedicine.*, 9(1), pp.4067–4078. Available at: http://www.ncbi.nlm.nih.gov/pmc/articles/PMC4149440/ [Accessed December 19, 2014].

Sill, T.J. & von Recum, H.A., 2008. Electrospinning: applications in drug delivery and tissue engineering. *Biomaterials*, 29(13), pp.1989–2006. Available at: http://www.ncbi.nlm.nih.gov/pubmed/18281090 [Accessed July 15, 2011].

Silva, G., 2006a. Nanostructure of the nervous system and the impact of nanotechnology on neuroscience. *Biotechnology*, 11, pp.1 – 12. Available at: http://www.eolss.net/Sample-Chapters/C17/E6-58-11-04.pdf [Accessed December 19, 2014].

Silva, G., 2006b. Neuroscience nanotechnology: progress, opportunities and challenges. *Nature reviews. Neuroscience*, 7(1), pp.65–74. Available at: http://www.ncbi.nlm.nih.gov/pubmed/16371951 [Accessed November 17, 2014].

Silver, J. & Miller, J.H., 2004. Regeneration beyond the glial scar. *Nature reviews. Neuroscience*, 5(2), pp.146–56. Available at: http://www.ncbi.nlm.nih.gov/pubmed/14735117 [Accessed March 7, 2012].

Simms, B. a & Zamponi, G.W., 2014. Neuronal voltage-gated calcium channels: structure, function, and dysfunction. *Neuron*, 82(1), pp.24–45. Available at: http://www.ncbi.nlm.nih.gov/pubmed/24698266 [Accessed July 18, 2014].

Smetters, D., Majewska, A. & Yuste, R., 1999. Detecting action potentials in neuronal populations with calcium imaging. *Methods (San Diego, Calif.)*, 18(2), pp.215–21. Available at: http://www.ncbi.nlm.nih.gov/pubmed/10356353.

Smith, A.D. & Bolam, J.P., 1990. The neural network of the basal ganglia as revealed by the study of synaptic connections of identified neurones. *Trends in neuroscience*, 13(7), pp.259–265.

Sontheimer, H. & Ransom, C.B., 1995. Whole-cell patch-clamp recordings. In W. Walz, A. A. Boulton, & G. B. Baker, eds. *Patch-Clamp Applications and Protocols*. New Jersey: Humana Press Inc., pp. 35 – 67. Available at: http://link.springer.com/10.1385/0-89603-311-2:37 [Accessed August 23, 2014].

Sørensen, A. et al., 2007. Long-term neurite orientation on astrocyte monolayers aligned by microtopography. *Biomaterials*, 28(36), pp.5498–508. Available at: http://www.ncbi.nlm.nih.gov/pubmed/17905429 [Accessed January 10, 2015].

Specht, C.G. et al., 2004. Ordered growth of neurons on diamond. *Biomaterials*, 25(18), pp.4073–4078.

Spitzer, N.C., 2010. How GABA generates depolarization. *The Journal of physiology*, 588(Pt 5), pp.757–8. Available at: http://www.pubmedcentral.nih.gov/articlerender.fcgi?artid=2834934&tool=pmcentrez&rendertype=abstract [Accessed December 14, 2014].

Spooren, W.P. et al., 1996. Ventral pallidostriatal pathway in the monkey: Evidence for modulation of basal ganglia circuits. *The Journal of comparative neurology*, 370(3), pp.295–312. Available at: http://www.ncbi.nlm.nih.gov/pubmed/8799857.

Stafstrom, C., 2007. Persistent Sodium Current and Its Role in Epilepsy. *Epilepsy Currents*, 7(1), pp.15–22. Available at: http://onlinelibrary.wiley.com/doi/10.1111/j.1535-7511.2007.00156.x/full [Accessed November 13, 2014].

Stanika, R.I. et al., 2012. Comparative impact of voltage-gated calcium channels and NMDA receptors on mitochondria-mediated neuronal injury. *The Journal of neuroscience : the official journal of the Society for Neuroscience*, 32(19), pp.6642–50. Available at: http://www.pubmedcentral.nih.gov/articlerender.fcgi?artid=3370824&tool=pmcentrez&rendertype=abstract [Accessed July 11, 2014].

Stein, V. & Nicoll, R., 2003. GABA Generates Excitement. *Neuron*, 37(3), pp.375–378. Available at: http://www.sciencedirect.com/science/article/pii/S0896627303000564 [Accessed November 16, 2014].

Stenger, D. et al., 1998. Microlithographicdetermination of axonal/dendriticpolarity in culturedhippocampalneurons. *J Neurosci Methods.*, 82(2), pp.167–73.

Stetter, O. et al., 2012. Model-free reconstruction of excitatory neuronal connectivity from calcium imaging signals. *PLoS computational biology*, 8(8), p.e1002653. Available at: http://www.pubmedcentral.nih.gov/articlerender.fcgi?artid=3426566&tool=pmcentrez&rendertype=abstract [Accessed January 4, 2015].

Stevens, M. & George, J., 2005. Exploring and engineering the cell surface interface. *Science.*, 310(5751), pp.1135–1138.

Stosiek, C. et al., 2003. In vivo two-photon calcium imaging of neuronal networks. *Proceedings of the National Academy of Sciences of the United States of America*, 100(12), pp.7319–24. Available at: http://www.pubmedcentral.nih.gov/articlerender.fcgi?artid=165873&tool=pmcentrez&rendertype=abstract.

Strachan, T. & Read, A., 1999. Genetic manipulation of animals. In *Human Molecular Genetics.* New York: Wiley-Liss, pp. 491–508.

Sullivan, M.R. et al., 2005. In vivo calcium imaging of circuit activity in cerebellar cortex. *Journal of neurophysiology*, 94(2), pp.1636–44. Available at: http://www.ncbi.nlm.nih.gov/pubmed/16079125 [Accessed December 29, 2014].

Sur, S. et al., 2012. A hybrid nanofiber matrix to control the survival and maturation of brain neurons. *Biomaterials.*, 33(2), pp.545–55. Available at:

http://www.pubmedcentral.nih.gov/articlerender.fcgi?artid=3210375&tool=pmcentrez&rendertype=abstract [Accessed September 14, 2014].

Takahashi, A. et al., 1999. Measurement of intracellular calcium. *Physiological reviews*, 79(4), pp.1089–125. Available at: http://www.ncbi.nlm.nih.gov/pubmed/10508230.

Tamura, A. et al., 2014. Both neurons and astrocytes exhibited tetrodotoxin-resistant metabotropic glutamate receptor-dependent spontaneous slow Ca2+ oscillations in striatum. *PloS one*, 9(1), p.e85351. Available at: http://www.pubmedcentral.nih.gov/articlerender.fcgi?artid=3893197&tool=pmcentrez&rendertype=abstract [Accessed November 15, 2014].

Tanaka, E. et al., 2002. Extrusion of Intracellular Calcium Ion After In Vitro Ischemia in the Rat Hippocampal CA1 Region. *Neurophysiology*, 88(2), pp.879–887.

Tang, S. & Whitesides, G., 2009. Basic Microfluidic and Soft Lithographic Techniques. In I. Gannot & J. Neev, eds. *Optofluidics: Fundamentals, Devices and Applications*. McGraw-Hill Companies, Inc, pp. 7–32. Available at: http://www2.egr.uh.edu/~nvaradar/private/Refs/Litho.pdf [Accessed November 20, 2014].

Tarsy, D., Vitek, J.L. & Lozano, A.M., 2003. *Surgical Treatment of Parkinson's Disease and Other Movement Disorders*, Totowa, New Jersey.

Taylor, A.M. et al., 2005. A microfluidic culture platform for CNS axonal injury, regeneration and transport. *Nature methods.*, 2(8), pp.599–605.

Taylor, A.M. et al., 2009. Axonal mRNA in uninjured and regenerating cortical mammalian axons. *The Journal of neuroscience : the official journal of the Society for Neuroscience*, 29(15), pp.4697–707. Available at: http://www.pubmedcentral.nih.gov/articlerender.fcgi?artid=3632375&tool=pmcentrez&rendertype=abstract [Accessed August 27, 2014].

Taylor, A.M. et al., 2010. Microfluidic local perfusion chambers for the visualization and manipulation of synapses. *Neuron*, 66(1), pp.57–68. Available at: http://www.pubmedcentral.nih.gov/articlerender.fcgi?artid=2879052&tool=pmcentrez&rendertype=abstract [Accessed September 17, 2014].

Taylor, A.M. et al., 2003. Microfluidic Multicompartment Device for Neuroscience Research. *Langmuir.*, 19(5), pp.1551–1556.

Taylor, A.M. & Jeon, N.L., 2010. Micro-scale and microfluidic devices for neurobiology. *Current opinion in neurobiology.*, 20(5), pp.640–7. Available at: http://www.ncbi.nlm.nih.gov/pubmed/20739175 [Accessed August 10, 2014].

Tepper, J.., Wilson, C.. & Koós, T., 2005. Feedforward and Feedback inhibition in Neostriatum. In *The Basal Ganglia VIII*. Oxford, pp. 457 – 466.

Tepper, J.M. et al., 2010. Heterogeneity and diversity of striatal GABAergic interneurons. *Frontiers in neuroanatomy*, 4(December), p.150. Available at: http://www.pubmedcentral.nih.gov/articlerender.fcgi?artid=3016690&tool=pmcentrez&rendertype=abstract [Accessed July 12, 2011].

Thames, S.F. & Panjnani, K.G., 1996. Organosilane polymer chemistry: A review. *Journal of Inorganic and Organometallic Polymers*, 6(2), pp.59–94.

Thomas, B. et al., 2013. A novel method for detecting 7-methyl guanine reveals aberrant methylation levels in Huntington disease. *Analytical biochemistry*, 436(2), pp.112–120.

Available at: http://www.pubmedcentral.nih.gov/articlerender.fcgi?artid=4090024&tool=pmcentrez&rendertype=abstract [Accessed September 10, 2014].

Thomas, V. et al., 2006. Mechano-morphological studies of aligned nanofibrous scaffolds of polycaprolactone fabricated by electrospinning. *Journal of Biomaterials Science, Polymer Edition*, 17(9), pp.969–984. Available at: http://www.tandfonline.com/doi/abs/10.1163/156856206778366022 [Accessed December 19, 2014].

Tseng, K. et al., 2001. Cortical Slow Oscillatory Activity Is Reflected in the Membrane Potential and Spike Trains of Striatal Neurons in Rats with Chronic Nigrostriatal Lesions. *The Journal of …*, 21(16), pp.6430–6439. Available at: http://www.jneurosci.org/content/21/16/6430.short [Accessed November 17, 2014].

Tuft, B.W. et al., 2013. Photopolymerized microfeatures for directed spiral ganglion neurite and Schwann cell growth. *Biomaterials*, 34(1), pp.42–54. Available at: http://www.ncbi.nlm.nih.gov/pubmed/23069708 [Accessed September 13, 2014].

Turner, R.S., 2009. *Basal Ganglia and The Regulation of Movement.*, Chichester, England: John Wiley & Sons Ltd.

Uttayarat, P. et al., 2005. Topographic guidance of endothelial cells on silicone surfaces with micro- to nanogrooves: orientation of actin filaments and focal adhesions. *Journal of biomedical materials research. Part A*, 75A(3), pp.668–80. Available at: http://www.ncbi.nlm.nih.gov/pubmed/16110489 [Accessed December 10, 2014].

Velve-Casquillas, G. et al., 2010. Microfluidic tools for cell biological research. *Nano today*, 5(1), pp.28–47. Available at: http://www.pubmedcentral.nih.gov/articlerender.fcgi?artid=2998071&tool=pmcentrez&rendertype=abstract [Accessed December 15, 2014].

Vogt, A.K. et al., 2005. Synaptic plasticity in micropatterned neuronal networks. *Biomaterials*, 26(15), pp.2549–57. Available at: http://www.ncbi.nlm.nih.gov/pubmed/15585257 [Accessed January 2, 2015].

Voldman, J., Gray, M.L. & Schmidt, M. a, 1999. Microfabrication in biology and medicine. *Annual review of biomedical engineering*, 1, pp.401–25. Available at: http://www.ncbi.nlm.nih.gov/pubmed/11701495.

Wagenaar, D. et al., 2005. Controlling Bursting in Cortical Cultures with Closed-Loop Multi-Electrode Stimulation. *The Journal of neuroscience : the official journal of the Society for Neuroscience*, 25(3), pp.680–688. Available at: http://www.jneurosci.org/content/25/3/680.short [Accessed November 14, 2014].

Wagenaar, D., Pine, J. & Potter, S., 2006. An extremely rich repertoire of bursting patterns during the development of cortical cultures. *BMC neuroscience*, 7, p.11. Available at: http://www.pubmedcentral.nih.gov/articlerender.fcgi?artid=1420316&tool=pmcentrez&rendertype=abstract [Accessed November 3, 2014].

Walboomers, X.F. et al., 1999. Attachment of fibroblasts on smooth and microgrooved polystyrene. *Journal of biomedical materials research*, 46(2), pp.212–20. Available at: http://www.ncbi.nlm.nih.gov/pubmed/10379999.

Wang, J. et al., 2012. The effects of electrospun TSF nanofiber diameter and alignment on neuronal differentiation of human embryonic stem cells. *Journal of Biomedical Materials Research - Part A*, 100(3), pp.632–645.

Wang, J.-Z. et al., 2013. Abnormal hyperphosphorylation of tau: sites, regulation, and molecular mechanism of neurofibrillary degeneration. *Journal of Alzheimer's disease : JAD*, 33, pp.S123–39. Available at: http://www.ncbi.nlm.nih.gov/pubmed/22710920 [Accessed January 17, 2015].

Wang, L. et al., 2013. Construction of oxygen and chemical concentration gradients in a single microfluidic device for studying tumor cell-drug interactions in a dynamic hypoxia microenvironment. *Lab on a chip*, 13(4), pp.695–705. Available at: http://www.ncbi.nlm.nih.gov/pubmed/23254684 [Accessed November 18, 2014].

Wang, Y. et al., 2012. Systematic prevention of bubble formation and accumulation for long-term culture of pancreatic islet cells in microfluidic device. *Biomedical Microdevices*, 14(2), pp.419–426.

Watters, O. et al., 2014. Automated analysis of intracellular calcium fluorescence in rat organotypic hippocampal cultures: comparison to a manual, observer based method. *Journal of neuroscience methods*, 223, pp.20–9. Available at: http://www.ncbi.nlm.nih.gov/pubmed/24325985 [Accessed August 2, 2014].

Weerakoon, P. et al., 2009. An integrated patch-clamp potentiostat with electrode compensation. *IEEE transactions on biomedical circuits and systems*, 3(2), pp.117–25. Available at: http://www.ncbi.nlm.nih.gov/pubmed/23853203.

Weiss, P., 1945. Experiments on cell and axon orientation in vitro; the role of colloidal exudates in tissue organization. *Journal of experimental zoology*, 100(3), pp.353–86.

Weiss, P., 1947. The problem of specificity in growth and development. *The Yale journal of biology and medicine*, 19(3), pp.235–278. Available at: http://www.ncbi.nlm.nih.gov/pmc/articles/PMC2602102/ [Accessed March 23, 2012].

Welling, A., 2009. Voltage-dependent calcium channels. *Biotrend reviews*, 1(4), pp.1–12. Available at: http://www.researchgate.net/publication/7664775_Voltage-dependent_calcium_channels/file/79e415092b58e6d9b2.pdf [Accessed August 25, 2014].

Whitesides, G. et al., 2001. Soft Lithography In Biology and Biochemistry. *Annual review of biomedical engineering*, 3, pp.335–73. Available at: http://www.annualreviews.org/doi/abs/10.1146/annurev.bioeng.3.1.335 [Accessed December 5, 2014].

Whitesides, G.M., 2006. The origins and the future of microfluidics. *Nature*, 442(7101), pp.368–73. Available at: http://www.ncbi.nlm.nih.gov/pubmed/16871203 [Accessed July 10, 2014].

Williams, J.D. & Wang, W., 2004. Study on the postbaking process and the effects on UV lithography of high aspect ratio SU-8 microstructures. *Journal of Micro/Nanolithography, MEMS, and MOEMS*, 3(4), pp.563–568. Available at: http://nanolithography.spiedigitallibrary.org/article.aspx?doi=10.1117/1.1792650 [Accessed November 2, 2014].

Wilson, C., 2010. Up and down states. , 3(6), pp.1–11.

Wilson, C.J. et al., 2000. Coupled Oscillator Model of the Dopaminergic Neuron of the Substantia Nigra Coupled Oscillator Model of the Dopaminergic Neuron of the Substantia Nigra. *Neurophysiology*, 83(5), pp.3084–3100.

Wilson, C.J., 2007. GABAergic inhibition in the neostriatum. *Progress in brain research*, 160, pp.91–110. Available at: http://www.ncbi.nlm.nih.gov/pubmed/17499110 [Accessed July 2, 2011].

Wilson, C.J. & Groves, P.M., 1981. Spontaneous firing patterns of identified spiny neurons in the rat neostriatum Charles J . Wilson and Philip M . Groves. *Brain*, 220(1), pp.67 – 80.

Wilson, C.J. & Kawaguchi, Y., 1996. The origins of two-state spontaneous membrane potential fluctuations of neostriatal spiny neurons. *The Journal of neuroscience : the official journal of the Society for Neuroscience*, 16(7), pp.2397–2410. Available at: http://www.ncbi.nlm.nih.gov/pubmed/8601819.

Wojcik, S.M. et al., 2004. An essential role for vesicular glutamate transporter 1 (VGLUT1) in postnatal development and control of quantal size. *Proceedings of the National Academy of Sciences of the United States of America*, 101(18), pp.7158–63. Available at: http://www.pubmedcentral.nih.gov/articlerender.fcgi?artid=406482&tool=pmcentrez&rendertype=abstract.

Wolf, A. & Wennemuth, G., 2014. Ca2+ clearance mechanisms in cancer cell lines and stromal cells of the prostate. *The Prostate*, 74(1), pp.29–40. Available at: http://www.ncbi.nlm.nih.gov/pubmed/24037789 [Accessed August 20, 2014].

Wood, C., Williams, C. & Waldron, G.J., 2004. Patch clamping by numbers. *Drug discovery today*, 9(10), pp.434–41. Available at: http://www.ncbi.nlm.nih.gov/pubmed/15109948.

Xia, Y. et al., 1996. Non-Photolithographic Methods for Fabrication of Elastomeric Stamps for Use in Microcontact Printing. *Langmuir*, 12(16), pp.4033–4038. Available at: http://pubs.acs.org/doi/abs/10.1021/la960387c [Accessed December 6, 2014].

Xia, Y. & Whitesides, G.M., 1998. Soft lithography. *Annual Review of Materials Science.*, 28(12), pp.153–84.

Xiao, R. et al., 2014. Quantifying Biased Response of Axon to Chemical Gradient Steepness in a Microfluidic Device. *Analytical chemistry*, 86(23), pp.11649–11656. Available at: http://pubs.acs.org/doi/abs/10.1021/ac504159g [Accessed December 22, 2014].

Xie, J. et al., 2014. Neurite Outgrowth on Electrospun Nano fibers with Uniaxial Alignment: The Effects of Fiber Density, Surface Coating, and Supporting Substrate. *ACS nano*, 8(2), pp.1878–1885. Available at: http://pubs.acs.org/doi/abs/10.1021/nn406363j [Accessed December 19, 2014].

Xu, H., Ferreira, M.M. & Heilshorn, S.C., 2014. Small-molecule axon-polarization studies enabled by a shear-free microfluidic gradient generator. *Lab on a chip*, 14(12), pp.2047–56. Available at: http://www.ncbi.nlm.nih.gov/pubmed/24781157 [Accessed December 22, 2014].

Yang, F. et al., 2014. Activated astrocytes enhance the dopaminergic differentiation of stem cells and promote brain repair through bFGF. *Nature communications*, 5, p.5627. Available at: http://www.ncbi.nlm.nih.gov/pubmed/25517983 [Accessed December 19, 2014].

Yang, F. et al., 2005. Electrospinning of nano/micro scale poly(L-lactic acid) aligned fibers and their potential in neural tissue engineering. *Biomaterials*, 26(15), pp.2603–10. Available at: http://www.ncbi.nlm.nih.gov/pubmed/15585263 [Accessed July 19, 2011].

Yang, I.H., Co, C.C. & Ho, C.-C., 2005. Alteration of human neuroblastoma cell morphology and neurite extension with micropatterns. *Biomaterials*, 26(33), pp.6599–609. Available at: http://www.ncbi.nlm.nih.gov/pubmed/15936072 [Accessed December 9, 2014].

Yang, Y., Wimpenny, I. & Ahearne, M., 2011. Portable nanofiber meshes dictate cell orientation throughout three-dimensional hydrogels. *Nanomedicine : nanotechnology, biology, and medicine*, 7(2), pp.131–6. Available at: http://www.ncbi.nlm.nih.gov/pubmed/21272664 [Accessed September 8, 2011].

Yao, L. et al., 2009. Effect of functionalized micropatterned PLGA on guided neurite growth. *Acta biomaterialia*, 5(2), pp.580–8. Available at: http://www.ncbi.nlm.nih.gov/pubmed/18835227 [Accessed June 4, 2013].

Yelnik, J., 2002. Functional Anatomy of the Basal Ganglia. *Movement Disorders*, 17.

Yu, T.T. & Shoichet, M.S., 2005. Guided cell adhesion and outgrowth in peptide-modified channels for neural tissue engineering. *Biomaterials*, 26(13), pp.1507–14. Available at: http://www.ncbi.nlm.nih.gov/pubmed/15522752 [Accessed September 13, 2014].

Yuan, Y. et al., 2013. Cadmium-induced apoptosis in primary rat cerebral cortical neurons culture is mediated by a calcium signaling pathway. *PloS one*, 8(5), p.e64330. Available at: http://www.pubmedcentral.nih.gov/articlerender.fcgi?artid=3669330&tool=pmcentrez&rendertype=abstract [Accessed September 7, 2014].

Yung, W., Häusser, M. & Jack, J., 1991. Electrophysiology of dopaminergic and non-dopaminergic neurones of the guinea-pig substantia nigra pars compacta in vitro. *The Journal of Physiology*, 436, pp.643–667. Available at: http://jp.physoc.org/content/436/1/643.short [Accessed November 17, 2014].

Yuste, R. et al., 2011. Imaging action potentials with calcium indicators. *Cold Spring Harbor protocols*, 2011(8), pp.985–9. Available at: http://www.ncbi.nlm.nih.gov/pubmed/21807854 [Accessed July 16, 2014].

Zhang, K. et al., 2014. Block-Cell-Printing for live single-cell printing. *Proceedings of the National Academy of Sciences of the United States of America*, 111(8), pp.2948–53. Available at: http://www.pubmedcentral.nih.gov/articlerender.fcgi?artid=3939871&tool=pmcentrez&rendertype=abstract [Accessed October 28, 2014].

Zhang, S. et al., 1999. Biological surface engineering : a simple system for cell pattern formation. *Biomaterials*, 20(13), pp.1213–1220. Available at: http://www.sciencedirect.com/science/article/pii/S0142961299000149 [Accessed December 9, 2014].

Zhao, Y. et al., 2010. Hormonal inhibition of endocytosis: novel roles for noradrenaline and G protein G(z). *The Journal of physiology*, 588(Pt 18), pp.3499–509. Available at: http://www.pubmedcentral.nih.gov/articlerender.fcgi?artid=2988514&tool=pmcentrez&rendertype=abstract [Accessed August 21, 2014].

Zhong, S. et al., 2006. An aligned nanofibrous collagen scaffold by electrospinning and its effects on in vitro fibroblast culture. *Journal of biomedical materials research. Part A*, 79(3), pp.456–63. Available at: http://www.ncbi.nlm.nih.gov/pubmed/16752400.

Zhou, M.-Y. et al., 2009. Effects of surface wettability and roughness of microchannel on flow behaviors of thermo-responsive microspheres therein during the phase transition. *Journal of colloid and interface science*, 336(1), pp.162–70. Available at: http://www.ncbi.nlm.nih.gov/pubmed/19394620 [Accessed December 7, 2014].

Zuccato, C., Valenza, M. & Cattaneo, E., 2010. Molecular Mechanisms and Potential Therapeutical Targets in Huntington ' s Disease. *Physiological review*, 90(3), pp.905–981.

Appendix

1. Abbreviations

3-NPA	3-nitropropionic acid
6-OHDA	6hydroxydopamine
AMPA-R	A-amino-3-hydroxy-5-methyl-4-isoxazolepropionic acid receptor
ANOVA	Analysis of variance
ATP	Adenosine triphosphate
BG	Basal ganglia
CAG	Cytosine Adenine Guanine
CLSM	Confocal laser scanning microscopy
CNS	Central nervous system
D1	Dopamine receptor type 1
D2	Dopamine receptor type 2
DAPI	4',6-diamidino-2-phenylindole
DETA	Trimethoxysilylpropyldiethylenetriamine
DIV	Days *in vitro*
DMEM-F12	Dulbecco's Modified Eagle's Medium/Nutrient F-12 Ham's medium
DMSO	Dimethyl sulfoxide
DNA	Deoxyribonucleic acid
DNase	Deoxyribonuclease
DRG	Dorsal root ganglia
DYN	Dynorphin
E	Embryonic day
ECM	Extracellular matrix
EGF	Epidermal growth factor
EGFP	Enhanced green fluorescent protein
E_K	Potassium-generated potential
E_{Na}	Sodium-generated potential
ENK	Enkephalin
EPSCs	Excitatory postsynaptic currents
EPSPs	Excitatory postsynaptic potentials

ER	Endoplasmic reticulum
E_{rev}	Reversal potential
F	Fluorescence
F_0	Background fluorescence
FCS	Fetal calf serum
FITC	Fluorescein isothiocyanate
GABA	Gamma-aminobutyric acid
GAD	Glutamate decarboxylase
GFP	Green fluorescent protein
GP	Globus pallidus
GPe	External part of the globus pallidus
GPi	Internal part of the globus pallidus
HD	Huntington's disease
HRP	Horseradish peroxide
Htt	Huntingtin protein
HVA	High voltage activated
IP_3R	Inositol trisphosphate receptors
iPSCs	Induced pluripotent stem cells
IPSPs	Inhibitory postsynaptic potentials
LGE	Lateral ganglionic eminence
LN	Laminin
LVA	Low voltage activated
MAP2	Microtubule-associated protein 2
MAP5	Microtubule-associated protein 5
MEAs	Multi-electrode arrays
mESCs	Mouse embryonic stem cells
MGE	Medial ganglionic eminence
MpA	Micro-grooves pre-seeded with astrocytes
MPL	Micro-grooves pre-coated with poly-L-lysine and laminin
MSNs	Medium spiny neurons

nAChR	Nicotinic acetylcholine receptors
NCM	Neuronal culture medium
NCX	Sodium-calcium exchanger
NGF	Nerve growth factor
NGS	Normal goat serum
NMDA	N-methyl-D-asparate
NMDA-R	N-methyl-D-aspartate receptor
NOS	Nitric oxide synthase
NPL	Nano-fibres pre-coated with poly-L-lysine and laminin
NPY	Neuropeptide Y
P	Postnatal
PA	Peptide amphiphile
PBS	Phosphate-buffered saline
PCL	Polycaprolactone
PD	Parkinson's disease
PDL	Poly-D-lysine
PDMS	Polydimethylsiloxane
PEB	Post-exposure baking
PEI	Polyethyleneimine
PFA	Paraformaldehyde
PLA	Polylactic acid
PLGA	Poly (lactic-co-glycolic acid)
PLL	Poly-L-lysine
PMCA	Plasma membrane calcium ATPase
PMMA	Polymethylmethacrylate
PNS	Peripheral nervous systems
PS	Polystyrene
PSF	Penicillin Streptomycin Fungizone
PV	Parvalbumins
Py	Phosphotyrosine

QA	Quinolinic acid
ROCs	Receptor operated channels
ROI	Region of interest
RyRs	Ryanodine receptors
SAMs	Self-assembled monolayers
SEM	Scanning electron microscope
SERCA	Sarco-/endoplasmic reticulum calcium ATPase
SN	Substantia nigra
SNc	Substantia nigra pars compacta
SNr	Substantia nigra pars reticulate
SOM	Somatostatin
SP	Substance P
STN	Subthalamic nucleus
TBS	Tris-buffered saline
TH	Tyrosine hydroxylase
Thal	Thalamus
TRITC	Tetramethyl rhodamine
TRPC	Transient receptor potential type C.
TSF	Tussah silk fibroin
TTX	Tetrodotoxin
UV	Ultraviolet
VGlut 2	Vesicular glutamate transporter 2
VL	Ventral lateral nucleus
VM	Ventral mesencephalon
VOCs	Voltage-operated channels
V_{rest}	Resting voltage
WT	Wild-type

2. Manuscripts published, submitted or in preparation.

Kamudzandu M, Yang Y, Roach P, Fricker RA (2015) Efficient alignment of primary CNS neurites using structurally engineered surfaces and biochemical cues

Kamudzandu M, Roach P, Fricker RA, Yang Y (2015) Nanofibrous scaffolds supporting optimal central nervous system regeneration: an evidence-based review

Kamudzandu M, Fricker RA, Roach P (2015) A complex five-port microfluidic-based functional CNS circuit